Freie Universität Berlin

GFZ Helmholtz-Zentrum Potsdam

Multi-scale and uncertainty assessment of contractional thick-skinned structures in petroleum basins of the Andean back-arc

Jan Witte

Neogene (syn-orogenic) conglomerates and volcaniclastics in synclinal position

(Pincheira piggy-back basin, ~22km west of Malargüe, Argentina, view south)

1. Gutachter:	Prof. Dr. O. Oncken GeoForschungsZentrum Potsam, Freie Universität Berlin
2. Gutachter:	Prof. Dr. Anne Bernhardt Freie Universität Berlin
Ort und Datum der Disputation:	Berlin, 30. September 2020

Multi-scale and uncertainty assessment of contractional thick-skinned structures in petroleum basins of the Andean back-arc

Dissertation

zur Erlangung des akademischen Grades eines Doktors der Naturwissenschaften (Dr. rer. nat.) in der Wissenschaftsdisziplin Geologie am Fachbereich Geowissenschaften an der Freien Universität Berlin

vorgelegt von

Jan Witte

aus Hameln

Berlin, Oktober 2020

Acknowledgements

Undertaking this PhD project has been truly a life-changing experience for me and it would not have been possible without the support and guidance that I received from many people.

First and foremost I would like to thank my thesis supervisor, Onno Oncken, for his patient and wise guidance throughout this project, for always caring about my work and for countless and highly inspiring discussions about structural geology (some of them in the outcrops!) and many other interesting topics.

I would also like to express my gratitude to Manfred Strecker, for his enriching support, his extremely valuable insights into Andean tectonics and, particularly, for engaging so deeply in the discussions around the highly complex structural interplay at the Santiago Basin in Peru.

Furthermore, I would like to thank all my co-authors, particularly Johnny Rebaza, Cinthia Alegria, Marco Raez and Massimo Bonora. A big “thank you” also goes to the Argentinian colleagues who helped so much with the field logistics, namely, Daniel Bogetti and his team in Mendoza. My sincere thanks to the fellow geoscientists at GFZ, Pia, Marcos, Io, Jonathan, Armin, Matthias and Bernd, for valuable technical discussions and for joining you at the “Sektionsfest” in the summer a couple of times, and having a great time there!

Completing this work would have been impossible without the tireless support of Franziska Alberg and I truly value all her continuous help and logistical support in coordinating hotel reservations, blocking work space, organizing meetings and keys and always cheering me up. A wholehearted thanks also goes to Regina Prero, for fantastic logistical support and coordinating with the IT team.

A special thank you goes to my very dear friends, Achim and Cindy Tappe, for always having an open ear for me and for their exceptional moral support and encouragement.

Thank you, mom and dad, for your unfailing emotional support and endless patience!

Widmung

Diese Dissertation möchte ich meinen wundervollen Eltern widmen, die mich immer in allen meinen Projekten unterstützen.

Eidesstattliche Erklärung

Hiermit versichere ich, dass ich die vorliegende Dissertation ohne unzulässige Hilfe Dritter und ohne Benutzung anderer als der angegebenen Literatur angefertigt habe; die aus fremden Quellen direkt oder indirekt übernommenen Gedanken sind als solche kenntlich gemacht.

Hameln, Juli 2020

“A ship is always safe at shore but that is not what it’s built for.”

Albert Einstein

CONTENTS

Chapters 3 to 6 in this Thesis correspond to the following published / submitted research papers:

Chapter 3

A new structural model of the Pachitea Basin, Peru: Interaction of thick-skinned tectonics and salt detached thrusting

Witte, J., Rebaza, J., Westlund, D., Stratton, M. and C. Alegria

2015, Journal of South American Earth Sciences, 63 (2015), p. 400-146.

doi.org/10.1016/j.jsames.2015.04.008

Chapter 4

Structural styles and tectonic evolution of the Santiago Basin, Peru – Implications for hydrocarbon traps

Witte, J. Strecker, M.R. and M. Raez

2018, in: G. Zamora, McClay, K.R. and V.A. Ramos, eds., Petroleum basins and hydrocarbon potential of the Andes of Peru and Bolivia: AAPG Memoir 117, p. 227-250.

doi.org/10.1306/13632122M1173770

Chapter 5

Uncertainty Quantification in Section-Balancing Using Pseudo-3D Forward Modeling – Example of the Malargüe Anticline, Argentina*

Witte, J. and O. Oncken

** At the time of the PhD disputation, this paper was under review at the Journal of Structural Geology.*

Chapter 6

Fracture evolution in oil-producing sills of the Rio Grande Valley, northern Neuquén Basin, Argentina

Witte, J., Bonora, M., Carbone, C. and O. Oncken

2012, AAPG Bulletin, v. 96, No. 7, p. 1253-1277.

doi.org/10.1306/10181110152

ZUSAMMENFASSUNG

Jede sorgfältige geologische Interpretation erfordert die Integration von Daten über mehrere Grössenordnungen hinweg und im Idealfall auch quantifizierbare Aussagen über die Unsicherheiten. Selbstähnlichkeit („fraktales Verhalten“) in Strukturelementen und die Notwendigkeit eine Unsicherheitsanalyse sind schon seit langer Zeit bekannt (z.B. Gibbs, 1983; Pollard & Aydin, 1988). Dennoch sind heutzutage weder eine sorgfältige Datenintegration über mehrere Grössenordnungen hinweg noch die Quantifizierung der Unsicherheit in der Strukturanalyse zum Standard geworden. Derzeit fehlen verfügbare Workflows zur Unsicherheitsquantifizierung. In diesem Dissertationsprojekt habe ich multi-skalierte Daten in vier Untersuchungsgebieten untersucht, welche in Erdölprovinzen im subandinen Back-arc liegen und von kompressionaler Basement-Tektonik dominiert werden. Zwei Gebiete liegen in Peru („Santiago“, „Pachitea“) und zwei in Argentinien („Malargüe“, „Rio Grande“) (**Fig. 1.1**). Für das Gebiet „Malargüe“ (s.u.), wo ein sehr hochqualitatives Datenset vorlag, habe ich eine neue Methode zur verbesserten Unsicherheitsquantifizierung entwickelt.

Für alle vier Gebiete standen KW-Industrie Datensätze zur Verfügung, darunter Bohrlochdaten, 2D-Seismik (ältere sowie neu reprozessierte), 3D-Seismik (nur „Rio Grande“), geologische Oberflächenkarten (einige davon neu erhoben im Rahmen dieses Projektes) und neue Magnetikdaten (nur „Pachitea“). Diese Strukturen wurden bisher nicht (oder nur teilweise) mit moderner struktureller Methodik untersucht. Neu im Rahmen dieses Projektes konstruierte strukturelle Transekten für die Regionen „Santiago“ und „Pachitea“ ermöglichen ein verfeinertes Strukturmodell, ein besseres Verständnis der tektonischen Entwicklung im Beckenmaßstab, ein besseres Verständnis des Einflusses von Evaporiten auf den Baustil sowie die Berechnung neue Verkürzungsraten. Über die Thick-Skin „Malargüe Antiklinale“ gibt es bereits genauere Untersuchungen. In diesem Dissertationsprojekt wird jedoch ein dreidimensionaler Ansatz vorgestellt, der auf einem neuen und außergewöhnlich gut kalibrierten pseudo-3D Modell der Antiklinale beruht und – unter Verwendung von Forward Modeling – einen neuen Workflow zur Quantifizierung von Unsicherheiten darstellt. Dieser Workflow trägt zur systematischen Reduzierung von Modellunsicherheiten bei und kann auch in anderen tektonischen Settings angewendet werden. Er hilft bei der Beantwortung relevanter Fragen rund um die Malargüe Antiklinale und trägt dazu bei, die Unsicherheiten des Strukturmodells deutlich besser als in früheren Arbeiten einzugrenzen und ermöglicht neue Einblicke in die Bildung der Antiklinale. Eine Thick-Skin Antiklinale bildet auch den strukturellen Kern der geklüfteten Trägergesteine (Intrusiva!) des Los Cavaos Ölfeldes am „Rio Grande“. Basierend auf neu erhobenen Aufschlussdaten und einer umfangreichen Kernstudie wurde hier eine statistische Kluftanalyse durchgeführt (teils im mm-Bereich) und in den kinematischen Kontext gestellt, um erstmals ein systematisches Verständnis der Entstehung und Entwicklung der in den magmatischen Ölreservoirs enthaltenen Klüfte zu erlangen. Die in diesem Dissertationsprojekt verwendeten Daten und Resultate, welche von Transekten im Beckenmaßstab bis hin zu Klüften im mm-Maßstab reichen, umfassen also acht Größenordnungen.

SUMMARY

Any thorough geological interpretation requires the integration of multi-scale data and, ideally, quantifiable statements on the uncertainties. Both, self-similarity ("fractal behavior") in structural elements and the necessity to conduct uncertainty analysis have been recognized for decades (e.g. Gibbs, 1983; Pollard & Aydin, 1988). However, at present, neither meticulous data integration across scale magnitudes, nor uncertainty quantification have become the norm in structural analysis. A lack of available workflows for uncertainty quantification exists. In this PhD Thesis I integrated and examined multi-scale data in four study areas, located in petroleum producing provinces of the Sub-Andean back-arc and dominated by contractional thick-skinned tectonics. Two study areas are located in Peru ("Santiago", "Pachitea") and two in Argentina ("Malargüe", "Rio Grande") (**Fig. 1.1**). For the "Malargüe" region, where an exemplary data set was available, I developed a new workflow to improve uncertainty quantification in kinematic modeling.

For all four regions typical data sets from the hydrocarbon industry were used, including well data, 2D seismic (vintage and newly reprocessed), 3D seismic (only "Rio Grande"), surface geological maps (some newly acquired) and new magnetics data (only "Pachitea"). Most of these structures have not (or only partially) been investigated with modern structural workflows to date. New structural transects for the "Santiago" and "Pachitea" regions reveal refined structural models, an improved understanding of the basin-scale tectonic evolution, a better understanding of the role of evaporites and new shortening rates. The thick-skinned "Malargüe Anticline" has been studied in more detail previously. In this PhD Thesis, however, a three-dimensional approach, based on an exceptionally well-constrained anticline, using a new forward modeling workflow around uncertainty quantification is presented. This workflow helps to systematically reduce model uncertainties and can also be applied in other tectonic settings. The new workflow helps to answer critical questions around the "Malargüe" region. Namely, it helps to constrain the structural model significantly better than previous models and to provide new insights into the formation of the Malargüe Anticline. A thick-skinned anticline also forms the structural core of the oil producing fractured intrusives at the Los Cavaos oil field in the "Rio Grande" region. Here, for the first time, a systematic statistical fracture analysis was conducted, based on outcrop work and an extensive core study. The analysis was conducted in kinematic context, to shed new light onto the characterization, genesis and evolution of these fractures contained within the igneous oil reservoirs. In this PhD Thesis, assessments ranging from basin-scale transects (longer than >100 km) to mm-scale fractures, nine orders of scale-magnitude are covered.

1. INTRODUCTION

1.1 Motivation

This PhD Thesis examines two major themes: (a) contractional thick-skinned tectonics, (b) multi-scale integration and uncertainty quantification in structural modeling. Understanding thick-skinned structures of the Sub-Andean domain using multi-scale approaches is critical in deciphering the tectonic evolution of that region. This is particularly important in less studied frontier areas where poorly understood kinematic interaction of thick-skinned structures with salt tectonics add complexity, such as in the Peruvian back-arc exist (Alemán & Marksteiner, 1993; Baby et al., 2005; Hermoza et al., 2006; Bertolotti & Moretti, 2009; Moretti et al., 2013).

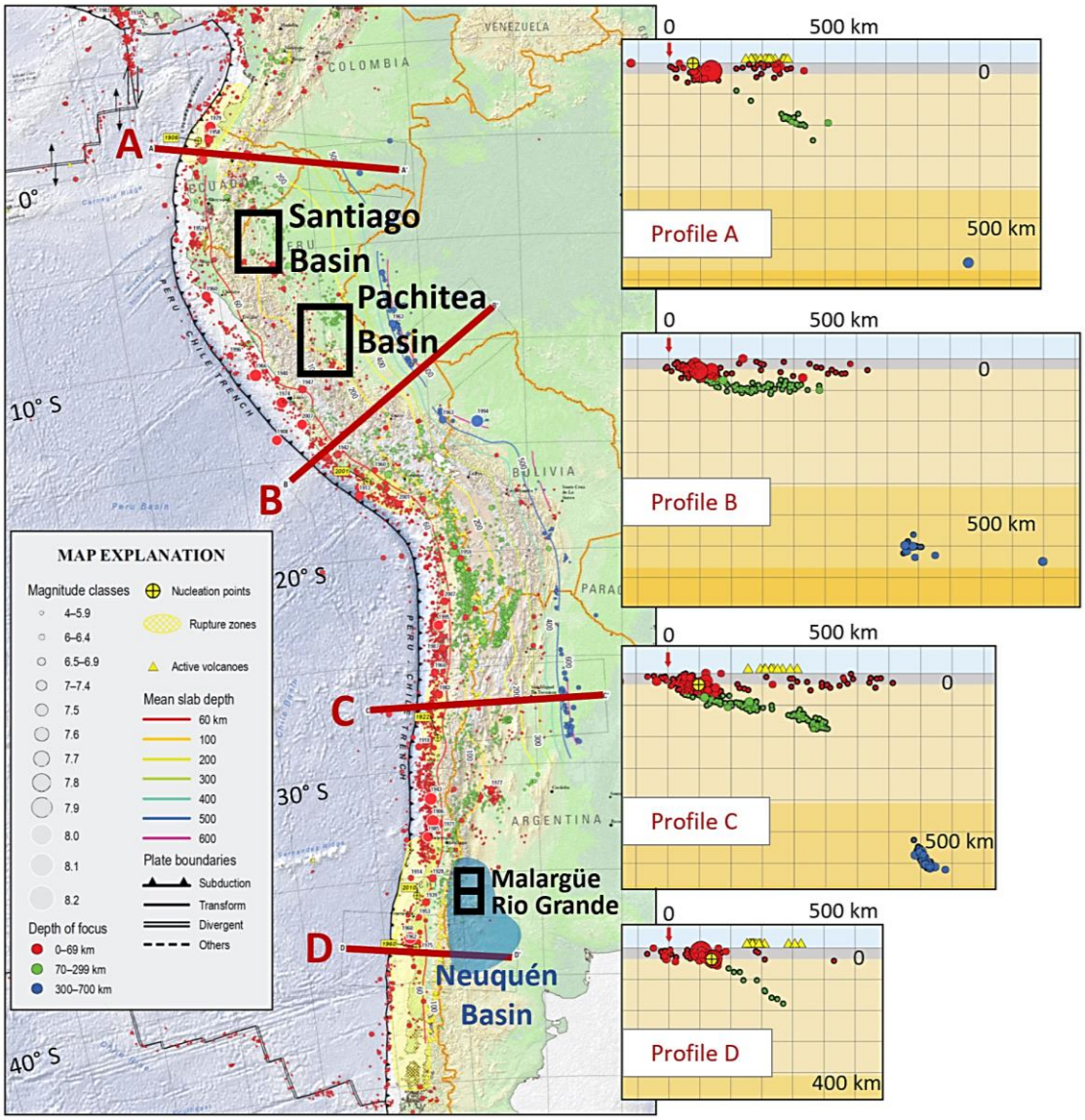

Fig. 1.1: Location map of the four study areas along the Sub-Andean back-arc (modified from Rhea et al., 2010). Note different subduction angles (Benioff Zones) along strike.

The importance of integrating multi-scale data and quantifying uncertainties in structural interpretations has been recognized for many years (e.g. z.B. Gibbs, 1983; Pollard & Aydin, 1988). Multi-scale data integration in oil producing igneous reservoirs, such as observed in the oil fields of the Rio Grande Valley, Argentina, have not been examined consistently (Bermudez & Delpino, 2008). No standardized workflows for uncertainty quantification in kinematic modeling are available (Mitra & Mount, 1998; Hilley et al., 2005). Both topics have a significant impact on scientific research, as well as reducing operating risks in the extraction of natural resources (Chalco 1961; Touzett, 1976; Quispesivana et al., 1997; Hermoza et al., 2011; Witte et al., 2018). These themes were investigated in four study areas located in the Sub-Andean domains of Peru and Argentina (**Fig. 1.1**). However, the concepts, methods and results presented here may also be applied in other tectonic provinces around the world.

The Andean Orogen and its back-arc span more than 8000 km from Venezuela to Fireland and owe their existence to the convergent plate boundary between the oceanic Nazca Plate to the west and the continental South American plate to the east (**Fig. 1.1**). Between ~15-20°S a major tectonomorphic element exists, the Bolivian Orocline, where the orogen's general strike changes from NW-SE in the North to N-S in the South (Carey, 1955; Isacks, 1988; Kley, 1999; Hinsch, 2001). At the subduction zone, which has been active since Jurassic times, the Nazca Plate is being subducted under the South American Plate to the east (Scheuber & Reutter, 1992). Andean mountain building is believed to have started in Mid- to Late Cretaceous times, while the modern Sub-Andean belt formed primarily during Neogene to recent times (Jacques, 2003a). *Please note that the structural timing will be discussed in detail in Chapters 3-6*. The present-day relative convergence rate (~65-80mm/yr) and vector (WSW-ENE) between the two plates are relatively constant along the entire collision zone (e.g. Rhea et al., 2010; Heidbach et al., 2008). However, significant along-strike variation exists in the subduction angle, including a number of flat-slab segments (e.g. Profile C, **Fig. 1.1**), causing varying responses in the geo-tectonic processes in the back-arc. This can result in marked broadening of the mountain chain, as well as the km-scale uplift of plateaus, such as the Altiplano (Isacks, 1988; Oncken et al., 2006; Martínez et al., 2016). The general tectonic architecture, kinematics and seismicity of the orogen have been investigated in detail by numerous authors and are largely understood (e.g. Isacks, 1988; Strecker et al., 1989; Sempere at al., 1997; Ramos et al., 2002; Jacques, 2003a, 2003b; Oncken et al., 2006; Ramos et al. 2006). Rich petroleum systems have formed and have been preserved in numerous back-arc basins along the Andean Orogen. Significant amounts of hydrocarbons in these basins are predominantly hosted in contractional or transpressional thick- and thin-skinned structures in Colombia, Peru, Bolivia, Argentina and southern Chile (Jacques, 2003b). Much less hydrocarbons are found in the Andean fore-arc, with the main reason being its proximity to the tectonically

highly active subduction zone where petroleum systems with commercial amounts of hydrocarbons are unlikely to be preserved over the geologic times.

1.2 Contractional thick-skinned structures (Chapters 3 and 4)

Traditionally, thick-skinned structures are defined as structures into which the (mechanical) basement is involved, while thin-skinned structures are defined as structures that involve only the sedimentary cover which is located stratigraphically above the basement (e.g. Fossen, 2010). Very often, however, a clear definition of the lithology and degree of structural involvement of the mechanical basement is not straightforward, due to the lack of precise data. The Peruvian segment of the Andean orogen is characterized by a slightly oblique convergence vector between the two plates. In the Sub-Andean foothills of northern Peru numerous 100 km-scale thick-skinned high-relief structures are developed, such as the Loreto Dome, the Shira Mountains Block or the Contaya Arch (e.g. Mathalone & Montoya, 1995) (**Fig. 4.13**). There is broad agreement on the general mechanisms, tectonic evolution, fundamental styles, kinematics, volcanism and scale-ranges of Sub-Andean thick-skinned contractional structures (Dickinson & Snyder, 1978; Gries, 1983; Strecker et al., 1989; Vergani et al., 1995; DeCelles & Giles, 1996; Zapata & Allmendinger, 1996; Ramos et al., 2002; Ramos et al., 2004; Zapata et al., 2005; Ramos et al., 2006; DeCelles, 2012; Strecker et al, 2012).

Structural linkage, such as deflection, focusing or triggering of thin-skinned structures in the sedimentary cover overlying basement warps or steps have been documented widely (Wiltschko & Eastman, 1983; Schedl & Wiltschko, 1987; Scisciani & Montefalcone, 2006; Kokkalas et al., 2012), but the exact kinematic mechanisms remain poorly understood. Things become even more complex when salt detachments are involved, which is the case in both, the “Santiago” and “Pachitea” study areas of this PhD Thesis. Poorly-constrained models showing the possible existence of deep and (partially) inverted thick-skinned half-grabens are documented from the Santiago Basin (e.g. Baby et al., 2005). Furthermore, interplay of thick- and thin-skinned structures, timing, shortening rates, as well as the position of basal detachments and the implications for extraction of natural resources (petroleum and minerals) remain poorly understood in the Peruvian back-arc (e.g. Wine et al, 2001a; Hermoza et al., 2006; Rait et al., 2009). Fundamental questions that presently remain open relate to the origin, configuration, lack of shortening amounts/rates, kinematic evolution of the basement, especially in areas with poor data coverage, such as the northern portions of the Santiago and Marañón Basins, as well as the e.g. very remote Madre de Díos Basin in southern Peru (e.g. Mégard, 1984; Mathalone & Montoya, 1995; Baby et al., 1997; Baby et al., 2013). At the “Malargüe Anticline” in Argentina (see

Chapter 5 for details), the question to which degree the present-day anticline was formed by pre-existing extensional grain causes a vigorous debate (e.g. Giambiagia et al., 2009; Turienzo, 2010; Mescua et al., 2012). With respect to contractional thick-skinned structures (which are examined in Chapters 3 and 4), the following key open questions can be formulated as follows:

- What controls the geodynamic situation and deformation style in the back-arc?
- What is the interaction between different structural styles and the role of structural inheritance?
- What is the impact of the evaporites on structural architecture?
- What are the structural timing and the shortening rates, based on the latest interpretations?
- What are the implications for the petroleum potential?

Very similar questions apply also to thick-skinned structures in the study areas ("Rio Grande" and "Malargüe", Chapters 5 and 6). There, however, they are examined from a slightly different perspective, to understand multi-scale fracture evolution and uncertainty quantification workflows.

1.3 Multi-scale analysis and uncertainty quantification (Chapters 5 and 6)

While Chapter 5 focuses on new workflows to quantify uncertainties and to better constrain thick-skinned structures, Chapter 6 examines the lower end of the multi-scalebar, by investigating the fracture evolution within the andesitic and oil producing sills of the northern Neuquén Basin.

Any robust geological interpretation requires the integration of multi-scale data and – ideally – should include a quantifiable statement about the limitations and uncertainties of the data and the related interpretation (e.g. Ramsey, 1967, Gibbs, 1983, Allmendinger, 2012). As more and more powerful computers and modeling software becomes available, the integration of multi-scale data is more and more common, although it is still not the norm, especially in commercial mineral resources projects. One characteristic of the Argentinian back-arc is the occurrence of igneous (andesitic) sills at ~35°S lat. (e.g. Spacapan et al., 2016; Spacapan et al., 2018), which play a major role in petroleum production. Quantifiable multi-scale fracture analysis has been conducted by researchers for many decades (Pollard & Aydin, 1988). Numerous multi-scale studies have examined oil-bearing sills in terms of emplacement parameters, maturation, migration, charge and entrapment (e.g. Gil-Imaz et al., 2006; Valentine & Krogh, 2006; Aarnes et al., 2008; Burchardt, 2008; Goulty & Schofield, 2008; Ventura Santos et al., 2009). However, integrative and systematic studies on the characteristics and evolution of oil-bearing fractures in sills are very scarce (e.g. Bermudez & Delpino, 2008; Delpino & Bermudez; Spacapan et al., 2016; Spacapan et al., 2018), which is frequently due to the lack of quality

data sets. In this PhD Thesis a multi-scale data set from the petroleum industry is utilized to systematically study the multi-scale characteristics and evolution of fracture sets hosted in andesitic sills of the northern Neuquén Basin (Chapter 6).

Another key theme of this PhD Thesis, uncertainty quantification, also relates to thick-skinned structures and multi-scale data integration. Quantifying these model uncertainties has a significant impact in scientific research, as well as in extraction of natural resources (minerals or petroleum). Traditionally, geologic interpreters have been attempting to semi-quantitatively judge the limitations and uncertainties of their (static and kinematic) models and it is well known that uncertainty increases with less data (quantity and quality) (e.g. Ramsey, 1967, Gibbs, 1983, Allmendinger, 2012). Uncertainties in geometry, such as thickness or dip, of the stratigraphic taper in a given basin is a first-order parameter in controlling the localization and spacing of thrust systems and has to be as well constrained as possible (e.g. Endignoux & Mugnier, 1990; Butler et al., 2006; Moretti & Callot, 2012, Allmendinger & Judge, 2013). However, very few systematic studies have been published to address this issue and to date established workflows are lacking (e.g. Bond et al., 2007; Allmendinger et al., 2012; Bond, Allmendinger & Jude, 2013; 2015; Berthelon & Sassi, 2016). The few available studies that have examined the challenge of uncertainty quantification, demonstrate quite different approaches, such as differential maps, strain ellipse and saturation curves (Victor et al., 2004; Poblet & Bulnes, 2007; Judge & Allmendinger, 2011).

Based on the data set from the thick-skinned "Malargüe Anticline", I developed a new workflow to quantify uncertainties in structural models, based on (trishear) kinematic forward modeling (**Fig. 5.5**). This workflow started with the construction of a (very) detailed and highly constrained (pseudo-) 3D model, which was initially tested through traditional restoration and finally reproduced by forward modeling. Subsequently, selected static and kinematic parameters, namely ramp angle and shortening, were varied systematically and the misfit area, between the different outcomes and the "fixed" present-day model, mapped. This allowed for the quantification of uncertainties in the model under varying parameters. Indications of dependencies between parameters were observed and lead to the recommendation to conduct further research. From the perspective of multi-scale integration and uncertainty quantification (*which are examined and discussed in more detail in Chapters 5 and 6*), the following key open questions can be formulated:

- How can the inventory of oil-bearing fractures in igneous reservoirs be better understood?
- How can the understanding of scale, dimension and evolution of these fractures be improved?
- How can uncertainty quantification better constrain multi-scale models?
- What are the implications of improved multi-scale (fracture) models for the petroleum potential?

In summary, the overall motivation of this PhD Thesis was to contribute new structural insight into large-scale and small-scale structures, with the main objective to reduce model uncertainties. The results and workflows presented herein can be applied in improving and fine-tuning geological models in research, as well as to reduce commercial and operational risks in oil and mineral extraction.

2. Data and methods

2.1 Overview

For this study a number of very different types of data were used, interpreted and integrated by through a variety of workflows. More importantly, these different data categories covered a broad spectrum of scales, ranging from the 100 km-scale of remote sensing data all the way to the cm- and mm-scale represented by core observations and thin sections. **Table 1** provides an overview of the different types and scales of data that were utilized within this study.

SCALE RANGE	BASIN	OIL FIELD	COMPARTMENT/ OUTCROP	WELL BORE	CORE	THIN SECTION
	~100 km	~1 - 10 km	~10 - 100s m	~1 - 10s m	dm-mm	mm (and sub-mm)
TYPICAL DATA	Satellite Imagery	Satellite Imagery	Satellite Imagery			
	Digita Terrain Data	Digita Terrain Data	Digita Terrain Data	(Digita Terrain Data)		
	2D Seismic	2D/3D Seismic	(2D)/3D Seismic	(2D/3D Seismic)		
	Geological Maps	Geological Maps	Geological Maps	(Geological Maps)		
	Grav / Mag	(Grav / Mag)				
			Outcrop	Outcrop	Outcrop	
			Well Logs	Well Logs	Well Logs	
				Drill Core	Drill Core	
	Focal Mechanisms	Focal Mechanisms	(Focal Mechanisms)	Geomechanical Data	Geomechanical Data	
				Sidewall Plug	Sidewall Plug	Sidewall Plug
					Poro/Perm Data	Poro/Perm Data
		(Dynamic Test Data)	Dynamic Test Data	Dynamic Test Data	(Dynamic Test Data)	
Santiago Basin	X	X	X	X		
Pachitea Basin	X	X	X	X		
Neuquén "Malargüe"	X	X	X	X	X	(X)
Neuquén "Rio Grande"	X	X	X	X	X	(X)

Table 1: Overview of typical multi-scale data (idealized) used in petroleum exploration projects and actual data used within each of the four study areas. The scale-gap between seismic data and well bore data (blue line) typically leads to increased spatial uncertainty in structural interpretations.

2.2 Remote sensing data

Remote sensing data was used in all four study areas. Traditionally, remote sensing data includes satellite imagery, aerial photographs and digital terrain data and is use to recognize, characterize and map first order structural elements (e.g. **Fig. 3.1**). In this study remote sensing data was used specifically to establish and confirm the fundamental tectonic framework in the regions, especially in areas of poor seismic, poor well data coverage and poor surface geology maps. Across almost the entire Sub-Andean domain remote sensing data is extremely valuable, as field access if often challenging (or impossible), geological maps are frequently old (and often faulty) and seismic coverage is never complete. The list below summarizes the types of remote sensing data (and corresponding resolution) that were used:

- Pachitea (Chapter 3): Nasa-DEM (90m res.), Landsat imagery (30m res.)
- Santiago (Chapter 4): Nasa-DEM (30m res), Landsat imagery (30m res.)
- Malargüe (Chapter 5): Nasa-DEM (90m res), Landsat imagery (30m res.)
  Aerial photographs (~3m res.)
- Rio Grande (Chapter 6): Nasa-DEM (90m res.), Landsat imagery (30m res.)

Different software packages were used to visualize, integrate and interpret these different sources of remote sensing data, namely, Global Mapper and MOVE 2020 (by Petroleum Experts, originally provided by Midland Valley). Hill shading analysis was applied in all four regions, to enhance visualizations and screen for geomorphological features, such as fault scarps or other lineaments. During multi-scale analysis, this information was then used to compare it against the smaller scale observations, such as map-scale, outcrop and even core-scale structures (e.g. in the Rio Grande area).

2.3 Surface geological data

Surface geological maps provide extremely useful calibration for regional (or oil field scale) structural models. However, in remote areas, such as the Sub-Andean domain, geological maps are often outdated and faulty, as they are not regularly updated due to poor accessibility. So the reliability of the existing maps is often questionable. To mitigate this challenge, new and proprietary surface geological was acquired (with significant logistical effort) for the “Pachitea”, “Rio Grande” and “Malargüe” areas (e.g. **Fig. 4.1**). This was particularly important for the “Malargüe” area, as the key objective there was to quantify model uncertainties and, hence, a precise surface geological data set was needed. Surface geological mapping included mapping stratigraphic and tectonic contacts, as well

as collecting strike-and-dip data of sedimentary strata and fracture data. The regions “Santiago” and “Pachitea” are characterized by heavy vegetation affecting the the surface geological data. Consequently, the data uncertainty there is much larger than at “Rio Grande” and “Malargüe”, located in quasi desert-like landscape with the strata extremely well exposed.

2.4 Magnetics data

In science or exploration projects, the advantage of potential data, such as gravity or magnetics data, is that it covers large areas and allows to detect deeply seated and long-wavelength structures, such as e.g. large lineaments. The disadvantage lies in its very limited resolution. So, ideally potential data should always be calibrated or integrated with more precise data, such as satellite imagery or seismic data. In this study airborne magnetics data was used for the “Pachitea” region to confirm and map first order lineaments (length or many tens of kms) and was, subsequently integrated with seismic and outcrop data (**Fig. 3.4**). *Please refer to the Chapter 3 for a more detailed discussion on how this data category was used during the workflow.*

2.5 Seismicity data

In structural analysis and modeling seismicity data, ideally, can be used to confirm – and sometimes to “pin-point” – the spatial position and kinematic attitude of active detachments. This is particularly valuable for detachments that are too deep to be captured by seismic sections. Seismicity data used in this PhD Thesis was extracted from the online catalogues of the USGS National Earthquake Information Centre (USGS, 2017). Spatial precision is known to be limited, particularly the vertical position. Nevertheless, seismicity data represents an important element in structural (kinematic) analysis and was used within this study: For the regions “Santiago” and “Malargüe” seismicity data was extracted from public sources and – even though sparse – plotted on structural maps and cross-sections (**Fig. 5.3**) and provided additional insight into the present-day kinematics of these very remote areas (particularly for “Santiago”).

2.6 Seismic data

For all four regions, seismic data of varying vintages (and quality) was available, mostly 2D seismic (e.g. **Fig. 4.7**). For the “Rio Grande” region a 3D seismic cube was available, from which several oil field-scale sections were extracted and interpreted (**Fig. 6.5**). All four study areas are located in

onshore settings where the quality of seismic imaging strongly suffers from surface effects (e.g. rough topography) and, therefore, varies greatly. The list below summarizes the type of seismic data and vintage that was used in the four regions:

- Pachitea (Chapter 3): 2D seismic (in depth), 2005
- Santiago (Chapter 4): 2D seismic (in time), 2007
- Malargüe (Chapter 5): 2D seismic (in time), 1970s-1990s
- Rio Grande (Chapter 6): 2D seismic (in time), 1970s-1980s
  3D seismic (in depth), extracted transects, 2005

Particularly the seismic data from the "Pachitea" region underwent full modern reprocessing, including depth-conversion, using a velocity model based on seismic check-shots from nearby wells. *Important note: the exact parameters of this depth conversion and those of the velocity model were not available to me.* The reprocessing of the "Pachitea" seismic dataset resulted in significantly enhanced imaging and, hence, allowed for detailed structural interpretations. In the other three regions, seismic time-to-depth conversion was achieved by "depth-stretching". This is done by manually stretching the seismic images, until they fit the drilled well tops (in the subsurface), as well as the recorded structural strike and dip data (at the surface). From experience, depth-stretching is estimated to cause vertical errors of up to +/-10 %, not much different from depth-conversion based on velocity models. The widely varying quality of the seismic images has a direct impact on the quality of the models and their uncertainty. Typically, the spatial uncertainty of reflectors increases significantly with depth and near velocity anomalies, such as e.g. volcanic rocks, which tend to absorb seismic energy and distort seismic images. *Please refer to Chapter 5 for a detailed discussion on how these uncertainties can impact structural models.*

2.7 Well data, log data and core descriptions

In integrative multi-scale structural analysis well log and core data typically provide important (and very precise) data in the ~1-10m scale range. High resolution well log data can even reach vertical and lateral resolutions of a few centimeters, while direct measurements of well exposed fractures in drill core can provide information in the mm and even sub-mm scale range. Thin sections (from outcrop samples, core or drill cuttings data) provide valuable information about the rock fabric in the sub-mm scale range, but were not used in this study. Formation tops and log data were used in all four study areas, mainly to calibrate the vertical position of key stratigraphic horizons in the seismic data, to

confirm formation isopachs and, in the case of the "Rio Grande" area, to map the lateral extent of intrusive sills and related cavity zones (**Figs. 6.6.A, 6.6.B**). An extensive core study was conducted for the "Rio Grande" area. This included the analysis of 22 cores over a period of more than 2 months and enabled the reconstruction of a fracture inventory and its evolution through time (e.g. **Fig. 6.9**). An important scale-gap exists between the compartment scale (typically seen in high resolution seismic data) and the reservoir scale (represented by well data). This is simply caused by the technological limitations of the registration method (seismic and logs). In consequence, this scale range is particularly prone to increase model uncertainty. This uncertainty creates limitations in the interpretations of all four study areas, but is particularly important for the discussions around uncertainty quantification of the "Malargüe" area.

2.8 Kinematic restoration (retrodeformation and forward modeling)

Traditional kinematic restoration of cross-sections was applied in each of the four study areas presented here (e.g. **Figs. 3.7, 4.5, 5.6**), although for the "Rio Grande" area the restored transect is not shown. The purpose of using traditional cross-section restoration is to test and corroborate structural interpretations (e.g. Ramsey, 1967, Gibbs, 1983). All of the kinematic restorations here were conducted using commercial industry software (MOVE 2020 by Petroleum Experts, originally provided by Midland Valley). The general kinematic workflow used for all structural models presented in this PhD Thesis consisted in the following steps:

- Load all data into structural software (DEM data, satellite imagery, surface geology, seismic, wells)
- Quality check (confirm spatial location and quality of data)
- Integrate all data categories, static structural interpretation (with a kinematic concept in mind)
- Kinematic restorations, to reconstruct the pre-deformational situation
- Forward modeling (only "Malargüe"), to systematically test parameters and map uncertainties

Please refer to the four papers in Chapters 3-6 for more details on the kinematic modeling workflows.

The algorithms used were Flexural Slip and Fault Parallel Flow and the present-day interpretations were flattened incrementally to key stratigraphic horizons. For the restoration of the evaporitic bodies (Pachitea Basin and Santiago Basin), abundant – and highly time-consuming - manual restoration was applied. The pins for restorations were set into the synclines and sometimes (if synclines were only partially preserved) into the crests of the anticlines. All kinematic restorations, including the forward

modeling, were conducted under a number of assumptions (simplifications of the natural conditions). The three key assumptions were:

- All rock material moved only within the plane of section
- Small (non-resolved) structures did not contribute to the shortening
- Pressure solution did not contribute to the shortening

Naturally, these simplifications affect model uncertainties. For a more detailed discussion please refer to the chapters on uncertainty discussion (particularly Chapter 5). Forward modeling, which represents another kinematic method to test present-day structural interpretations, was also applied: By varying a number of key parameters (e.g. ramp angle, shortening) and by contracting the pre-deformational strata, one can test the geometric outcome of structures and compare it with the present-day situation (**Fig. 5.7**). The parameters were then adjusted and another forward-run was conducted until, eventually, the present-day structure was reproduced. For the "Malargüe" region this workflow was used intensely, refined, kinematic parameters varied systematically and the misfit between the forward model and the present-day static model recorded. Please refer to Chapter 5 for a more thorough discussion.

3. A NEW STRUCTURAL MODEL OF THE PACHITEA BASIN, PERU: INTERACTION OF THICK-SKINNED TECTONICS AND SALT DETACHED THRUSTING

3.1 Abstract

We present four new structural transects, a new seismo-stratigraphic correlation, a refined structural model and new shortening rates for the Pachitea Basin (=PB), Peru. Our results are based on the integration and detailed interpretation of newly acquired industry seismic (2D, 2005 vintage), existing well data, existing and proprietary surface geology data and newly acquired aero magnetic data (2007 vintage). Our assessment confirms the presence of at least four distinct structural styles in the area, thick-skinned structures, thin-skinned detachment thrusting, salt-tectonics and localized strike-slip tectonics. Based on seismo-stratigraphic correlations we conclude that the oldest rocks carried to outcrop by the San Matias (=SM) thrust are of Jurassic age. We interpret the thin-skinned master detachment to be located in varying positions, directly below or above, autochtonous salt pillows. Timing assessment of the SM thrust sheet reveals that it has been active from at least ~5 Ma to post-2 Ma, supporting regionally published timing data for this latitude. Positive topographic surface expressions indicate ongoing contraction along the mountain front of the Peruvian Eastern Cordillera (=EC). Across the PB we calculate between 2.6% and 5.5% for thick-skinned shortening and at least 25.5% for the thin-skinned shortening. For the SM thrust sheet we calculate a slip-rate of ~1-1.6 mm/yr, which is in line with published slip rates on individual thrusts from around the world. Observations along the SM thrust system indicate that thin- and thick-skinned systems interact mechanically, and that they have been active intermittently. We conclude that the location of salt pillows as well as pre-existing or growing basement-involved structures helped trigger the SM thrust. Different types of salt bodies are present in the PB, autochtonous pillows, slightly thrusted pillows and allochtonous diapirs. Our results provide new insight into the structural interplay, particularly how thick-, thin-skinned and salt tectonics interacted to form the present-day structural configuration. The interplay of the distinct structural styles has direct control on the trapping styles of hydrocarbons in the area. Trapping potential for hydrocarbons in the PB is related to thick-skinned (basement-involved) structures, located in the SM footwall, as well as classic thin-skinned thrusting (salt or shale detached) and possibly to wrench-related structures. In order to unlock the exploration potential of this area additional seismic, outcrop work and geochemical data are necessary. Future research should focus on apatite fission track analysis and GPS stations on some of the key basement-cored structures.

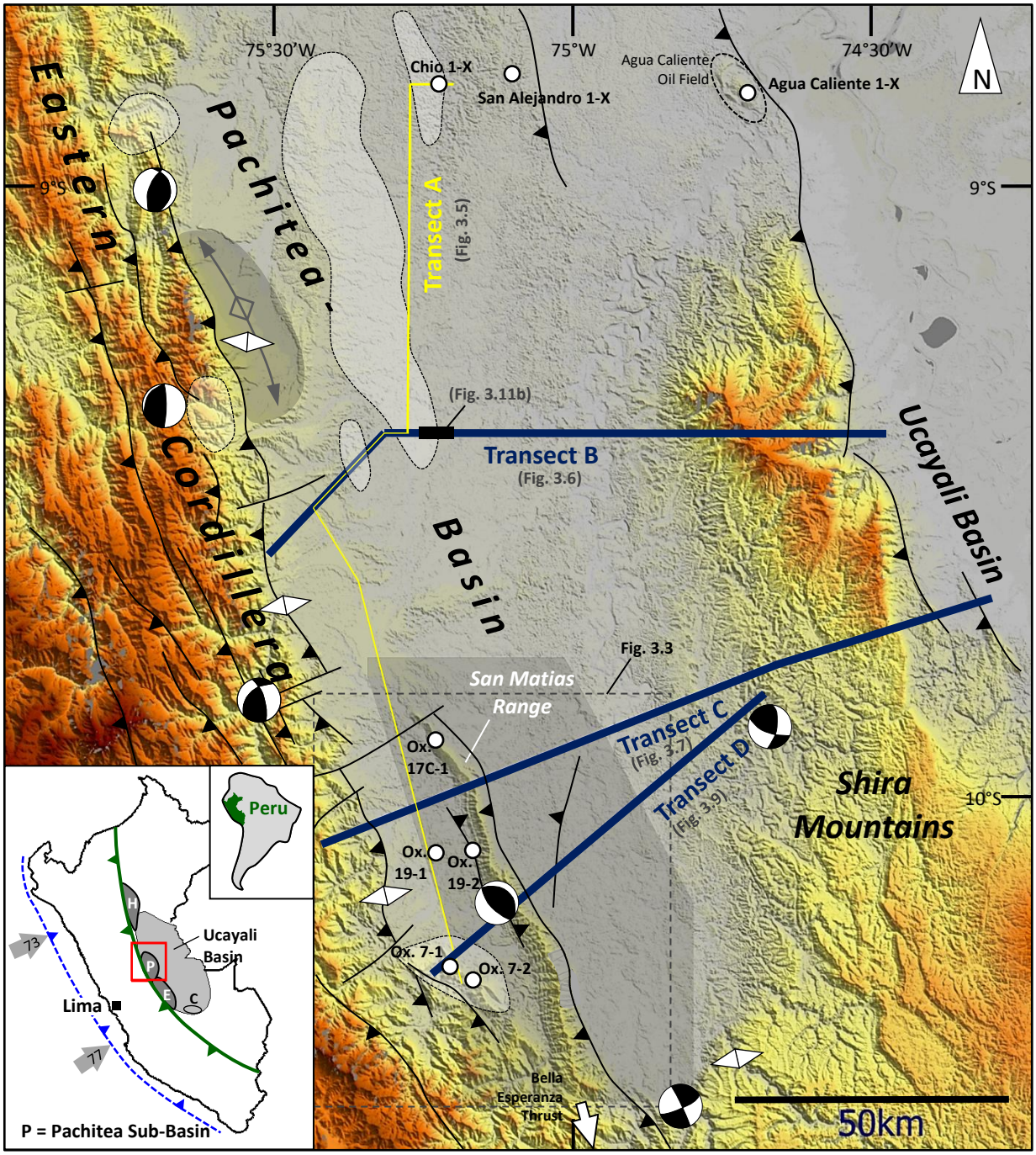

Fig. 3.1: Geomorphologic map of the PSB, showing key wells, location of transects and aero magnetic data (grey shaded area). Blue = main structural transects; yellow = regional correlation transect. White shaded areas = salt pillows (modified after Hermoza et al., 2006). White diamonds= Present day maximum horizontal stress direction (source Haidbach et al. 2008); beachball diagrams represent present-day focal mechanisms (from Devlin et al., 2012). Inset: grey arrows indicate subduction direction and velocity (mm/yr); blue dashed line = approximate position of Peru-Chile Trench; green line = Subandean deformation front; H, P, E = Huallaga, Pachitea, Ene Basins; C=Camisea field complex.

3.2 Introduction – regional context

The polyphase Ucayali Basin (Fig. 3.1) has been explored for many decades and amongst the key findings are (a) flat-slab subduction (angle of ~5°) due to the buoyancy of the aseismic Juan-de-Fuca and Nazca ridges (Pilger, 1981; Dumont, 1996; Rhea et al., 2010; Espurt et al., 2007), (b) the presence of major, basement-seated, inverted fault systems, (c) the active eastward propagation of the Subandean deformation belts (Megard, 1984; Wine et al., 2002; Hermoza et al., 2006), (d) the basin's limits are controlled by large arches, with dominant ENE-WSW and NW-SE trends, also controlling the hydrocarbon accumulations (Jacques, 2003a, b), (e) the presence of at least three detachment levels, Devonian shales (Cabanillas Fm.), Permian shales (Ene Fm.) and Jurassic evaporites (likely Pucara Group) (e.g. Hermoza et al., 2006), (f) the existence of four tectonosedimentary packages (Fig. 3.2), separated by major unconformities: firstly, a pre-Hercynian section, overlying the crystalline basement, comprising clastics and carbonates. The second package comprises

Late Permian e Early Triassic clastics and volcanics, associated with a major rift-event (Mitu Group) and subsequent Triassic-Jurassic marine series, including black shales, evaporites and limestones (Pucara Group) and, eventually, continental red beds (Sarayaquillo Formation). This package is truncated by the erosion related to the Nevadan Orogeny, causing a regional base-Cretaceous unconformity, a regional seismic marker. The third package consists of Cretaceous, westward thickening continental clastics, originating from the Brazilian shield to the East. Finally, the Andean cycle (Late Turonian-Early Coniacian), marked by the deposition of synorogenic packages, many of which are characterized by growth strata (Megard, 1984; Mathalone & Montoya, 1995).

The ongoing orogeny is accompanied by repeated intra-Tertiary unconformities and by a marked Upper Eocene-Oligocene marine flooding event depositing the Pozo shale, a regional seismic marker (e.g. Hermoza, 2004). Subsequent contractional pulses, affecting the Subandean basins, are documented, such as the Early to Mid-Miocene Incaic event (Mathalone & Montoya, 1995) and the Miocene Quechua I, II and III tectonic phases (terminology used by Megard, 1984). Thick Plio-Pleistocene synorogenic clastics cover most of the present-day Ucayali plains. Abundant geomorphological evidence for modern deformation of these sediments has been documented (Dumont, 1996). The present-day convergence of the Nazca Plate along the Peruvian coast is directed towards the ENE (N79°) at a rate that varies between 73 mm/yr at 8°S and 77 mm/yr at 14°S (Dewey & Lamb, 1992; Jaillard et al., 2000; Hampel, 2002; Audin et al., 2008; Rhea et al., 2010).

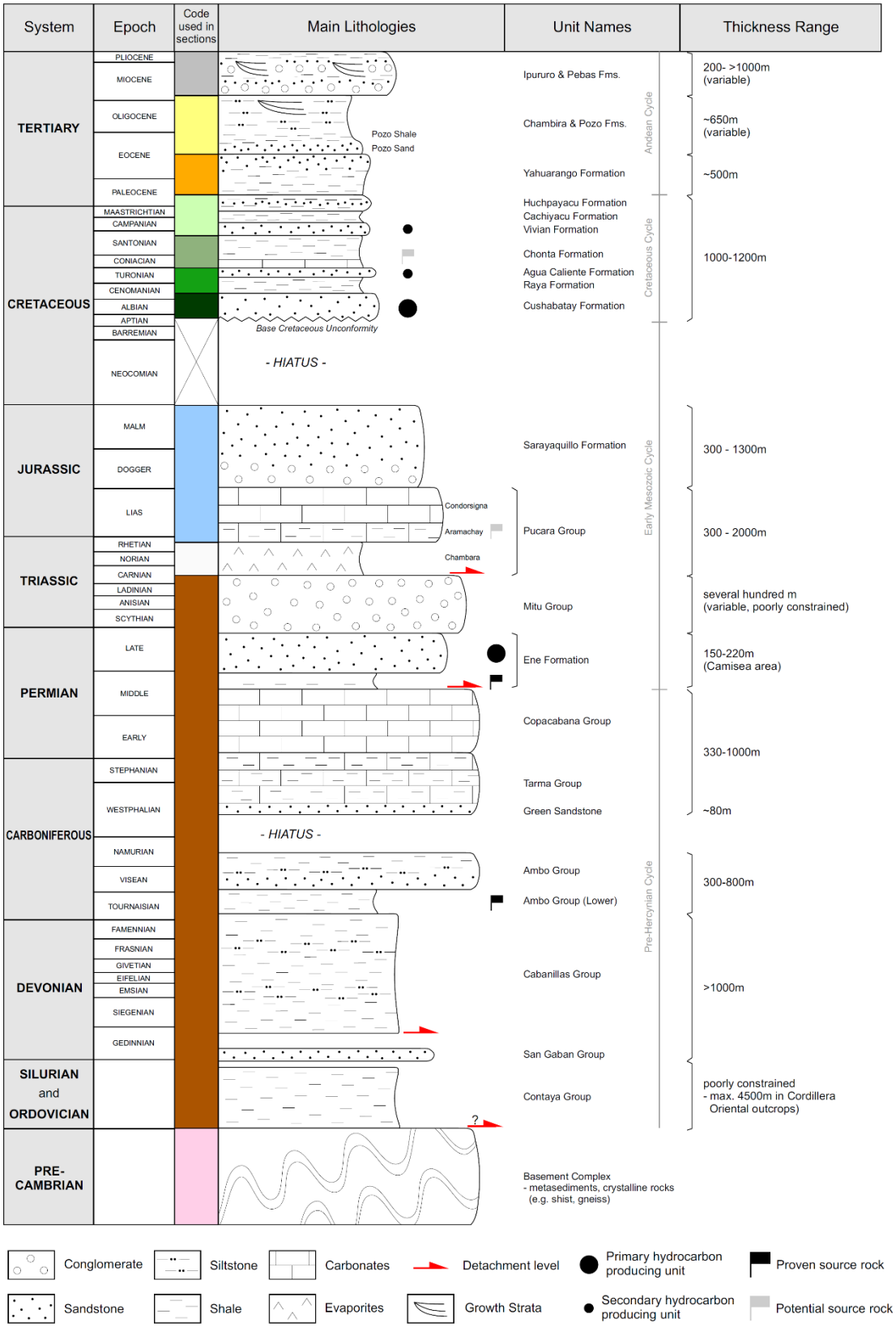

Fig. 3.2: Stratigraphic chart of the greater Ucayali Basin; compiled from various sources (Mathalone & Montoya, 1995; Rosas et al., 2004; Allca, 2007).

The regional stress field is dominated by WSW-ENE directed σ_{Hmax}, implying a present-day σ_{Hmax} almost perpendicular to the Andean chain (Heidbach et al., 2008) (Fig. 3.1). From the southern Shira Mountains (=SHM) into the Ene Basin, stress vectors become more heterogeneous, ranging from NW-SE to steep NE. Most of the shallow seismicity (0-35 km depth) occurs along the EC, while deeper events (70-150 km) are found in the SHM (USGS, 2017). Focal mechanism data confirm that the PB is under W-E directed compressional regime with local strike-slip movements around the SHM block (Devlin et al., 2012). Seismicity is observed as far as the much more external Moa Divisor structure (Navarro Zelasco, 2010).

3.3 Pachitea Basin

The asymmetric PB (between 9° and 11°S) is part of the Peruvian Sub-Andean basins and is located ~280 km NE of Lima, Peru (Figs. 3.1, 3.3) (Megard, 1984; Mathalone & Montoya, 1995). The structural geometries in the PB, and adjoining Ene Basin, are controlled by the interplay of basement-involved high-angle fault systems, resembling former half-grabens, with overlying shallower low-angle thrust sheets (Martinez et al., 2003; Hermoza et al., 2006; Allcca Torres, 2007; Espurt et al., 2008; Gautheron et al., 2013). In the West the basin is overthrust by the EC, to the East it is bounded by the uplifted basement block of the SHM. To the South it continues into the tectonically much higher shortened Ene Basin, while to the North it gradually deepens into the main Ucayali Basin. The westerly adjoining and highly inverted Pucara Basin is characterized by sinistral transpression and thin-skinned thrusting along rift-associated fault systems during Andean contraction (Rosas et al., 2007). The oldest strata that crop out along the western margin of the PB are of Jurassic age (Pucara Gp.). Towards the East the PB pinches out onto the eastern basement high of the SHM (compiled from Gil Rodriguez et al., 1999; Jaillard et al., 2000; INGEMMET, 1997). The SHM block has been characterized as a rift-related, basement-cored structure, formed in Late Permian times, that was inverted transpressionally during Andean contraction (Gil Rodriguez, 2002), acting as a buttress to the advancing Subandean foldbelt (Wine et al., 2002; Martinez et al., 2003). Sanchez Alvarez (2007) suggests a sole detachment at 21-24 km depth, which was reactivated during Upper Miocene times, between 7.2 and 5.3 Ma. He determined the related shortening across the central Ucayali basin to range between 3 and 5.5%. Finally, Espurt et al. (2008), focusing on the southeastern limb of the SHM block, and based on seismic, surface geology and well data, conclude that it is an up-thrusted block controlled by eastward verging basement-hosted low-angle thrusts and shallow, thin-skinned back thrusts, with deformed Plio-Pleistocene units on its eastern limb. Section balancing reveals that across the Ene and South Ucayali Basin the shortening is homogeneous along strike at ca. 56 km or 30% (Espurt et al., 2008), while Gil

Rodriguez et al. (1999) calculate the shortening of the internal Subandean zone at the PB to be 50%. The topographically mostly flat PB is divided by a marked N-S oriented topographic ridge, roughly parallel to the basin's main axis, the SM Range, representing the leading edge of a thrust sheet (Figs. 3.1, 3.3). Just like the southern Ucayali Basin, which hosts the giant hydrocarbon fields (Camisea complex), the PB has been the target of oil exploration. Several oil and condensate pools have been found (e.g. Agua Caliente Field, Fig. 3.1) and oil shows are common in well tests and as surface seeps (Fig. 3.3).

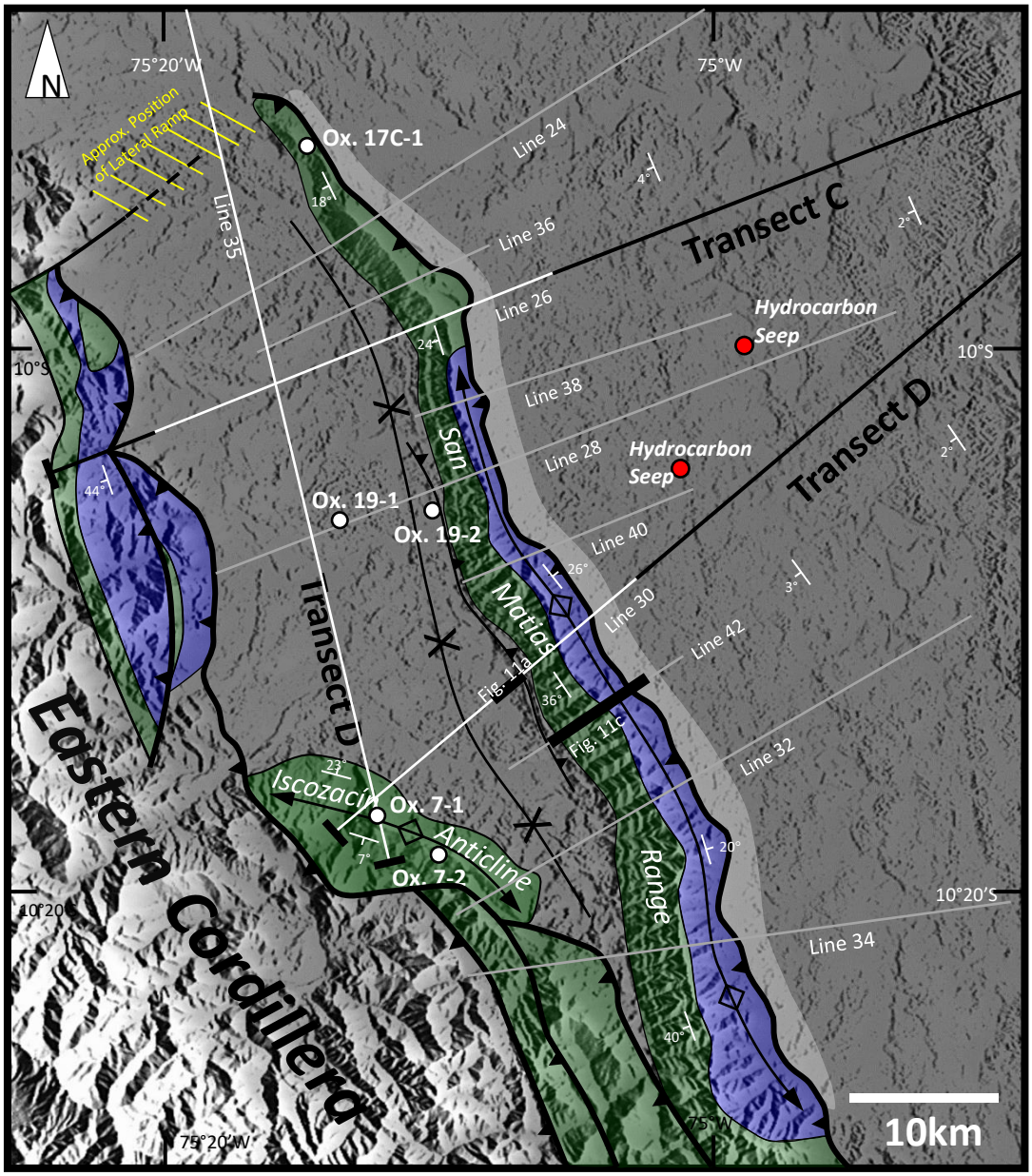

Fig. 3.3: Simplified surface geology (modified from INGEMMET, 1997), dip data, seismic data and transect location across the SM Mts.; grey seismic lines represent overall project and white lines are shown here. Blue = Jurassic outcrop; green = Cretaceous outcrop. White shaded area = approximate outline of basement-involved reverse fault system in SM footwall.

Several proven petroleum systems, functioning in the adjoining Ucayali basin, are also known to exist in the PB (Fig. 3.3). Proven and potential source intervals have been identified in the Ucayali and PB, such as the Devonian/Carboniferous shales of the Ambo and Cabanillas Groups, the Permian black shales of the Ene Fm., the Late Triassic-Early Jurassic black shales of the Aramachay Fm., as well as shales of the Cretaceous Raya and Chonta Formations (Disalvo et al., 2008; Mathalone & Montoya, 1995; Rosas et al., 2007). The main reservoirs in the Ucayali basin are Paleozoic clastics (Camisea area), while in the PB - to date - various Cretaceous sandstones, such as Cushabatay, Agua Caliente and Vivian Formations, are hydrocarbon bearing (Mathalone & Montoya, 1995; Martinez et al., 2003).

3.4 Motivation for study

The five wells that exist in the PB (Oxapampa area, drilled in the 1960s) (Figs. 3.1, 3.3) have hydrocarbon shows, but lack modern data sets. Seismic data are sparse throughout the area and typically range from medium to poor quality, especially in the highly deformed domains, where velocity and imaging problems are common. Exploration risks are lack of structural understanding, particularly with respect to structural interplay, timing and migration pathways. No integrative structural interpretation of the PB has been presented to date.

Regarding the Andean structural timing of the PB, there is general agreement that the main deformation occurred during Neogene times: Espurt et al. (2008) state that the Subandean zone in the Ucayali basin developed since Mid Miocene times (15e10 Ma); Allcca Torres (2007) concludes that the thrusting and inversion of the SM and SHM domains occurred in Neogene times, around 10 Ma; shortening transfer in the Subandean domain started at 14 Ma in the Camisea Basin and the SHM basement thrusts has been determined to have cooled around 4-5 Ma, based on AH-data (Gautheron et al., 2013). Bertolotti & Moretti (2009) document that the Andean compression in the foreland of the northern Ucayali basin is active since Upper Miocene times, while Hermoza et al. (2011) conclude a Neogene age for the Andean reactivation of the Paleozoic structures in the PB. In conclusion, due to the absence of detailed timing assessments, more precise age dating of the Andean deformation is currently lacking.

Scientific controversy exists around the following geologic aspects of the PB:

(1) The stratigraphic age of the oldest units cropping out in the SMM thrust sheet: Based on outcrop data, Gil Rodriguez (2002) state that thick clastics, specifically conglomerates, up to 1000mthick, crop out in the Gavilan Creek of the SMM, above the detachment (Fig. 3.3). These have been traditionally assigned to Jurassic age, but have recently been considered to be of Permo-Triassic age (Mitu Group), overlying the Ene Formation, above a detachment in black shales (Allcca Torres, 2007). Based on lithologic similarities with outcrops in the Pongo Paquitzapango (~320 km SE, in the Ene Basin) and age dating of macro-fossils, the author proposes that these sediments belongs to the Ene Formation, but fail to show data from the fossil dating assessment. Hence, uncertainty remains around the stratigraphic age of the strata above the SMM detachment.

(2) The impact of evaporites on deformation: Several authors have recognized the presence and importance of evaporites in the western Ucayali and PB: Hermoza et al. (2006) conclude that the evaporites are restricted to inverted Triassic-Jurassic grabens, while Gil Rodriguez et al. (1999) compare the evaporite detachments in the PB with the ones reported from the Huallaga and Santiago basins (located 400 km and 600 km north of PB, respectively) and state that in the PB the main salt-detachment is located at the base of the Pucara Group. Bertolotti & Moretti (2009) conclude that the structural impact of the up to 700 m thick Late Pucara evaporites in the northern Ucayali basin has been poorly studied and is generally underestimated, while recent research reveals that the evaporitic pillows may help control localization of early thin-skinned deformation (Moretti et al., 2013). Hence, even though the authors acknowledge the importance, there is still significant controversy as to the stratigraphic position of the salt-related detachments and the exact location of the salt-detachments.

(3) Detailed understanding of the complex Cenozoic deformation history and structural interplay: Growth strata in Neogene units have been documented by several authors (Mathalone & Montoya, 1995; INGEMMET, 1997), but have not been put in context with the thick-skinned and thick-skinned systems and not been investigated for interaction and structural interplay.

(4) The deformation and trapping potential of the deeper and “masked” Paleozoic structures: Prospective structures have been discovered in the southern Ucayali Basin (Camisea complex) but not yet in other parts of this basin. Some authors have mentioned the importance of deep prospective structures, particularly masked Paleozoic structures (Hermoza et al., 2011).

In summary, four major uncertainties exist with respect to the structural understanding of the PB:

(1) the age of the oldest rocks outcropping in the SM; we present a new regional stratigraphic correlation which clearly shows that the outcropping rocks in the SMM are Jurassic in age which has implications for the structural model and shortening rates in the area. (2) The role of evaporites on deformation; we explain the structural linkage of the salt welds with the thick-skinned inversion structures, we show new evidence of the exact location of the salt-related detachments and evidence for allochtonous salt pillows in the PB. (3) Detailed understanding of the structural timing and interplay; we present refined structural interpretations, based on newly acquired airborne magnetic data, new 2D seismic and new seismic correlations, that show how thick- and thin-skinned structures interact and that additionally reveals new aspects about the structural timing in the area. (4) Deformation and trapping potential of the deeper structures; we show an example of anticlinal structures, probably a structural trend, in pre-Cretaceous units, located in the sub-thrust domain below the SM Mountains, which are indicative of a new prospective play-fairway.

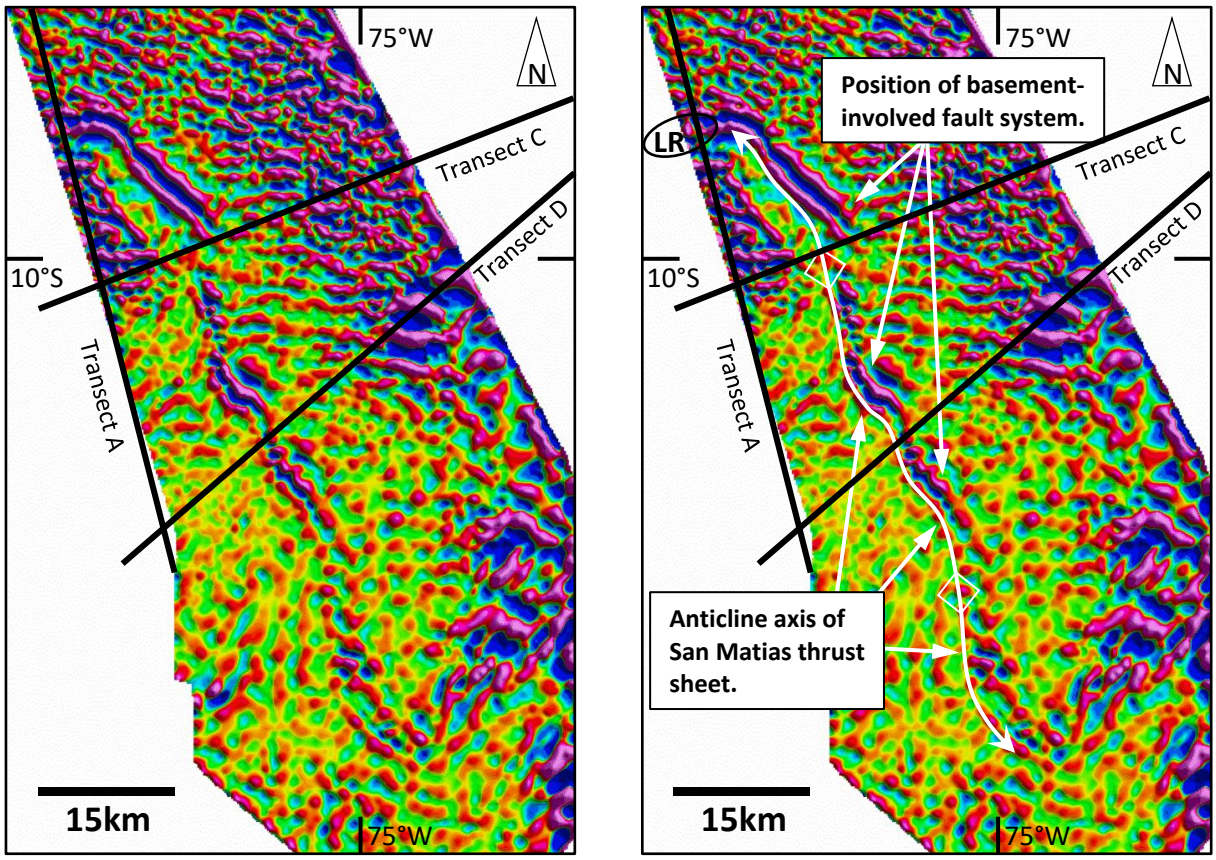

Fig. 3.4: Band-pass filter 800e3200 m of the total magnetic field data, showing basement-involved, segmented lineaments in the footwall below the San Matias thrust. Left: uninterpreted. Right: interpreted. LR = approximate location of a lateral ramp.

3.5 Data used

For the structural interpretation we integrated the following data: public domain elevation data (90 m resolution, NASA), regional stress data (Heidbach et al., 2008), focal mechanism data (Devlin et al., 2012), newly acquired airborne magnetic data (2007) (Fig. 3.4), published geological surface maps (INGEMMET, 1997), unpublished geological maps and reports, proprietary geological field data from the SM range, 9 2D seismic lines (PSDM, 2005 vintage), well data from 8 nearby wells (Ox. 7-1, Ox. 7-2, Ox.19-1, Ox.19-2, Ox.17C, San Alejandro-1X, Chio-1X, Agua Caliente-1X) and published literature.

3.6 Methodologies

Digital elevation data, present-day stress data, focal mechanism data, regional tectonic lineaments and salt pillows were integrated into a structural-geomorphological map (Fig. 3.1) which depicts the location of the 4 structural transects present herein. A second geomorphological map of the southern PB was generated to show surface geology, tectonic elements, dip data, oil seeps and locations of seismic lines used in this project (Fig. 3.3). Airborne magnetic data was acquired in 2007, covering the SM topographic ridge, with the aim to detect, to better understand and laterally map basement-involved lineaments (Fig. 3.4). The total magnetic field data had a 800 m - 3200 m band-pass filter applied, as it highlights very well the magnetic-structural anomalies associated with the SM thrust system. The lateral resolution of this data is ~1 km.

Using well data from the Chio-1X, Ox.19-1 and Ox. 7-1 wells and seismic lines, a basin-longitudinal cross-section was constructed, Transect A (182 km long) (Fig. 3.5), for regional correlation purposes and to constrain the age of the oldest strata outcropping at the SM range. Additionally, based on elevation data, seismic data, well data and surface geological data three transverse transects were constructed; Transect B (112 km long), Transect C (132 km long) and Transect D (77 km long) (Figs. 3.6, 3.11). Transects C and D were restored to kinematically test the model robustness (Figs. 3.7, 3.9). The construction of each of the transects was done by integrating all structurally relevant data into a static structural model (in depth-domain). While Transect A is shown here with a vertical exaggeration of 4x, in order to better visualize the thin salt layers and subtle dip changes, Transects B, C, and D are shown in true-dip scale. Transects C and D were restored to kinematically test the structural model robustness. The thin-skinned structures were restored (flattened) to the top of the Yahuarango Formation, representing one of the youngest Andean pre-deformational units, while the thick-skinned structures in Transect C were restored to the top of the Basement (Fig. 3.7). The algorithms used to restore the cross-sections are flexural slip and fault parallel flow. The pins necessary for the restorations were placed in undeformed areas, preferably in the synclines. The restorations were made under the assumption that all rock volume flowed only within the plane of section. Finally, for better understanding of the spatial variations in structural styles, a pseudo-3D structural model was constructed.

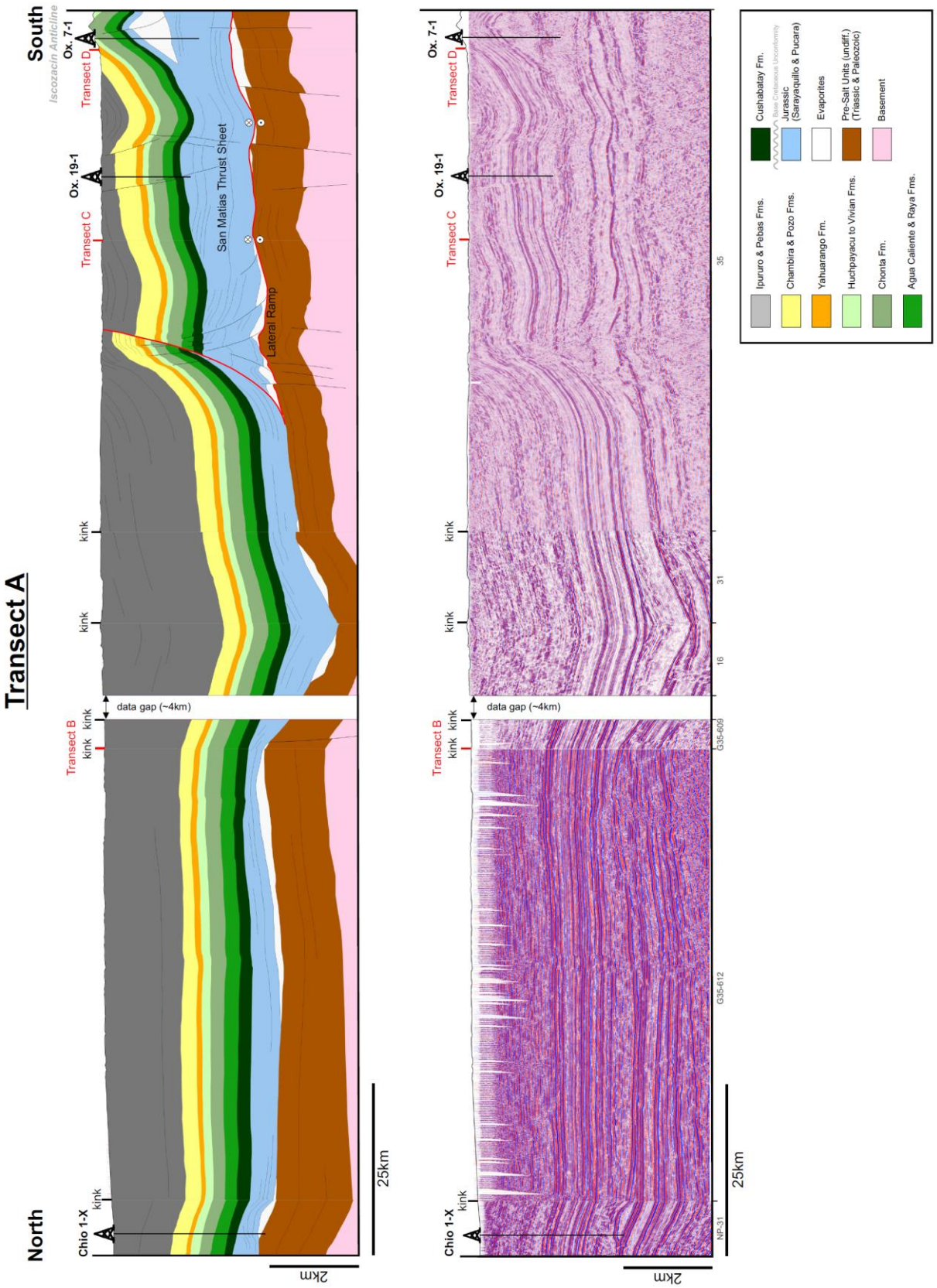

Fig. 3.5: Regional cross-section in basin-longitudinal direction, from Chio 1-X well to Ox. 7-1 well. Vertical exaggeration: 6x.

3.7 Results

The northern portion of the basin-longitudinal Transect A (Fig. 3.5) reveals tectonically quiet Paleozoic, Jurassic, Cretaceous and Tertiary strata with local salt-pillows in the lower part of the Jurassic section. While in the northern part of the section, the strata rest almost horizontally, the southern part of the transect is characterized by a structurally more complex setting: the allochtonous SM thrust sheet, transported on the SM thrust, rests on a series of salt-pillows or salt-welds. The Jurassic section within the SM thrust sheet is thicker than the Jurassic section in the autochtonous domain to the north. Just north of the northern leading edge of the SM thrust sheet northward uplifted Jurassic to Tertiary strata are observed. The thrust transport direction of the SM thrust sheet is from West to East (away from the observer in Fig. 3.5). Most of the basement-involved faults show indications of slight inversion.

Transect B (Fig. 3.6) is a transverse section that represents the northern portion of the tectonically quiet PB. Here the basin consists in a westerly deepening wedge of Paleozoic, Mesozoic and Cenozoic units in a monoclinal setting (structural dips generally <5°) with occasional salt pillows. Correlation from the Chio 1-X confirms that these pillows are stratigraphically hosted in the lower Jurassic section. Local thin-skinned east-vergent thrusting is associated with the salt-pillows (Figs. 3.6 and 3.11b). The apparent eastward thinning of the Jurassic units is due to the successively deeper level of erosion caused by the base-Cretaceous unconformity. In the eastern portion of the transect Cretaceous strata crop out (west flank of SHM). Further into the SHM increasingly older units crop out, eventually Paleozoic strata.

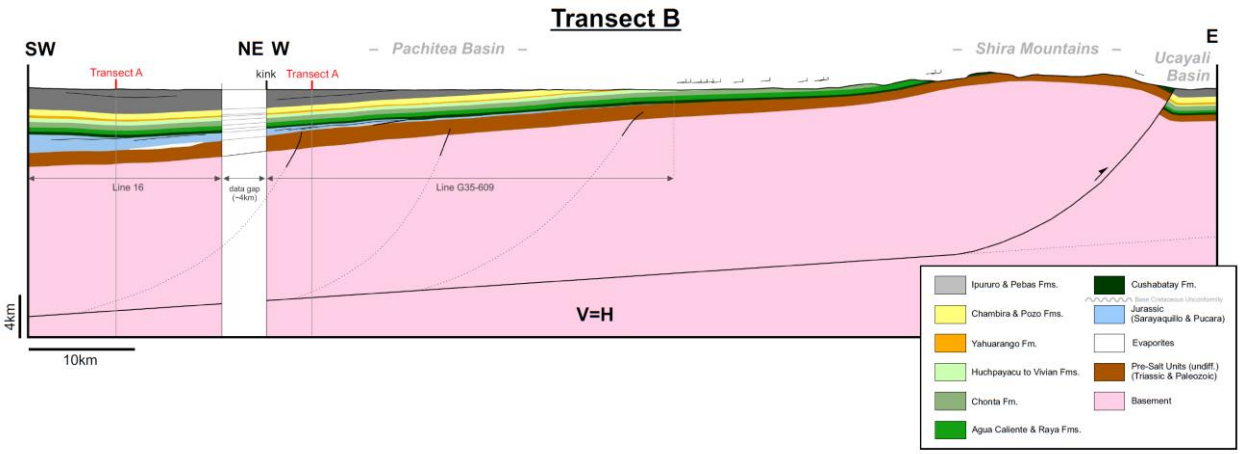

Fig. 3.6: Transect B, depicting the structural situation of the northern Pachitea Basin. Note: Shira East-Flank simplified. Basement faults have been adapted schematically from Devlin et al. (2012).

Fig. 3.7: Transect C, representing the structural situation of the central Pachitea Basin and restoration to Top Yahuarango Formation. Note: Shira East-Flank simplified.

The transverse Transect C (Fig. 3.7) represents the central part of the PB, near the northern end of the SM Mountains. Structurally it represents the eastern leading edge of the SM thrust sheet where Jurassic, Cretaceous and Tertiary strata in the hanging wall are thrust over Jurassic, Cretaceous and Tertiary strata in the footwall (Fig. 3.8). The eastern part of the section represents the gradually climbing strata onto the western flank of the SHM high. Two different structural styles can be recognized in this section. Firstly, high-angle reverse faults, affecting the basement, the Paleozoic, Mesozoic and locally the Cenozoic section. The SMM deep structure comprises a basement-involved positive structure with several fault branches. The second structural style that is observed is the thin-skinned SM thrust sheet (Fig. 3.8).

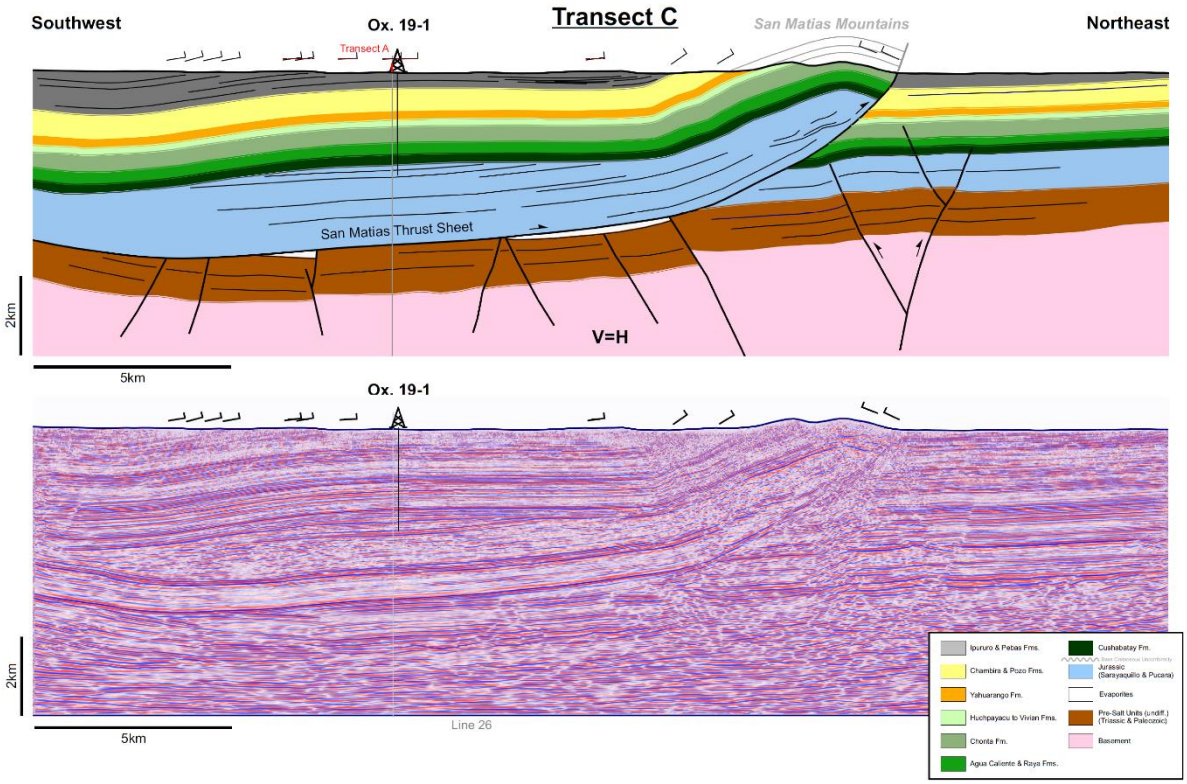

Fig. 3.8: Detail of Transect C showing the configuration of the San Matias Thrust Sheet.

The transverse Transect D (Figs. 3.9 and 3.10) represents the southern sector of the PB from the Iscozacín Anticline to the SHM. The eastern portion of the transect, as seen consistently in the other transects, reveals a constant, monoclinal setting (dip <5°). The section reveals thin-skinned as well as thick-skinned structural styles: In the western and central parts of this section, at basement and Paleozoic levels, a system of basement-seated, high-angle reverse faults is observed, with varying vergence, affecting the Paleozoic and locally the Cretaceous and Tertiary sections. The basement-involved structure under the SM thrust has no clearly marked vergence and reveals several secondary

faults branching away from the master fault (Fig. 3.10). The SM thrust sheet carries Jurassic, Cretaceous and Tertiary strata over Jurassic, Cretaceous and Tertiary in the footwall. The basal thin-skin detachment is located above the Jurassic evaporites (salt-pillows, salt-welds).

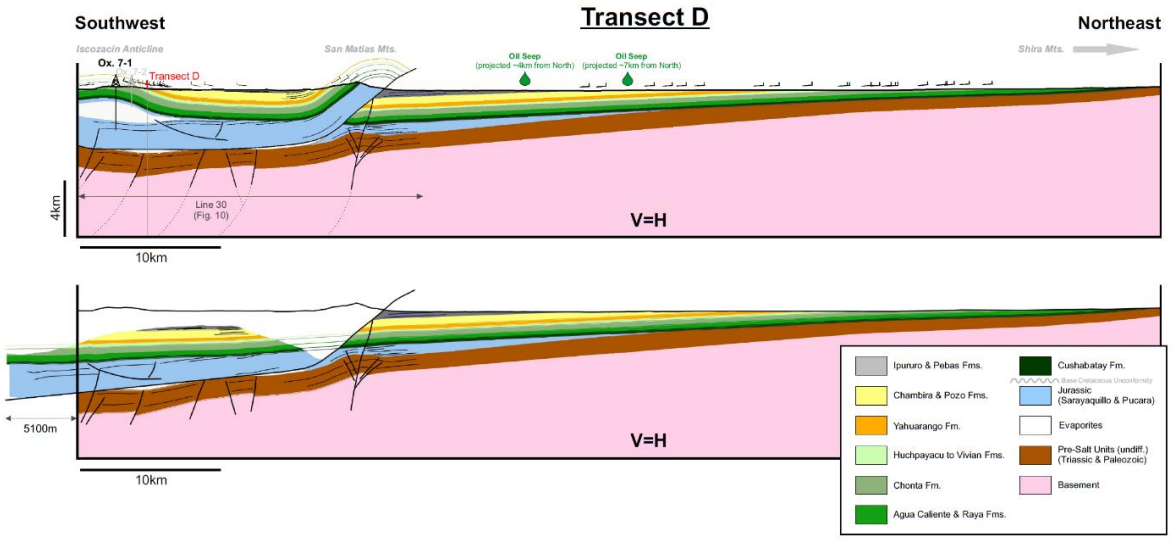

Fig. 3.9: Transect D, representing the structural situation of the southern Pachitea Basin and restoration to Top Yahuarango Formation.

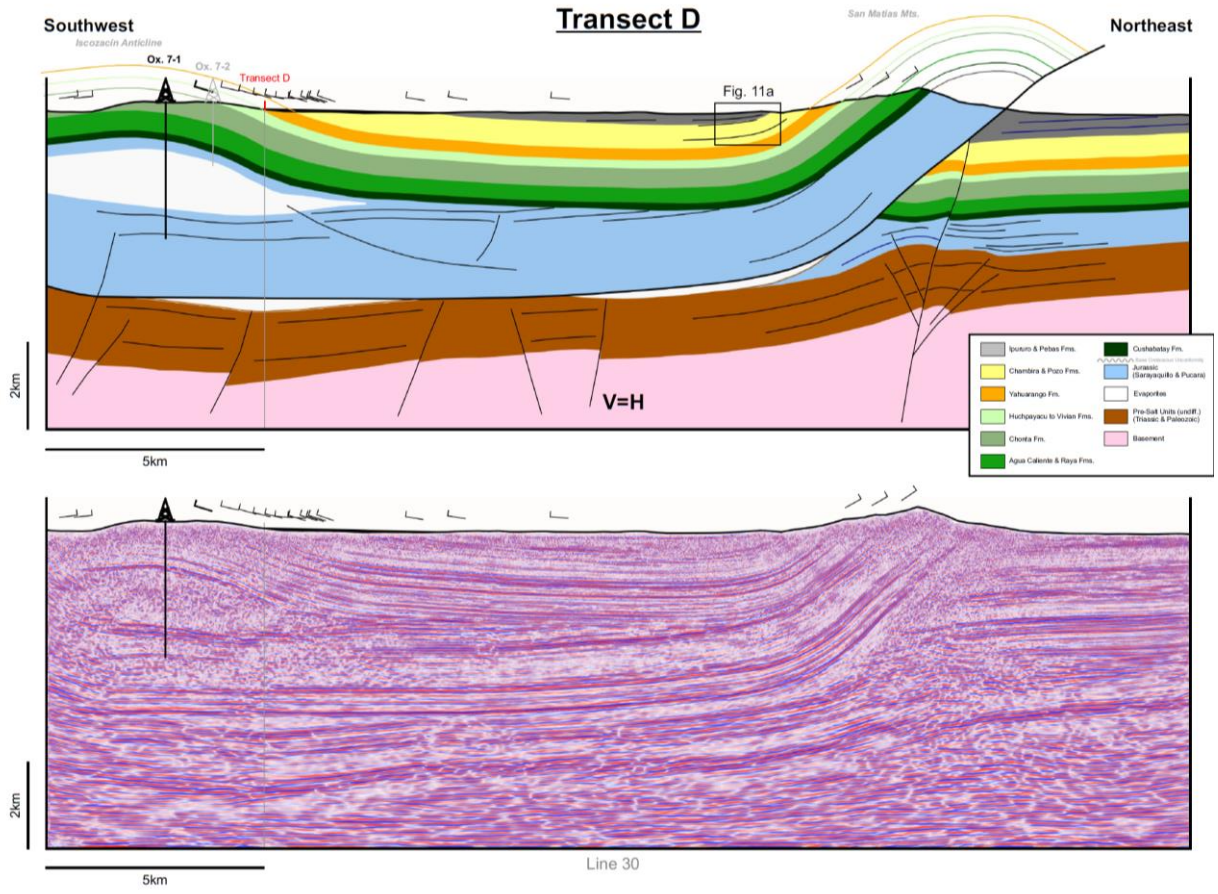

Fig. 3.10: Detail of Transect D showing the San Matias Thrust Sheet.

3.8 Discussion

3.8.1 Thin-skinned thrusting at the San Matias Mountains

Thin-skinned thrusting occurs in two domains of the PB, at the EC front and the SM Mountains. Due to its impact on the structural models and on exploration risks, the understanding of the stratigraphic age of the oldest carried units, particularly at the SM thrust sheet, is of fundamental importance. The data clearly shows that the SM thrust sheet rides on a low-angle detachment, with a ~20 km wide horizontal flat, ramping up with ~35° under the SM Mountains. To our knowledge, no reliable and clearly documented published data is available on the stratigraphic age of the oldest outcropping rocks at SMM. Below is a summary of the publicly available data to date.

Arguments supporting Paleozoic age outcrops are (1) poorly documented Permian age dating of macro-fossils (sea urchins) from Bella Esperanza Thrust, south of the SM ridge (Gil Rodriguez, 2002), (2) poorly documented Permo-Triassic age, based on palynology samples from the Ox. 7-1 well and seismic-to-outcrop correlation (Gil Rodriguez, 2002), (3) questionable lithostratigraphic correlation from the Camisea area (>300 km away), description of sand and limestones as Ene Formation with overlying Mitu Group conglomerates, based only on lithologic character, but without documented age dating (Allcca Torres, 2007). Arguments supporting Jurassic age outcrops are (1) the regional geologic context along the EC thrust front where Jurassic outcrops and base-Pucara detachments have been consistently documented (e.g. INGEMMET, 1997; Hermoza et al., 2006), (2) regional context with the Huallaga Basin where low-angle detachments and related Jurassic evaporites in outcrop have been confirmed (Megard, 1984; Hermoza et al., 2005), (3) regional geologic outcrop data shows that south of the first-order Tambo fault zone (Ene basin and south) Paleozoic detachments prevail, while north of this zone (PB and north) base-Jurassic detachments dominate, all theway to Huallaga (Espurt et al., 2008).

Based on the regional seismoestratigraphic correlation (Transect D, Fig. 3.5) with a well-tie of Jurassic strata at the Chio 1-X well (Perupetro, 1998), we interpret the oldest rocks at outcrop level in the SMM to be of Jurassic age, likely Pucara Group strata. These decollements could be located in the Chambara Formation (evaporites) or the Aramachay Formation (black shales) (Fig. 3.2). Salt-hosted detachments have been documented from other Peruvian basins, such as the nearby Huallaga basin (Megard, 1984; Hermoza et al., 2005) and from around the world (e.g. Davis & Engelder, 1985; Jackson, 1995).

3.8.2 Thick-skinned tectonics

Ongoing thick-skinned inversion of pre-existing extensional systems is widespread across Peru and may form significant oil accumulations (Mathalone & Montoya, 1995; Hermoza et al., 2006). In the PB similar structural styles occur in two regions, the eastern SHM and the SM footwall. The SM basement-involved system reveals fault angles of 60°-80°, varying vergence and geometries locally resembling flower-like structures up to ~3.5 km wide and 170 m high (Figs. 3.8 and 3.10). Strike-slip movements in the southern PB have been documented (Devlin et al., 2012). The seismic quality in the footwall gradually decreases towards the west. Even though the magnetic data has a lower spatial resolution than seismic data, it reveals an anomaly which is offset laterally by several km from the axis of the SM thrust anticline. The SM thick-skinned system (sub-thrust), which has not been described in the literature in detail, can be mapped over >70 km (Fig. 3.4). In map view the magnetic anomaly reveals that the deep fault system consists in separate segments with slight strike variations. We interpret this sub-thrust fault system to be a trend of inverted preexisting normal faults, likely overprinted by a transpressional component, which is strongly evidenced by: (a) the steep dip of the master faults, (b) sub-vertical flexure zones above the faults (in Mesozoic strata), indicating a near-vertical component of the fault movements below, (c) the occurrence of flower-like structural geometries, (d) the segmented and dog-legged nature of the map-view pattern (Fig. 3.4), a typical geometry of inherited and reactivated normal faults (Lowell, 1979; McClay et al., 2002; Fossen, 2010).

3.8.3 The role of evaporites on deformation

Salt bodies in the Ucayali Basin and their impact on thin-skinned thrusting have been recognized previously (e.g. Moretti et al., 2013). However, there is still significant uncertainty as to their exact stratigraphic location. We observe large salt bodies in the PB (>20 km wide and up to 1200 m thick) (Fig. 3.5) and categorize them into three different types, (a) autochtonous salt, resting directly on the Triassic-Paleozoic package (e.g. the pillow below the Iscozacín Anticline (Figs. 3.5 and 3.9)), (b) slightly thrusted salt-pillows (e.g. central part of Transect A, Fig. 3.5) and (c) autochtonous salt diapirs (e.g. the salt body coring the Iscozacín Anticline (Fig. 3.5)). Seismic shows that evaporitic bodies focus the thin-skinned thrusting, such as the SM master thrust located near a salt-weld layer at the base of the Jurassic sequence (base of Pucara Group) (Fig. 3.11a). The precise location of the detachment varies: While in the south the SM master detachment is located above the autochtonous salt, it is located beneath it near the northern leading edge of the thrust sheet (red line in Fig. 3.5). The Pucara Group contains up to three members, the Chambara (evaporites), Aramachay (shales) and Condorsigna

(limestones) (Rosas et al., 2007) (Fig. 3.2). We propose that the salt-related detachments of the SM thrust sheet are closely related to the evaporites of the Chambara Member.

Local lithological variation and related rheological heterogeneities could cause the master detachment to take slightly different positions around the Chambara evaporites. We interpret the salt body inside the Iscozacín Anticline as a salt diapir that has migrated to its present location in recent geologic times. In the absence of growth strata on the flanks of the anticline, which could help to date the structure, we suggest that the structuring occurred very recently. From the sparse seismic data here it is not possible to determine the exact vertical and lateral components of the salt migration. For this reason our preferred interpretation is that of a salt diapir which formed mostly through (sub-) vertical salt migration, due to the following reasons: (a) the very fresh and dome-like topographic surface expression which spatially coincides with the salt body and (b) a marked radial drainage pattern, associated with the dome. Salt migration can be very fast, reaching several meters per year (e.g. Jackson, 1995) and a very recent salt migration could explain why the two exploration wells Ox. 7-1 and Ox. 7-2 were dry holes, as hydrocarbon expulsion may not have been captured by this extremely young structure. From these two wells it is known that the salt inside the Iscozacín structure is not pure halite. Instead, halite and gypsum are intercalated with clastics (shale, sandstone, conglomerates) and the evaporite content ranges between ~20% and 70% (per meter drilled). A salt feeder is not observed which could be due to (a) the location of the feeder between seismic lines or (b) the feeder thickness being below the seismic resolution. Counter-regional faults may act as feeders and feeders are thin, narrow features are typically not seen on seismic (Diegel et al., 1995; Rowan, 1995). Salt feeders may typically lie below the lowest point of the salt base (Hudec & Jackson, 2006) and the possibility of multiple feeders has to be considered. However, multiple feeders would complicate the shape of the canopy base (Hudec & Jackson, 2006) and due to the fact that the base of the salt body at the Iscozacin Anticline is flat, we conclude that the structure was fed by a single feeder, possibly through a combination of subvertical and lateral salt migration.

3.8.4 Restoration and shortening

In order to test the robustness of the structural model, Transects C and D were kinematically restored to the top of the Yahuarango Formation. The hanging wall cut-off of the SM anticline was reconstructed by down-plunge projection (~2.1° northward plunge). Regarding the hanging-wall cut-off, based on the geometric reconstruction, we calculate the eroded bed length at the SM thrust at Transect D for the top Cushabatay to be at least 3.0 km (Fig. 3.9). The restorations reveal that the shortening is different between both transects: While on Transect C the SM thrust has 2.9 km tectonic

transport (2.2%) (Fig. 3.7), on Transect D the shortening of this structure is 5.1 km (6.6%) (Fig. 3.9). The thin-skinned tectonic transport on the frontal thrust of the EC on Transect D has been calculated to be 14.2 km (18.4%), which is a minimum value, as the hanging wall cut-off is eroded. Hence, total minimum thin-skinned shortening here is 19.6 km (25.5%). The thick-skinned shortening in Transect C has been calculated to be 3.4 km (2.6%) (Fig. 3.7), values which are in line with published data, such as Sanchez Alvarez (2007) who suggests the thick-skinned shortening across the central Ucayali basin to range between 3 and 5.5%. The depth to detachment below the SHM of around 20 km has been adapted from Devlin et al. (2012), a value that seems reasonable given the wavelength of the SHM block. The total shortening for the internal Subandean zone at the PB has been calculated to be 50% by Gil Rodriguez et al. (1999). Placing these shortening rates in a more regional context, there are indications that the shortening gradually increases southward from the PB: Shortening across the PB is 25.5% (this paper), while Espurt et al. (2008) mention ~56 km or 30% across the Southern Ucayali and Ene Basins and Baby et al. (1997) document 191-231 km of shortening across the EC in Bolivia.

At the northern end of the SM range, seismic and surface data shows that the SM structure plunges towards the northwest, loses tectonic transport and displays a notable strike-rotation. Also, passively northward-lifted strata above the northern leading edge of the SM thrust sheet are observed on Transect A (Figs. 3.3 and 3.5). Based on these observations we interpret this area as a lateral or oblique ramp in the subsurface, located between the northern tip of the SMM and the EC. Due to sparse seismic, the exact geometric configuration of this lateral ramp cannot be mapped. The foreland-ward tectonic transport on the SM thrust at the latitude of Transect C is 2.9 km and, due to mechanic-kinematic constraints, has to decrease to almost zero at the lateral ramp. Transect C is about 19 km from the northernmost tip of the SMM, which would imply a reduction of tectonic transport from 2.9 km to practically 0 km over a distance of 19 km. This seems reasonable as no major rotational accommodation is necessary.

3.8.5 Structural timing and interplay

Numerous deformational events since Paleozoic times have been documented from the Ucayali Basin (Jaillard et al., 2000; Megard, 1984) and the Andean Orogeny has been divided into 6 distinct compressional pulses, ranging from Albian to Late Miocene (Megard, 1984). Angermann et al. (1999) and Sdrolias & Müller (2006) found that the convergence rate of the Nazca Plate has been steadily decreasing since the Early Miocene. Oncken et al. (2012) mention that the acceleration of shortening in the Andes correlates with waning plate convergence rates; the authors conclude that in the Central

Andes (as far north as 13°S) after ~15 Ma deformation localization at the orogenic scale and substantial weakening of the eastern flank of Andes occurred. This implies that during the time span representing the observed structures of the PB the kinematic regime has slowed down over the last ~30 Ma. Based on our observations and interpretations, we suggest that initially the pre-existing structures were inverted by Andean compression. Typically, these pre-existing structures in the Subandean domain require little shortening to be inverted (e.g. Giambiagi et al., 2003). With ongoing west-east directed Andean compression eventually, the mechanically weak layers (Jurassic shales and evaporites) in the PB failed and propagated eastward as the large SM thrust sheet.

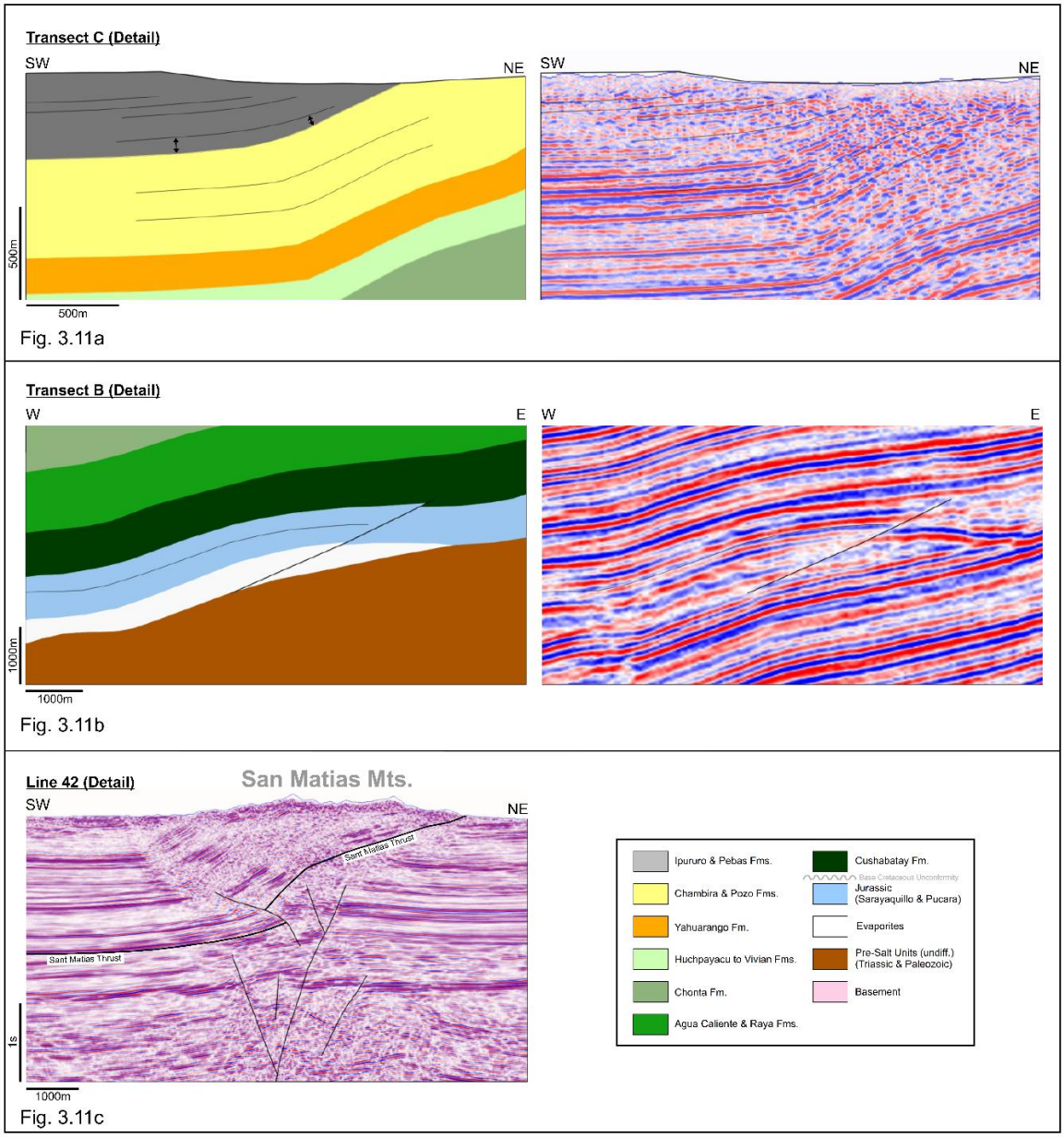

Fig. 3.11a: Indications of growth strata in the shallow section. Fig. 11b: Thin-skinned thrust originating from salt-pillow. Fig. 11c: San Matias Thrust displaced by deeper structure.

Paleozoic and Precambrian outcrops about 30 km west of the present-day eastern topographic front of the EC (e.g. Hermoza et al., 2005) are a good indicator for the approximate location of where the thin-skinned San Matias thrust system steps down westward into Paleozoic rocks and eventually converges with the intra-basement detachment.

We observe that locally very young intra-Ipururo reflectors display evidence of convergence, indicating syn-depositional structural growth (Fig. 3.11a). The Ipururo Formation has been assigned Pliocene age (INGEMMET, 1997) which is defined from 5.333 Ma (upper boundary) to 2.58 Ma (lower boundary) (IUGS, 2014). Hence, this would imply that the SM thrust was advancing and continued thin-skin deformation occurred in the PB at least from 5.333 Ma to post-2.58 Ma. In the northern part of the PB, particularly closer to the EC thrust front, tilted shallow seismic reflectors and subtle positive topographic expressions of Quarternary-Pleistocene strata (Fig. 3.1) indicate ongoing deformation. Under the assumption that the SM thrust was active from ~5 Ma to ~0.5 Ma and based on the tectonic transport revealed by the structural transects, we calculate the slip range to be between ~1 mm/yr to ~1.6 mm/yr, values which seem reasonable when compared to slip-rates documented from other basins, such as 1 mm/yr from thrusts in Iran (Fattahi et al., 2006), 0.15 mm/yr to ~2 mm/yr from thrust faults in the Dinarides (Kastelic & Carafa, 2012) and ~2.0 mm on active thrusts in Argentina (Schmidt et al., 2011). The thin-skinned SM detachment consistently ramps up to surface at the western limb of the underlying basement-involved structure (Figs. 3.7, 3.8). In consequence, we interpret these two different structural styles as mechanically linked structures, where the ramping of the thin-skinned detachment is triggered in response to the growing e or already existing e underlying thick-skinned structure. It has been shown that basement topography, such as basement warps or basement faults may deflect, focus or trigger thin-skinned structures (Wiltschko & Eastman, 1983; Schedl & Wiltschko, 1987).

We observe that the general monoclinal situation of the PB is partially the result of the tilting (rotation) of the SHM block. Fault-branches originating from the deep thick-skinned systems locally displace the SM thrust (Fig. 3.11c), which implies that the thick-skinned system was active after the SM thrust sheet was in place. If the growing (or existing) thick-skinned system was the trigger for the SM thin-skinned thrust, as suggested above, it would imply that thick- and thin-skinned systems were active intermittently or synchronously. Similar interaction of thick- and thin-skinned systems have been reported from other regions around the world, such as the Apennines, Italy (Scisciani and Montefalcone, 2006) or Greece (Kokkalas et al., 2012).

A pseudo 3-dimensional model of the PB was built from the transverse sections (Fig. 3.12) and visualizes the thick- and thin-skinned systems, as well as the salt tectonic structures in their true spatial context. It becomes obvious that the SM thrust structure is visible on the two southern transects (C, D), but has disappeared on the northern transect (B). It also becomes clear how the thick-skinned eastern shoulder of the SHM block controls the slope of the entire basin floor. Salt structures are limited to the western sector of the PB, where originally autochtonous salt was present and helped trigger thin-skinned thrusting.

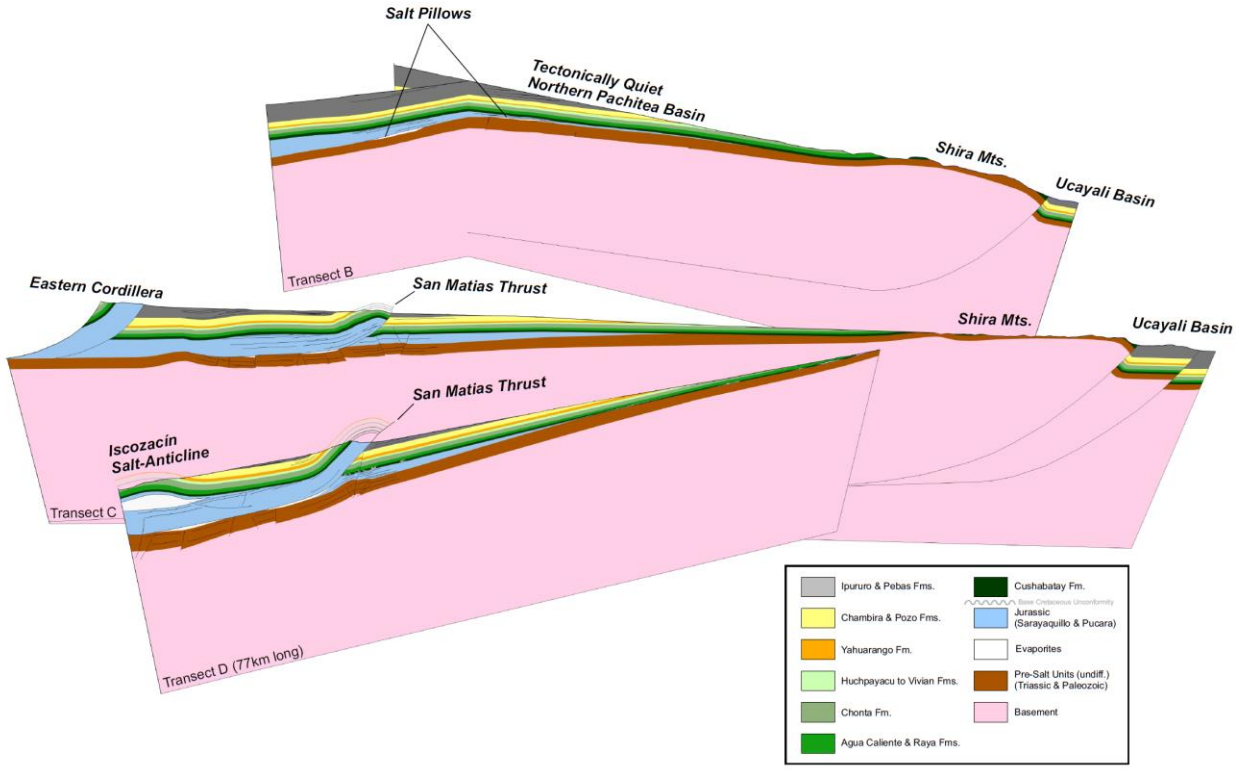

Fig. 3.12: 3D-Visualization of the three Transects, B, C and D, representing varying structural styles in the Pachitea Basin. View towards the Northwest.

3.9 Conclusions

The principal objective of this study is to integrate new data, particularly new seismic interpretations, into an improved and more robust structural model of the PB than previously published, with the secondary aim to better understand hydrocarbon exploration risks in this area.

We have shown that, based on a newly conducted seismo-stratigraphic correlation, and the geological context, the oldest outcropping rocks carried on the SM thrust are Jurassic in age, which has direct implications for the structural models here. Based on detailed seismic interpretations and kinematic restorations we confirm the importance of salt bodies on the thin-skinned detachments in the area. We propose that the existence of allochtonous salt diapirs is due to salt migration through sub-vertical feeders and that the related diapir-cored anticline, which has a marked topographic expression, is likely too young to have captured hydrocarbons. We have shown that the deformation history in the PB is complex, very likely with intermittent activity of thick- and thin-skinned systems. For the first time we document a basement-involved fault system, possibly an inverted system, in the footwall of the SM thrust, with significant vertical relief and lateral extension over >70 km. This thick-skinned system apparently hosts anticlines with a pre-Cretaceous structural component, an observation that has implications on the pre-Cretaceous prospectivity in the region.

Apparently thin- and thick-skinned systems interact mechanically and we propose that the SM thrust sheet was localized and triggered principally by two elements, firstly pre-existing (or growing) thick-skinned structural relief and, secondly, the location of pre-Cretaceous salt-pillows which act as weakness zone for thrust initiation. Calculated thin-skinned slip rates of 1-1.6 mm/yr are comparable with slip rates documented from individual thrust in other parts of the world (e.g. Schmidt et al., 2011). Indications of converging seismic reflectors in the Ipururo Formation and fresh topographic surface expressions, such as domes and deflected river courses, indicate that thrusting occurred in the PB in post-Pliocene times. Our timing assessment (active thrusting from at least 5Ma to post-2 Ma) is consistent with published timing data at that latitude (Megard, 1984; Sebrier et al., 1988; Mercier et al., 1992; Hérail et al., 1996; Noble et al., 1990; Gil Rodriguez, 2002; Hermoza et al., 2005; Espurt et al., 2008). One of the key observations is that the SM thrust is the easternmost salt-detached thin-skinned structure related to the Andean orogen at this latitude (~10°S).

We conclude that significant exploration potential may remain in the pre-Cretaceous succession and confirm, hence, similar observations made by Hermoza et al. (2011). However, the Paleozoic succession is very poorly understood and future research efforts, including field work, additional

seismic and drilling, will be necessary to de-risk these plays. Amongst the key exploration risks in the PB, are recent structuring or trap modification and surface connection of the Cretaceous reservoirs. However, it has been shown that even under non-ideal circumstances, large accumulations of light hydrocarbons can be preserved (Chiarelli, 1978; Mcgregor, 1996).

For future research in the PB we recommend apatite fission track analysis, to further constrain the uplift history of the basement blocks and GPS stations along the major thrust systems, to quantify present-day shortening rates. For future exploration de-risking we recommend the acquisition of more densely spaced seismic, particularly along the thrust systems (EC and SM thrust systems) with the aim to further improve the understanding of timing of structural closure in comparison with hydrocarbon expulsion.

3.10 Acknowledgements

We are thankful to the management of Gran Tierra Energy, particularly Dana Coffield, Doug Hamilton, Roger Fife, Carlos Monges and Hugo Pelliza, for allowing us to publish the data and our interpretations.

4. STRUCTURAL STYLES AND TECTONIC EVOLUTION OF THE SANTIAGO BASIN, PERU – IMPLICATIONS FOR HYDROCARBON TRAPS

4.1 Abstract

The Santiago Basin of the northern Peruvian sub-Andes is a structurally complex region related to a combination of thin- and thick-skinned deformation and the impact of salt tectonics during Andean deformation. Oil shows in this basin are very common, and even though the first exploration campaigns started in the 1940s, no commercially exploitable hydrocarbons have been discovered yet.

We present three basin-scale structural transects and refined structural interpretations, based on vintage 2-D seismic data and well tops that help elucidate the relationships between thin-skinned and deep-seated, thick-skinned structures. Two dip sections were kinematically restored to the top of the Yahuarango formation, one of the youngest pre-Andean units. We calculated the depth to the intra-basement detachment to be approximately 20 km (12 mi), a value that correlates with other thick-skinned detachments and earthquake hypocenters from the region.

We recognized a varied inventory of salt-related structures, which we interpret to be part of the approximately 800-km (500-mi)-long Peruvian Salt Belt. The onset of salt movement occurred soon after salt deposition, likely through sediment loading. Our data suggest that Miocene-Pliocene basin deformation starting at 5.3 Ma has been sustained until the present-day. Shortening ranges from 7.31 km (4.54 mi) to 7.56 km (4.70 mi) (5.9% and 6.1%, respectively), corresponding to Miocene-Pliocene deformation rates of 1.3–1.4 mm/yr. These values are significantly lower than those of adjacent regions in the sub-Andes. This may be related to the combined effects of pressure solution, strain accommodation, or deflection by crustal-scale faults farther west.

4.2 Introduction

The deformation characteristics and architecture of thin-skinned and thick-skinned tectonic provinces are well known and are associated with fold-and-thrust belt and broken-foreland end-member scenarios of orogenic evolution, respectively (Dickinson & Snyder, 1978; Gries, 1983; DeCelles & Giles, 1996; DeCelles, 2012; Strecker et al., 2012). Whereas deformation in thin-skinned foreland fold-and-thrust belts generally mimicks a self-similarly growing orogenic wedge and successively advances toward the foreland with a well-defined deformation front, reverse-fault-bounded basement uplifts of broken forelands rather record spatially disparate, highly diachronous deformation patterns (Dahlen, 1984; Jordan & Allmendinger, 1986; Hain et al., 2011). Deciphering the nature of shortening in complex structural orogenic provinces that combine both deformation styles in one area is, however, a challenging task.

The Santiago Basin of northern Peru, located between 3 and 5°S latitude, is such a complex structural environment (Fig. 4.1). The Santiago Basin has been explored for many decades; although eight exploration wells have been drilled and helped establish the stratigraphy (Figs. 4.2, 4.3), no economic quantities of hydrocarbons have been found (Alemán & Marksteiner, 1993; Baby et al., 2005, and references therein). Despite these investigations and exploration efforts, there is an ongoing debate concerning the tectono-sedimentary evolution of this basin. In light of these issues, we address the following, still poorly understood, basin-evolution mechanisms of the Santiago Basin: (a) the role of salt tectonics (e.g., Alemán & Marksteiner, 1993; Alemán & Marksteiner, 1997; Witte et al., 2011); (b) the apparent lack of vergence of the thin-skinned structures (Alemán & Marksteiner, 1993; Mathalone & Montoya, 1995; Alemán et al., 1999); (c) the thick-skinned structures below the Triassic–Jurassic section and their relationship with surface anticlines and possible Permian-Triassic half graben (e.g., Baby et al., 2005); (d) the timing of regional deformation, interplay of structures, and detachment levels in the Santiago Basin and the adjacent northern Marañón Basin (e.g., Wine et al., 2001a; Hermoza et al., 2006; Rait et al., 2009); and (e) the impact of deformation on the timing and formation of hydrocarbon traps (Chalco, 1961; Touzett, 1976; Quispesivana et al., 1997). In our analysis we consequently focus on the Cenozoic history of deformation and refrain from further study of Paleozoic and Mesozoic structures, unless they have been involved in compressional reactivation during the Andean orogeny.

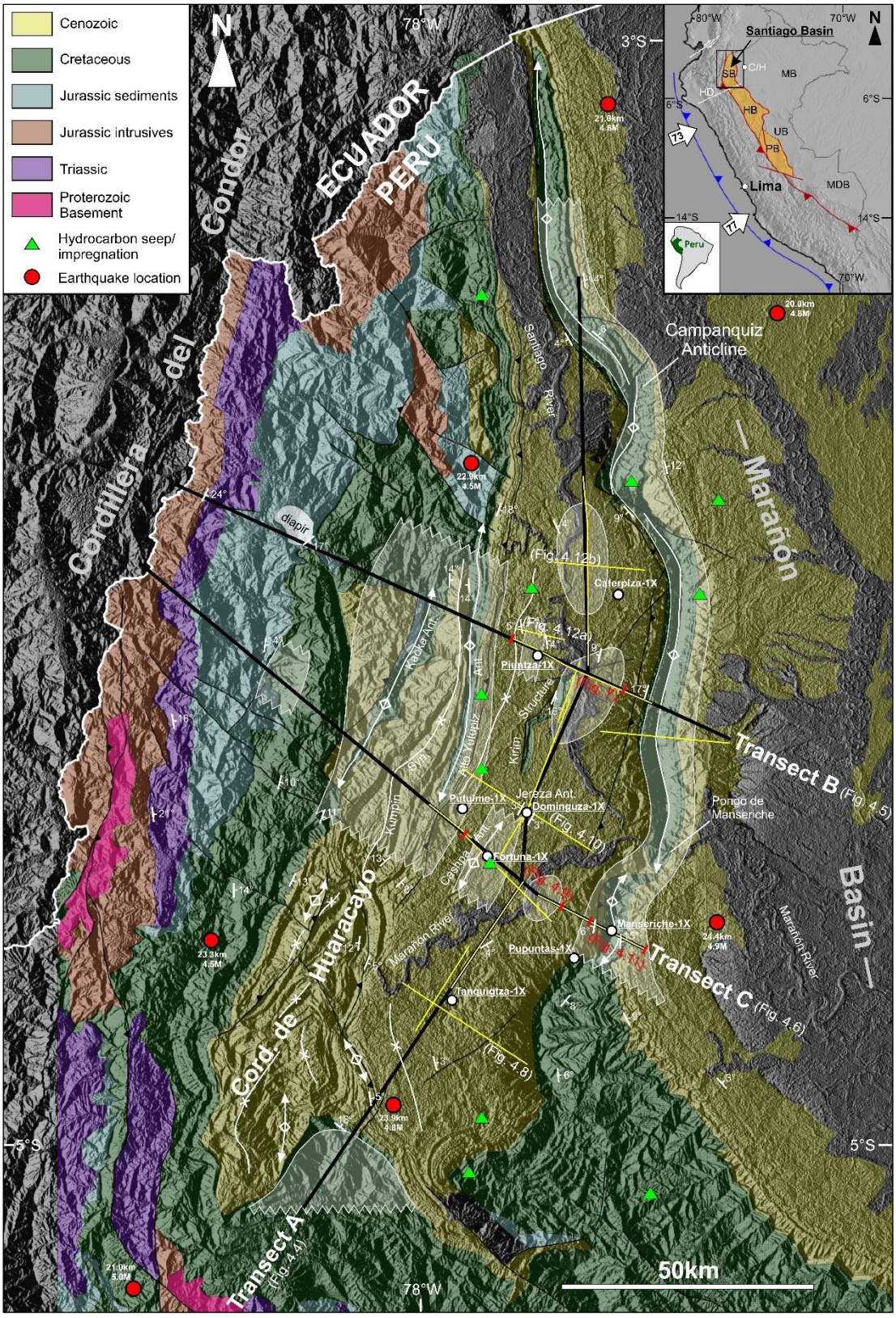

Fig. 4.1: Overview map and data location; gray = Quaternary; seismicity extracted from USGS (2017); transparent white = possible salt pillows; yellow lines = 2-D seismic lines; inset: subduction zone (blue) and major thrust systems (red) of Peru; numbers = plate convergence rate in mm/year; MB = Marañón Basin; HB = Huallaga Basin; UB = Ucayali Basin; PB = Pachitea Basin; MDB = Madre de Díos Basin; C/H=location of Chapuli-1X and Huitoyacu-1X wells; HD = Huancabamba Deflection.

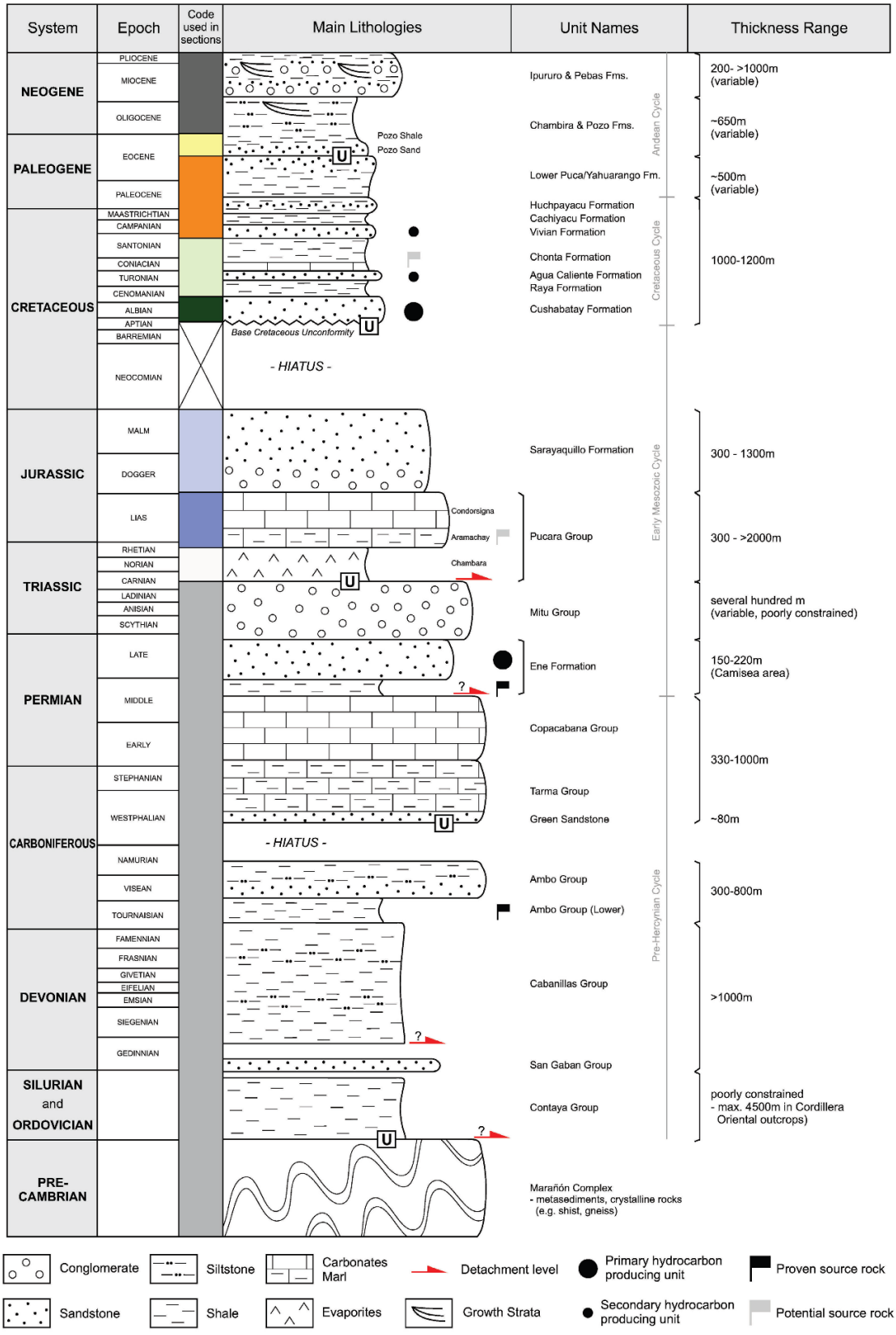

Fig. 4.2: Generalized stratigraphic chart of the Santiago and western Marañón basins; the presence of pre-Triassic strata within the Santiago Basin is speculative; U = unconformity; modified after various sources (Wine et al., 2001a; Encarnación, 2008; Chacaltana et al., 2012).

4.3 Geological framework

The Santiago Basin results from a polyphase deformation history, and it constitutes a region where thin- and thick-skinned thrusting are intimately linked. Proterozoic to Cretaceous units associated with the thick-skinned structures of the Cordillera del Condor delimit the western Santiago Basin, whereas Cretaceous to Miocene units within the thin-skinned, basin-scale Campanquiz Anticline bound the basin to the east (Fig. 4.1). To the north the basin gradually narrows and extends into Ecuador, whereas in the south it transitions into the adjoining Huallaga Basin without a sharp boundary. Plio-Pleistocene synorogenic clastic deposits cover most of the present-day Santiago Basin.

Previous work on the Santiago Basin has covered (a) the presence of major basement-controlled, inverted fault systems (e.g., Baby et al., 2005), even though these have not been fully seismically imaged; (b) the active eastward propagation of the sub-Andean contractional belts (Megárd, 1984; Rocha et al., 2008; Baby et al., 2014; Eude et al., 2015); (c) the presence of thin-skinned contractional structures with opposing (east- and west-directed) vergence (Alemán & Marksteiner, 1993); (d) the coexistence of different structural styles, such as thrusting and strike-slip faulting, as well as transpressional inversion of pre-existing extensional faults (Rocha et al., 2008); (e) variable present-day convergence rates of the Nazca Plate along the northern Peruvian coast of 6.8 cm (2.7 in.) at 1°S latitude versus 73 mm (2.9 in.)/yr at 8°S latitude with east-northeast-directed plate motion (N79°; Dewey & Lamb, 1992; Jaillard et al., 2000; Hampel, 2002; Audin et al., 2008; Rhea et al., 2010); (f) the regional present-day tectonic stress field with an east–west orientation of σ_{Hmax}, which is approximately perpendicular to the Cordillera del Condor and the axis of the Campanquiz Anticline (Heidbach et al., 2008); and, (g) seismicity that occurs throughout the region. For example, shallow seismicity (0–35 km (0–22 mi) depth) appears to occur mainly along the western topographical margin of the Santiago Basin (i.e., along the Alto Yutupiz structural trend and its northern and southern continuations) and along the Campanquiz Anticline, whereas deep-seated seismicity is associated with the subduction of the Nazca Plate (70–150 km [43–93 mi]; USGS, 2017).

Four principal tectono-sedimentary units, separated by major unconformities, exist within the greater Santiago Basin (Fig. 4.2). The unit with the oldest rocks (Ordovician, Silurian, Devonian) does not crop out in the Cordillera del Condor (INGEMMET) and is represented by a pre-Hercynian section comprising clastics and carbonates that overlie Proterozoic metamorphic rocks. These Proterozoic sections crop out in the Cordillera del Condor to the west of the basin (Fig. 4.1). The presence of pre-Triassic (Ordovician to Permian) strata in the Santiago Basin is speculative, due to lacking well or outcrop data. These units are overlain by volcanoclastics of the Triassic Mitu Group; these rocks are

associated with a major rifting event (e.g., Sempere et al., 2002). A subsequent Triassic–Jurassic thermal sag episode resulted in the deposition of marine strata that include black shales, evaporites, and limestones (Pucara Group; Rosas et al., 2007) and late Jurassic continental red beds (Sarayaquillo formation; Fig. 4.2). The areal extent and significance of evaporites in the greater Andean context is unknown. The salt-bearing tectono-sedimentary units are truncated by an angular unconformity related to the late Jurassic–early Cretaceous Nevadan orogeny (Martinez et al., 2003; Bump et al., 2008). The angular unconformity is superseded by middle Cretaceous to recent sediments, associated with the Andean orogeny (e.g., Bump et al., 2008; Baby et al., 2014). The majority of the synorogenic Tertiary units are characterized by growth strata and repeated unconformities (Megárd, 1984; Mathalone & Montoya, 1995). These units also include the Pozo Shale, an important regional seismic marker horizon related to Upper Eocene–Oligocene marine flooding. The Pozo Shale attains a thickness of up to several hundred meters (e.g., Hermoza, 2006).

The separation of the Santiago Basin from the well-known Marañón–Oriente Basin (Alemán et al., 1999), which is located farther east, occurred during the late Miocene through the formation of the Campanquiz Anticline (Alemán et al., 1999; Gil Rodríguez et al., 2001; Wine et al., 2002a; Kennan, 2008). Both, the Marañón and Oriente basins have evolved from a series of originally extensional Permian-Triassic basins that had transitioned into a Mesozoic continental back-arc basin complex (e.g., Mathalone & Montoya, 1995). Abundant geomorphological evidence for Quaternary deformation in these basins has been documented, attesting to protracted, youthful shortening in this area (Dumont, 1996).

Key petroleum source rocks in the Santiago Basin are represented by organic shales of the Cretaceous Chonta and Raya formations, as well as the Jurassic Pucara formation (Wine et al., 2001a). Sandstones of the Cretaceous Cushabatay and Vivian formations and the Eocene Pozo formation represent the reservoir rocks (Fig. 4.2; Wine et al. 2001a; Chacaltana et al., 2012). Information on different phases of deformation capable of generating potential hydrocarbon traps have been documented (e.g., Megárd, 1984), but a detailed and integrated analysis of the exact timing has been lacking.

4.4 Data and methods

We integrated published geological data and our new interpretation of seismic reflection data to construct a geological map and three structural transects (two dip and one strike transects; Figs. 4.1, 4.4, 4.5, 4.6) superimposed on SRTM public-domain elevation data (30 m [98 ft] resolution, NASA). In

particular, the available geologic data are based on published geological surface maps (scale 1:100,000) and surface dip data (INGEMMET), outcrop information, fault traces and formation contacts from our proprietary data base, unpublished geological maps and industry reports, well tops from six wells (Piuntza-1X, Putuime-1X, Manseriche-1X, Fortuna-1X, Tanguintza-1X, Dominguza-1X), and 12 2-D seismic lines (2007 vintage; Fig. 4.3). A simple depth stretch was used to pseudo-depth convert the seismic data. Well tops and surface-dip data were used to calibrate the depth stretch. The oldest unit reached by the drilling in the Santiago Basin is the Cushabatay formation (Figs. 4.2, 4.3). To better determine the thickness and extent of the Triassic–Jurassic and pre-salt sections for our transects, we used outcrop data in the Cordillera del Condor and sporadic well penetrations in the adjoining Marañón Basin (Baby et al., 2005; Rocha et al., 2008).

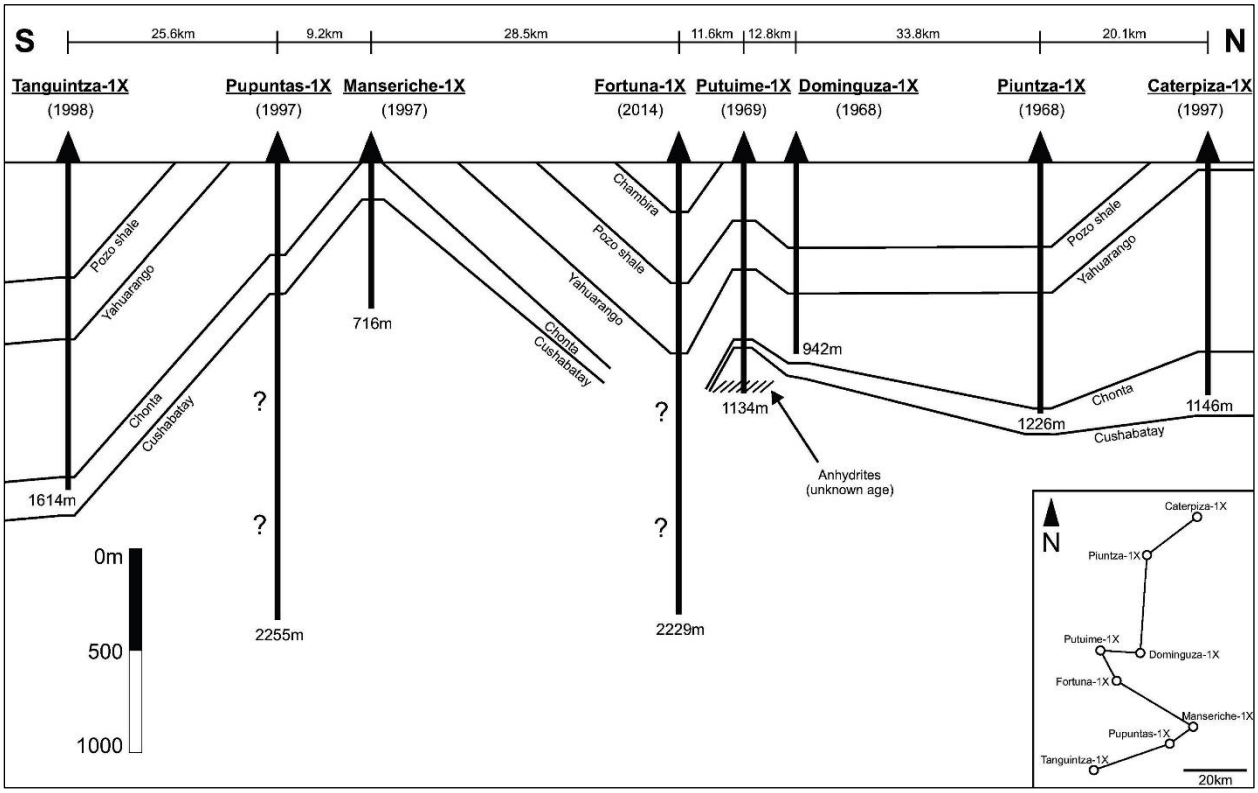

Fig. 4.3: Stratigraphic correlation panel across the Santiago Basin, from south to north, hung on the Yahuarango Formation. Numbers below well name indicate completion year. Values below wells indicate total depth reached. Question marks indicate zones where no further tops are documented.

Due to the lack of data, the Triassic and pre-salt sections are shown as an undifferentiated pre-salt unit (Fig. 4.2). Seven local-scale transects were constructed to depict the different structural styles across the basin (Figs. 4.7–4.12). To constrain the extent of the late Triassic–Jurassic evaporates within our structural transects, we created a map of the "Peruvian Salt Belt" based on regional surface and

subsurface data (Prueher et al., 2005; Hermoza et al., 2006; Sanchez Alvarez, 2007; Zelasco, 2010; Moretti et al., 2013; Witte et al., 2015; INGEMMET geological maps; Fig. 4.13). The two dip sections (transects B and C; Figs. 4.5, 4.6) were kinematically restored using the algorithms flexural slip and fault-parallel flow from Midland Valley Move™ 2016 software to validate model robustness. The thin-skinned structures were restored to the top of the Yahuarango formation, one of the youngest Andean pre-deformational units, and up to 500 m thick, whereas the thick-skinned structures were restored to the top of the Paleozoic–late Triassic pre-salt unit. The pins used for the restorations were placed in the synclines where the least amount of flexural slip is expected. The kinematic restoration rested on the assumption that all rock material only flowed in the plane of section—an approximation, in consideration of the flow of plastic rocks (salt, shale). As the restoration is line-length based (and not a full 3-D restoration), the three-dimensional salt flow cannot be quantified here. To approximately represent the salt correctly during the restoration, the post-deformational surface area of salt was manually redistributed between the pre- and post-salt stratigraphic units (e.g., Rowan, 1993; Rowan and Ratcliff, 2012).

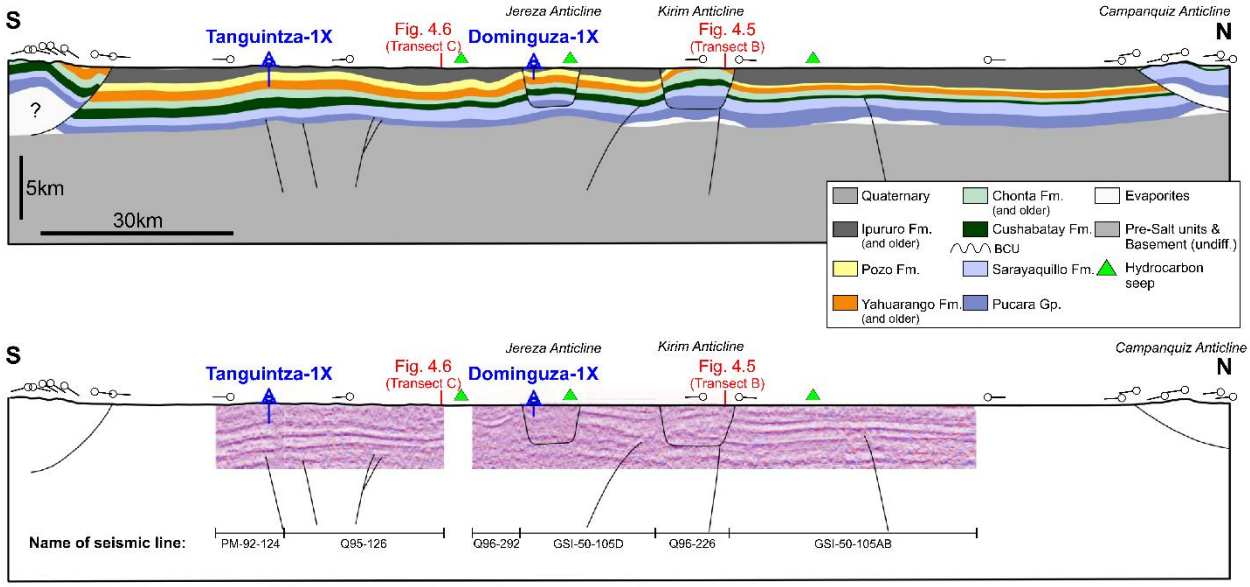

Fig. 4.4: Transect A, strike-section through the Santiago Basin, 2x vertical exaggeration; numbers below seismic lines indicate names of seismic lines; for location see Fig. 4.1.

4.5 Structural styles

4.5.1 Cordillera del Condor

The Cordillera del Condor lies to the west of the Santiago Basin (Fig. 4.1). It constitutes Proterozoic, Paleozoic, Mesozoic, and Cenozoic strata that dip 20° to the east (INGEMMET, 1995). Our interpretation of the structural style of the Cordillera del Condor is shown in transects B and C (Figs. 4.5, 4.6) and is based solely on outcrop data, as no seismic or well data exist in this region. In our interpretation, we show that the Cordillera del Condor results from a steeply dipping blind reverse fault within the Proterozoic and Paleozoic sections. The overlying Mesozoic and Cenozoic strata constitute a drape and deform passively above this structure. Shortening of this thick-skinned structure is transferred to the Mesozoic section through Triassic–Jurassic evaporites, which trigger a passive roof thrust (e.g., Couzens-Schultz et al., 2003).

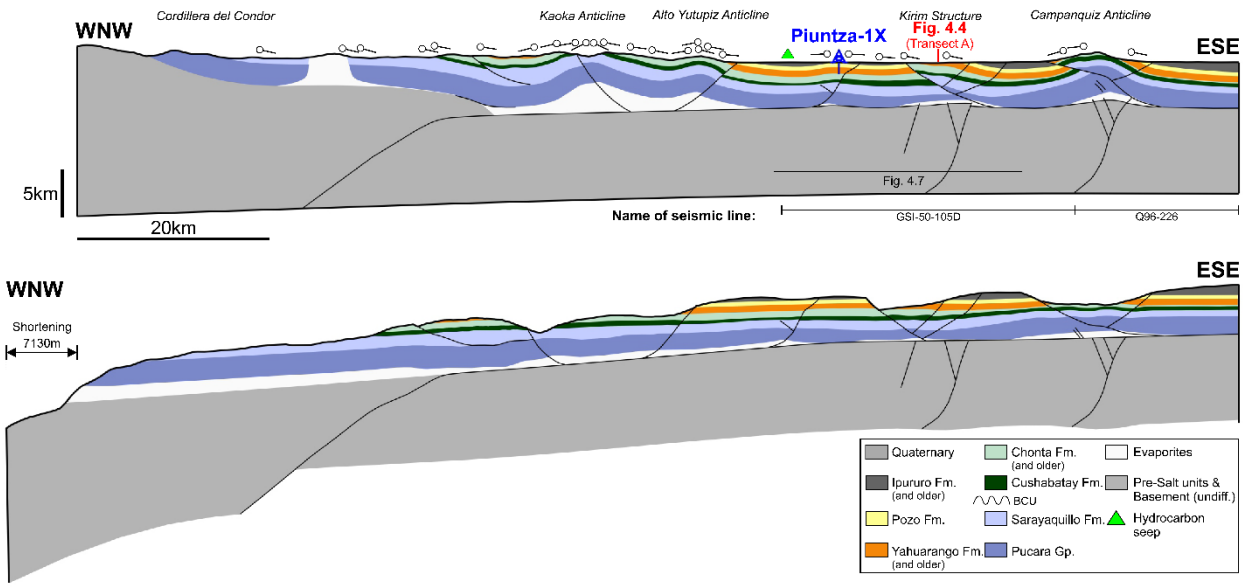

Fig. 4.5: Transect B original (top) and restored (bottom), not exaggerated (true-dip); numbers below seismic lines indicate names of seismic lines; location see Fig. 4.1.

4.5.2 Kaoka Anticline, Kumpin Syncline, and Alto Yutupíz Anticline

To the east of the Cordillera del Condor lies an array of three thin-skinned structures. From west to east, these structures are the Kaoka Anticline, the Kumpin Syncline, and the Alto Yutupiz Anticline (Figs. 4.1, 4.5, 4.6). The Kaoka Anticline can be traced for more than 40 km (25 mi) in north-northeast–south-southwest direction, and its width varies between 4 and 7 km (2 and 4 mi). The oldest exposed unit is the Jurassic Sarayaquillo formation.

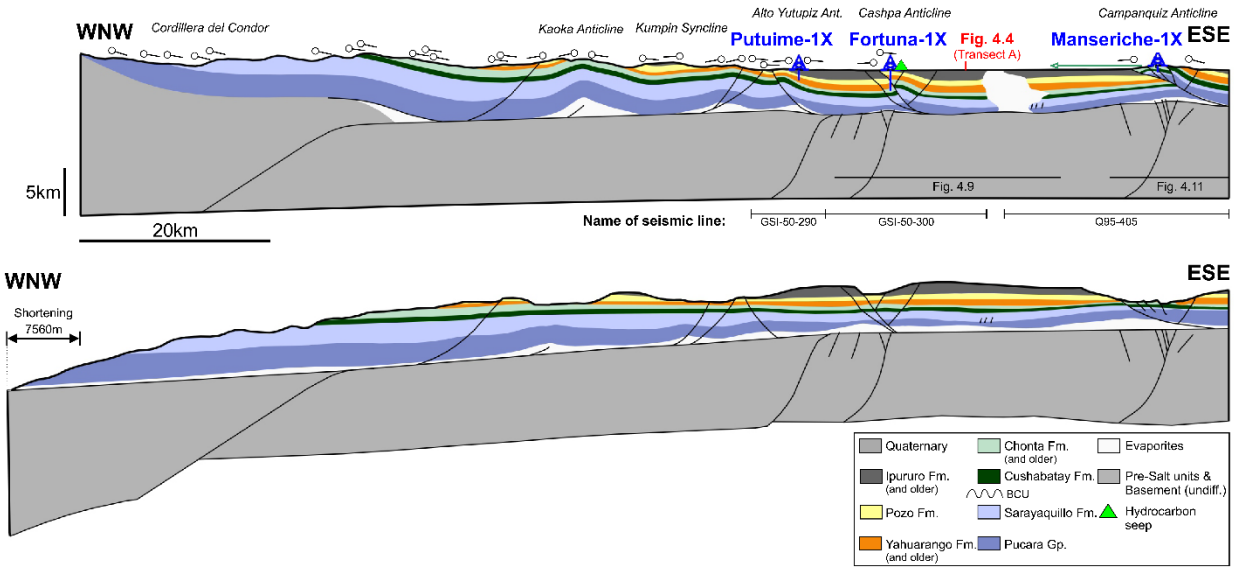

Fig. 4.6: Transect C original (top) and restored (bottom); green arrow indicates thickening in the Cretaceous section toward salt dome, not exaggerated (true-dip); numbers below seismic lines indicate names of seismic lines; for location see Fig. 4.1.

The Kumpin Syncline is about 45 km (28 mi) long; it is about 14 km (9 mi) wide in the south and 3–5 km (2–3 mi) wide in the north. The youngest rocks exposed in outcrop are Neogene strata of the Chambira formation. The Alto Yutupiz Anticline can be traced in outcrop for more than 70 km (43 mi) in a north-northeast–south-southwest direction, and it is typically 3–6 km (2–4 mi) wide. The oldest rocks exposed within this structure belong to the Cretaceous Chonta formation. None of the three structures shows a very pronounced vergence, and structural dips on the limbs are gentle (generally <20°), although the Alto Yutupiz Anticline exhibits a slight eastward vergence. On our structural transects, all three structures were modeled based on surface geology, as neither seismic nor well data exist here. We interpret these features as salt-cored structures (Figs. 4.5, 4.6). Autochthonous salt has not been directly confirmed in the subsurface at the longitude of the Alto Yutupiz Anticline, but we infer the presence of salt due to information from avaliable nearby seismic data and the regional geometric position of the synclinal cores here. The Putuime-1X well, however, penetrates a 122-m (400-ft)-thick unit of pre-Cushabaty anhydrites—possibly an intra-Sarayaquillo formation lens or, alternatively, migrated (allochthonous) evaporites from pre-Jurassic units (Witte et al., 2011).

4.5.3 Piuntza Anticline

The anticline drilled by the Piuntza-1X well is located to the east of the Alto Yutupiz anticline (Figs. 4.1, 4.5, 4.7). The oldest unit cropping out at the axis of this anticline is the Eocene-Oligocene Pozo formation, and both limbs are represented by the Ipururo formation at outcrop level, dipping approximately 4°. As seen in the seismic data, a slight eastward vergence exists (Fig. 4.7). The structure is interpreted as a thin-skinned thrusted anticline with a detachment related to a small salt pillow at the core. Based on the seismic data, the pre-salt units do not exhibit evidence for major deformation below this anticline. A dip line located a few km north of the well reveals converging reflectors of the Ipururo Formation on the forelimb of this anticline (Fig. 4.12), indicating ongoing deformation of the structure during Miocene-Pliocene times (see "Discussion" below for structural timing).

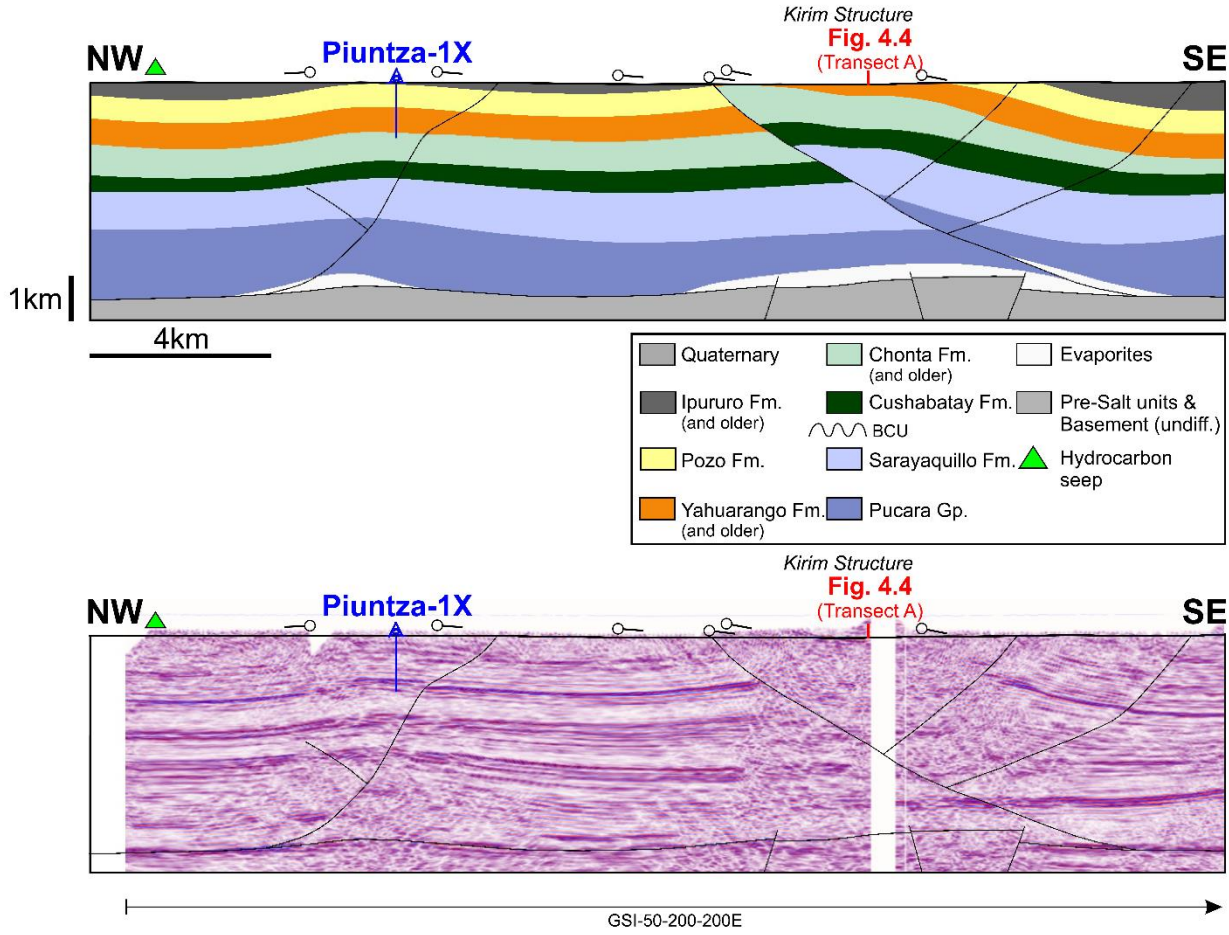

Fig. 4.7: Interpretation of the anticline drilled by the Piuntza-1X well and the Kirim-Structure (both top) and seismic data (bottom), not exaggerated (true-dip); number below seismic line indicates name of seismic line; for location see Fig. 4.1.

4.5.4 Tanguintza Anticline

This anticline drilled by the Tanguintza-1X well is located in the southern portion of the Santiago Basin (Fig. 4.1); this structure is manifested in two cross sections (Figs. 4.4, 4.8). The oldest stratigraphic unit at outcrop level is the Pozo formation. The anticline forms an east-vergent, thin-skinned structure with Jurassic to Cenozoic strata affected by thrusting. According to outcrop data, the fore- and backlimbs involve dips ranging from 3 to 12°. Divergent seismic reflectors at the core of the structure indicate the presence of a weak detachment, possibly associated with a salt weld or small pillow. A west-vergent backthrust was formed here, affecting Jurassic to Cenozoic strata. The pre-salt units are poorly represented, but do not seem to exhibit major changes in relief.

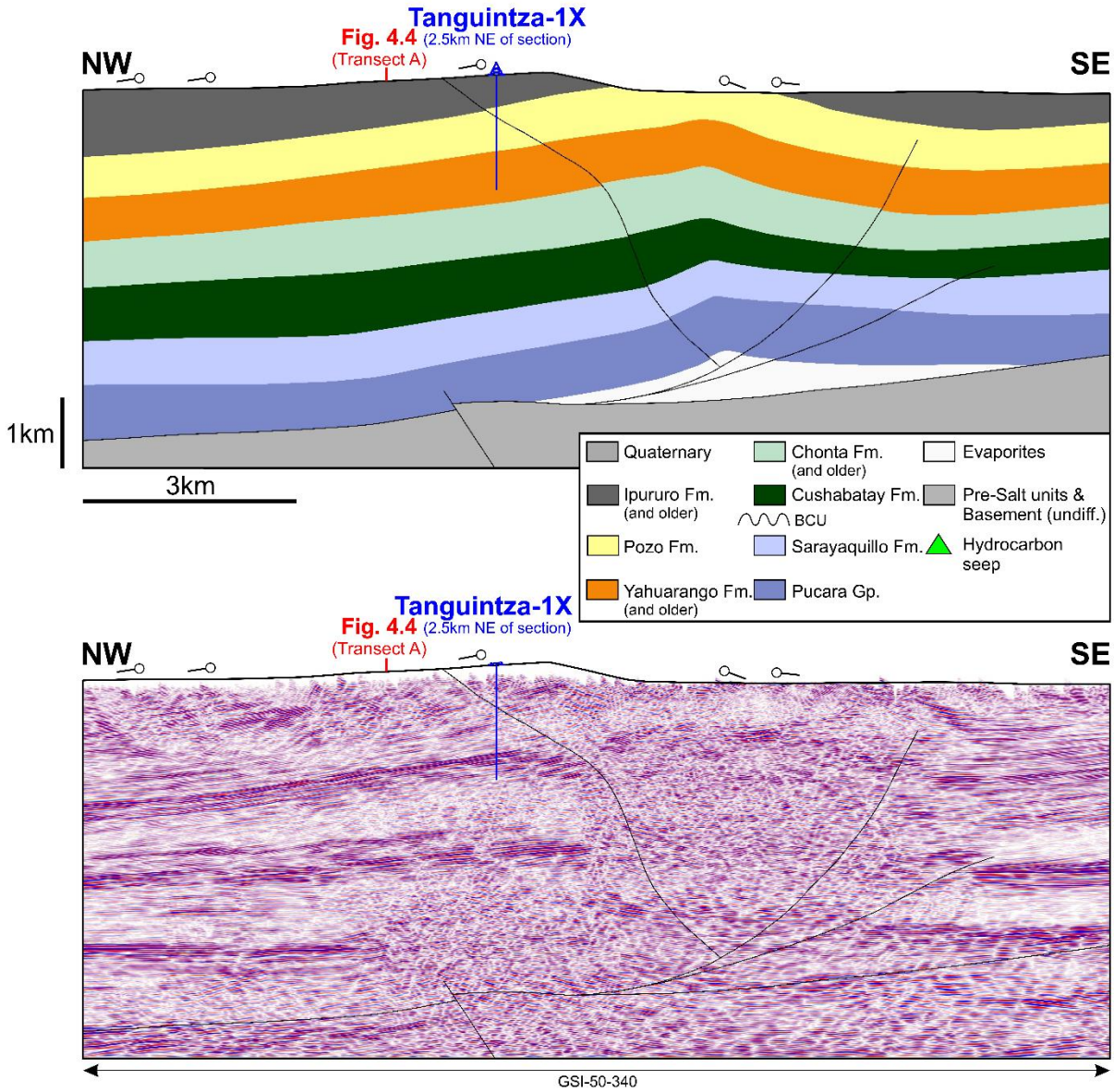

Fig. 4.8: Interpretation of the anticline drilled by the Tanguintza-1X well (top) and seismic data (bottom), not exaggerated (true-dip); number below seismic line indicates name of seismic line; for location see Fig. 4.1.

4.5.5 Cashpa and Jereza Anticlines

The Cashpa and Jereza anticlines are located about 15 km (9 mi) southeast of the Alto Yutupiz Anticline (Fig. 4.1). The Cashpa Anticline is a west-vergent, thin-skinned structure with the basal detachment inferred to be located at the top of the pre-salt units (Fig. 4.9), although the presence of salt here is uncertain. The forelimb of the structure is dissected by an additional thrust originating at the top of the pre-salt units. The seismic data, although of poor quality, reveal that the pre-salt units are affected by high-angle faults creating minor relief. At outcrop level, the crest and limbs of this structure are represented by the gently dipping Ipururo formation (3–5°). The Jereza Anticline, which has been drilled by the Dominguza-1X exploration well (Fig. 4.3), at surface represents a rather simple four-way dip closure with the Ipururo formation at outcrop level (Fig. 4.1). The fore- and backlimbs of this structure have dips of about 3–5°, and a thrust affecting the western limb is documented at surface. The seismic data (Fig. 4.10) reveal a west-vergent structure developed above a thrust fault, detaching at the top of the pre-salt units; this structure cuts Jurassic, Cretaceous, and Cenozoic strata. The presence of a salt weld at the core of the structure, however, is questionable.

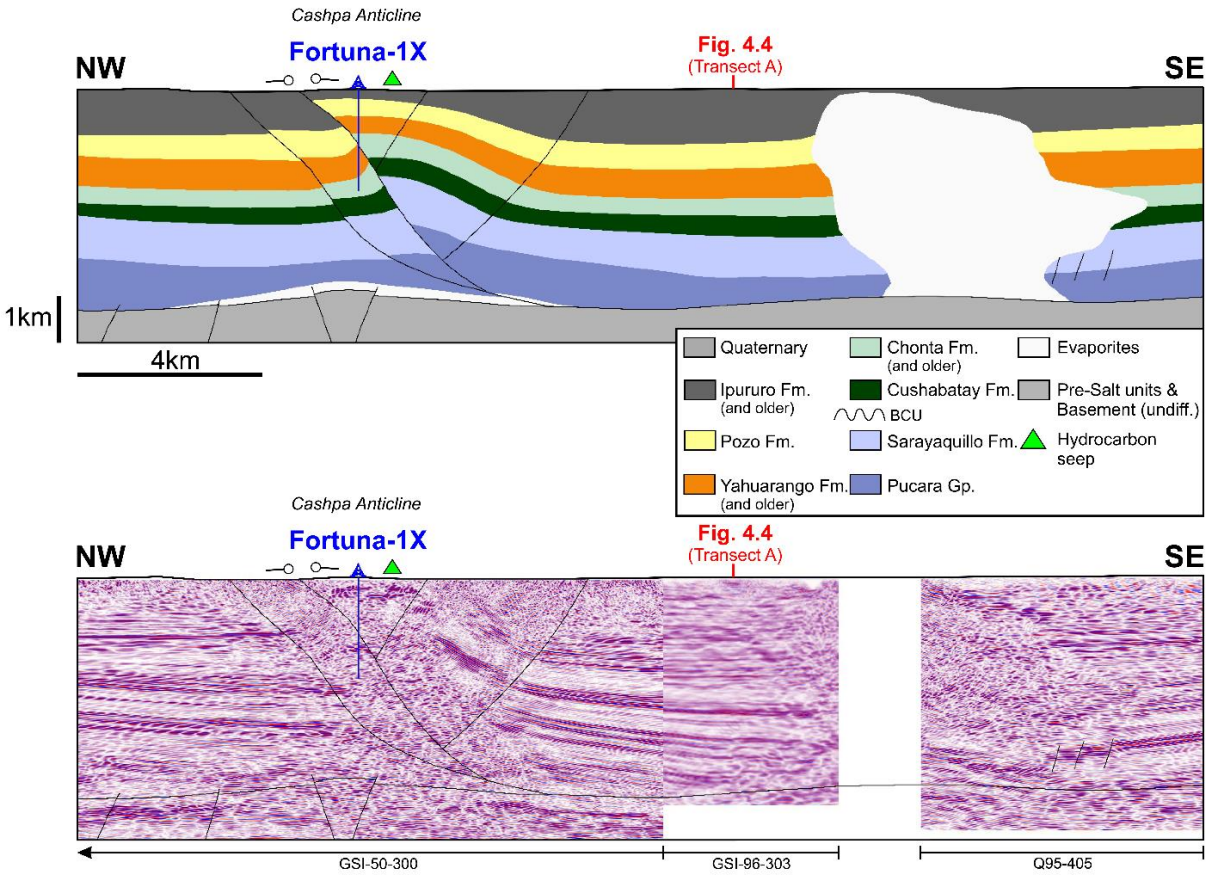

Fig. 4.9: Interpretation of the Cashpa Anticline drilled by the Fortuna-1X well (top) and seismic data (bottom), not exaggerated (true-dip); number below seismic line indicates name of seismic line; for location see Fig. 4.1.

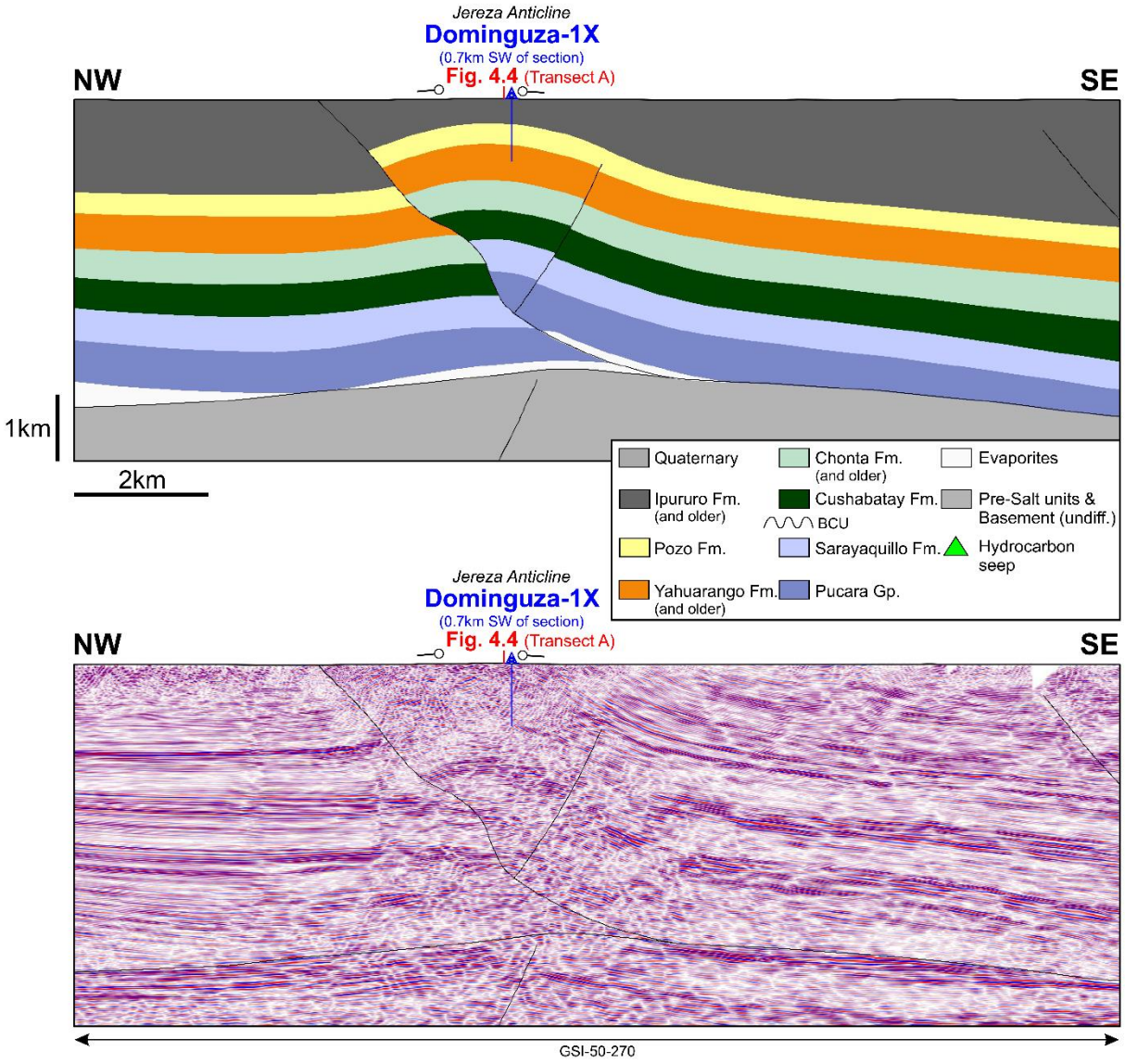

Fig. 4.10: Interpretation of the Jereza anticline drilled by the Dominguza-1X well (top) and seismic data (bottom), not exaggerated (true-dip); number below seismic line indicates name of seismic line; for location see Fig. 4.1.

4.5.6 Kirim Anticline

The Kirim Anticline is located between the Piuntza-1X well and the Santiago River (Fig. 4. 1); it is imaged on several seismic reflection profiles and presented on the geologic cross sections (Figs. 4.4, 4.5, 4.7). Continuous southwest–northeast-oriented outcrops of the Cretaceous Agua Caliente formation can be traced for more than 22 km (14 mi) before being covered by Quaternary deposits of the Santiago River, but the Kirim Anticline continues in the subsurface for several kilometers northeastward. Seismic reflection data reveal a west-vergent, thrusted anticline that involves Jurassic to Cenozoic (Ipururo formation) strata. The limbs of the anticline dip approximately 10–15° toward

the southeast, whereas the underlying thrust fault has variable dips between 20 and 30° toward the southeast. Two east-vergent backthrusts also occur, each with a throw of several tens of meters. The west-vergent master thrust is exposed over a length of 22 km (14 mi) at outcrop level (Fig. 4.1). At the position of Transect B (Figs. 4.5, 4.7), a clear forelimb is not developed. We interpret this structure as a thin-skinned thrust fold, with the detachment related to a possible salt layer near the top of the pre-salt units. Based on the seismic reflection data, the pre-salt units are affected by high-angle faults creating minor structural relief (Fig. 4.7).

4.5.7 Campanquiz Anticline

The Campanquiz Anticline is a west-vergent, thrust-related structure (Figs. 4.1, 4.11). Based on seismic reflection data and the regional position of the thin-skinned detachment, we interpret this structure as a fault-bend fold with the basal detachment hosted in ductile Triassic–Jurassic evaporates. This setting suggests that, upon continued contraction, the fold was cut by a west-vergent thrust, which further amplified the structure. The Campanquiz Anticline is of major importance for the understanding of the structural and stratigraphic evolution of this region, as it forms the key structure that separates the Santiago and Marañón Basins from each other (Fig. 4.1). The anticline can be traced in outcrop for a length of more than 180 km (112 mi), from the Manseriche-1X well in the south to the Ecuadorian border in the north. The anticline is generally 10 km (6 mi) wide at outcrop level and segmented by transfer faults in several locations (INGEMMET, 1998; Fig. 4.1). The oldest units exposed in outcrop are the Cretaceous Agua Caliente and Cushabatay formations. The Jurassic Sarayaquillo formation is very close to outcrop level but is not exposed. The master thrust has a flat-ramp-flat geometry, as seen on both transects B and C (Figs. 4.5, 4.6, 4.11); the lower segment of the thrust dips at 15–20° to the southeast, the middle part at 40–55° (southeast), and the upper portion at 15–25° (southeast). Jurassic to Cenozoic strata (Ipururo formation) are involved in the formation of this structure. Forelimb dips range between 25 and 35° toward the northwest, whereas backlimb dips reach 30–35° (southeast). At the position of the Manseriche-1X well, the fold crest is dissected into a small stack of four duplexes (Transect C; Fig. 4.11), whereas at Transect B, the crest of the Campanquiz Anticline is more intact (Figure 5). On the backlimb, a backthrust developed, displacing Mesozoic and Cenozoic strata by a few tens of meters. Underlying the thin-skinned detachment there are steeply dipping (65–77°) contractional faults with variable vergence that do not offset the Jurassic section.

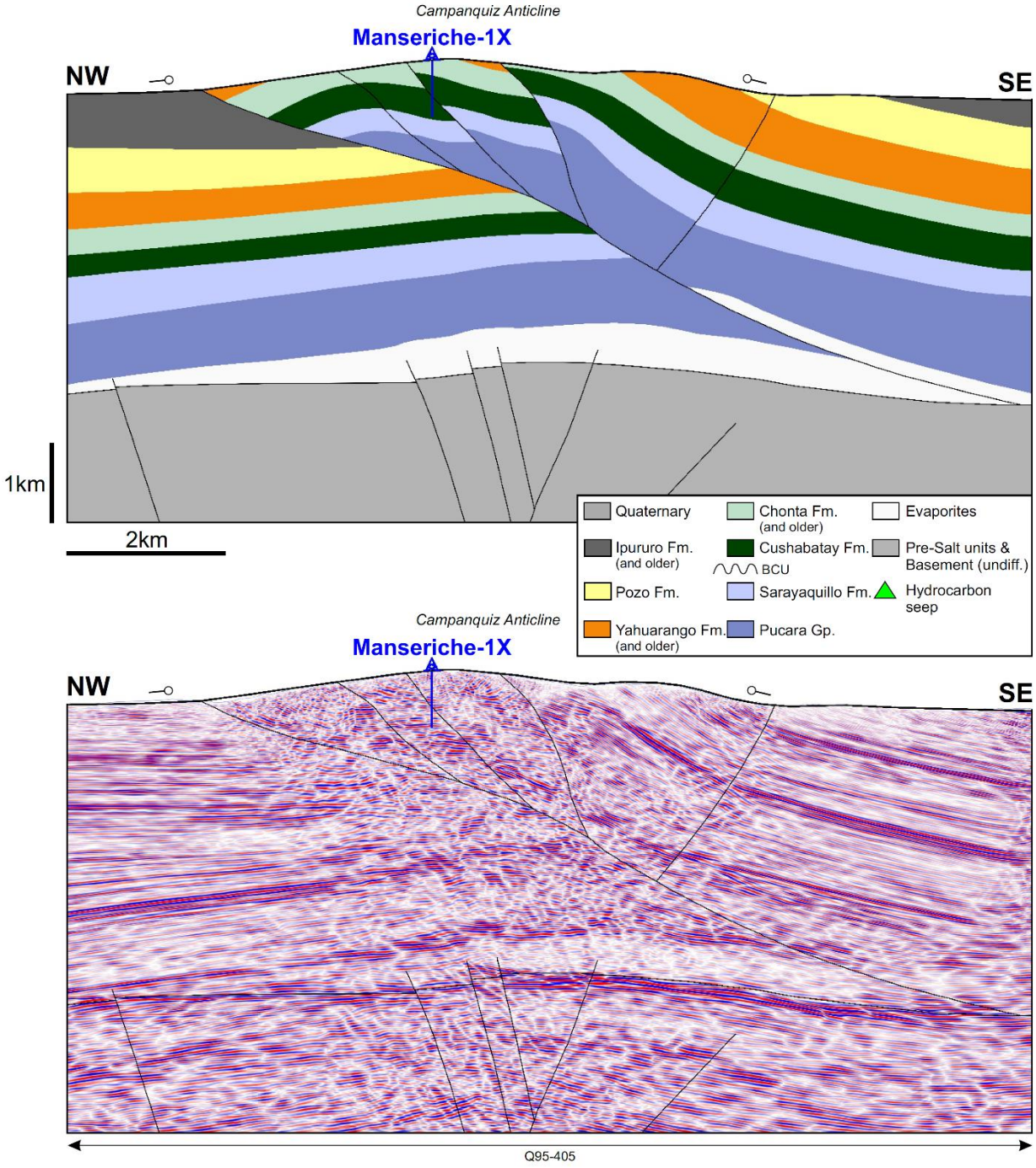

Fig. 4.11: Interpretation of the Campanquiz anticline drilled by the Manseriche-1X well (top) and seismic data (bottom), not exaggerated (true-dip); number below seismic line indicates name of seismic line; for location see Fig. 4.1.

4.6 Thick-skinned tectonics

In the Santiago Basin there are two domains where thick-skinned structures are observed. The first structural domain is represented by the Cordillera del Condor (Fig. 4.1). Here, the crystalline basement, together with the Paleozoic and Mesozoic sections, represents a large thrust-sheet that has been thrust and uplifted over a steep, west-dipping ramp (~32-34°; Figs. 4.5, 4.6). The vertical relief of this structure is in the order of ~3 km (~2 mi). The second domain of thick-skinned deformation is located along the axis of the Santiago Basin, as revealed by the seismic sections (Figs. 4.4, 4.5, 4.6). This low-lying domain of thick-skinned contraction and virtually no horizontal shortening exhibits relatively subtle vertical structural relief, never reaching more than a few hundred meters (e.g., Figs. 4.4, 4.5, 4.6, 4.9, 4.11). In this domain we observed indications of high-angle reverse faults rooted inside the pre-salt units; these structures rarely penetrate the overlying Mesozoic section. The observed angles of the master faults are generally between 65 and 77° (varying dip). Based on seismic reflection data, the strike of the thick-skinned master fault underlying the Campanquiz Anticline can be inferred and suggests an approximate strike azimuth of 14° (north-northeast), approximately parallel to the basin axis and the Campanquiz Anticline. Correlating the thick-skinned faults underlying the Kirim Anticline, a strike azimuth of approximately 32° (northeast) can be determined. Using the method of Groshong & Epard (1994) for transects B and C (Figs. 4.5, 4.6), we calculated the depth to the thick-skinned detachment to be 20.6 km (12.8 mi) for the northern dip-transect (B) and 19.9 km (12.3 mi) for the southern dip-transect (C). Interestingly, these depths do approximately coincide with earthquake-hypocenter locations in the region (Fig. 4.1). Based on these conditions, we propose that the deeper segments of these reverse faults sole out into a regional intra-basement detachment at a depth of approximately 20 km (12 mi), as suggested by previous researchers (Baby et al., 2005; Sanchez Alvarez, 2007; Devlin et al., 2012).

4.7 Thin-skinned salt tectonics

Our structural analysis of the Santiago Basin has revealed the existence of several salt-related structures at varying evolutionary stages (Figs. 4.5, 4.9). Divergence of seismic reflectors near the base of the Jurassic units, which is clearly seen in numerous locations across the basin (e.g., Figs. 4.9, 4.10, 4.11), suggests the presence of a plastic layer (shale or salt) in the subsurface; it can also be observed how low-angle detachments sole out into this plastic layer (Figs. 4.10, 4.11). The most prominent structural style is associated with salt-cored anticlines that are cut by thin-skinned thrust faults (e.g., the Campanquiz Anticline). Other anticlines are salt-cored but show little to no thrust faulting (e.g., the Kaoka and Alto Yutupiz Anticlines). Diapirs are also present, as shown by seismic reflection data

from an area approximately 8 km (5 mi) downstream from Santa Maria de Nieva on the eastern banks of the Marañón River (Figs. 4.1, 4.6, 4.9). Here, an irregular body without a coherent internal signal is imaged on several seismic reflection lines. Immediately above the apex of this structure, a topographic anomaly was observed rising about 20–80 m (66–262 ft) above the regional topography. We thus interpreted this feature as a salt diapir. Normal faulting affecting the Jurassic section on the eastern flank of the inferred diapir may reflect the reactive (extensional) origin of the mobilized salt (Fig. 4.9). Local folding at shallow levels (topographic anomaly and deformed shallow reflectors) could indicate diapir rejuvenation associated with the squeezing of a buried diapir. Thickening of the Cretaceous section on the eastern flank of the structure would be compatible with early salt inflation and subsequent salt evacuation (Mark Rowan, personal communication 2017); see green arrow in Transect C, Fig. 4.6). The geometries of the salt pillows and diapiric bodies observed here are broadly compatible with those documented from different salt basins around the world (e.g., Boigk, 1981; Davis & Engelder, 1985; Hudec & Jackson, 2006).

To test the robustness of the structural model, the thin-skinned structures of transects B and C were kinematically restored to the top of the Eocene Yahuarango formation (Figs. 4.5, 4.6), whereas the underlying thick-skinned structures were restored to the top of the pre-salt units. The restorations reveal that in terms of absolute and relative amount thick-skinned and thin-skinned shortening is very similar in both transects. For Transect B (present-day length 121 km [75 mi]), we calculated a total horizontal shortening of 7.1 km (4.4 mi) (5.9%). For Transect C (present-day length 123 km [76 mi]), we calculated a total horizontal shortening of 7.5 km (4.6 mi) (6.1%). Overall, these values are in line with published data from the central Ucayali Basin of Peru, where Sanchez Alvarez (2007) documented shortening across a thick-skinned area in the range of 3–5.5% where the depth to the intra-basement detachment has been documented to be approximately 20 km (12 mi) (Devlin et al., 2012). However, these values are significantly lower than those reported from areas north and south of the Santiago Basin, such as in the Eastern Cordillera of Colombia (Mora et al., 2013) and the adjacent Huallaga Basin of Peru, where Hermoza et al. (2005) documented 80 km (50 mi) (40%) of shortening. Possible explanations for the marked contrast in horizontal shortening around the Santiago Basin could be due to (with decreasing importance) (a) the influence of the Huancabamba Deflection (Fig. 4.1), a major orogenic deflection separating domains with distinct structural styles (Atherton et al., 1983; Fildani et al., 2008); (b) strain accommodation or deflection caused by orogen-scale/crustal-scale strike-slip zones, a known deflection mechanism (e.g., Marshak, 2004), and reported from the Gulf of Tumbes/Guayaquil at the Ecuadorian coast (Witte & Bourgois, 2009); (c) the existence of deep-seated, blind detachments, as documented from the Catskill Mountains (Marshak, 1986); and (d) diffuse

compaction and pressure solution (e.g., Schmidt et al., 1993). Up to 30% of orogenic shortening may be accommodated by pressure solution, as documented from the Swiss Jura Mountains (e.g., Plessmann, 1972). An additional explanation for masked shortening might involve basement folding, as documented in the Sierras Pampeanas reverse fault-bounded basement uplifts of Argentina, where strain is accommodated by deformation of basement rocks causing large-scale drape folding and tilting (Jordan & Allmendinger, 1986; Strecker et al., 1989). However, we did not observe these deformation styles in the Santiago Basin and, hence, conclude that this mechanism is not contributing here.

4.8 Discussion

Based on the synopsis of our structural and regional observations, we discuss here the different structural, tectonic, and petroleum-related implications that are relevant for the Santiago Basin.

4.8.1 Structural styles of the Santiago Basin

Thick-skinned inversion of preexisting extensional systems during Andean compressional tectonics has been documented in different areas of Peru (Mathalone & Montoya, 1995; Hermoza et al., 2006; Scherrenberg et al., 2014, 2016; Witte et al., 2015), Ecuador (Baby et al., 2013), Colombia (Mora et al., 2006, 2009; Parra et al., 2010), and Argentina (Jordan & Allmendinger, 1986; Mon & Salfity, 1995; Hain et al., 2011). A discussion regarding the presence, location, and characteristics of the early Mesozoic rift system in Peru has been ongoing for years (Mathalone & Montoya, 1995; Sempere et al., 2002; Spikings et al., 2016). The main Triassic rift unit, the Mitu Group, has been established as a stratigraphic unit (e.g., Dalmayrac et al., 1980; Megárd, 1984; Kontak et al., 1985), but typically it is seen in the lower, noisy part of the seismic data. Very few well penetrations of this unit exist across Peru. For this reason, establishing a reliable and detailed regional correlation of these synrift units is very difficult. The lateral extent of sediments of the Mitu Group (or equivalents) is assumed to be discontinuous, as it is related to local rift depocenters (e.g., Gil Rodríguez, 2002; Baby et al., 2005; Spikings et al., 2016). We propose that, at the latitude of the Santiago Basin, the Triassic rift-related units may be absent, as they are neither imaged on seismic reflection data nor reported from outcrops in the Cordillera del Condor (Spikings et al., 2016; Faccenna et al., 2017); in addition, wells in the westernmost sector of the Marañón Basin did not reach the pre-Jurassic units.

Inverted thick-skinned structures in sub-Andean domains typically exhibit a component of oblique or strike-slip motion (e.g., Cooper et al., 1995; Sanchez Alvarez, 2007; Espurt et al., 2008; Giambiagi et

al., 2013). For the Santiago Basin, it has been proposed that the thick-skinned system represents an array of strike-slip faults where the majority of the structural relief in the post-salt section is due to transpression (Tankard, 2002). We did not observe unambiguous manifestations of large flower structures in the seismic data and therefore do not favor a structural model for the formation of compressional basins and ranges associated with a dominant strike-slip regime, as was previously proposed. In addition, these thick-skinned structures have been interpreted as pre-existing half grabens, whereby the rift-bounding faults were inverted during Andean contraction (e.g., Baby et al., 2005; Spikings et al., 2016). Alternatively, the steeply dipping faults could represent newly formed Cenozoic (Andean) reverse faults following inherited anisotropies, and with a minor transpressional component. In summary, based on our observations within the Santiago Basin and in light of the regional context, we suggest that Triassic rift-related strata are absent here and that the steeply dipping, basement-rooted faults may represent reactivated normal faults associated with Andean contraction.

4.8.2 Spatiotemporal kinematic evolution of the Santiago Basin

A number of constraints regarding deformation ages have been documented for the Santiago Basin. It has been shown that northern Peru and the Santiago Basin have been subjected to multiple phases of deformation, from the Paleozoic to the present day (e.g., Megárd, 1984; Rocha et al., 2008). There is general consensus that the rapid uplift and relief-building of the Campanquiz Anticline occurred during the Miocene-Pliocene (Rocha et al., 2008); this is confirmed by apatite fission-track thermochronology data, which indicate cooling and rapid exhumation from 10 Ma onward (Alemán & Marksteiner, 1993; Valdivia et al., 2006). More recent apatite fission-track thermochronology has revealed two cooling events, one between 16–12 Ma and a younger one beginning at about 5 Ma (Valdivia et al., 2006). This is compatible with the deformation of Miocene-Pliocene reflectors from the region of the Chapuli-1X and Huitoyacu-1X exploration wells, about 120 km (75 mi) northeast of the Pongo de Manseriche (Fig. 4.1), as documented by Witte et al. (2011). These authors also suggested that late Miocene reactivation of salt detachments led to the modification of salt-cored anticlines in the Santiago Basin. At the Balsapuerto Dome (Fig. 4.13), based on 40Ar/39Ar age dating, thrusting is known to have ended between 12 to 10 Ma (Prueher et al., 2005). Apatite fission-track data from the intermontane Bagua Basin (Fig. 4.13) indicate exhumation associated with thrusting and folding ended after 8.6 Ma (Naeser et al., 1991).

Based on apatite fission-track data, Alemán & Marksteiner (1993) demonstrated Miocene-Pliocene deformation from the Campanquiz and Huaracayo ranges. Inspection of geological maps and seismic data confirms that the deformation of the Ipururo formation strata is ubiquitous in the Santiago Basin (e.g., INGEMMET, 1997; Figs. 4.1, 4.12). Seismic sections through these units reveal the presence of growth strata in several places (Fig. 4.12). Importantly, the Ipururo formation has been assigned a Pliocene age (INGEMMET, 1997); this would imply that deformation must have been ongoing at several locations across the Santiago Basin from at least 5.3 Ma to post-2.5 Ma (the age of the top of the Ipururo formation; Fig. 4.14). In addition, neotectonic observations suggest that deformation may have continued until the present day (Alemán & Marksteiner, 1993; Encarnación, 2008; Chacaltana et al., 2012; USGS, 2017).

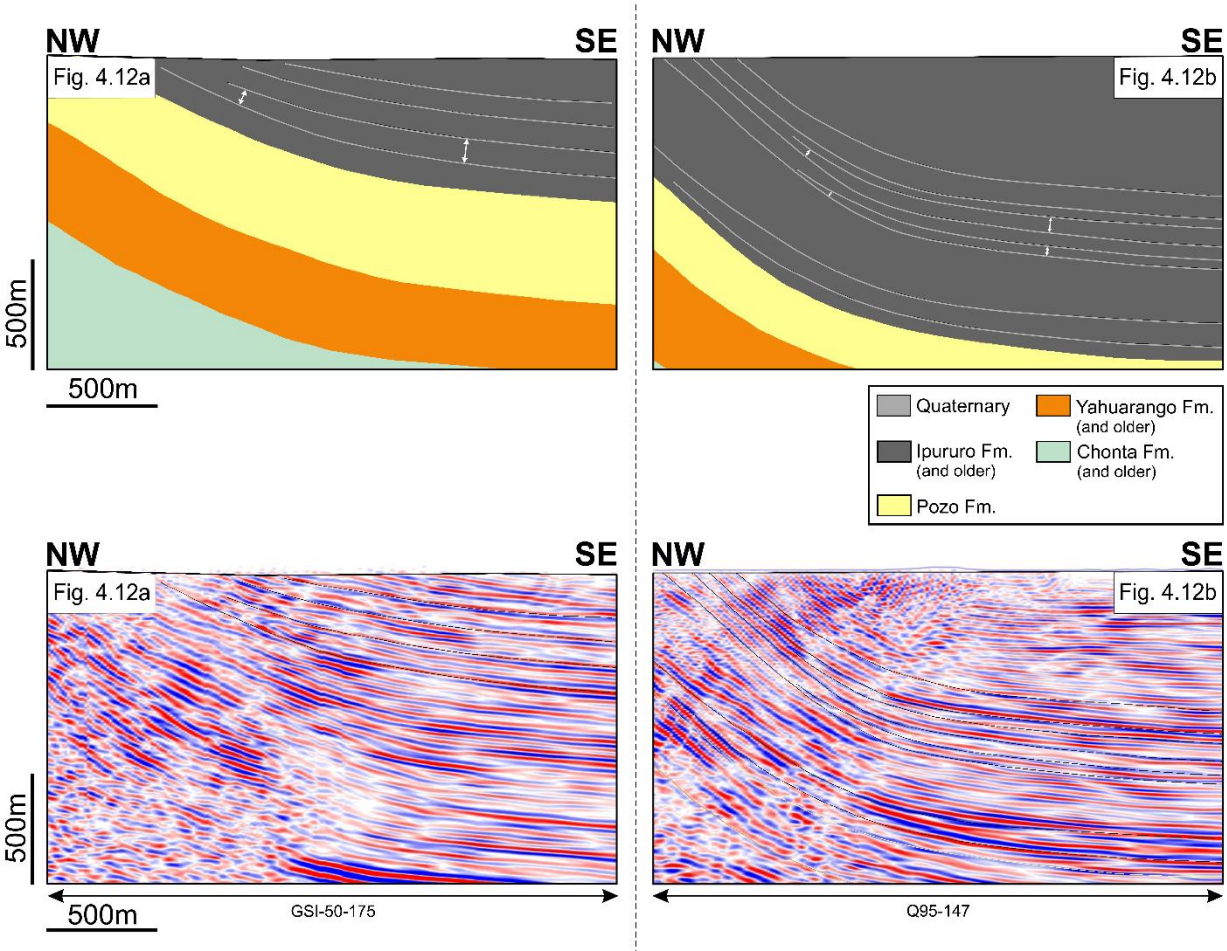

Fig. 4.12. a (left): Interpretation of converging Ipururo Formation reflectors on the eastern flank of the anticline drilled by the Piuntza-1X well (top) and seismic data (bottom); number below seismic line indicates name of seismic line; for location see Fig. 4.1.

Fig. 4.12b (right): Interpretation of converging Ipururo Formation reflectors on the eastern flank of an anticline north of the Caterpiza-1X well (top) and seismic data (bottom); number below seismic line indicates name of seismic line; for location see Fig. 4.1.

Based on the tectonic transport revealed by the kinematic restoration, we calculated the overall rate of contraction across the Santiago Basin to have been between 1.3 and 1.4 mm (0.05 and 0.06 in.)/yr. These values are reasonable, although much lower, when compared to slip rates greater than 5 mm (0.2 in.)/yr documented for areas between the structurally similar Eastern Cordillera and the Llanos Basin of Colombia (Mora et al., 2013). Possible pre-Neogene salt-related deformation is assumed not to have triggered significant amounts of horizontal shortening in the Santiago Basin, but rather vertical or subvertical salt flow or accumulation. The regional tectonic context indicates that pre-Cretaceous, salt-related relief exists in the Santiago Basin, which had been eroded to the base of the Cushabatay formation (e.g., Megárd, 1984; Mathalone & Montoya, 1995). This observation indicates pre-Cretaceous tectonic deformation, possibly related to early salt pillowing, caused by differential loading stresses associated with orogenic processes. Local thinning of the early Cretaceous strata (Cushabatay formation) suggest that early salt movements continued throughout this period. It is likely that salt movements in the Santiago Basin occurred intermittently during both before and after the formation of the Base Cretaceous Unconformity (BCU).

In light of our observations and interpretations we suggest that, initially, the mechanically weak layers (Triassic–Jurassic shales and evaporites) in the Santiago Basin triggered a shallow thin-skinned thrust system, likely during the late Jurassic Nevadan orogeny (Martinez et al., 2003; Bump et al., 2008). It is well known that salt layers, salt pillows, or salt welds may trigger and focus thin-skinned detachments in extensional or contractional settings due to the mechanical weakness of the evaporites (e.g., Hudec & Jackson, 2006; Moretti et al., 2013). Bertolotti & Moretti (2009) concluded that the structural impact of the up to 700-m (2297-ft)-thick Pucara evaporites in the northern Ucayali Basin of Peru has been generally underestimated, whereas recent research has revealed that the evaporitic pillows may help control the localization of early thin-skinned deformation there (Moretti et al., 2013; Witte et al., 2015). Subsequently, during continued contraction, the deeper thick-skinned thrust systems were active, either originating from possible inherited extensional structures or as newly generated Andean reverse faults. Typically, such preexisting structures in the sub-Andean domain require little shortening to be inverted as has been demonstrated in other sub-Andean regions (e.g., Giambiagi et al., 2013). Further contractional modification of these deep-seated structures likely occurred during the Andean orogeny, starting in the Eocene (Megárd, 1984). One possible mechanism to explain why salt-detached, thin-skinned structures can be spatially correlated with deep-seated thick-skinned structures would be a mechanical soft link, whereby deep-seated relief (or active structural growth) triggers ramps in higher stratigraphic levels. Such a mechanism has been previously documented in the Pachitea Basin of Peru (Witte et al., 2015) and other contractional mountain belts around the

world (e.g., Wiltschko & Eastman, 1983; Schedl & Wiltschko, 1987; Scisciani & Montefalcone, 2006; Kokkalas et al., 2012). Accordingly, the thin- and thick-skinned systems may have been active intermittently or synchronously. Seismicity in this region indicates that the deeper structures of the Santiago Basin are currently active, accommodating ongoing convergence between the Nazca and South American plates (Rosenbaum et al., 2005; Sallares & Ranero, 2005; Oncken et al., 2012).

4.8.3 The Santiago Basin in the context of regional salt tectonics

The Santiago Basin is an integral part of a 50–200-km (31–124-mi)-wide belt (Fig. 4.13) between the Ecuadorian order and the Tambo strike-slip zone in the Pachitea-Ene Basin of Peru. Here, widespread salt-detached anticlines, salt pillows, salt welds, and sporadic diapirs have been documented (Benavides, 1968; INGEMMET, 1995, 1997, 1998, 1999; Wine et al., 2001b; Moretti et al., 2013; Witte et al., 2015). We propose calling this belt the Peruvian Salt Belt (Figs. 4.13). The first comprehensive cross sections showing the characteristics of salt tectonics in the Santiago Basin represented the early Mesozoic salt as a virtually continuous layer with a thickness of up to 4 km (2 mi; Alemán & Marksteiner, 1993; Mathalone & Montoya, 1995). Earlier studies also demonstrated that evaporites in Peru are often interlayered with sediments (e.g., at the Tiraco/Callanayacu Dome, Huallaga Basin; Fig. 4.13; e.g., Wine et al., 2001b). This phenomenon is also known from the Iscozacín Anticline (Fig. 4.13), where up to several hundred meters of evaporites interlayered with red beds have been drilled. Hermoza et al. (2006) presented a map of the lateral extent of salt pillows in the Pachitea Basin. Based on a recent 2-D seismic survey from the Pachitea Basin, Moretti et al. (2013) and Witte et al. (2015) demonstrated how salt welds and salt pillows can focus and trigger thin-skinned salt detachments.

In addition, Bertolotti & Moretti (2009) documented up to 700-m (2297-ft)-thick Jurassic evaporites in the northern Ucayali Basin. The lubricating effect of salt layers on low-angle thrusting has been confirmed from the Huallaga Basin (e.g., Hermoza et al., 2005). Early Mesozoic low-relief salt pillows have also been documented from the northwestern part of the Marañón Basin, where the Situche structural complex has been interpreted as marking the eastern feather-edge of these evaporites (Fig. 4.13; Rait et al., 2009). The stratigraphic age of the evaporites in this salt belt is still only weakly constrained and may range from the Triassic to early Jurassic times (e.g., Hermoza et al., 2006; Moretti et al., 2013; Witte et al., 2015), although there are some authors that claim a late Permian age (Calderón et al., 2017). Among the four major tectonic domains across Peru, the Peruvian Salt Belt is the only zone where widespread salt-related structures occur and may potentially form hydrocarbon traps (Domain II in Figs. 4.13, 4.15). We interpret some of the thin-skinned thrusts associated with the more evolved folds in the Santiago Basin as breakthrough thrusts, which have dissected former

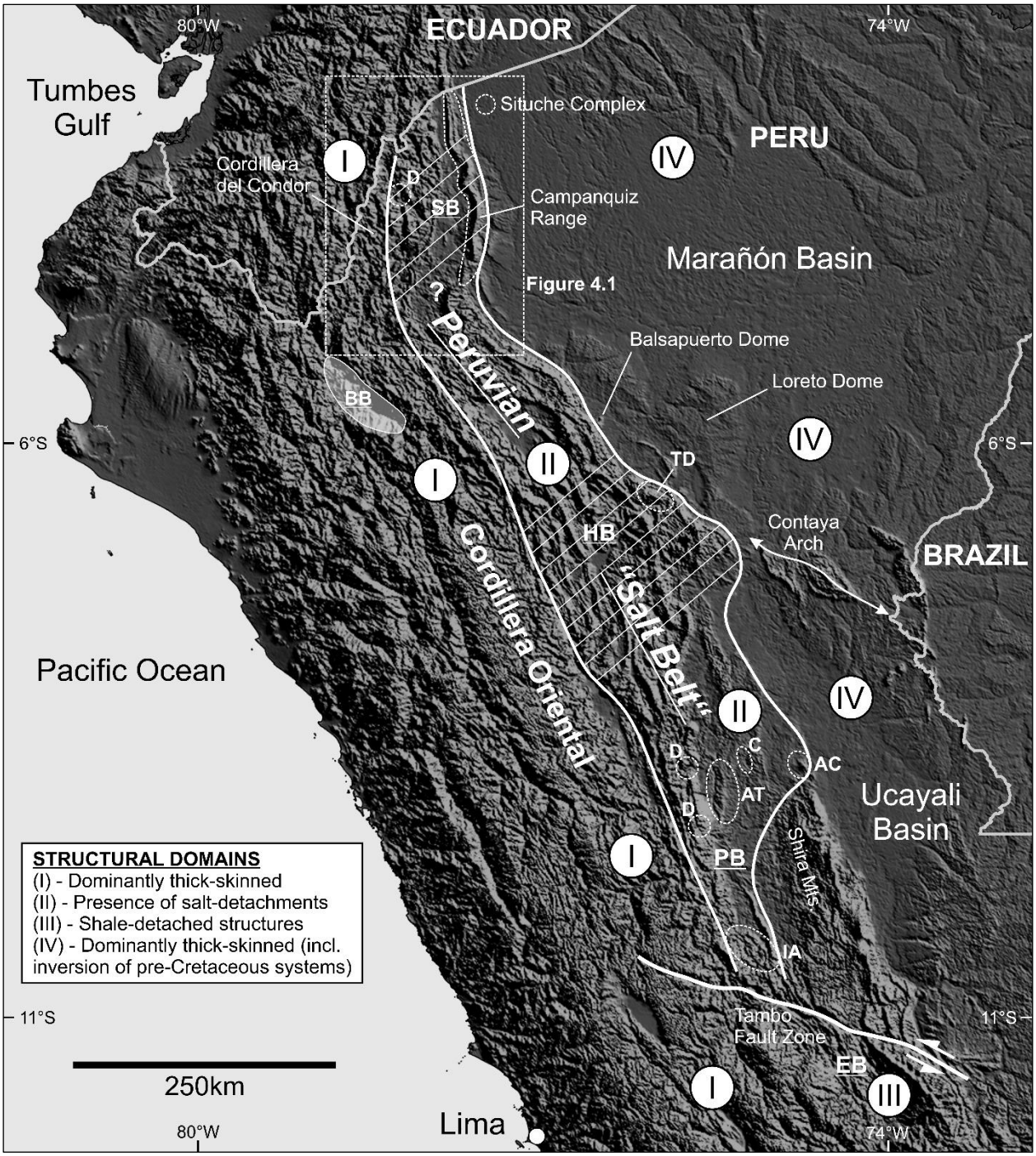

Fig. 4.13: Salt occurrences in Peru, based on surface and subsurface data. Hatched areas indicate regions where salt structures are common. Dashed outlines = individual salt structures (TD = Tiraco dome; AC = Agua Caliente; C = Chío; AT = Aguaytía; IA = Iscozacín Anticline; D = salt diapir or pillow at outcrop). Basins: SB = Santiago Basin, BB = Bagua Basin, HB = Huallaga Basin, PB = Pachitea Basin, EB = Ene Basin. Salt presence between Santiago and Huallaga Basin and at Situche Complex is uncertain. Salt is absent at Balsapuerto Dome, Loreto Dome, Contaya Arch (CA), and Shira Mountains. Roman numbers indicate domains of different structural styles (see text for more details).

detachment folds upon continued contraction, a similar process to that described from the salt-cored structures of the Zagros fold belt (e.g., McQuarrie, 2004). The southern continuation of the Salt Belt,

the Ene Basin, is also dominated by thin-skinned thrusting (Ene Basin, Domain III). Here, however, the main detachment level is rooted in Paleozoic shales (Wine et al., 2002b; Chacaltana et al., 2011). Domain I is represented by the highly inverted (and deeply eroded), thick-skinned structures of the Cordillera Oriental, and Domain IV is located in the Andean foreland basins (Marañón and Ucayali basins); here thick-skinned structures dominate, including deep-seated and inverted pre-Cretaceous systems (Bump et al., 2008; Calderón et al., 2017).

4.8.4 Impact of structural evolution on petroleum system

Previous work on the Santiago Basin has shown that the earliest, unambiguously documented onset of salt movement predates thin-skinned deformation; the onset of salt growth and diapirism in the Santiago Basin can be constrained to Albian–Aptian and Coniacian–Santonian, possibly triggered by sediment loading (Witte et al., 2011). Different degrees of salt movement have been shown to have been active in the Santiago Basin, beginning in the Jurassic until the Cenozoic. The early onset of salt structuring that we propose here has direct implications for hydrocarbon systems in the sub-Andes. We suggest that the fast deposition of thick red beds of the Sarayaquillo formation likely triggered the first salt movements through sediment loading (Fig. 4.14). Subsequently, regional compression during the Nevadan orogeny may have reactivated salt movements and possibly caused widespread uplift and erosion, resulting in the Base Cretaceous Unconformity.

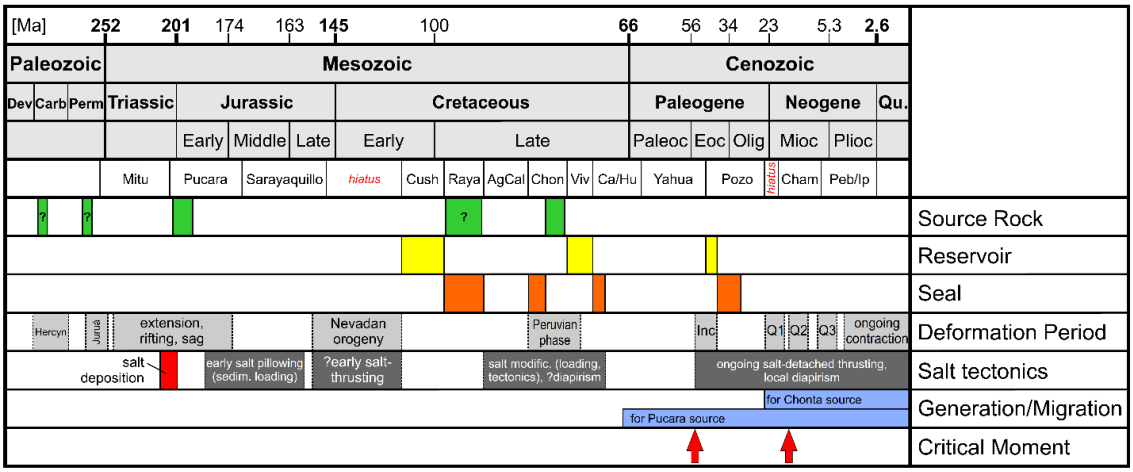

Fig. 4.14: Petroleum systems event chart for the Santiago Basin. The Hercynian, Juruá, Nevadan, Peruvian, Incaic, and Quechua contractional tectonic phases have been adapted from different sources (Megárd, 1984; Rosas et al., 2007; Chalcatana et al., 2012). Presalt units and events are speculative.

Subsequent Cretaceous sedimentation of the Cushabatay, Raya, Agua Caliente, Chonta, and Vivian formations along with the Peruvian compressional phase (Megárd, 1984) during the late Cretaceous likely caused renewed salt movements. We also inferred in our analysis that sedimentary loading related to the deposition of the thick Yahuarango and Pozo formations likely caused further salt flow. With the onset of the Andean orogeny in Peru (e.g., Megárd, 1984), salt movements may have accelerated and culminated in salt-detached, thin-skinned thrusting and diapir squeezing during the Miocene, a process that has continued until the present day.

Regarding possible hydrocarbon source intervals, Encarnación (2008) suggested that a potential Pucara source rock would have reached maturity during the Lower Paleocene; the critical moment for such a source rock is marked by the onset of deformation (and trap deformation) during the Lower Eocene (Fig. 4.14). The assumed younger source rock, the Chonta formation, reached maturity only during the late Oligocene (Encarnación, 2008), and the critical moment here is defined by the formation of traps during the early Miocene. Assuming that pre-Paleocene salt relief had already existed in the basin, west-east directed migration inside the Santiago Basin would have been complicated from this time on and would only be possible via a “fill-and-spill” mechanism. North–south-directed petroleum migration (parallel to the north–south-oriented proto-salt ridges) would, however, involve simpler migration pathways (Rocha et al., 2008). Early salt movements could have also favored early trap formation, potentially catching migration pulses from older, still unproven pre-Jurassic source rocks.

Hydrocarbon seeps in the Santiago Basin, including impregnations and gas seepages, have so far only been documented from areas along and east of the Alto Yutupiz Anticline (Fig. 4.1). This could indicate that presently active migration and remigration occur only in this zone. Several surface occurrences of hydrocarbons correlate spatially with thrust faults, which could reflect preferred migration routes. Where seeps correlate with Cretaceous outcrops, this could be evidence for exhumed source intervals and/or charged paleo-reservoir sections that are being eroded.

4.9 Conclusions

The Santiago Basin in the Peruvian sub-Andes is characterized by the complex interaction of thick-skinned, thin-skinned, and salt-structural styles (Fig. 4.15). Our assessment of the history of the Santiago Basin provides new insight into these structural styles, the kinematic evolution, and implications for the petroleum systems. The thick-skinned system has only been poorly documented

to date, which is mainly due to poor seismic imaging and limited recording depth. The east-vergent Cordillera del Condor, located about 70 km (43 mi) west of the Santiago Basin, however, is a clear expression of a highly uplifted, first-order thick-skinned structure with Proterozoic basement exposed at outcrop level. Our shortening calculations for the thick-skinned system (5.9% and 6.1%, respectively) fall in the same range as previously published values from the Peruvian sub-Andean domain (~3-5.5%). Section restoration indicates that significant pre-Paleogene relief existed across multiple structures in the Santiago Basin, mainly due to pre-existing salt relief (pillows). We did not observe unambiguous manifestations of large flower structures in the seismic data and therefore do not favor a structural model with a dominant strike-slip regime. Our timing analysis of the Santiago Basin confirms that first salt movements likely occurred as early as the middle Jurassic, due to sedimentary loading. Subsequent salt modification throughout the Cretaceous and Cenozoic was caused by a combination of orogenic and sedimentary forces. Salt deformation culminated in salt-detached thrusting, diapir growth, and diapir squeezing in Neogene times and is believed to continue to the present day.

We confirm the presence of salt in the Santiago Basin, as suggested by previous research, but propose a more nuanced view of the salt-related structural styles and the impact of salt tectonics on petroleum prospectivity. We document that high-relief salt pillows preferably occur along a longitudinal zone just east of the Cordillera del Condor (Figs. 4.1, 4.15), whereas farther east—due to less salt abundance—low-relief salt pillows occur. Salt welds are not directly observed (due to low seismic resolution) but are likely to occur below the core of salt-detached synclines—due to salt withdrawal— and also on salt-related thrusts throughout the basin. Sporadic salt diapirs, reaching up to several kilometers in vertical relief, are documented from the eastern flank of the Cordillera del Condor and the basin center. According to the regional evidence of salt-related structures along the Peruvian sub-Andes, the Santiago Basin can be characterized as part of a larger evaporite province, the Peruvian Salt Belt (Fig. 4.13).

Regarding hydrocarbon exploration, we conclude that the early onset of salt flow was favorable for the generation of structural relief in the post-salt plays (Fig. 4.14), potentially capable of entrapping hydrocarbons early on (“old traps”). Structures related to the deeply seated and thick-skinned faults, on the other hand, will be probably located too deep to constitute attractive drilling targets. Salt-cored footwall traps, such as targeted by the Fortuna-1X well, would seem much more feasible, although they may pose operational issues related to mobile shales. At the time of the critical moments for

both source rocks (Pucara and Chonta), significant salt-related structural relief already existed in the Santiago Basin, generating attractive trapping potential.

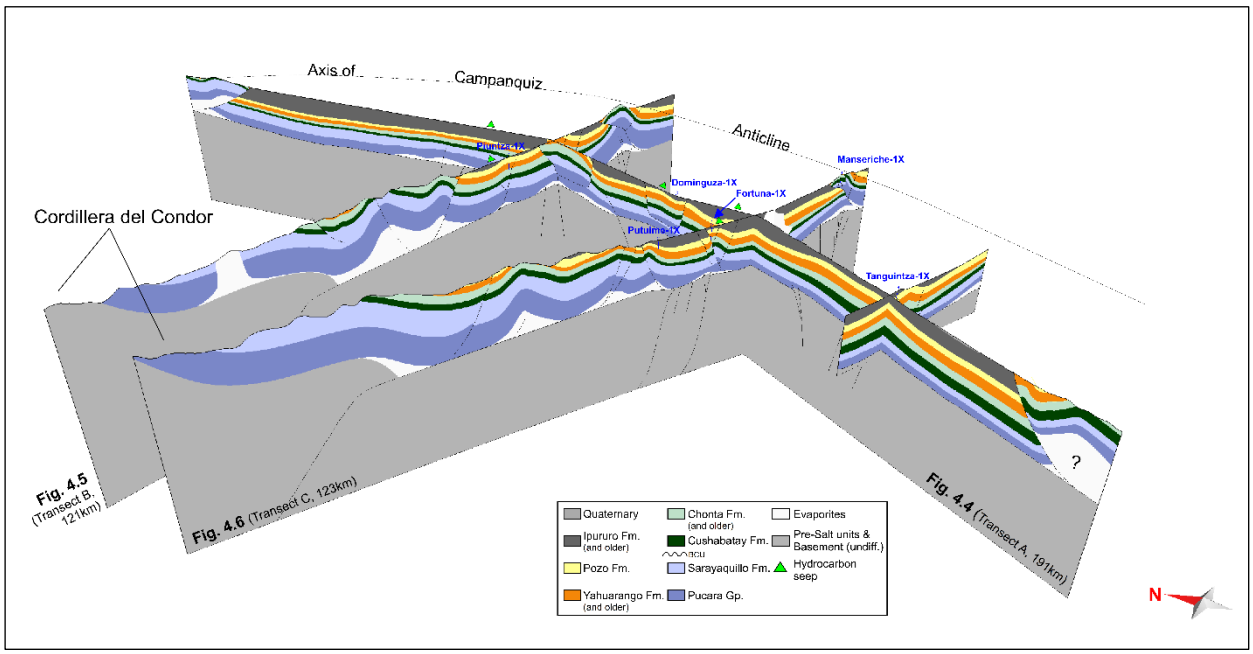

Fig. 4.15: Oblique view of the pseudo-3-D structural model (2x vertical exaggeration, view to the northeast).

Subsequent thrusting through Miocene-Pliocene and recent times increased the breaching risks of prospective structures, as documented by several oil seeps throughout the basin. These observations should be taken into consideration during future exploration efforts.

4.10 Acknowledgements

We would like to express our gratitude to Perupetro S.A. for providing well and seismic data. We are also thankful to M. Rowan for taking the time to discuss aspects of salt tectonics in the data as well as O. Oncken and M. Parra for discussing various aspects of the structural styles and regional Andean tectonics. M. Strecker acknowledges the STRATEGY project funded by the German Science Foundation (DFG project STR 373/34-1) for support. We also thank two anonymous reviewers for their comments, which helped to improve the final version of the manuscript.

5. UNCERTAINTY QUANTIFICATION IN SECTION-BALANCING USING PSEUDO-3D FORWARD MODELING – EXAMPLE OF THE MALARGÜE ANTICLINE, ARGENTINA

5.1 Abstract

Quantifying uncertainty in balancing is an insufficiently resolved challenge. We present a new workflow to assess uncertainty. In contrast to conventional restoration, we focus on forward modeling and mapping uncertainty in solution space. We test the approach by applying trishear as the most appropriate mechanism reproducing associated fault-fold systems. We present a new structural model of the exceptionally well exposed, thick-skinned Malargüe Anticline (=MA), located in the Malargüe Foldbelt (=MFB), Neuquén Basin (=NB), Argentina. Several structural models of varying quality have been published by oil explorers and researchers, but lack detailed kinematic assessment.

To minimize uncertainty, we systematically vary the key modeling parameters “shortening” and “ramp angle” to reduce the cross-sectional area difference, the misfit, between model and observation. We find that the misfit is highly sensitive to these two parameters. The total uncertainty for a single structure w.r.t. these values rarely undercuts 7%. Apparently dependencies exist between these parameters. We recommend this method be extended to other parameter combinations and tectonic settings. Our analysis results in new shortening rates for the MA (up to 1.57 mm/yr) and a refined genetic model, whereby the anticline was generated during Andean contraction, rather than evolving from a pre-existing structure.

5.2 Introduction & Motivation

Geometric-spatial uncertainties represent a significant challenge in the building of balanced cross-sections and different methods have been shown to estimate or even quantify the range of uncertainty in such geometric models (e.g. Victor et al., 2004; Poblet & Bulnes, 2007; Allmendinger et al., 2012; Berthelon & Sassi, 2016). Balanced cross-sections are the result of very different data sources, e.g. seismic data, well data, outcrop data, topography data. Uncertainty is added during acquisition, processing and interpretation of this data with additional uncertainty added by spatially unresolved structures and also by the assumption of plane parallel flow (e.g. Allmendinger et al., 2012, Bond, 2015). Finally, standard balanced section construction as a standard inverse problem mostly relies on restoration using a set of procedures and preservation rules as quality control applying them to the data and rarely resulting in more than a single section. Because of the non-uniqueness of inverse problems based on limited data this provides insufficient information on uncertainties in the solution, or differences therein between competing solutions. Even though numerous sources of uncertainty in structural balancing are known to exist, only very few investigations localize or quantify uncertainty in a precisely calibrated 3D structural model:

Detailed investigation of uncertainty quantification in cross-sections found that the uncertainty related to eroded hanging wall cut-offs is not the main source for shortening error in balanced sections. This component only accounts for about 15% of the error (Allmendinger et al., 2012; Allmendinger & Judge, 2013). The authors identify geometrical uncertainties (shape, thickness) of the pre-contractional stratigraphic wedge as the main cause for error in shortening, causing a portion of up to ~56-70% of the shortening error, which may propagate into a shortening error of up to 8-11% in relation to the overall area balancing, as shown for examples from the North American Cordillera. A new method to quantify errors in balanced cross-sections is presented by Judge & Allmendinger (2011). The researchers highlight the fact that balanced sections are typically based on incomplete data sets (underconstrained) and identify the stratigraphic thickness, depth to decollement and eroded hanging wall cut offs as the main parameters impacting shortening error. The software “AreaErrorProp” presented in their research is based on the parameter “shortening amount” and quantifies the amount of shortening as well as the absolute and relative Gaussian errors, based on vertices defining the circumference of the deformed wedge and the position of the decollement (Judge & Allmendinger, 2011). An increasing number of vertices eventually leads to a saturation of the shortening curve and reduced the error bars. The method is applicable to both, restoration as well as to forward modeling, but is focused on yielding the shortening uncertainty with less information on the structural detail within the section. Recovering the latter is not currently possible with an inverse

approach due to both, the lack of data usually characterizing the geological standard situation, and to the lack of physics-based geometric algorithms that provide a complete description of the deformation. Forward approaches have attempted to explore uncertainty more successfully. Victor et al. (2004) used seismically imaged and predicted stratigraphy. Poblet & Bulnes (2007) employed strain ellipses as markers for misfit minimization between forward model and observation in nature and laboratory.

Here, we focus on extending the approach of misfit minimization to better assess uncertainty in thick skinned structures. The distribution of strain in thick-skinned structures has been investigated exhaustively and there is general agreement about the main drivers controlling the 3D strain distribution within these structures. Key physical parameters controlling strain distribution, depending on the structure type, relate to mechanical-rheological effects within thick-skinned structures (Pei et al., 2014; Hughes et al., 2014), and to the existence of (pre-existing) weakness zones (Endignoux & Mugnier, 1990; Miller et al., 1992; Bergh et al., 1997; Flöttmann & Hand, 1999; Beacom et al., 2001; Cardozo et al., 2003; Hilley et al., 2005; Butler et al., 2006; Amrouch et al., 2010; Caër et al., 2015; Surpless et al, 2015). The impact of modeling parameters, on the other hand, such as variations in the P/S ratio, the trishear angle (Allmendinger, 1998; Cardozo et al., 2003) or the dip of the master detachment has been clearly demonstrated in another set of studies (Hardy & Ford, 1997; Cristallini & Allmendinger, 2001). Some of the remaining problems around the quantification of thick-skinned structures are related to misinterpretations of complex forelimbs due to poor seismic data (Mitra & Mount, 1998) and the general over-simplification of natural conditions (Hilley et al., 2005). To our knowledge kinematic modeling results with consistently analyzed quantifiable uncertainties of thick-skinned fault propagation anticlines, and showing along-strike variations of the structure have not been published.

We, hence, state the key motivations for our analysis: (a) develop a new workflow for uncertainty quantification and to test it on the extremely well exposed thick-skinned MA, (b) to conduct detailed kinematic modeling workflows and to compare different independent methodologies, (c) to document the uncertainty parameters of the deformation (shown here for selected parameters) and (d) to provide new insight into the discussion about the origin of the MA. We present 12 new cross-sections (location see **Fig. 5.1**), based on 30 2D seismic lines, 56 wells, new and proprietary surface geology data, remote sensing data, new kinematic restorations and new shortening rates for the MA.

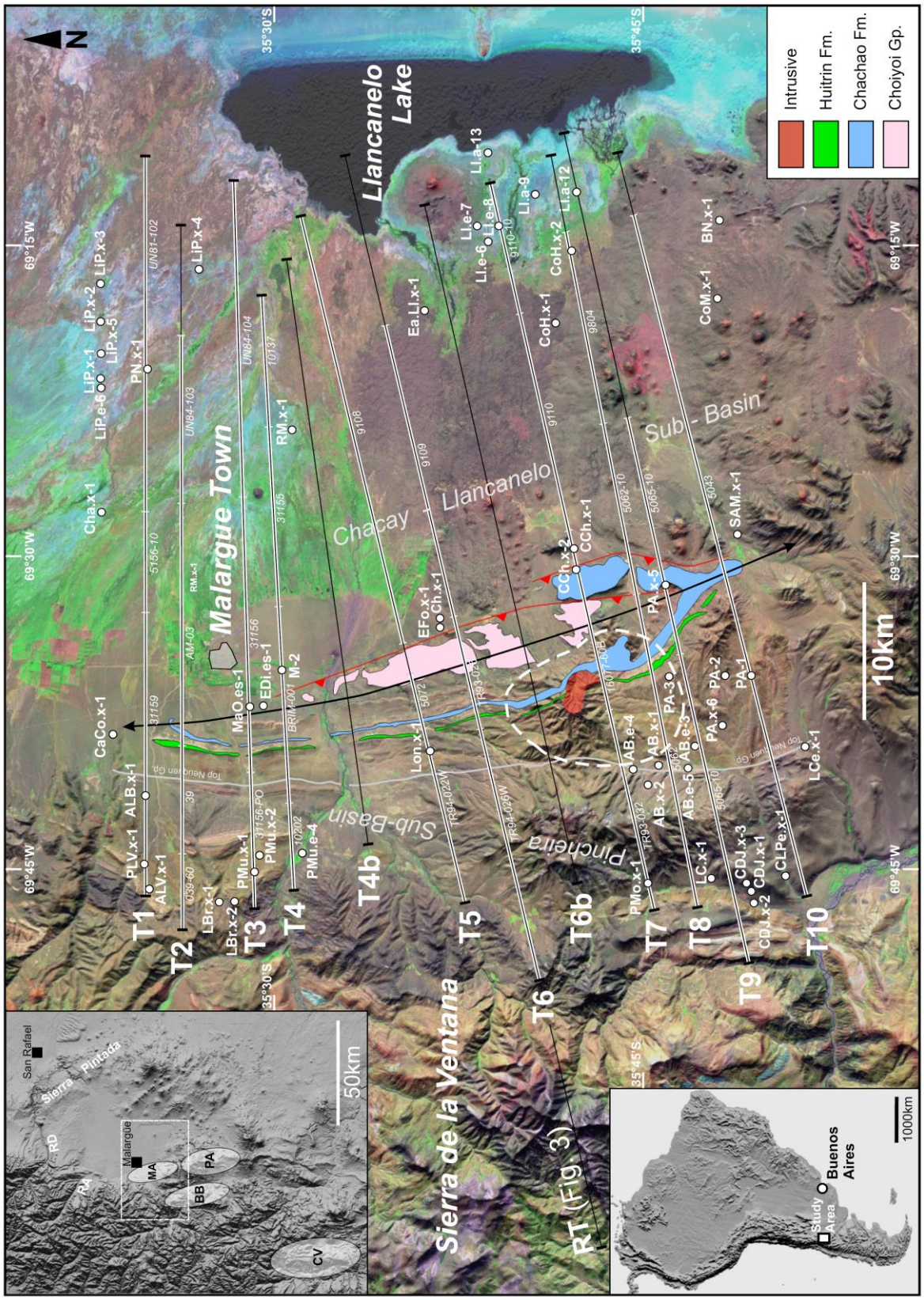

Fig. 5.1: Overview of the Malargüe Anticline and data location. Inset: Location of study area. Dashed white line: area affected by abundant secondary intrusions from main intrusion (sills and dikes). RT = Regional Transect (**Fig. 5.3**). Inset: RD=Diamante River, RA=Atuel River, MA=Malargüe Anticline, BB=Bardas Blancas Anticline, PA=Palauco Anticline, CV=Cordillera del Viento.

5.3 Geotectonic Setting

The study area, the MA, is located in the northern NB, Argentina (**Fig. 5.1**). The NB developed from a series of Permian-Triassic (half-)grabens and later evolved into a Mesozoic back-arc basin that was subsequently overthrust from the west during Andean compression (Vergani et al., 1995). The stratigraphy and the general structural styles of the northern NB are well understood (**Figs. 5.2, 5.3**): in the vicinity of the MA the preserved basin fill varies between 4-5 km and several thin-skinned detachments are known to exist, especially within the shaly and evaporitic units of upper Jurassic and lower Cretaceous age (Auquilco, Vaca Muerta, Huitrin Fms.) (Giambiagi et al., 2008; Yagupsky et al., 2008; Turienzo et al., 2012).

Shortening is still active, even near the center of the NB (Messager et al., 2010) and numerous Cenozoic volcanic complexes exist (Kay et al., 2006). Our study area is located in the thick-skinned MFB of the northern NB (36°S). The exact stratigraphic location of the detachments within the mechanical basement are somewhat uncertain: Due to the general erosional level of the northern NB the intra-basement detachments are not typically exposed at outcrop level, but various authors interpret the position of the sole detachment to be at around 10 to 14 km depth (Manceda & Figueroa, 1995; Giambiagi et al., 2008). There is general agreement that the MFB, of which the MA is part, is a hybrid foldbelt, where thin- and thick-skinned structures and orogenic wedges coexist (e.g. Giambiagi et al., 2009; Giambiagi et al., 2012; Mescua et al., 2012). For the area of the Diamante River (location see **Fig. 5.1**), based on detailed field mapping and balanced cross-sections, Turienzo (2010) concludes that the MFB developed in Mio-Pliocene times and presents deformation ages from 14.8Ma to 2Ma. According to published information, the MFB was contracting in the northern section between 15Ma and ~7Ma (Giambiagi et al., 2009), between 15.8Ma and 6.7Ma at the Bardas Blancas anticline, between 10.8Ma and 8.14Ma at the Palauco anticline, and between 7Ma and 1Ma at the Malargüe anticline where in Late Pliocene to Early Pleistocene times the coherent fold was broken by a series of faults (Silvestro & Kraemer, 2005; Giambiagi et al., 2008; Giambiagi et al., 2009).

Detailed analysis of the structural styles and kinematics of the MA have been provided (Silvestro and Kraemer, 2005; Giambiagi et al., 2009; Giambiagi et al., 2012). At surface level, the structure is about 40km long, 8km wide in the south and 3 km wide in the north, with an east-vergence and plunges to the north and south. Along the fold axis two distinct strike-trends are observed, a NNW-SSE trend in the south and a N-S trend in the north (**Fig. 5.1**). In its core, the Permo-Triassic basement is exposed, consisting in volcanics, volcanoclastics and intrusives (Choiyoi Group) and the sedimentary cover is welded to it; this unit is considered the mechanical basement, due to its brittleness in contrast to the

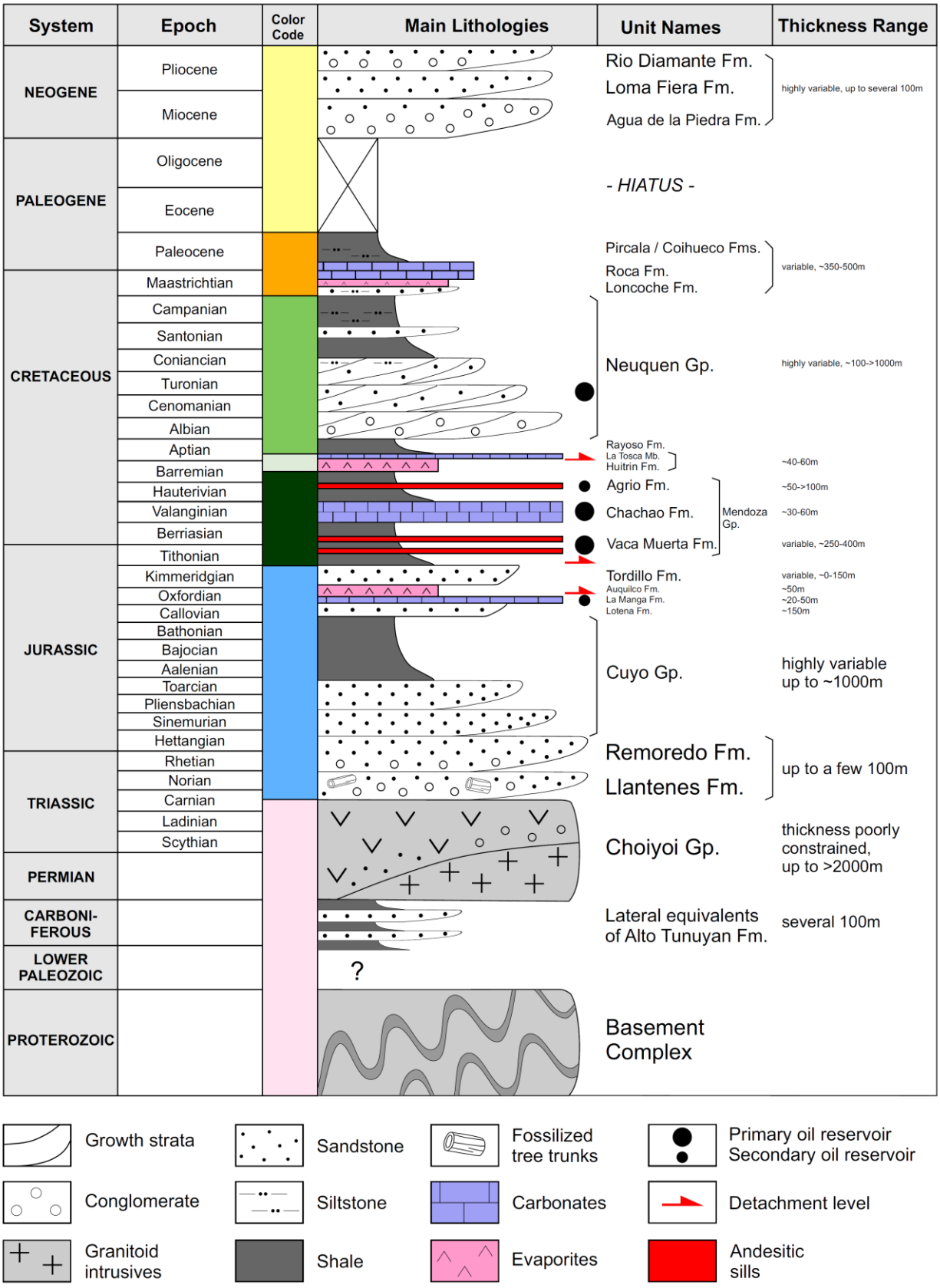

Fig. 5.2: Stratigraphic chart of the greater study area. Compiled from different sources (Giambiagi et al., 2008; Turienzo et al., 2012; Yagupsky et al., 2008).

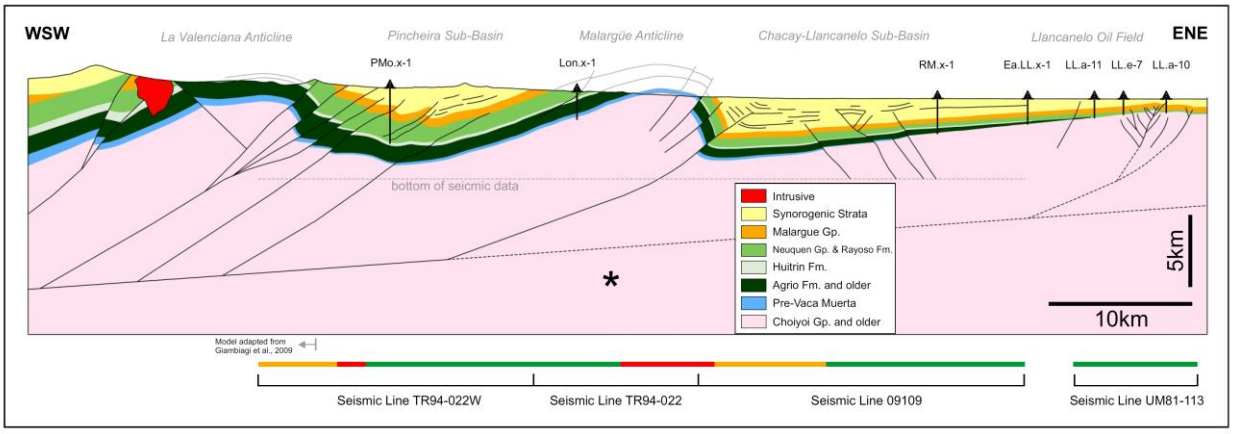

Fig. 5.3: Regional Cross-Section shows the key structures in the study area. Asterics indicates approximate longitudinal and vertical position of the nearest shallow seismic event recorded in the area since 1975, a M=3.6 earthquake in the Sosneado area. Colour bar indicates seismic data quality (green = good, orange = medium, red = poor). For location of transect see **Fig. 5.1**.

sedimentary cover. It does, however, not represent the Precambrian crystalline basement which comprises a very different composition and is also located much deeper with the exact position of the interface unkown (Manceda & Figueroa, 1995; Silvestro & Kraemer, 2005; Giambiagi et al., 2009). Regarding the forelimb of the MA, we confirm the observation made by previous authors that the master thrust at the MA does not reach the surface (Silvestro & Kraemer, 2005; Giambiagi et al., 2009) (**Figs. 5.3, 5.4**). According to our observations the master thrust partially dissects seismic reflectors within the Neogene section, but does not penetrate the surface and is therefore considered a blind thrust. Regarding the backlimb, some authors show that this part of the MA is generally very gently deformed (Giambiagi et al., 2009; Silvestro & Kraemer, 2005) and that no basement-cover detachment occurs there (Giambiagi et al., 2009). We confirm that the backlimb is indeed generally very gently deformed, just slightly rotated, but we would contradict in that we do observe local basement-cover detachments on the backlimb. This is clearly documented by seismic and well data around the Agua Botada oil field (**Fig. 5.5**, transects T7, T8. T9). These local thin-skinned thrusts are not very pronounced in terms of structural relief and transport but they are clearly present and accommodate some of the thin-skinned contraction. The interaction of basement and cover has been examined in a detailed way and a broad spectrum of basement-cover interaction mechanisms have been described (Turienzo & Dimieri, 2005; Giambiagi et al., 2009). Messager et al. (2012) reveal evidence that the Meson and Sosneado thrusts (~50 km north of MA), based on terrace age dating at the Atuel River, indicate active thrusting between Mid- and Late Pleistocene (**Fig. 5.1**). Documented shortening rates are 0.5mm/yr for the MA (Giambiagi et al., 2009) and 0.4mm/yr for the Diamante River area (Turienzo,

2010). A vigorous scientific debate is ongoing about the question whether the MA is a newly formed structure that was generated during Andean contraction or if it formed as an inversion feature above pre-existing normal faults. Some authors favor a model of inverted pre-existent extensional faults (Giambiagi et al., 2009; Dimieri & Turienzo, 2012; Mescua & Giambiagi, 2012), while Mescua et al. (2012) favor a more differentiated model where the dominant process is that of inversion of pre-existing extensional system, combined with the generation of new faults related to the recent contraction. On the other hand, Turienzo (2010) concludes that at the Atuel and Diamante Rivers clear evidence for tectonic inversion is not observed.

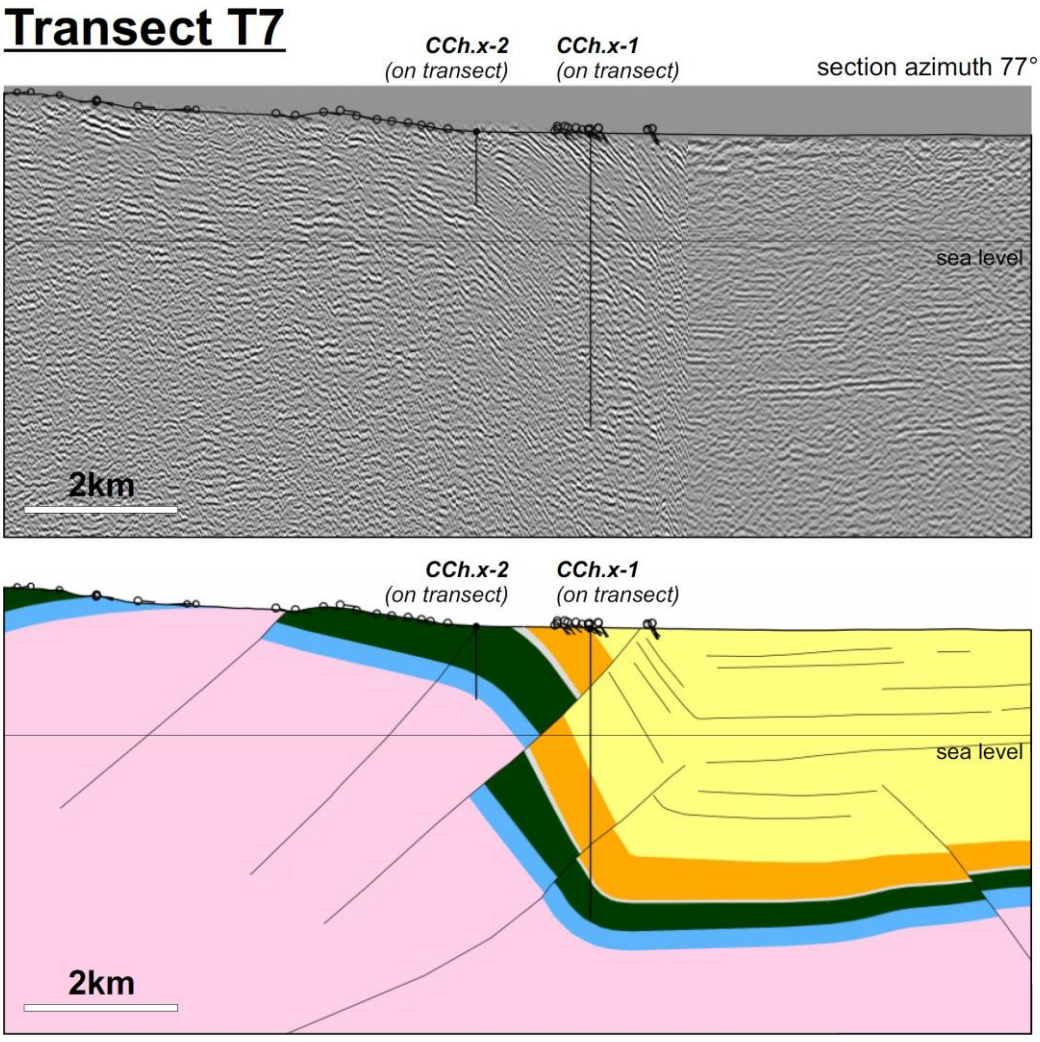

Fig. 5.4: Detail of Transect T7, showing data situation (above) and structural interpretation (below) near the fore limb of the MA. True-dip section. See **Fig. 5.1** for location.

Previous workers have shown that the key factors controlling the kinematics of the MA are the competence contrast between basement and cover, the composition and fabric of the basement, the

strength and degree of mechanical anisotropy, the presence and thickness of growth-strata and the geometry of the basement master fault (Giambiagi et al., 2009). Furthermore Mescua & Giambiagi (2012) concluded that the inversion of major Mesozoic normal faults during Andean compression may have contributed significantly to uplift and deformation; the authors state that the stress-field orientation is suitable for the inversion of Mesozoic normal faults.

However, no clear definitions have yet been provided about which rocks are defined as the crystalline basement, the economic basement and the mechanical basement. This is mainly due to the poorly known deeper stratigraphy: the oldest rocks cropping out – or reached by drilling – in the vicinity of the MA are of Permo-Triassic age (Choiyoi Group). Older units crop out at the Sierra Pintada and at the Cordillera del Viento (locations see **Fig. 5.1**). At the Cordillera del Viento recent research confirmed the presence of ~2200m thick Carboniferous strata in outcrop, while Precambrian crystalline basement was not documented there (Llambias et al, 2007; Giacosa et al., 2014). At the Sierra Pintada, Manassero et al., (2009) report ~3050m of pre-Choiyoi strata, mostly Ordovician, Siluro-Devonian and Permo-Carboniferous clastics, resting unconformably above a Grenvillian age crystalline basement (1.2GA).

5.4 Database & Methods

The following data was used for the construction of the structural models: digital terrain data (NASA DEM, 90m resolution), satellite imagery (Landsat Thematic Mapper, 30m resolution), surface geological maps (1:50.000), air photos covering the anticline (resolution ~3m), a total of 541.3 kms of 2D seismic (30 lines, 1970s-1990s vintage) and 56 wells (well reports, formation tops, partial log data). The wells reach a maximum of 2500m below sea level (~3980m below terrain). Precise information on stratigraphic thicknesses was obtained through detailed outcrop mapping. Based on the dense data situation, stratigraphic thicknesses at surface level and down to about 2500m below sea level are considered to be very precise. Eroded hanging wall cut-offs at the MA are considered to involve a larger uncertainty. The quality of the seismic data varies significantly across the study area. Most of the seismic data is considered moderate to poor, locally good in quality but the core of the MA remains seismically unresolved (**Fig. 5.4**). A total of 12 cross-sections were constructed across the MA (**Figs. 5.5, 5.6**), to capture the structural styles and to represent the along-strike variability of its geometry (transects T1, T2, T3, T4, T4b, T5, T6, T6b T7, T8, T9 and T10). The support transects T4b and T6b are based on surface geology, topography data and data from adjoining transects (no nearby seismic

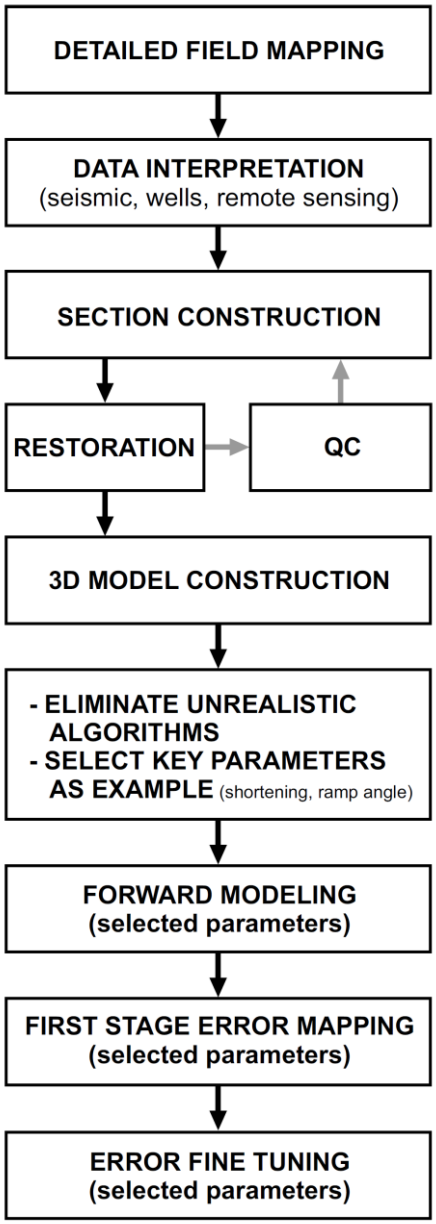

Fig. 5.5: Work flow used in this paper.

available). Transects T6b, T7, T8 and T9 are located in an area with very thick volcanics on the backlimb (dashed outline in **Fig. 5.1**). The location of the transects was very carefully chosen to ensure the availability of nearby and suitable 2D seismic data and wells. Wherever possible, the transects were constructed as closely as possible to the wells and seismic lines and wells were always projected on-strike, to minimize projection distance.

Conventional restoration of the interpreted seismic lines was used initially to constrain the basin fill geometry. This served as a starting model and basis for the subsequent forward modeling.

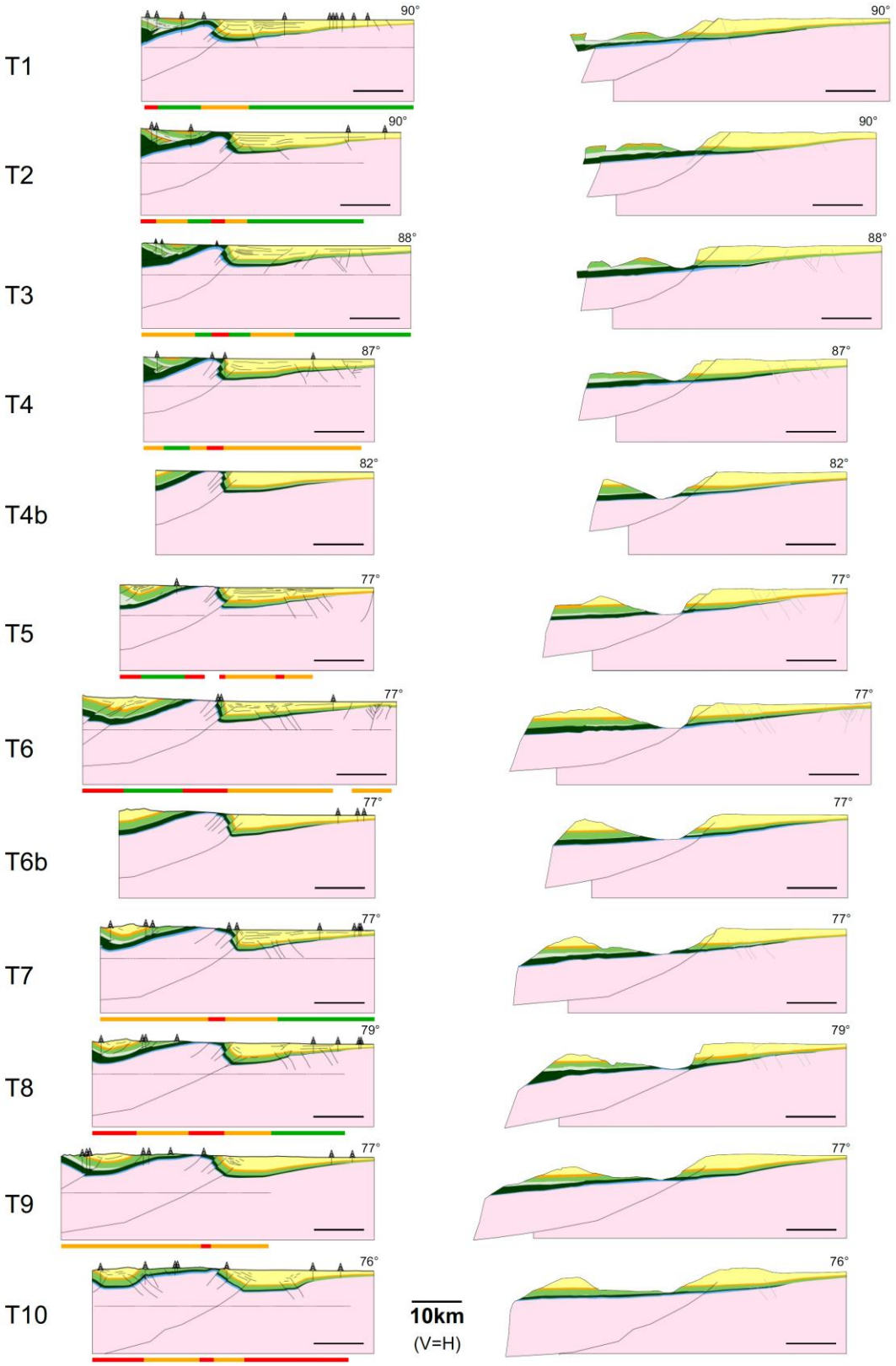

Fig. 5.6: Serial transects across the MA (see Figs. 1, 2 for location and stratigraphic color code). The strike azimuth of each section is indicated. Scale bar inside each section = 10km. Colour bars indicate seismic data quality (green=good, orange=medium, red=poor).

We base forward modeling on a number of key conditions. These are: (a) preservation of area, (b) plane strain, (c) strain compatibility and (d) kinematic modeling is limited to observable ("mappable") structures only. Additionally, forward modeling requires a reliable and geometrically well-defined marker horizon that can be consistently observed in surface and subsurface data. The marker of choice for the MA was the Top Choiyoi Gp. which satisfies these requirements. Kinematic section balancing was conducted by using state-of-the-art structural modeling software (MOVE 2019.1). Field observations at the core of the MA revealed that most deformation at the Choiyoi Group level appears ductile. Initial forward modeling runs quickly revealed that certain algorithms, such as simple shear or fault-parallel flow, produced unrealistic (non-geological) geometries for the overall shape of the MA (**Fig. 5.7**), even when widely varying key modeling parameters. Hence, these algorithms were eliminated from the analysis. Subsequently the trishear algorithm was identified – under a forward modeling workflow – to deliver the most similar geometries to the present-day situation. This algorithm was also found by previous authors to best represent the natural geometries at the MA (Giambiagi et al., 2009).

The trishear algorithm depends on a number of additional parameters that need to be defined for each modeling run, these are: trishear angle, trishear angle offset, trishear apex, propagation/slip (P/S) ratio, angular shear, number of trishear zones and fault tip position. In summary, the forward kinematic workflow was conducted in two phases: (I) Identification of the trishear algorithm as the appropriate algorithm for this setting and defining the trishear parameters; (II) Detailed uncertainty analysis using the trishear parameters defined during (I). Forward modeling test runs immediately revealed that very small variations of some of the trishear parameters resulted in highly unrealistic fold geometries (**Fig. 5.7**). These parameters were tested during a number of initial forward modeling runs, to obtain geometrically realistic results and, hence, to exclude certain parameters (and parameters ranges) from the subsequent workflow. The trishear parameters which were excluded from the workflow can be separated into two groups: (1) the ones that even upon minor variations result in non-geological (highly unrealistic) fold geometries (trishear angle offset, P/S ratio, fault tip position) and (2) the ones that upon minor variations result in approximately geological geometries, but nevertheless are extremely different from the observed geometries at the MA (trishear angle, trishear apex, angular shear, number of trishear zones). Based on the initial test runs, it was concluded to set the trishear angle to 98°, to set the trishear angle offset to 55°, to set the trishear apex to neutral, to set the P/S ratio to 0, to set the angular shear to -17°, to set the number of trishear zones to 1 and to set the fault tip position to neutral (0 km).

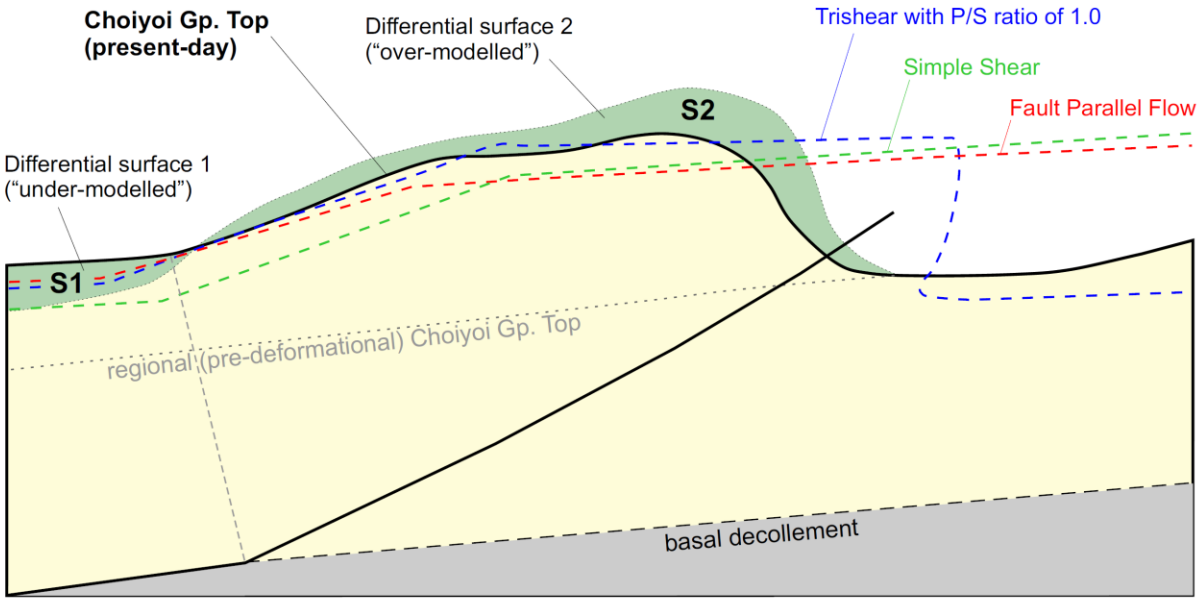

Fig. 5.7: Sketch illustrates differential misfit area (green) between present-day Top Choiyoi Gp. (top of yellow polygon) and "over-balanced" Top Choiyoi Gp., obtained through forward-modeling from regional (grey dashed line). S1 + S2 = total differential area used for statistical uncertainty evaluation. Algorithms, producing unrealistic geometries, such as Simple Shear (green), Fault Parallel Flow (red) or Trishear with a Propogation/Slip ratio of 1.0 (blue) were eliminated empirically from the work flow.

These parameters were then kept constant throughout the workflows. In order to understand how sensitive the end result of the forward models are, ramp angle and shortening were systematically varied (see below). Misfit curves were generated, showing the misfit between observed and modeled marker horizon (see above), enabling us to detect the uncertainty minima in each transect (**Figs. 5.8, 5.9**). 71 Scenarios with variable shortening and 56 scenarios with variable ramp angles were run. In this study we define "error" as the disagreement between a measurement and the true value (which can have numerous sources, such as the actual measurement, data processing and interpretation). We use the "misfit" as a measure to quantify "uncertainty". Uncertainty contains several sources of error, resulting from assumptions about the modeling conditions, heterogeneity of deformation etc. (e.g. ISO, 2008). The present-day magnetic declination of the study area is around +1.5° (British Geological Society website, 2019) and due to this very low value (well below the precision of a typical geological compass), the field measurements were not corrected.

5.5 Structural Styles

From north to south, 12 cross-sections reveal the asymmetric structural architecture of the MA (**Fig. 5.6**). A relatively simple, ~20 km long and monoclinal backlimb forms the western part of the structure

and from transect T7 on southwards starts to reveal a minor kink, located above the foot of the basal ramp in the subsurface. The crest of the MA at the Choiyoi Gp. level is a relatively narrow feature north (~2-3 km wide), gradually increasing in width towards the south. In the southern cross-sections (T8 to T10) the crest becomes increasingly broad and the overall anticline takes on a "box-like" geometry. Observations from seismic data, well data and geometric constraints reveal that the forelimb dip varies from north to south: the dip increases from 41° in the northernmost section to about 72-73° in the central sections (T4b and T5). From there on it gradually decreases towards the south to reach maximum dips around 37° in the very south. It is also dissected by two to three secondary faults sub-parallel to the master fault. Mounted onto the backlimb in the northern sections T1 to T5 is a thin-skinned duplex-system which has been well documented by the wells of the small Puesto Muñoz and La Brea oil fields. There the basal thrust system of this duplex unit detaches in the plastic shales of the Vaca Muerta formation, which is tectonically thickened in this area. The passive roof detachment is located at a higher stratigraphic level, at the evaporitic base of the Huitrin formation (La Tosca member). This passive roof detachment causes significant westward backthrusting and decoupling of the overlying strata, but is not developed in the southern sections. T7, T8 and T9 show some minor thin-skinned thrusting detached in Vaca Muerta shales, but no backthrusting. The underlying basement-seated master thrust at depth shows measurable geometric variation from north to south: The ramp dip angle varies between 27° in the northern sections (T1, T2, T3), then decreases towards T6 and T6b where it reaches 19°. It then increases again towards the south to reach 28° at T10. In all positions the master thrust cuts through and dissects the apex of the frontal syncline of the MA. Growth strata related to the master thrust are observed in different positions along the structure, but seem to be most pronounced in the north (sections T1 to T4).

5.6 Uncertainty quantification analysis

To demonstrate the workflow of uncertainty mapping, we selected two critical parameters, "shortening" and "ramp angle". Judge & Allmendinger (2011) demonstrated that in shortening analysis an increasing number of polygon-vertices eventually leads to a saturation of the shortening curve and reduced error bars. One of our key intentions here was to compare the error analysis for the geometrically extremely well constrained MA with their error quantification.

5.6.1 Uncertainty quantification curves – variable shortening

Under constant ramp angle forward modeling was conducted for each transect, with increasing amounts of forward-shortening and for each case the misfit surface between the observed and

forward-modelled Top Choiyoi was recorded (according to definition set in Chapter 1 Introduction & motivation). After reaching a minimum misfit, forward modeling was continued until the misfit area started increasing again, hence, making sure to map the minimum with confidence. For each transect the misfit is expressed in % (km^2 of differential surface in relation to the reference area) (**Fig. 5.7**). The overall shortening used in the forward modeling experiment ranges from just over 2000m (for transect T1) to around 12.000m (for sections T6b and T7) (**Fig. 5.8**). It also becomes clear that most of the uncertainty minima fall into a range of around 1.5 to 4%. Sections T6b and T7 are located near a major volcanic center and are believed to be affected by greater model uncertainty. They reveal a higher minimum uncertainty of just above 7%.

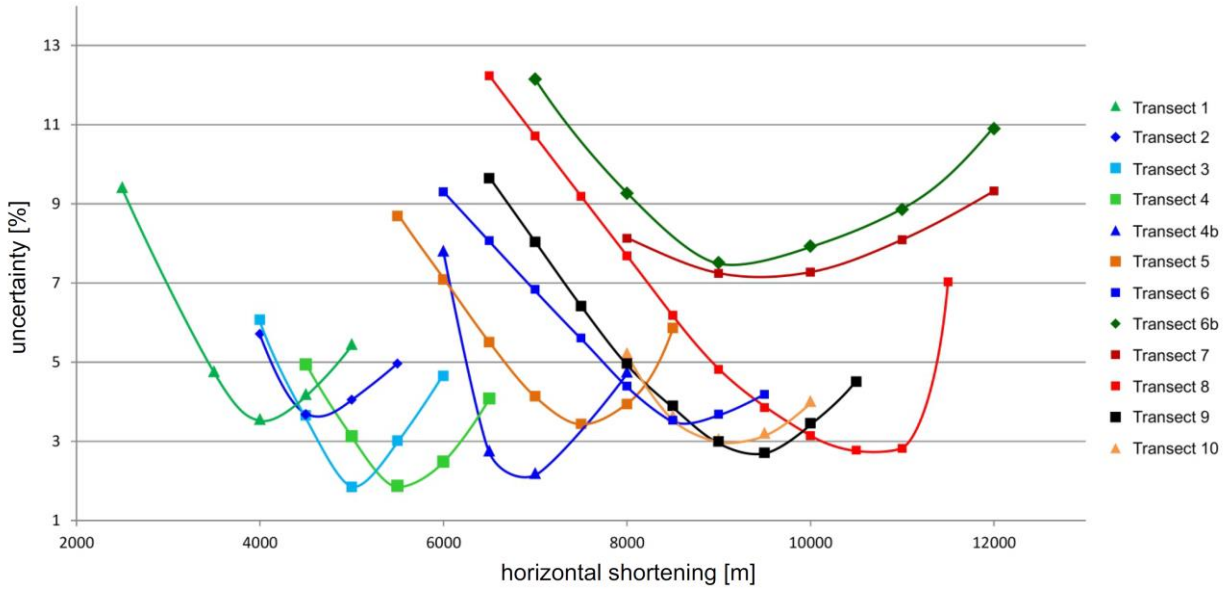

Fig. 5.8: Graphs showing uncertainty minima for variable "shortening" of all 12 transects. Uncertainty is expressed in % (km2 of misfit area in relation to reference area).

5.6.2 Uncertainty quantification curves – variable ramp angle

In order to test the model for the sensitivity of the ramp angle, a second set of modeling scenarios was run. This time using the shortening obtained from the previous variable shortening runs and keeping the shortening constant. The ramp angle was varied systematically. By increasing the ramp angle and recording the differential surface, an uncertainty minimum was established for each transect (**Fig. 5.9**). During the experiment the overall ramp angles were varied between 15° (central transects T6 and T6b) and 29° (northern transects T3 and T1). The majority of the minima of the uncertainty curves for each transect fall into a range of around 1.5% to 3.5%. However, for transect T7, which is located near a major volcanic center (greater model uncertainty), it was not possible to reduce the uncertainty minimum to below ~9%.

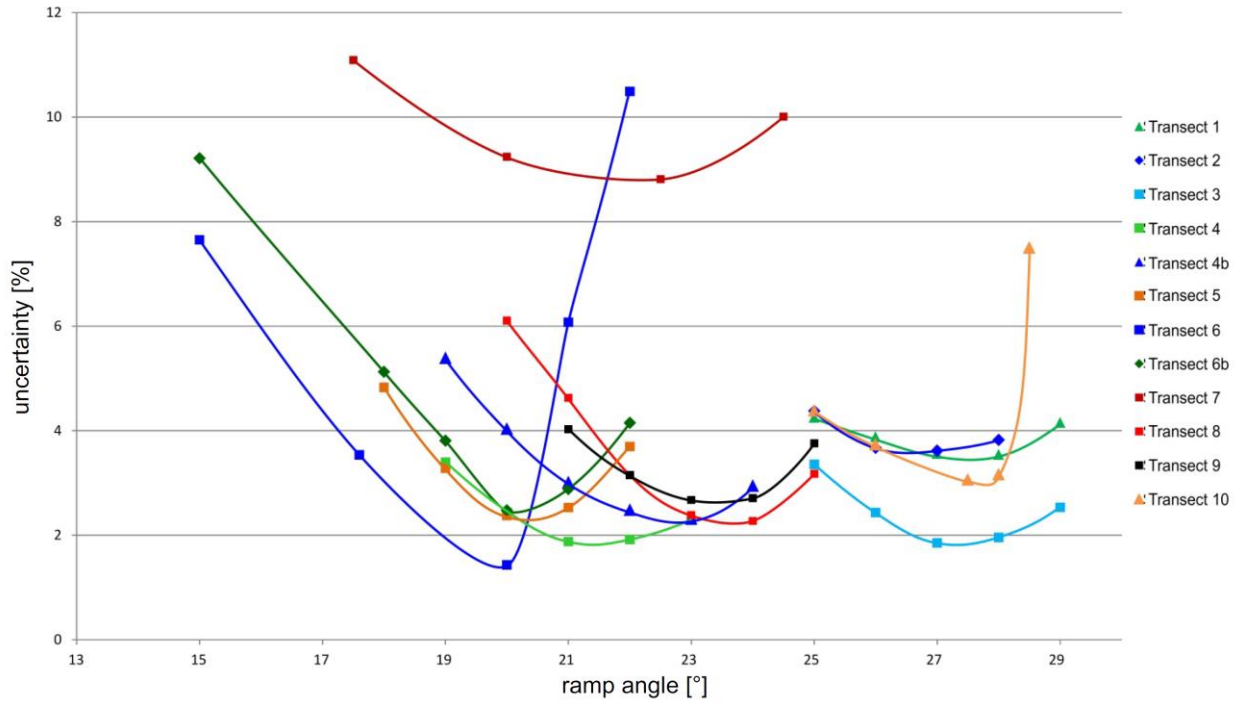

Fig. 5.9: Graphs showing uncertainty minima for variable "ramp angle" of all 12 transects. Uncertainty is expressed in % (km2 of misfit area in relation to reference area).

5.6.3 Uncertainty fine-tuning & Indications of Dependencies

To further fine-tune the minimum uncertainties, 288 forward models, with varying shortening and ramp angle, were run (between 21 to 42 per transect, using only transects with seismic data). A number of cross-plots were generated around the previously identified uncertainty minima (**Fig. 5.10**). For the northern transects T1, T2, T3 and T4 these plots exhibit rather confined uncertainty minima which fall into small and well-defined parameter ranges, creating slightly elongated "bulls-eyes" (blue and lilac colors in **Fig. 5.10**). Different degrees of elongation of the uncertainty minima are indicative of different degrees of influence of the variable parameters, i.e. dependencies. More elongated (oval) minima indicate a less defined solution and less dependency of the resultant uncertainty on that parameter. For the central and southern transects T5, T6, T7, T8 and T9 the uncertainty minima are less constrained and the cross-plots show rather elongated areas of minima. The southernmost transect T10 again exhibits a more confined, yet still elongated, shape of the uncertainty minimum area. Even though the uncertainty minima fields exhibit different degrees of elongation in the cross-plots, the variations of the two selected parameters (ramp angle and shortening amount) and the resulting uncertainty are in the same order of magnitude.

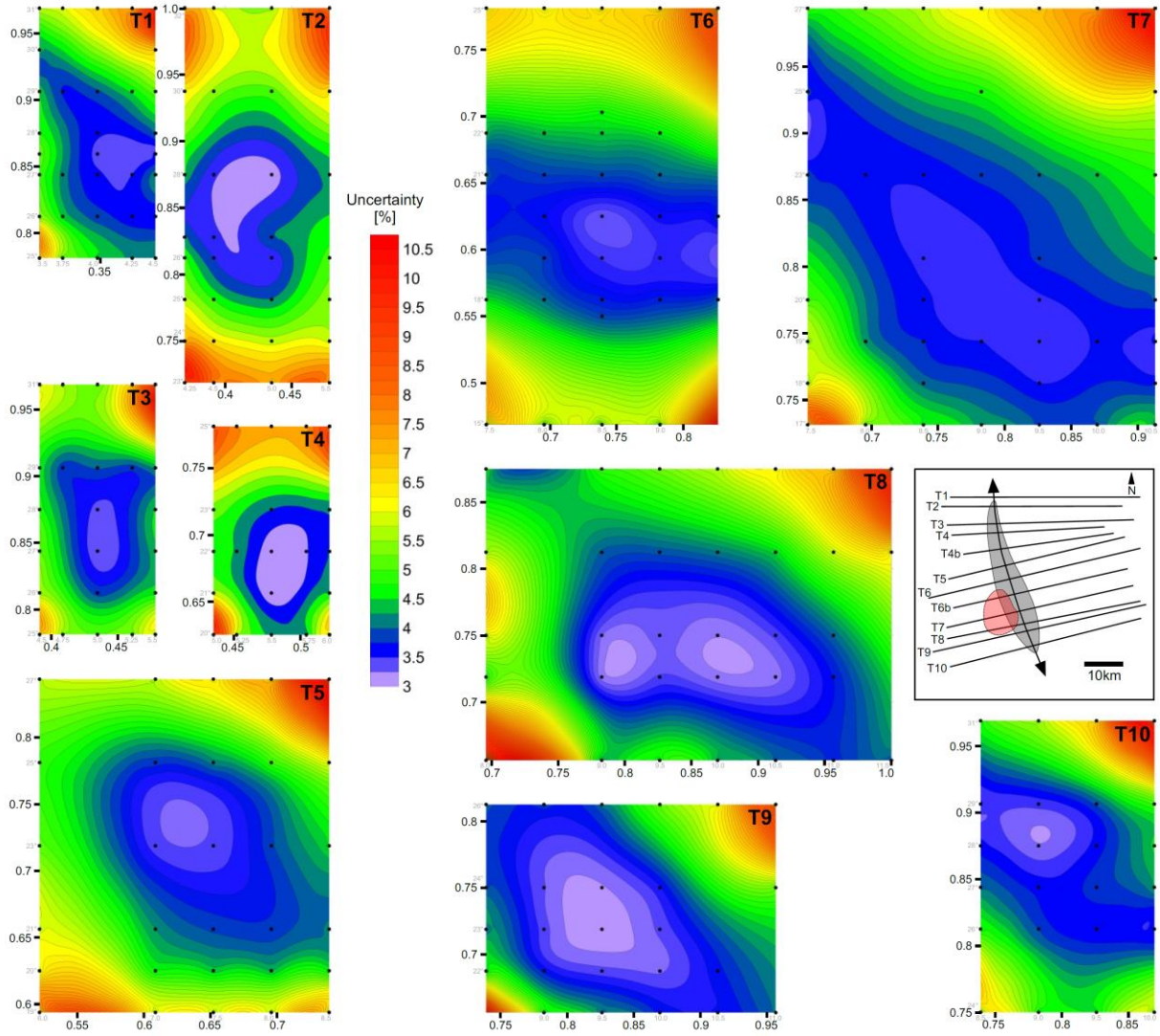

Fig. 5.10: Cross-plots showing uncertainty fine-tuning. X-Axis: Horizontal shortening expressed as relative value to maximum shortening observed in data set (absolute values in grey, [km]). Y-Axis: Ramp angle expressed as relative value to maximum ramp angle observed in data set (absolute values shown in grey, [°]). Colour coding = modeling error [%]. C.I. = 0.25%. Black dots represent data points for each modelled scenario. Map: transect locations with respect to MA Anticline, red=occurrence of volcanics.

The cross-plots reveal that for variations of shortening and ramp angle of ±5% the model uncertainty can be kept below 3%, generally. These results indicate that in several cases, by varying the two selected parameters “shortening” and “ramp angle” alone, a sharp uncertainty minimum cannot be found, an observation that hints at a dependency between these two parameters. Another explanation for poorly defined uncertainty minima, especially at transects T6b and T7 could be related to the presence of a large Miocene volcanic complex (particularly T7) and less well control, resulting in larger geometric model uncertainties there (**Fig. 5.1**). As mentioned above, the influence of the

other trishear-related parameters (trishear angle, trishear angle offset, trishear apex, P/S ratio, angular shear, number of trishear zones and fault tip position), were not analyzed systematically, as their influence on the outcome is so strong that even small variations very quickly result in very large and/or unrealistic deviations from the present-day fold geometries.

5.6.4 Global Uncertainty Maps

A number of parameters from the forward modeling, for which the model is highly sensitive, were eliminated from the workflow (e.g. trishear apex, trishear angle, P/S) (**Fig. 5.7**). Two selected parameters to which the model is sensitive were established as the key drivers: shortening and ramp angle. To further test the dependence or independence of these two parameters, the workflow of choice was to generate global uncertainty maps (cross-plots), one for the scenario "variable shortening" and another one for the scenario "variable ramp angle" (**Figs. 5.11, 5.12**). For all transects, a total of 71 scenarios were modelled with varying shortening, and 56 scenarios with varying ramp angle. The horizontal axis shows the variance of the modelled parameter (increasing shortening or ramp angle), the vertical axis represents a standardized geographic position for the data points of each transect (northern transects are plotted at the top and southern transects at the base of the map). As a third dimension, the actual uncertainty (in %) is assigned to each data point, gridded and contoured, thus visualizing areas of reduced or increased uncertainty for all transects. The global uncertainty map for variable shortening reveals that the minima for the northern and central transects T1 to T6 are consistently lined up in a "valley" where uncertainties are 1% to 4% (blue colors in **Fig. 5.11**). For transects 6b and 7, where the minimum uncertainties are higher than in the other transects, the map reveals a "saddle" with errors above 7% (green colors in **Fig. 5.11**). The three southernmost transects T8, T9 and T10 again exhibit lower minima, around 3% to 4% (blue colors). The southern transects T8, T9 and T10 again show low minima, aligned in a "valley" (blue colors), with no more than 3% minimum misfit. For the variable "ramp angle" a similar picture emerges (**Fig. 5.12**), where the northern and southern sections exhibit a consistent valley (with values around ~2-4%). At section T7, however, larger minimum uncertainties are observed (~6-7%), forming a "saddle" in the map.

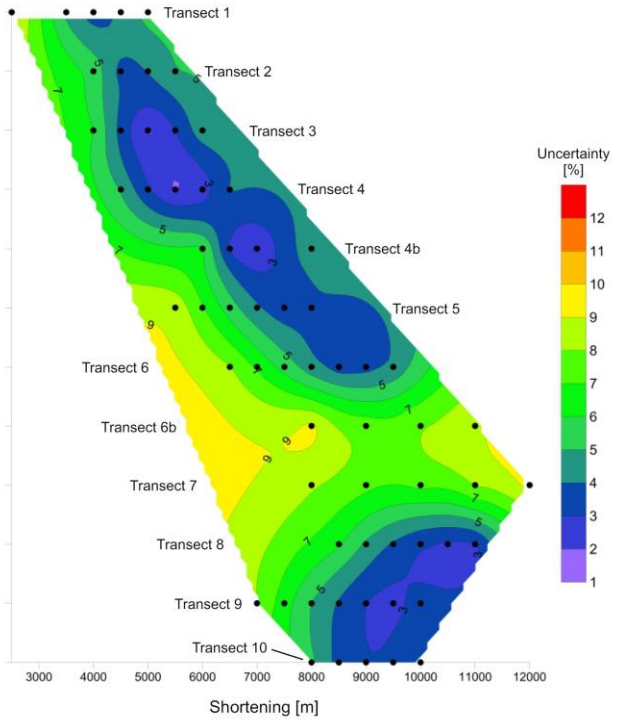

Fig. 5.11: Global uncertainty map for the variable "shortening". Vertical axis = standardized position of each transect.

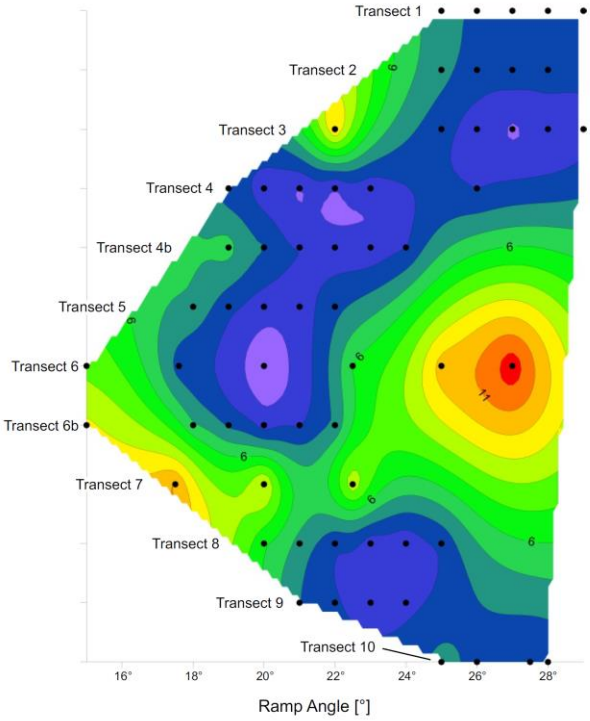

Fig. 5.12: Global uncertainty map for the variable "ramp angle". Vertical axis = standardized position of each transect.

5.7 Discussion

5.7.1 Boundary Conditions & Sources of Error

Initially, a number of trishear modeling parameters were excluded from the workflow based on a number of empirical test runs covering a range of variations. The criteria for exclusion were based on how realistically the forward modeling would reproduce the observed MA, even under minor variation. Based on the comparison between the forward model and the pseudo-3D model of the MA built here, the outcomes of these parameters can be categorized into two groups (a) non-geological (b) geological, but extremely different from the MA geometry. Minor variations of the parameters trishear angle offset, P/S ratio, fault tip position produced highly unrealistic (non-geological) fold geometries, while the parameters trishear angle, trishear apex, angular shear and number of trishear zones resulted in geological yet extremely different geometries from the observed MA. Further research would be required to establish a full and detailed "impact hierarchy" of these parameters.

One of the key findings regarding parameters controlling the outcome of contractional deformation is the correct assumption of the conceptual model, the structural styles and their evolution (Endignoux & Mugnier, 1990; Bond et al., 2007; Groshong et al., 2012; Woodward, 2012; Berthelon & Sassi, 2016). There is broad agreement that uncertainties in geometry (e.g. thickness, dip) of the stratigraphic taper in a given basin is a first-order parameter in exerting control on the outcome of kinematic deformation, such as the localization and spacing of thrust systems and the magnitude of internal shortening and, hence, has to be as well constrained as possible to obtain robust results in structural-geometric reconstruction (Endignoux & Mugnier, 1990; Boyer, 1995; Artoni & Casero, 1997; Butler et al., 2006; Buiter, 2012; Moretti & Callot, 2012; Smart et al., 2012; Allmendinger & Judge, 2013). Another parameter, the influence of the basal detachment, has been studied intensely in the past and authors coincide in that the location, the geometry (trajectory) and properties have a major impact on the uncertainties in the resulting models (Chalaron et al., 1995; Brooks et al., 2000; Graveleau et al., 2012). We acknowledge that the location and trajectory of the basal detachment at the MA also represents a large source of uncertainty. Based on the highly constrained 3D structural model of the MA (which is the result of dense multi-scale, as well as new proprietary outcrop data), backward and forward kinematic modeling and thorough uncertainty analysis of selected parameters, we confirm that the MA represents a fault-propagation fold (as discussed in e.g. Giambiagi et al., 2009). We argue, however, that the MA represents a highly evolved fault-propagation fold where the master thrust partially dissects the foreland syncline.

The largest errors here are associated with the deep subsurface, where neither wells nor seismic data allow for precise calibration, namely the exact position and trajectory of the basal detachment. No well has penetrated the flat portion of the decollement and it also located too deep to be represented correctly by seismic data. Here horizontal and vertical errors of up to several thousand meters have to be assumed. However, the spatial location of step-up point of the ramp (where the ramp departs from the regional detachment) can be constrained by the dip change in the back-limb ('return to regional', i.e. dip domain change from "steep" to "flat") and the geometric position of the regional detachment (**Figs. 5.3, 5.7**). Nevertheless, the exact location and angle of the basal detachment have to be considered a significant source of uncertainty for the static and kinematic models. General control on stratigraphic thicknesses here is considered excellent, due to the large number of bore holes throughout the study area (56 wells), the detailed surface geological mapping (in strike and dip direction across the anticline) and the additional support of air photos with a horizontal resolution of ~3 meters.

5.7.2 Method by Judge & Allmendinger (2011)

We use two independent methods to determine the shortening across the MA, firstly a commercial structural restoration software (MOVE 2019.1). Secondly, and to compare our results, the shortening was calculated by an independent method, utilizing the software AreaErrorProp 3.1.0 (Judge & Allmendinger, 2011) (**Fig. 5.13a**). Each software calculates the shortening in a completely different manner. While MOVE obtains the shortening amount through displacement vectors of particles, AreaErrorProp uses polygons which are defined by increasing numbers of nodes to asymptotically narrow down a saturation value for the shortening.

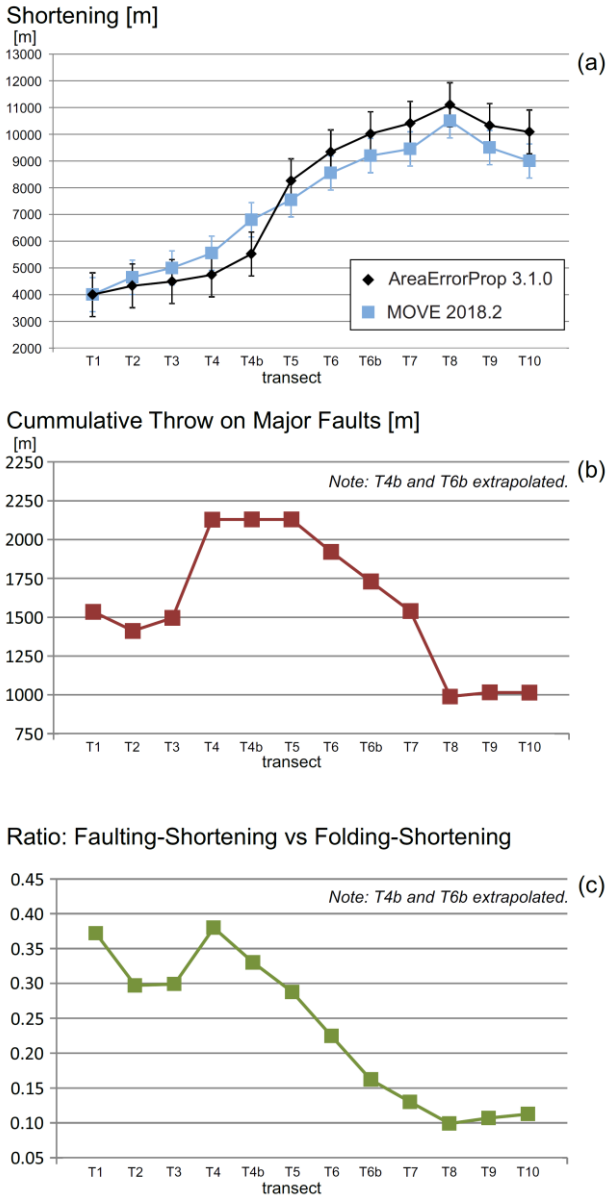

Fig. 5.13: Fold parameters along the MA, obtained from kinematic modeling (see text for more details).

For each transect forward modeling was carried out for the top of the Choiyoi Group as a reference horizon. The results for the calculation of shortening between both methods are almost identical (**Fig. 5.13a**).

This high degree of coincidence between two completely independent methods confirms the model robustness. Error bars of +/-10% are indicated, as the majority of the uncertainty values in this study falls within this range (these errors result from spatial uncertainties in the position of the nodes defining the polygons). It becomes apparent that the shortening varies significantly across the MA, as follows: The smallest amount of shortening is found at the northernmost section T1 where the contraction equals 4.0km, while the highest shortening is observed at transect T8 where the amount is 11.0km. The cumulative throw on major faults, indicative of the amount of brittle shortening, also exhibits along-strike variation, whereby the highest throws are observed in the central portion of the MA, between transects T3 and T5 (**Fig. 5.13b**). The ratio of faulting-related shortening versus folding-related shortening generally decreases from north to south (**Fig. 5.13c**), indicating that the shortening in the northern segment of the MA (~T1 to T4b) is accommodated by more brittle deformation, while in the south the shortening is related to more ductile deformation (folding).

Saturation analysis conducted for the Top Choiyoi Group at transects T2 and T6 at the MA, based on the workflows proposed by Judge & Allmendinger (2011), confirms that by increasing the amount of polygon nodes to beyond ~15-20 does not substantially change the shortening values (**Fig. 5.14**): a saturation effect occurs early on. One key difference between the two workflows is that the analysis presented by Judge & Allmendinger (2011), represents an integrative method, while our approach is parameter-specific. In summary, we state that uncertainty analysis in kinematic restoration of thick-skinned structures cannot be done conclusively by only looking at an isolated parameter. Our uncertainty assessment is based on a few exemplary parameters, to demonstrate the workflow. However, it appears that in these data sets uncertainties of controlling parameters are interdependent and screening of the entire multi-dimensional solution space (each parameter representing one dimension) is necessary to obtain quantifiable uncertainty information.

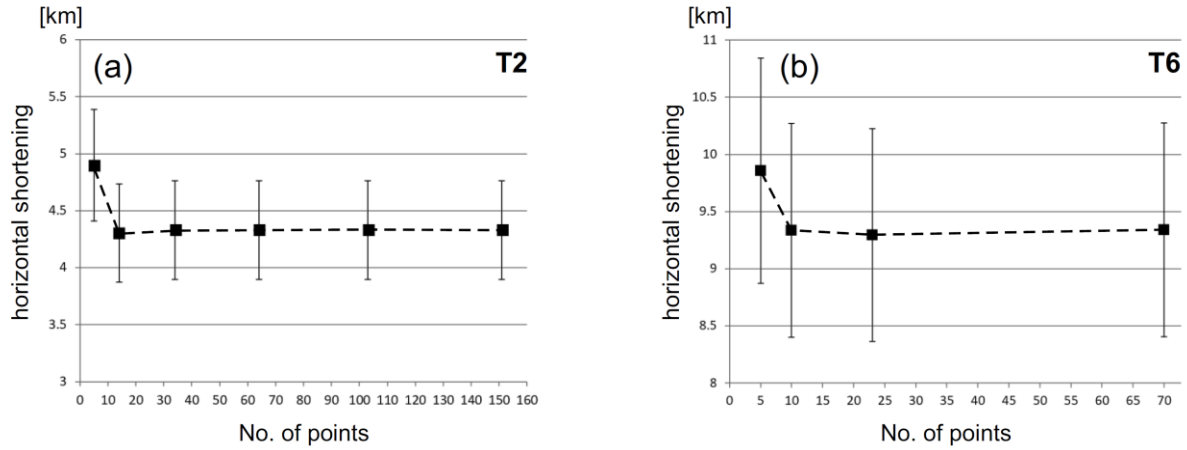

Fig. 5.14: Saturation of shortening curve according to AreaErrorProp analysis for sections T2 (**Fig. 5.14a**, left) and T6 (**Fig. 5.14b**, right). Error bars indicate +/-10% of error.

5.7.3 Limitations of Traditional Uncertainty Analysis

In structural analysis, kinematic restoration has been commonly used to validate geometric models (e.g. Gibbs, 1983, Suppe, 1983). Traditional workflows can be considered an inversion method, whereby typically one geometric (static) model solution can be confirmed, or at least narrowed down to a "most preferred solution" that is restorable without geometric contradictions. Such a workflow is, however, not exhaustive in terms of testing all possible geometric solutions. Furthermore, such a workflow is only valid under certain assumptions or boundary conditions, such as (a) preservation of area, (b) plane strain, (c) strain compatibility and (d) kinematic modeling is limited to observable ("mappable") structures only. A complete numerical inversion of such models is, however, not feasible currently, which is mainly due to the large amount of parameters and the resulting degrees of freedom and their inter-dependencies, as well as due to a lack of more complex algorithms allowing to restore any deformation based on observational constraints. This refers to parameters such as shortening, ramp angle, trishear angle, number of trishear zones, internal shear angle etc. (Erslev, 1991). Furthermore, traditional inversion methods – even in a simple structural model – would not deliver one definite solution, rather a range of outcomes within which the preferred solution can be selected. Typically, kinematically restored models are underconstrained due to the nature of the data category, data density and data quality (Bond, 2015). However, improved workflows to quantify uncertainty are needed as the traditional crude error estimation is highly imprecise and not standardized. The experience of the interpreter is an important criterion in the quality of model construction and also the estimation of uncertainties (Bond, 2015), but is also not standardized.

Previous methods for uncertainty quantification allow to determine uncertainties based on certain conditions (e.g. Judge & Allmendinger, 2011), such as constant area and by adding spatial uncertainties of critical nodes of the observed polygons. These methods also utilize spatial uncertainties of constructed points which are defined empirically (and increase significantly with depth). The major advantage of these methods lies in the straightforward mathematical workflow to determine the uncertainty. Disadvantages of such methods are the lack of involving small-scale and realistic elements of the model, such as strain-distribution, detailed geometry of faults and variations in the displacement field, as indicated by Cristallini & Allmendinger (2001). The work flows proposed by Poblet & Bulnes (2007) require strain ellipses as markers for misfit quantification, however, measurable strain data or strain markers are typically not available over larger areas, such as km-scale anticlines. Victor et al. (2004) utilized geometrically well constrained structures, based on detailed seismic and stratigraphic data, to quantify uncertainty. The approach, however, did not systematically examine the solution space nor explore interdependencies of modeling parameters.

The intent of forward modeling workflows is to minimize the deviation or misfit between observed geometric elements (nodes, formation boundaries etc.) and the model. The standard approach is to run different forward-scenarios (often on a try-and-error basis) until one (!) geometric solution is found. However, most often forward modeling is not used to systematically record the misfits. We propose that our method be applied in a complementary way to the one used by Judge & Allmendinger (2011). This will allow to not only determine the correct shortening amount, but also to quantify uncertainties of smaller-scale elements, such as e.g. varying ramp angles. Furthermore, forward modeling not only provides quantification of the misfit, but also helps to detect interdependencies. This will help to further improve geometric solutions and to understand the range of uncertainties.

To illustrate the concept, our new method to quantify uncertainties in kinematic restoration is demonstrated for selected parameters, shortening and ramp angle. We encourage alternative parameters or combinations of parameters be tested also. Our method could also be expanded to other kinematic restoration algorithms than Trishear, and can even be applied in varying tectonic environments, such as e.g. extensional settings. If numerous parameters are analyzed at the same time for misfits and interdependencies, the calculations would quickly become too complex for (semi-)manual modeling, due to the multi-dimensional nature of the data sets. It is important to note that for multi-parameter misfit analyses the number of necessary models will increase according to the number of parameters. In that case numerical modeling would be the tool of choice to quantify uncertainties.

5.7.4 Implications for the Malargüe Anticline

Based on our analyses, a number of observations can be made with respect to the overall structural model and genesis of the MA: In map view the MA consist in two segments with slightly different strike orientations, a northern segment (NNW trending) and a southern segment (NW-trending). This observation has been made by previous researchers (e.g. Giambiagi et al., 2009). Furthermore, we recognize that in cross-section the geometry of the MA varies from north to south (**Fig. 5.6**). These along-strike variations could be expressions of different pre-existing structural grain or different rock properties during contraction, or both.

As the MA was actively contracting between 7MA and 1MA and was broken by faulting in the early Pleistocene (Silvestro & Kraemer, 2005; Giambiagi et al., 2008; Giambiagi et al., 2009). Based on our models, the horizontal shortening rates can be determined to be 0.57 mm/yr near the northern plunge and 1.57 mm/yr in the south. These shortening rates are to be considered minimum values, as effects such as pressure solution or sub-seismic shortening may add to the overall shortening. These values are slightly higher than the ones reported for the MA (0.5 mm/yr) and comparable to those at the Bardas Blancas structure (2.2 mm/yr) and Palauco Anticline (2.6 mm/yr) (Giambiagi et al., 2009). Turienzo (2010) documents a slip rate of 2.5 mm/yr from the Atuel River, while Messager et al. (2012) report uplift velocities associated with the Sosneado Thrust of 0.39 to 1.19 mm/yr during Mid- to Late Pleistocene.

Additionally, we observe that the vertical relief, the ramp dip angle, the fold width and the width of the forelimb vary significantly between the northern and southern segment (**Fig. 5.15**). All these observations support the hypothesis that the fold may have evolved from two separate domains which merged into one coherent anticline during contraction. These observations alone do not answer the question if the MA evolved out of a pre-existent extensional system. Different fold geometries between the north and the south may also be explained by intra-Choiyoi compositional changes (presence of volcanics, sills, dikes around transects T6b, T7, T8, T9). These probably lead to varying mechanical responses along strike and result in different fold geometries. The effect of poorly constrained internal composition and resulting mechanical effects regarding rheology and elasticity on model uncertainty has been documented previously (Gerbault et al., 1998; Buiter, 2012). Recent research confirms the influence of mechanical stratigraphy, internal friction and geomechanical constraints on errors and uncertainty in deformation analysis (Moretti & Callot, 2012; Smart et al., 2012).

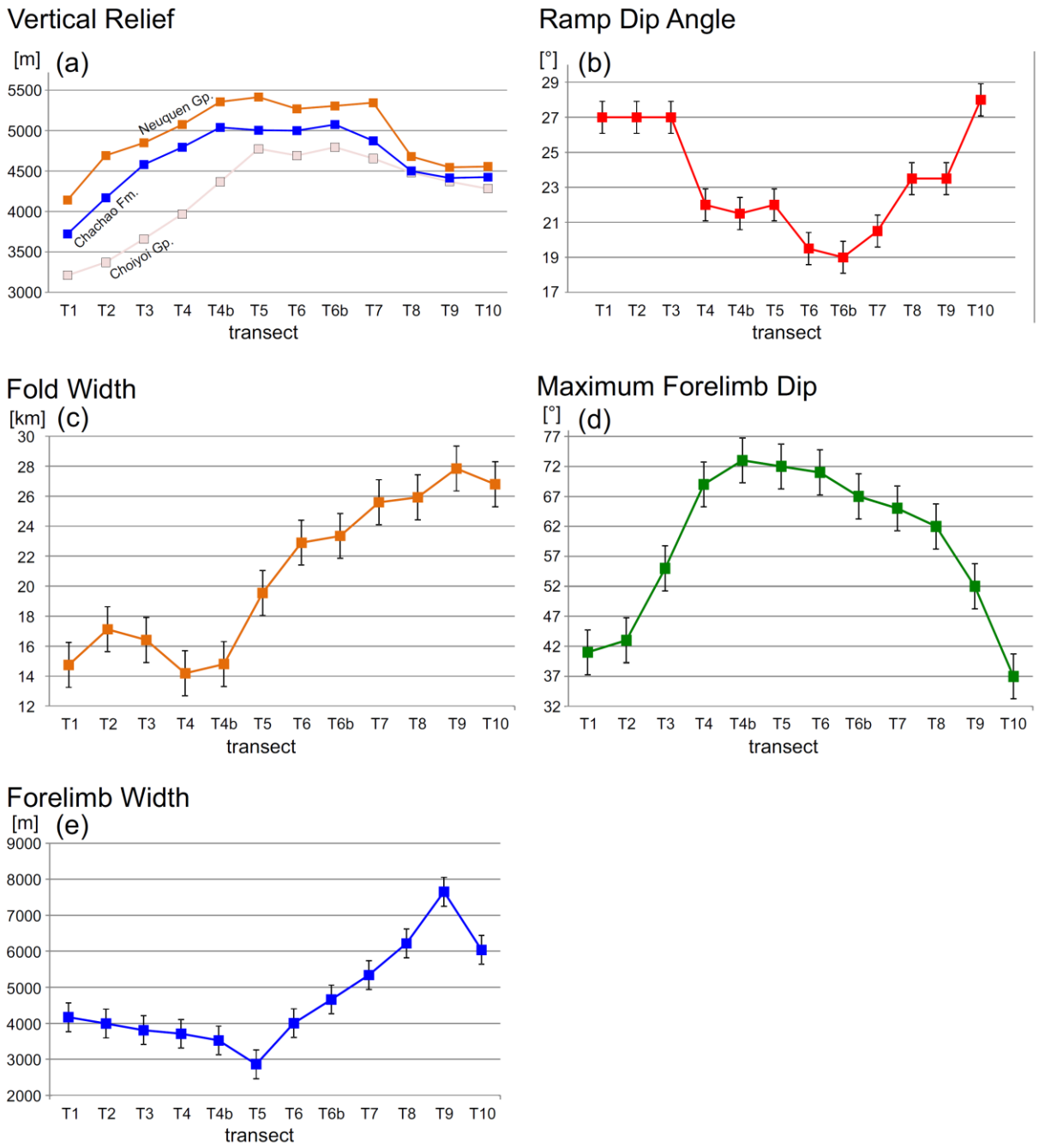

Fig. 5.15: Fold parameters obtained from observation of static structural models.

The often-neglected influence of internal strain and synchronous internal small-scale deformation (ductile and brittle) during contraction have also been recognized as a source of uncertainty in structural reconstruction (Groshong & Epard, 1994; Smart et al., 2012; Allmendinger & Judge, 2013; Caër et al., 2015). But this influence has not been fully understood to date. However, the ramp angles at the MA, established here through forward modeling, range between ~17-29° (e.g. **Fig. 5.9**) and do

not represent dip angles of extensional faults which are typically in the 50-80° range (e.g. Ramsay, 1967). In fact they are much more indicative of reverse faults (thrust) which are commonly in the 10-40° range.

Another argument helps to understand why the inverted half-graben model for the MA cannot be supported: If the MA was generated as an inverted half-graben with an assumed dip of 65° of the master fault, and under a horizontal shortening of >10 km, the vertical uplift of the crest of the MA would be >6 km, which clearly contradicts the data. We, therefore, favor the concept that the MA formed as a new structure (fault propagation fold) during Andean contraction. However, it is possible that certain elements of the master detachment, such as branch-points of splays, are caused by pre-existing structural elements, as shown e.g. for structures in the Rhenish Massif (Oncken et al., 1999). We demonstrate that isopach maps of the pre-Andean (i.e. pre-orogenic deposits) do not show clear evidence of thickness anomalies along the MA fault-fold system that could be indicative of depositional patterns controlled by pre-existing extensional structures (**SUPPL. Figs. 5.S1, 5.S2**).

The MA was established between 7MA and 1MA (Silvestro & Kraemer, 2005; Giambiagi et al., 2008; Giambiagi et al., 2009). At this time the anticline was in place as a migration barrier between the Pincheira Sub-Basin to the west and the Chacay-Llancanelo Sub-Basin to the east. This means that from this time on no hydrocarbon migration was possible across this barrier (kitchen shut-off). However, migration is still possible within the foreland basin, either eastwards towards the Llancanelo oil field or westwards, into the MA forelimb. The northernmost and southernmost portions of the forelimb remain undrilled to date and some limited exploration potential for small oil accumulations remains there. Past wells drilled in the central part of the forelimb may not be valid tests (old wells, partial technical failures). Porous and fractured reservoirs could potentially represent attractive targets in this highly strained structural position. However, complex seismic imaging and challenging drilling operations will have to be overcome to test this play. Furthermore, we confirm the “piggy-back” nature of the Pincheira Sub-Basin, which has been uplifted well above regional likely causing anomalous maturity and potentially unexpected reservoir pressures there. The position of the Pincheira Sub-Basin, the MA and the Llancanelo structure also provides further (indirect) evidence of an eastward-propagating regional detachment at depth, gradually rising towards the Andean foreland (**Fig. 5.3**).

5.8 Conclusions

In this paper we present new methods and results on uncertainty quantification for a highly constrained pseudo-3D model of the MA based on systematic mapping of uncertainty using forward modeling. The model is based on the integration of detailed field mapping data and detailed subsurface data. To demonstrate a new workflow for uncertainty quantification we tested two independent shortening calculations and combined them with forward modeling methods. Two selected parameters were chosen to illustrate the work flow to map the solution space: We were able to show that the parameters ramp angle and amount of shortening are two key drivers for uncertainty sensitivity in the case of the MA. We acknowledge that previous research has demonstrated the importance of stratigraphic-geometric uncertainties and eroded hanging-wall cut-offs as the main source for error in section balancing (e.g. Allmendinger & Judge, 2013).

Through forward modeling we have shown that varying the ramp angle (while leaving the shortening constant) leads to uncertainty variations of 2-7.5% in area, while varying the amount of shortening (and leaving the ramp angle constant) leads to uncertainty variations of 1.5-9% in area. Global uncertainty maps show that these observations are consistently valid for sections along the entire MA analyzed here (**Figs. 5.11, 5.12**). However, transects located in regions with abundant volcanics and, hence, stiffer stratigraphy and lower model confidence, reveal larger uncertainties. Fine tuning of uncertainties reveals that even variations of up to 10% in ramp angle or shortening amount will keep the error in area generally below 5% (**Fig. 5.10**). The effect of other variables on the kinematic workflow, such as the fundamental deformation style (controlled by the algorithm), P/S ratio or angular shear can be excluded from the workflow or kept constant, if they result in unrealistic fold geometries. A key outcome of this analysis is that there are strong indications for uncertainty dependencies between ramp angle and shortening. We, therefore, recommend to always screen the entire multi-dimensional solution space and carefully watch for uncertainty dependencies between key drivers.

5.9 Acknowledgements

We would like to thank Dr. Gerhard Haase and Daniel Boggetti and his team at PyT Consultora in Mendoza for their support, field logistics and access to geological surface maps.

5.10 Appendix

Test for anomalous thickness patterns in pre-orogenic units

In order to understand and define the structural style (type of fold) of the MA, we conducted isopach mapping of two pre-Andean (pre-orogenic) sedimentary units, the Valanginian Chachao Fm., consisting in rigid limestones and forming one of the main regional marker beds, and the underlying Vaca Muerta Fm. (plastic shales) (**Figs. 5.S1, 5.S2**). We intended to test the forelimb for thickness anomalies (thickening or thinning) which could be indicative of a fault-bend fold kinematic mechanism (e.g. Ramsay, 1967). The map reveals no anomalous thickening (or thinning) along the forelimb in neither of the two stratigraphic units. This observation is confirmed by geometric observations from seismic data, well data and outcrop data. This implies that no significant ductile deformation occurred along the fore-limb of the MA during folding. Additionally, the two isopach maps served as a test to detect any anomalous thickness patterns (particularly abrupt thickness-increases), which would be indicative of pre-existing tectonic structures at the location of the MA, such as “rift-like” or “half-graben” geometries, as have been documented for nearby Triassic-Jurassic depocentres (Giambiagi et al., 2003). Alternatively, for lower values of limb rotation such thickening could also be interpreted as resulting from pervasive distributed strain. Neither of the maps show any clear indications of thickness anomalies that could resemble pre-existing extensional structures nor significant ductile thickening or thinning. This implies that for the stratigraphic levels of the Vaca Muerta and Chachao Formations pre-existing depositional thickness anomalies can be ruled-out.

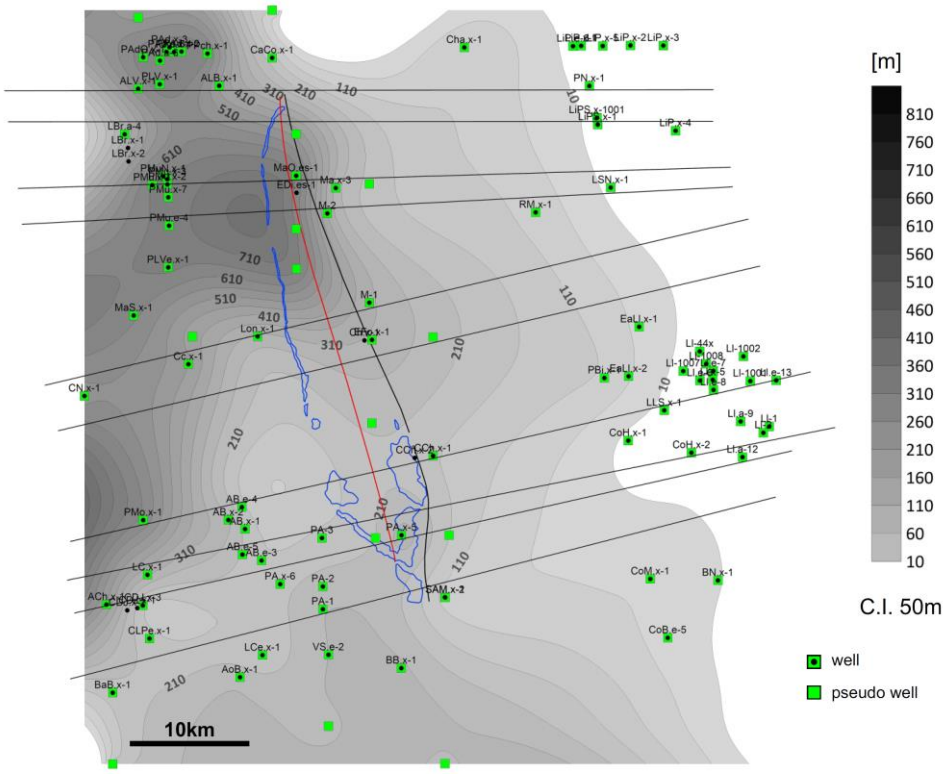

Fig. 5.S1: Isopach map of the Vaca Muerta Formation, based on well, outcrop, seismic and model data. Blue polygon = outcrop of main marker (Chachao Formation). Red line = anticline main axis; black line = approximate position of main thrust at basement level (in subsurface).

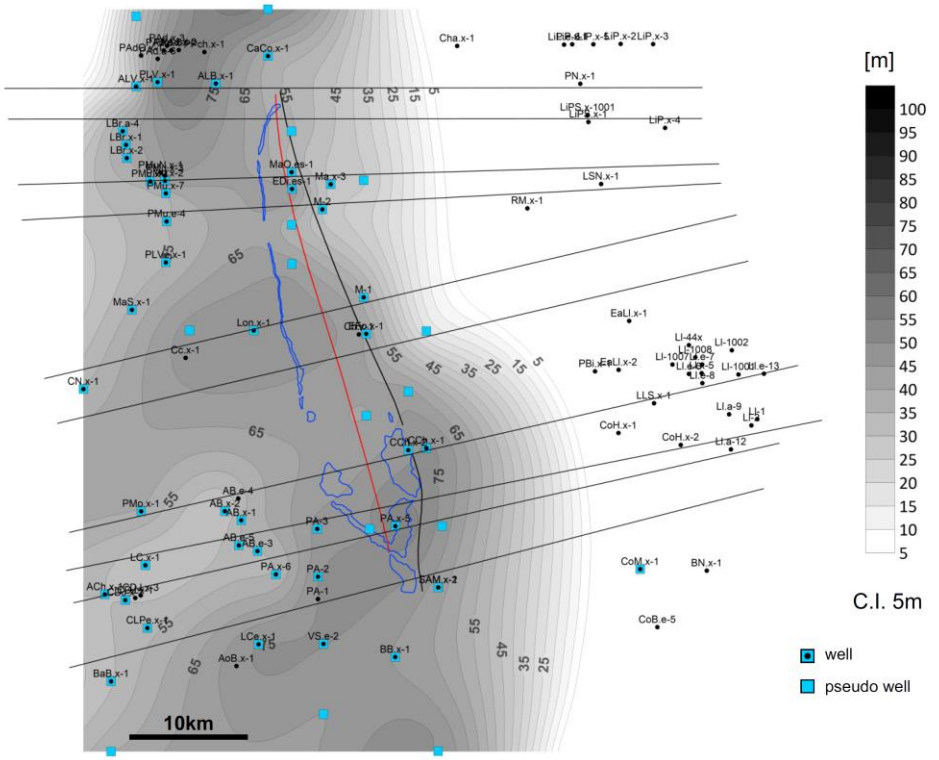

Fig. 5.S2: Isopach map of the Chachao Formation (based on same data sources as **Fig. 5.S2**). Tectonic elements as **Fig. 5.S2**.

6. FRACTURE EVOLUTION IN OIL-PRODUCING SILLS OF THE RIO RANDE VALLEY, NORTHERN NEUQUÉN BASIN, ARGENTINA

6.1 Abstract

Oil-producing sills are commonly considered atypical reservoirs, although they can hold significant exploration potential. The need for a better understanding of fracture properties and petroleum system characteristics for this and similar igneous rock plays is the main motivation of our study. We explore the evolution of this play type by an analysis of the Los Cavaos oil field, located in the Malargüe fold belt of the Neuquén Basin, Argentina, integrating multiscale fracture data from outcrops and subsurface. The field was created by a combination of intrusions and mild Miocene-Pliocene inversion. Production stems from thick cavity zones in naturally fractured andesitic sills emplaced inUpper Jurassic shale source rocks. Orientation patterns, fracture spacing, and length of fracture sets in the sill are consistent over several orders of magnitude. Large multiply connected and weakly cemented fractures are responsible for excellent interconnectedness in the reservoir. Fracture density is correlated with fault proximity, indicating a cogenetic evolution during active deformation. Abundant fractures in core with strike-slip to oblique striations support transpressional overprint during and after fracture formation. Although it is challenging to separate cooling from tectonic fractures, we propose two phases of fracturing, marked by a coexistence of subvertical and oblique fractures together with transpressional striae. Petrographic evidence suggests initial local oil expulsion and migration through microfractures, with opening displacements of 0.01 to 1 mm, followed by subsequent charging of the evolving intra-sill cavity system as well as the bulk fracture system during cooling and mild deformation. We suggest that the observed patterns may be extrapolated to sills in similar geotectonic settings.

6.2 Introduction

Oil-bearing naturally fractured sills exist around the world (Petford & McCaffrey, 2003) but are not commonly considered reservoirs, which is why they are poorly understood and underexplored. Producing sills form complex oil fields, posing high risks to explorers and engineers. Key parameters in these reservoirs are maturation, charge, entrapment, fracture quality, and geometry of the intrusion. Petroleum-bearing sills have been examined in several studies focusing on emplacement parameters (Gil-Imaz et al., 2006; Valentine & Krogh, 2006; Burchardt, 2008; Goulty & Schofield, 2008; Gressier et al., in press) or maturation, migration, charge, and entrapment mechanisms (de Araujo et al., 2005; Aarnes et al., 2008; Ventura Santos et al., 2009). However, few integrative studies, particularly on systematic fracture analysis in this play type are available, and they are commonly based on model data and rarely compared with the subsurface or outcrop. Our study sheds new light on sill emplacement, fracture properties, oil charge, and trapping in the Miocene andesitic sills of the Rio Grande Valley (RGV) oil fields in the Neuquén Basin (Figs. 6.1A, 6.1B).

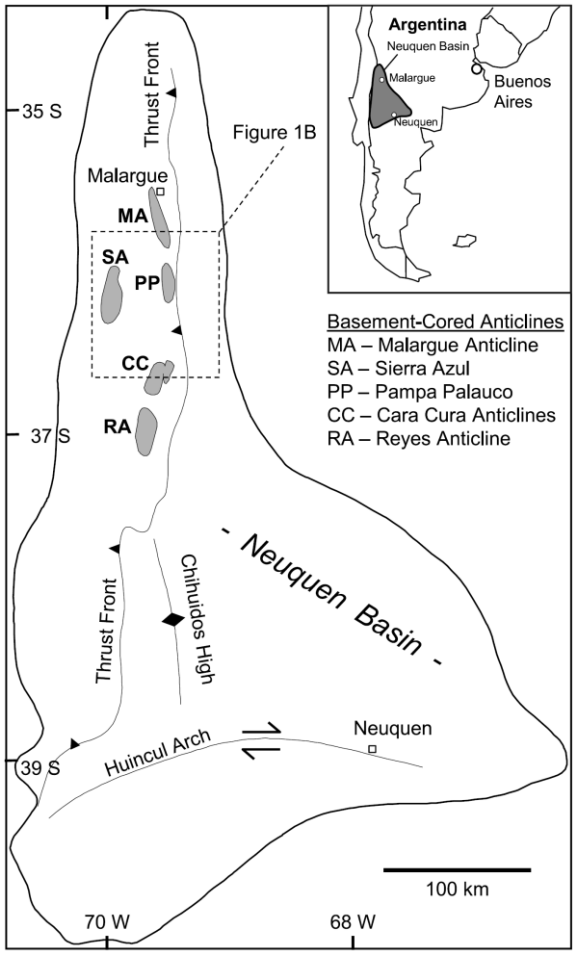

Fig. 6.1A: Map of the Neuquén Basin with tectonic elements and study area (dashed square) (modified from Legarreta et al., 2004; IHS, 2008).

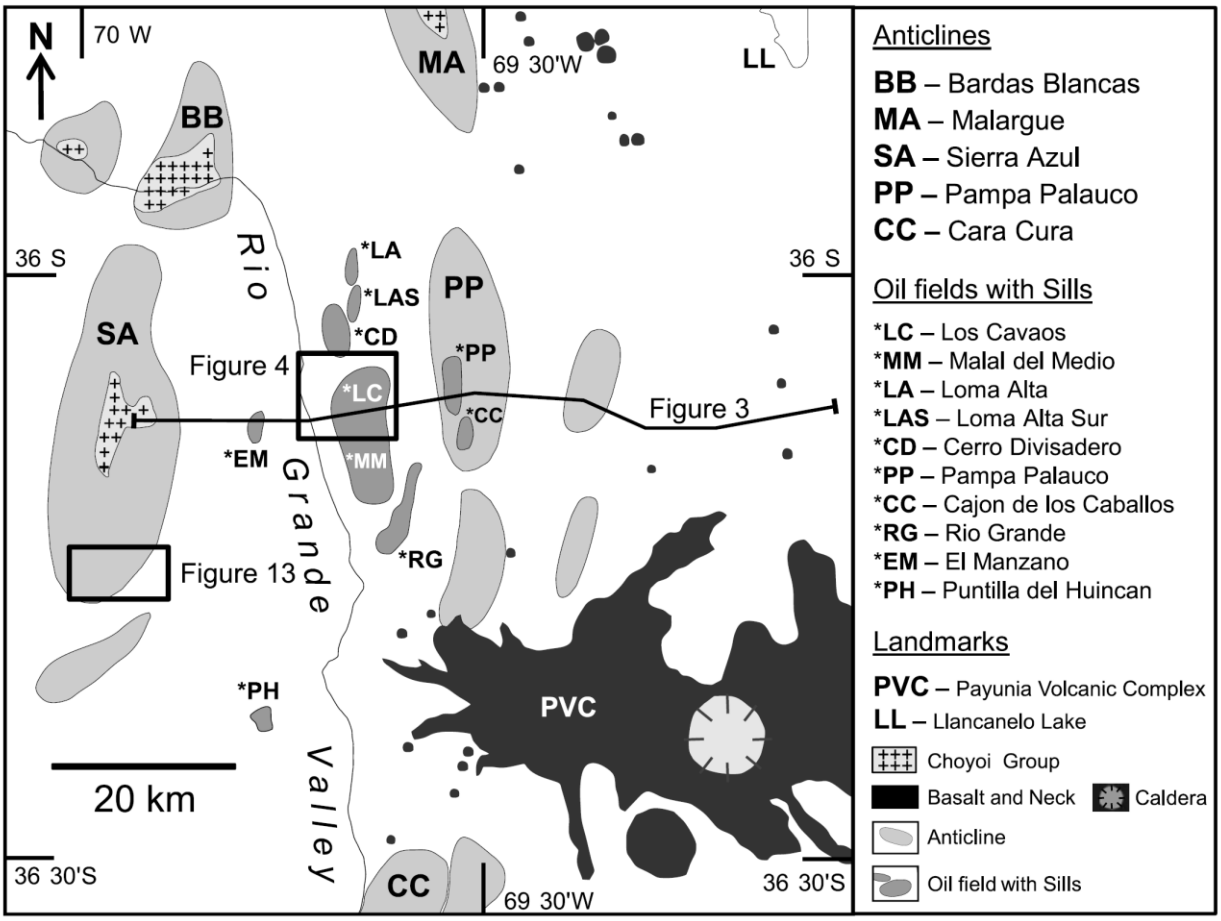

Fig. 6.1B: Simplified map of the Rio Grande Valley with subsurface (Fig. 6.4), outcrop study areas (Figure 6.13), and regional transect (Figure 6.3).

Here, hydrocarbons are produced from naturally fractured andesites that are hosted in and enclosed by shales of the Vaca Muerta Formation, the main source rock in the basin (e.g., Villar et al., 1998) (Fig. 6.2). Two central fields, Los Cavaos and Malal del Medio, are surrounded by several satellites. Typical estimated ultimate-recovery volume in this play is less than 25 million bbl per field. Initial rates of as much as 10,000 bbl/d per well triggered fast development drilling without fully understanding the production mechanisms. Now, almost 30 yr later, infill and near-field drilling are increasingly challenging. Thermal modeling of sills in the nearby Altiplanicie del Payun region revealed that source rock fractures and convective water flow are important in oil migration and charge (Rodriguez et al., 2007; Rodriguez Monreal et al., 2009).

For the petroleum systems at RGV, the function of fractures in oil charge and reservoir quality of sills remains poorly understood (Bermudez & Delpino, 2008; Delpino & Bermudez, 2009). The need for a better understanding of fracture properties and petroleum system characteristics for this and similar igneous rock plays is the main motivation for our study. We integrate multiscale fracture data from

outcrops and the subsurface. Secondarily, we hope that our insights will lead to improved exploration and production in this play and to reduced uncertainty in exploring for similar reservoirs worldwide. Our results clarify the control that igneous structures and fractures have on reservoir quality and performance and how they control reservoir flow and storage capacity in sill reservoirs.

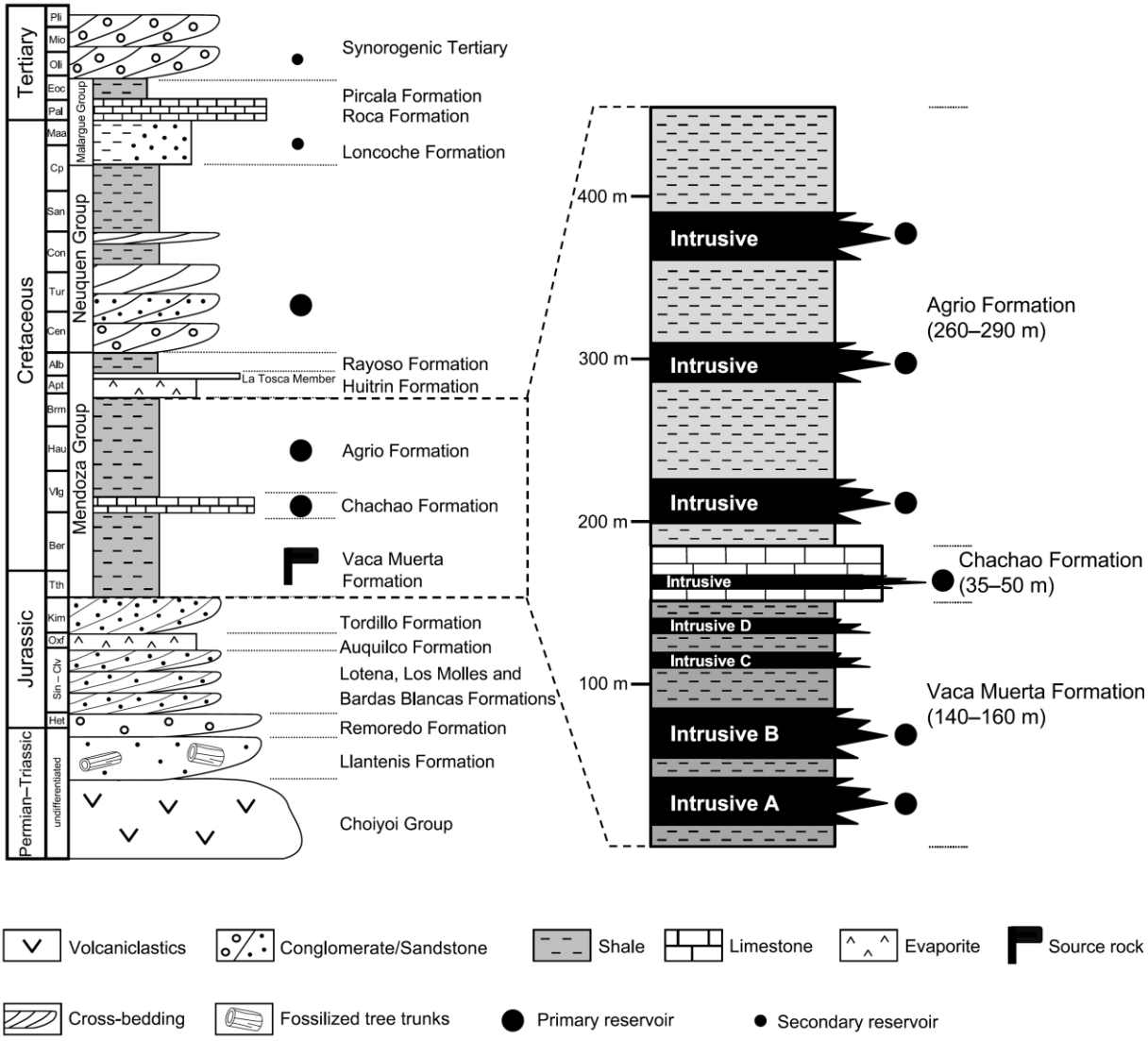

Fig. 6.2: Stratigraphic column of the study area. Pli = Pliocene; Mio = Miocene; Oli = Oligocene; Eoc = Eocene; Pal = Paleocene; Maa = Maastrichtian; Cp = Campanian; San = Santonian; Con = Coniacian; Tur = Turonian; Cen = Cenomanian; Alb = Albian; Apt = Aptian; Brm = Barremian; Hau = Hauterivian; Vlg = Valanginian; Ber = Berriasian; Tth = Tithonian; Kim = Kimmeridgian; Oxf = Oxfordian; Sin-Clv = Sinemurian to Callovian; Het = Hettangian.

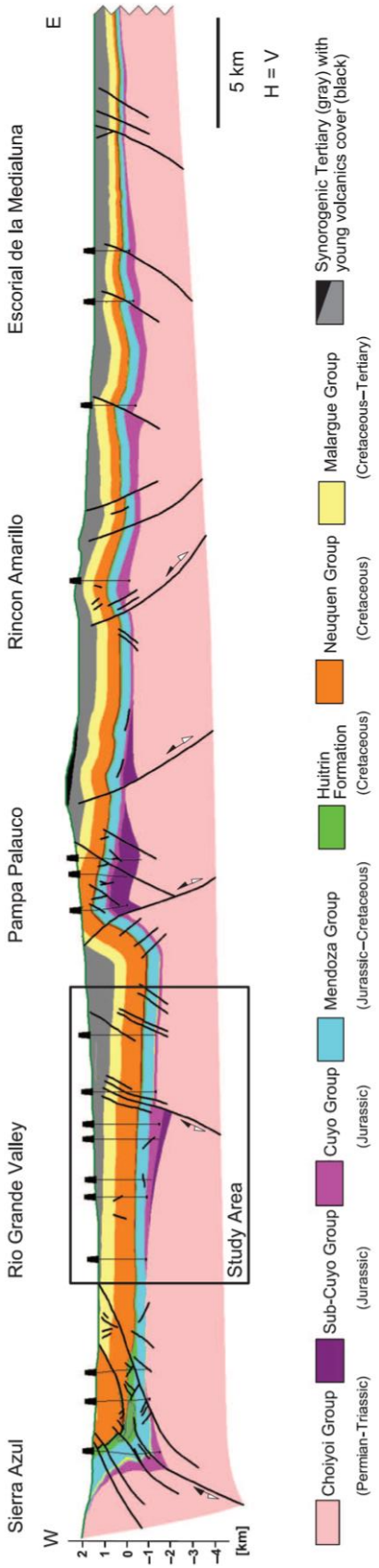

Fig. 6.3: Regional structural transect of the study area.

6.3 Geotectonic setting

The Neuquén Basin developed out of a series of Permian-Triassic grabens and later evolved into a Mesozoic back-arc basin that was subsequently overthrust from the west during Andean compression (Vergani et al., 1995). Shortening is still active, even near the basin center (Messager et al., 2010). Numerous Cenozoic volcanic complexes exist (Kay et al., 2006). Our study area, the RGV, is located in the thick-skinned Malargüe fold belt of the northern Neuquén Basin (36°S). A regional transect reveals that the RGV is located in a low-lying domain between inverted first-order structures (Fig. 6.3). The Malargüe fold belt was contracting in the northern section between 15 Ma and approximately 7 Ma (Giambiagi et al., 2009), between 15.8 Ma and 6.7 Ma in the Bardas Blancas anticline, between 10.8 Ma and 8.14 Ma in the Palauco anticline, andbetween7Ma and1Ma in the Malargüe anticline (Silvestro & Kraemer, 2005; Giambiagi et al., 2008; Giambiagi et al., 2009). Radiometric cooling ages from andesites in the northern Neuquén Basin range from 10.5 Ma to 7Ma (Linares & Gonzales, 1990; Baldauf et al., 1997; Combina & Nullo, 2005; Giambiagi et al., 2008). One andesite sample from an RGV well yielded a late Miocene Ar-Ar cooling age (unpublished Repsol internal report, 2006). We believe, therefore, that the bulk of the sill intrusions in the greater RGV area occurred during the late Miocene, likely between 10.5 Ma and 7 Ma.

6.4 Database and methods

Our study encompasses (1) subsurface and surface data from RGV and (2) data from analog outcrops in the nearby southern plunge of the Sierra Azul range (Fig. 6.1B).

6.4.1 Deformation styles from seismic data

A regional transect from vintage regional two-dimensional (2-D) seismic data (1970s and 1980s), local transects extracted from a three-dimensional (3-D) seismic cube (2005) across the RGV, and a structural map from seismic data depict the structural context and configuration of the Los Cavaos field (Figs. 6.3–6.5). Transect construction was conducted using 2-D Move restoration software (version 5.0b), incorporating satellite images, elevation data, wells, and formation tops of the main stratigraphic units. We used the top Neuquén Group, top Huitrin Formation, and top Chachao Formation as marker beds. The estimated vertical depth error is less than 10%, having thus negligible effects on the structural interpretation.

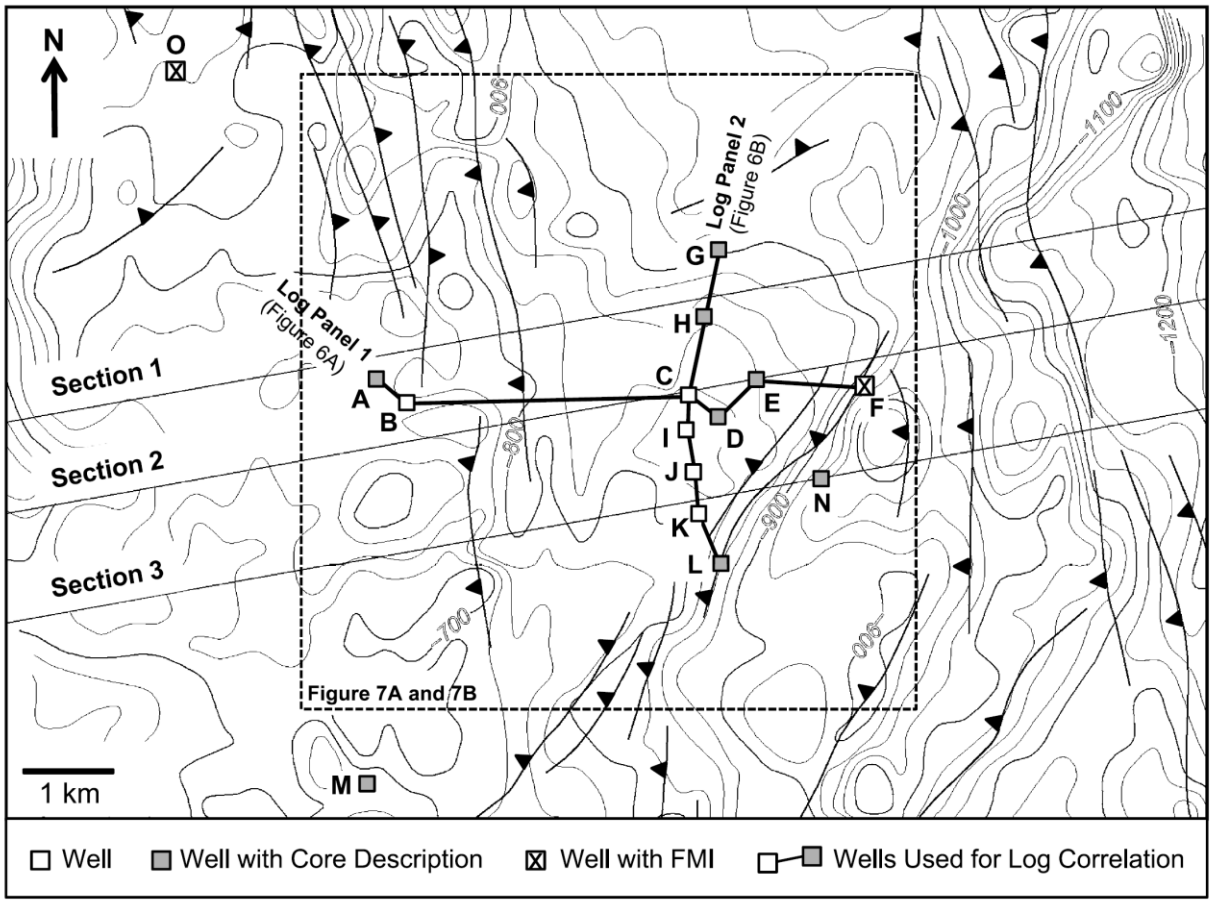

Fig. 6.4: Structural map of a near–top Chachao pick; below mean sea level (CI = 82 ft [25 m]). CI = contour interval; FMI = Formation MicroImager.

6.4.2 Fracture and cavity zone attributes from logs, core and outcrop

Logs from more than 50 wells were used for depth calibration and, from 13 key wells for correlation panels (Figs. 6.6A, 6.6B), including gamma-ray (GR), caliper, resistivity, and sonic logs. Logs were also used to map the gross thickness and cavity zone in sill A (Figs. 6.7A, 6.7B). Gamma-ray, resistivity, and sonic logs are particularly useful tools in the identification of an intrusive, but the resolution depends on contrast with the host sedimentary rocks and the composition of the sills (e.g., Schutter 2003). We found low GR readings particularly diagnostic for detecting sills with a mostly intermediate chemical composition. They are hosted in organic shales (hot background), hence creating a marked log contrast. Delpino & Bermudez (2009) noted that more acidic sills with a high potassium-feldspar content may also be marked by an inverted GR contrast (log reading higher than host rock), an effect we observed in one well (well B, Fig. 6.6A). Because of the poorly conductive matrix of the sills, high resistivity readings are indicative of intrusives, as are high sonic readings (fast lithology). Caliper logs, identifying the borehole morphology, and density readings, detecting density variations in the sills, were used to map the extent of the cavity zone (Fig. 6.7B).

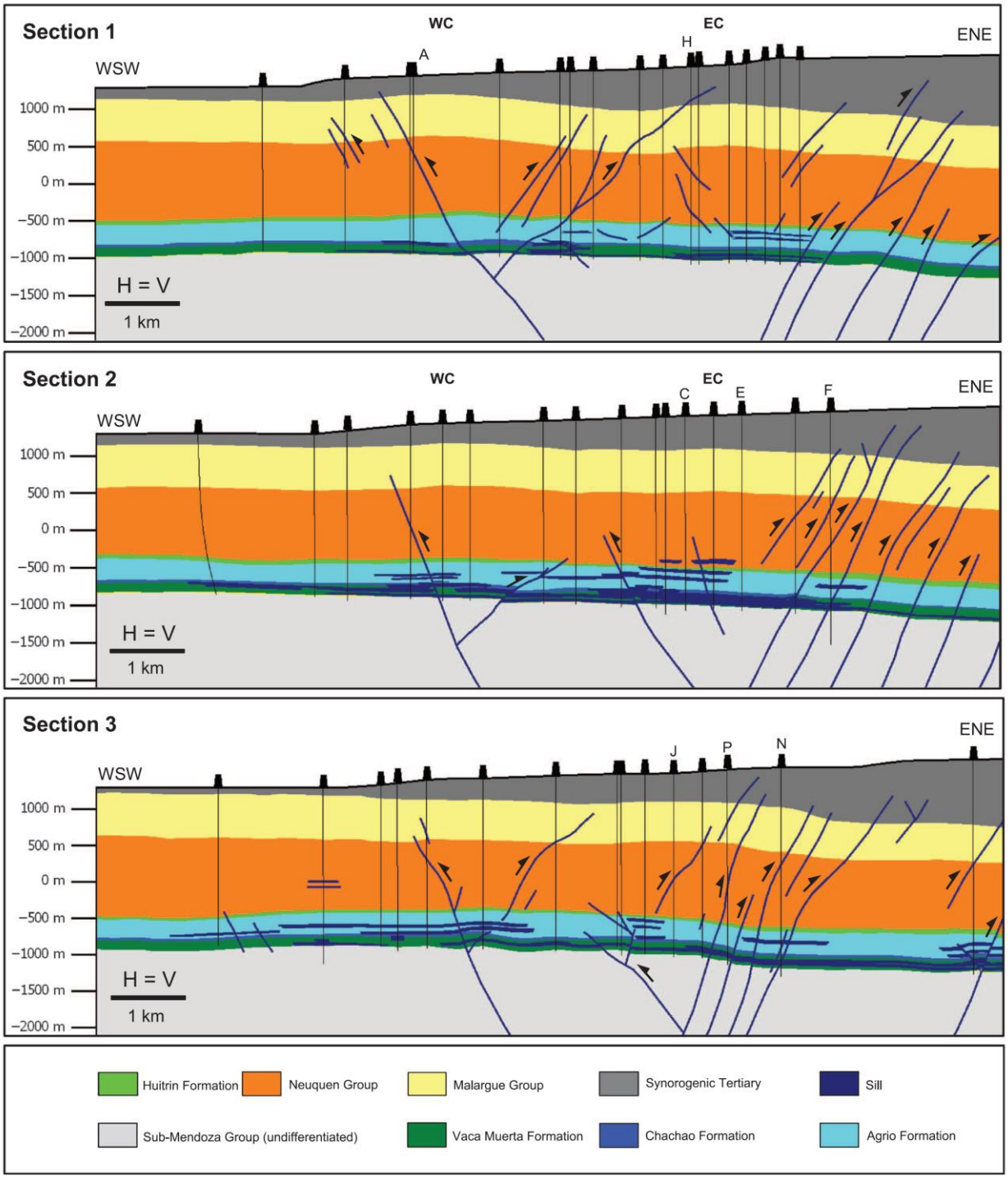

Fig. 6.5: Oil Field-Scale cross sections across Rio Grande Valley. WC = western culmination; EC = eastern culmination.

We analyzed 22 cores from 14 wells, including 7 oriented cores. All wellbores and main fracture sets are subvertical. A variety of fracture shapes, dimensions, opening displacements (apertures), mineral fills, and kinematic indicators are present (Figs. 6.8–6.11). Fracture apertures were collected in wells

D, F, and G along the core axis as a scan line. From 92 ft (28m) of core, we recorded 45 apertures from sill A and 58 from shales (Fig. 6.12) using a logarithmically graduated comparator (Ortega et al., 2006).

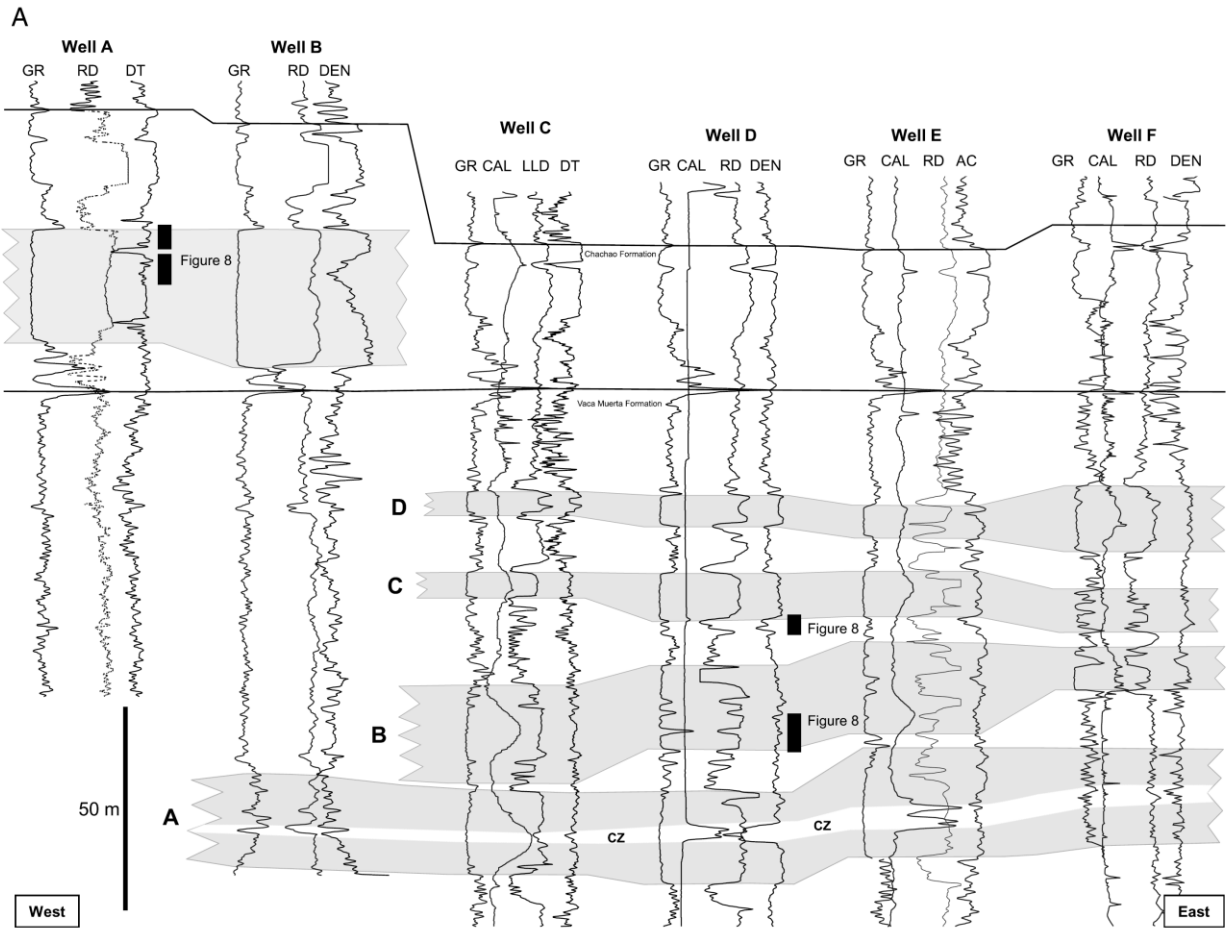

Fig. 6.6A: Log-panel 1 (west-east direction), flattened at the Vaca Muerta Formation. Black bars indicate cores. Intervals shaded in gray indicate sills A to D. (B) Log-panel 2 (north-south direction), flattened at the Vaca Muerta Formation. Black bars indicate cores. GR = gamma ray; RD = deep resistivity; DT = sonic; DEN = density; CAL = caliper; LLD = laterolog deep; AC = acoustic; CZ = cavity zone; RHOB = bulk density. GR = gamma ray.

We applied the concepts of Nelson (2001) to separate natural from induced fractures. The two sills examined in outcrop were chosen for similar composition, geometry, stratigraphic setting, and geographic proximity to RGV (Figs. 6.13–6.15). Fracture orientations were measured at 21 stations across both sills; at 3 stations across a 1640-ft (500-m) wide pavement of the western sill, the orientation, aperture, spacing, and length were registered in a counting box of 269 ft^2 (25 m^2), oriented in a way that each side formed a scan line perpendicular to one of the main fracture sets (Fig. 6.14A). Image data from two wells were used to detect fracture orientation patterns (Figs. 6.4, 6.16A). We measured apertures with a millimeter ruler and determined spacing by measuring the distance

between individual fracture positions along the scan lines. Fracture lengths of as much as 33 ft (10 m) were measured with a tape measure. Fracture height and interconnectedness were determined qualitatively to gain an understanding of the vertical extent and general abundance of intersections between the different sets. No usable kinematic indicators and sparse mineral fills were observed. Orientation measurements from reoriented cores yielded 36 fracture planes (Figs. 6.16A, 6.16B).

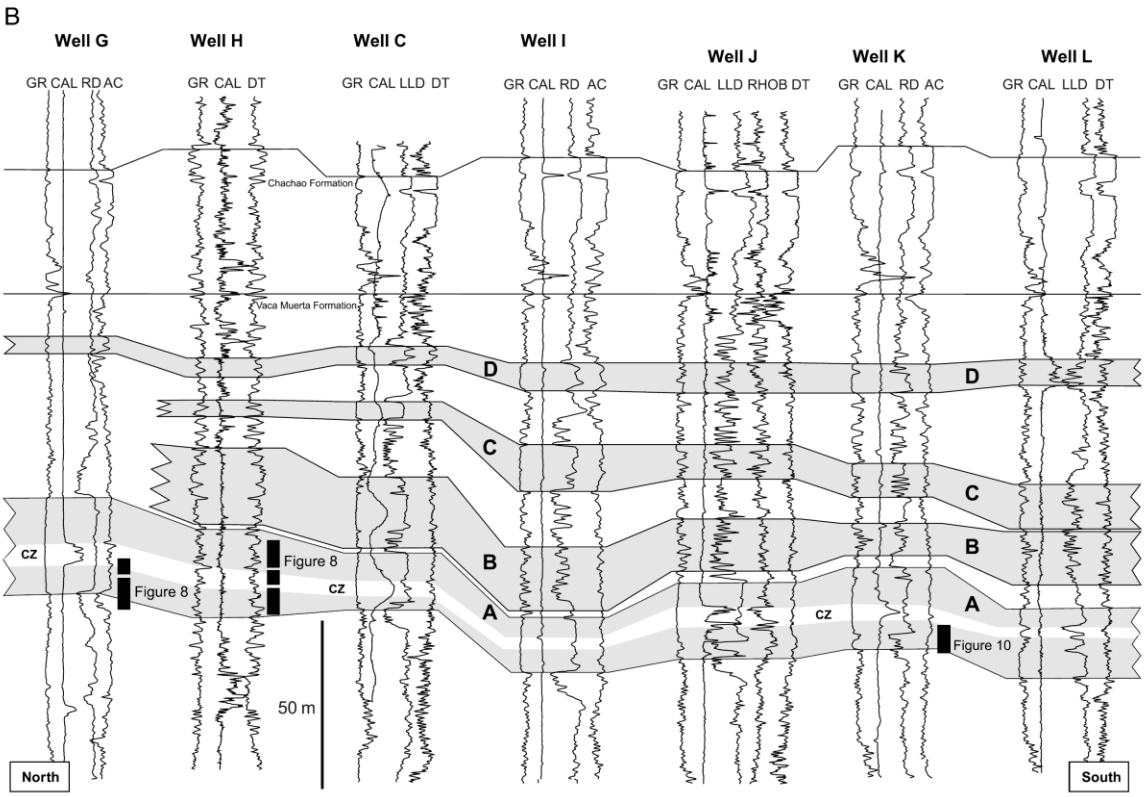

Fig. 6.6B: Continued.

For seven cores, we calculated the vertical fracture index defined by the number of fractures per vertical length of wellbore (e.g., Narr, 1996) (Fig. 6.16A). To test the consistency of fracture orientation in younger stratigraphic units, orientations were registered in Tertiary volcaniclastic rocks at five well-pad locations at the oil field (Fig. 6.16B).

6.4.3 Remote sensing interpretation

Satellite images were used to support the recognition of geometry of the two sills in outcrop and, second, to map kilometer-scale lineaments across RGV for multiscale analysis. Satellite images were referenced into 2-D Move, and lineaments were traced for orientation analysis. The interpretation was based on the physiographic expressions of drainage channels using only pronounced straight

features with lengths greater than 1640 ft (>500m). Cross-referencing with published lineaments confirmed the predominant directions (Yagupsky et al., 2008). Finally, we tested the multiscale properties of the faults and fractures by comparing the orientation patterns of lineaments from satellite imagery, fault traces from 3-D seismic data, outcrops, and subsurface fractures (Fig. 6.16A).

6.5 Results

6.5.1 Deformation styles from seismic data

A subtle structural relief of 1640 ft (500 m) at approximately 7 mi (~12 km) is observed as the elevation of the mapped horizon increases from east to west (Fig. 6.4). Fault corridors of north-northwest–south-southeast and southwest-northeast orientations are found. The most prominent fold is a northeast-plunging structural nose, approximately 4 mi (~6 km) long and 2 mi (3 km) wide. The bounding faults on its southeast flank dip steeply (70–80°) to the west, are reverse or transcurrent, and have offsets on the order of 33 to 49 ft (10–15 m; Fig. 6.5). In the south, the forelimb of the nose dips 12° to the east-southeast (locally, 20°). Backlimb dips are approximately 4°. The vertical structural relief across the structure is approximately 1000 ft (~300 m; Vaca Muerta level). The remainder of relief is found between the fault zone and the hinge. Toward the north, the nose loses relief with dips of 5° and less.

6.5.2 Sill geometries from well logs

Within the Vaca Muerta Formation, up to four distinct intrusive bodies are present, as well as two lower sills (sill A, sill B) and two upper sills (sill C, sill D), with thicknesses ranging from 3 to 98 ft (1–30 m). Sill A, the focus of our study, can be correlated for at least 6 mi (10 km; Fig. 6.7A). Near the center of sill A caliper readings, decreased densities or slow sonic log behavior indicate the presence of several-meters–thick and laterally continuous void spaces that we designate as a cavity zone (Figs. 6.6A, B). The cavity zone is confined within the sill, and its thickness varies in accordance with sill thickness (Fig. 6.7B).

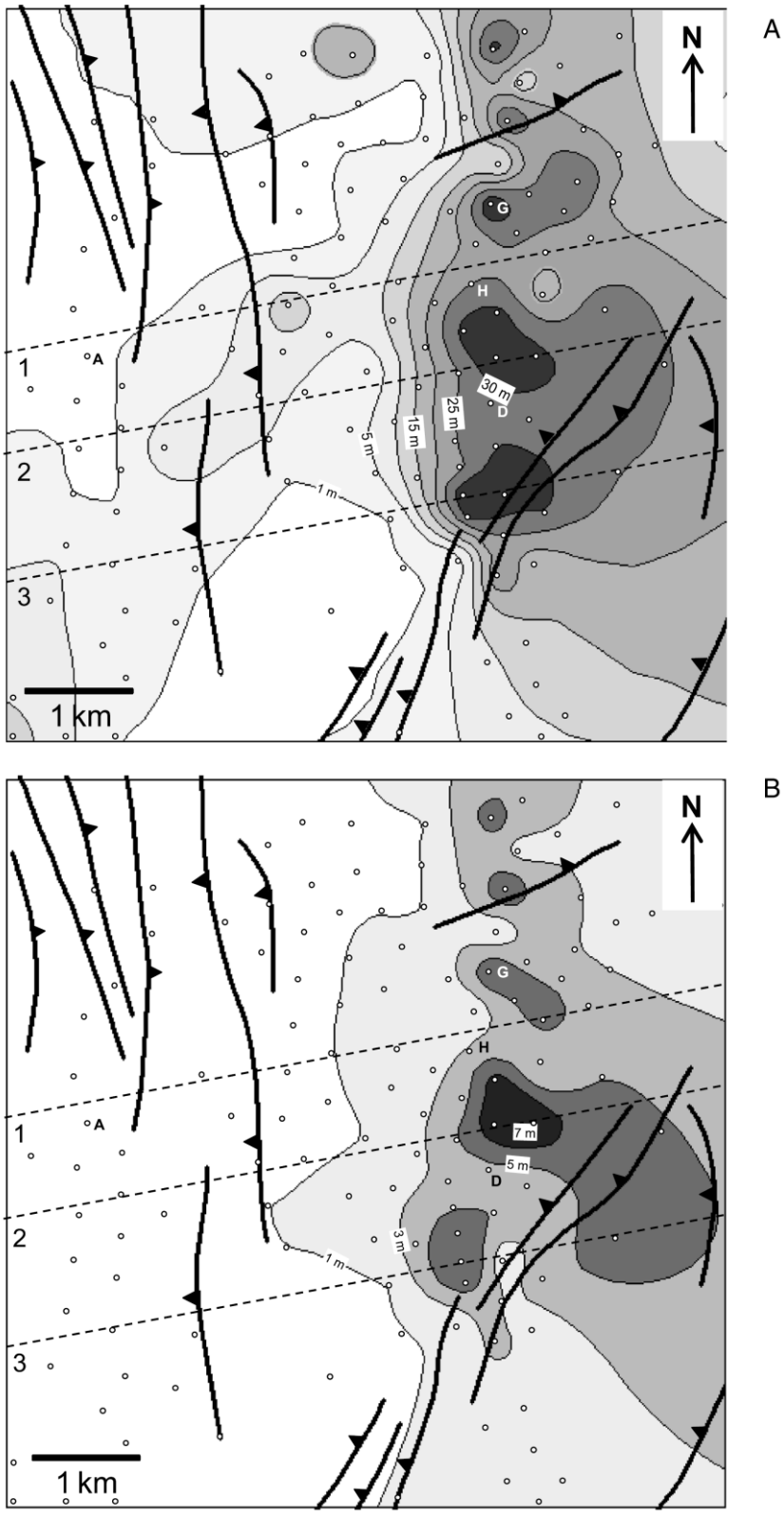

Fig. 6.7: (A) Gross thickness of sill A. (B) Gross thickness of cavity zone within sill A. The maps are based on log data points from approximately 80 wells. In some wells, core data were used for the confirmation of intrusives and the cavity zone. The dashed lines with numbers along them show the locations of Section 1, Section 2, and Section 3 shown in Fig. 6.5.

6.5.3 Fracture and cavity attributes from core

For orientation analysis, 8 cores from sills were examined, yielding 253 fractures. Twenty-five percent are subvertical, 20% are oblique (dips mostly between 45 and 65°), and 55% are sub-horizontal. Full spatial orientation data were obtained from reoriented cores, yielding 13 fractures from sills and 23 fractures from other stratigraphic units (Fig. 6.16A). Four sets of fractures are found: system 1 (northeast), system 2 (east-northeast), system 3 (southeast), and system 4 (north-northwest). The image logs in well F confirm the presence of systems 1, 2, and 4. The fracture orientations at well O are not consistent with the main sets. Fracture height and length can only be determined in a limited way because of core dimensions. Numerous vertically oriented fractures have minimum heights of several meters (Figs. 6.8, 6.9C).

We analyzed fracture spacing by calculating vertical fracture indices for seven wells, which mostly ranges between 2.2/m and 3.8/m but is higher in two well locations near faults, well K (6.3/m) and well F (13.6/m; Fig. 6.16A). The analysis of open and sealed fractures reveal that, of 253 fractures, 37%are closed, 58% are partly open, and 5% are open. Aperture analysis yielded 106 data points from three wells (D, F, and G), 59 from sills, and 47 from Vaca Muerta shales (Fig. 6.12). Regarding fill, 44% of the fractures reveal dead-oil lining, 19% have calcite fill, 4% show quartz fill, and 33% have no mineralization. Open or partly open fractures of no preferred orientation are found to be commonly oil coated. Vertical fractures are commonly weakly cemented, and no sequential cementations are seen.

We attempted to examine crosscutting relationships but, because of only a few intersections, we could not determine this parameter. Kinematic indicators found on 56 fracture planes include striae and stylolithsFig. 6. 11A, C). Sixty-three percent of these surfaces are sub-horizontally striated (rakes, <25°), 29% have oblique striae, and 9% reveal subvertical striae. Of all 56 striated surfaces, 21% are compressional and/ or transpressional whereas 13% are transtensional and/or extensional; for the remainder, no clear motion sense can be determined. Abundant nonsystematic fracture networks are found at the sill-shale interface (Figs. 6. 9B, 6.10D), showing no preferred orientation or kinematic indicators; they commonly display submillimeter apertures and are fully oil impregnated. Up to 3-ft (1-m)–thick vesicle layers with vugs of several centimeters across are locally oil stained but poorly connected to the fracture network (Figs. 6.9A, 6.11B). Cored intervals from cavity zones have anomalously lowrecoveries (<10%) and consist of poorly consolidated, argillaceous gray greenish material,with crystalline rock fabrics poorly preserved. In core, these zones represent 3- to 10-ft (1–3-m) thickness but, because of the poor recovery, are underrepresented by approximately 70%.

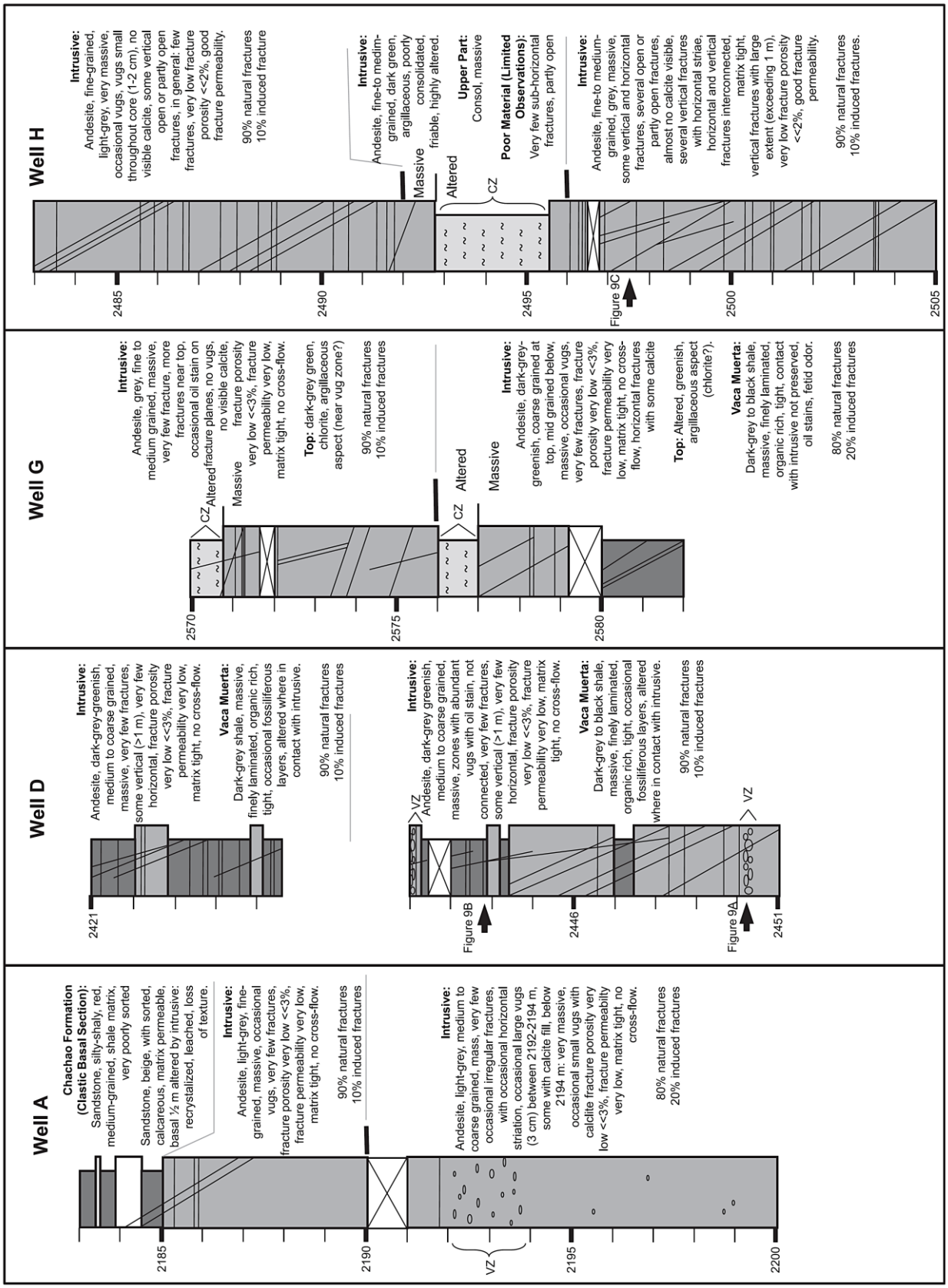

Fig. 6.8: Core descriptions. Dark gray indicates Vaca Muerta; light gray indicates intrusives; fracture angles are not to scale; black arrows mark photographs. Core quality and recovery is very good because of the hard, igneous material. VZ = vesicle layer; CZ = cavity zone.

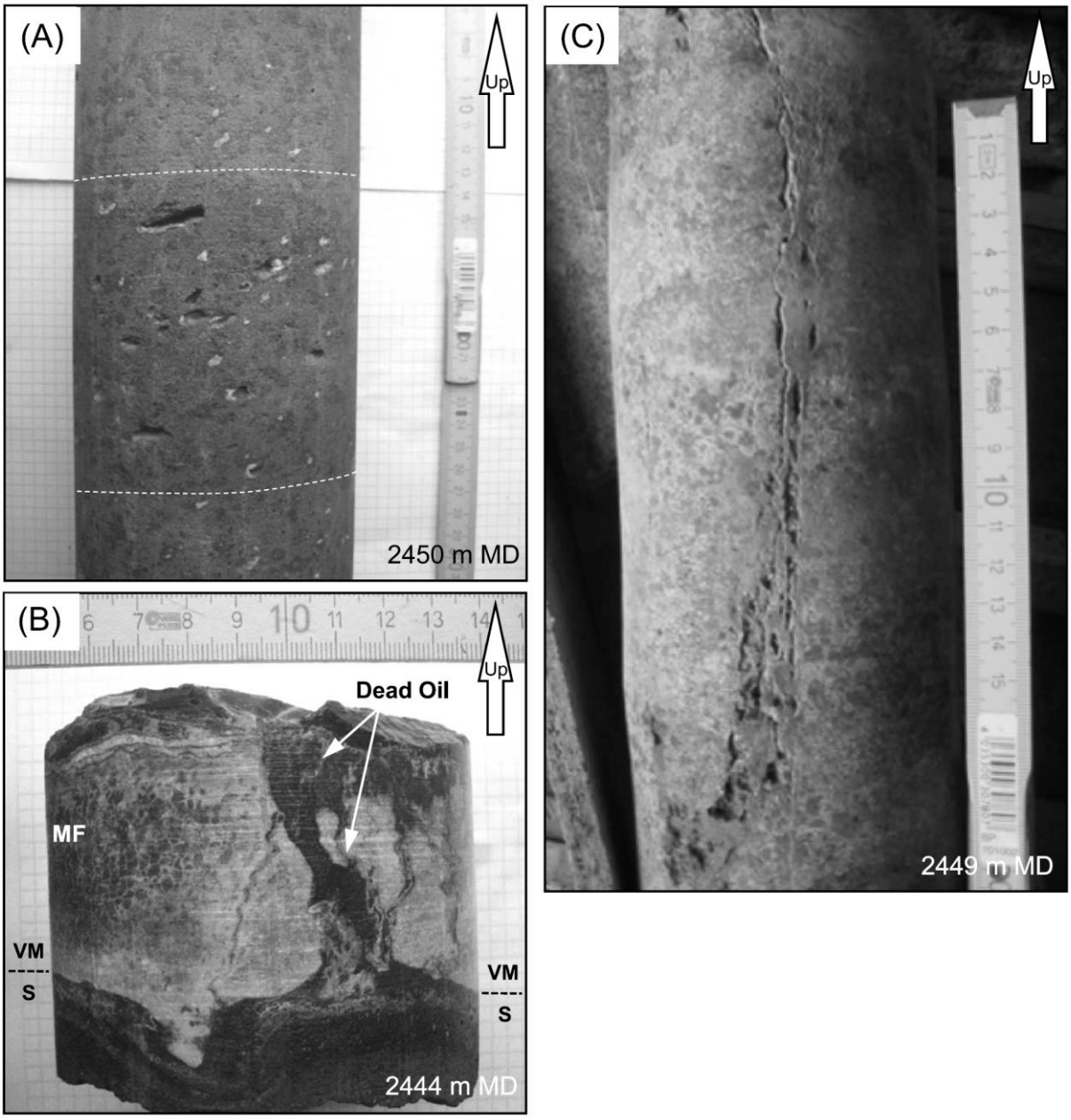

Fig. 6.9: (A) Well D: vug zone, partly mineral filled. (B) Well D: upper contact of the intrusive (S) and Vaca Muerta Formation (VM), oil stain in irregular fractures. (C) Well H: large vertical fracture and vugs. The scale is in centimeters. MF = microfractures; MD = measured depth.

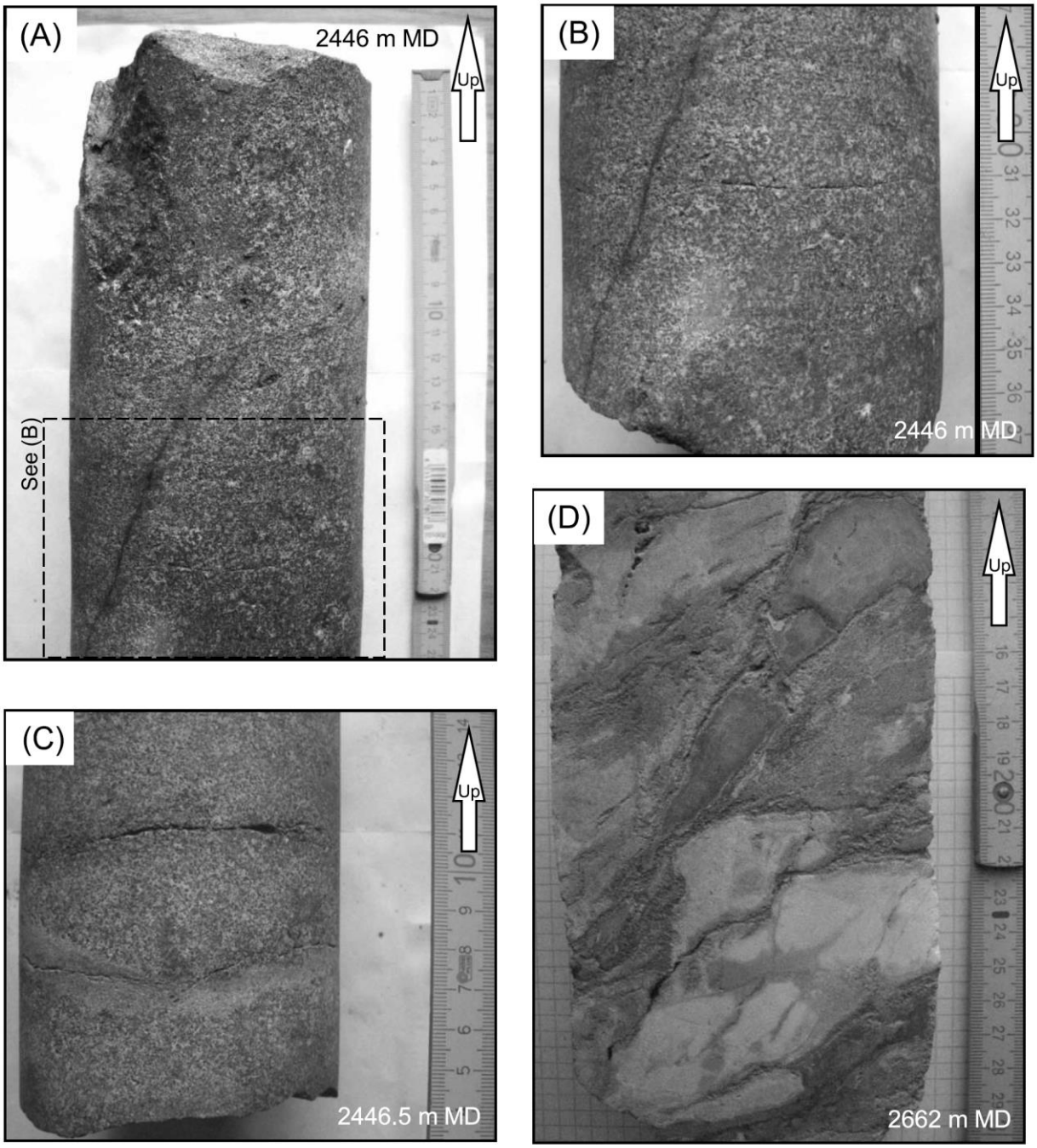

Fig. 6.10: (A) Well K: two connected oil-stained fractures in the intrusive. (B) Well K: subvertical oil-stained fracture and subhorizontal partly open fracture in the intrusive. (C) Well K: subhorizontal partly open fractures in the intrusive. (D) Well F: Vaca Muerta Formation, abundant oilimpregnated fractures. The scale is in centimeters. MD = measured depth.

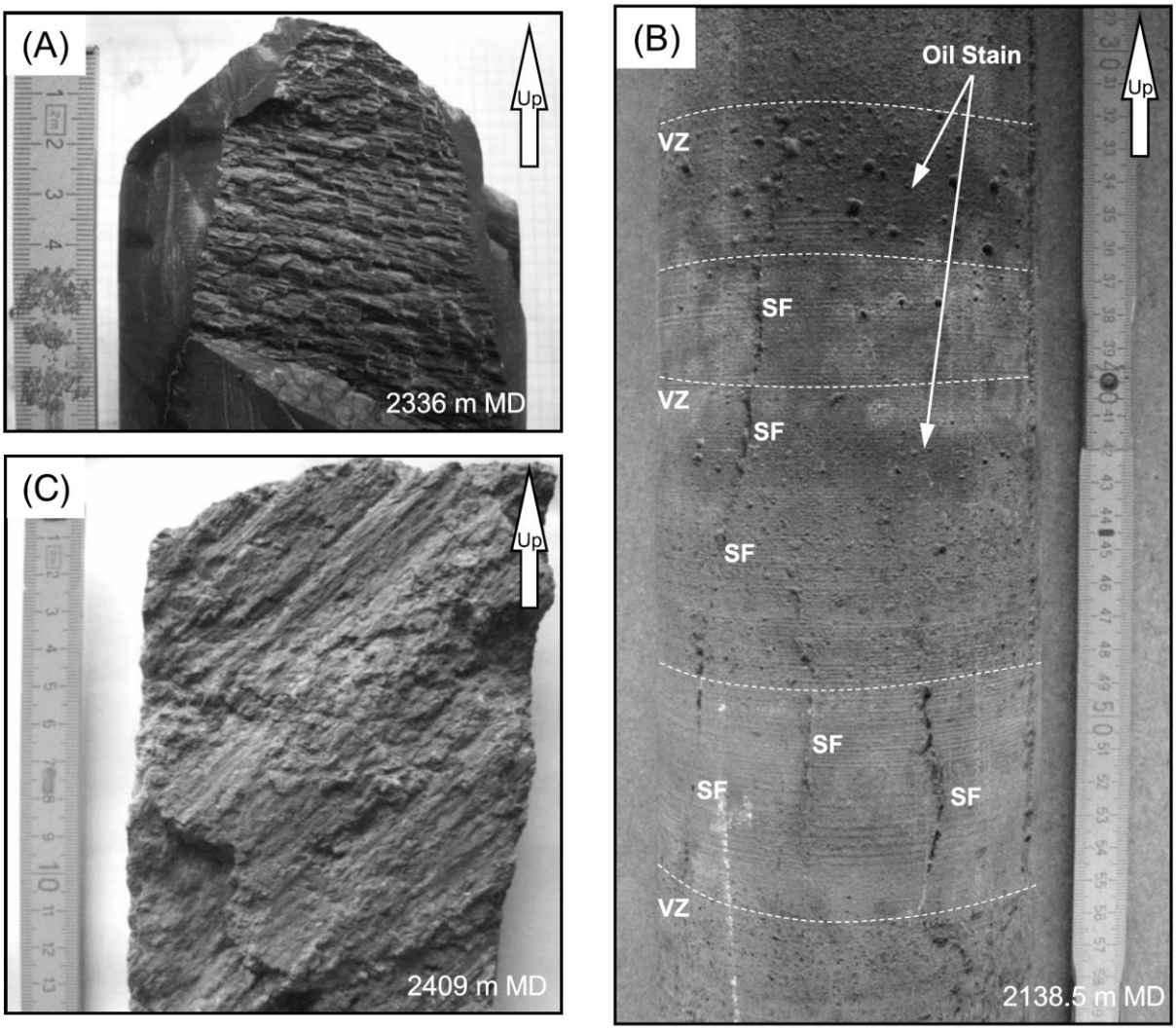

Fig. 6.11: (A) Well L: subvertical fracture with horizontal striae in the shales of the Agrio Formation indicate nearhorizontal movement. (B) Well M: intrusive with vesicle zones (VZ) connected by vertical fractures (SF). (C) Well N: subvertical fracture in the intrusive lined with dead oil. Striae indicate dextral transpression. The scale is in centimeters. MD = measured depth.

6.5.4 Lateral fracture attribute variations from outcrop

Five main sets are recognized: system A (east-northeast–northeast), B (southeast), C (north-northwest), D(north-northeast–northeast), and E (south-southeast–southeast). The exact fracture spacing of the two main sets (A and B) was measured at the pavement, ranging from approximately 0.3 to 3 ft (~0.1–1 m; Fig. 6.14A, B). Semiquantitative observation confirms approximately constant spacing across both intrusives. Only the center of the eastern intrusive displays wider spacing, with block sizes of several meters. Here, a coarse grain fabric is found with crystals several centimeters across. In log-log plots, fracture apertures from the pavement reveal straight distributions over more than two orders of magnitude (Fig. 6.12). Commonly, the fracture length of the longest fractures exceeds 66 ft (20 m) (beyond outcrop dimension). For lengths of as much as 33 ft (10 m), the two main sets show slightly different distributions (Fig. 6.14C). By projecting the line of best fit to the vertical axis in the log-log plot, a theoretical maximum fracture length of several tens of meters can be determined for both sets, which is in good agreement with qualitative outcrop observation.

The outcrop observation for the analysis of vertical height confirms that subvertical and sub-horizontal fractures are sill confined (Fig. 6.15). The presence of numerous multiple intersections between vertical and horizontal fractures indicates good interconnectedness (Fig. 6.15C). Orientation data from five well pads at Los Cavaos revealed four main fracture systems: set 1 (northeast-southwest), set 2 (west-east), set 3 (northwest-southeast), and set 4 (north-south). The orientations of sets 1, 3, and 4 broadly coincide with the other observation scales. System 2 is not well represented because of undersampling. Outcrop work allowed us to separate systematic from nonsystematic fractures. The fractures of the main systems in both intrusives are systematic, straight, planar, and bed confined, and commonly show lateral extents of at least several meters. The rock textures and vesicle layers in the outcrops are similar to those seen in the core. Probably as a result of weathering effects, no cavity zones, few striae, and practically no mineral fills were observed.

6.5.5 Large-scale lineament orientation from remote sensing

Fifty-six lineaments were obtained from satellite imagery, showing four main sets: set 1 (northeast-southwest), set 2 (west-east), set 3 (northwest-southeast), and set 4 (north-south; Fig. 6.16B). These orientations coincide with the fault orientations from the seismic mapping of a horizon near the top of the Chachao Formation and also with fracture orientations from subsurface and well pads.

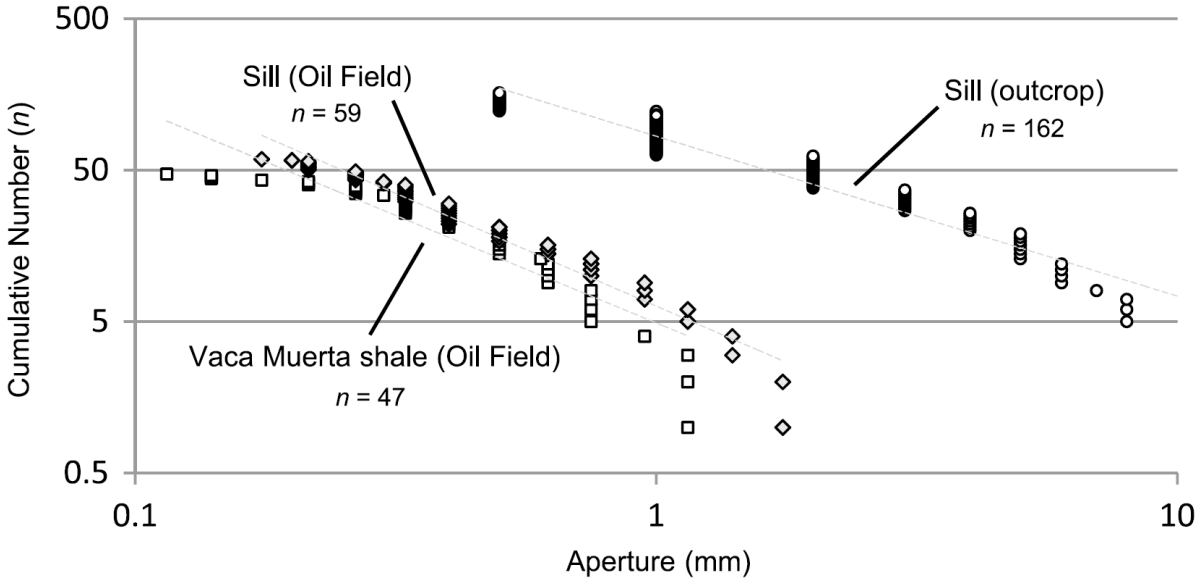

Figure 6.12: Fracture apertures from sills in outcrops and subsurface.

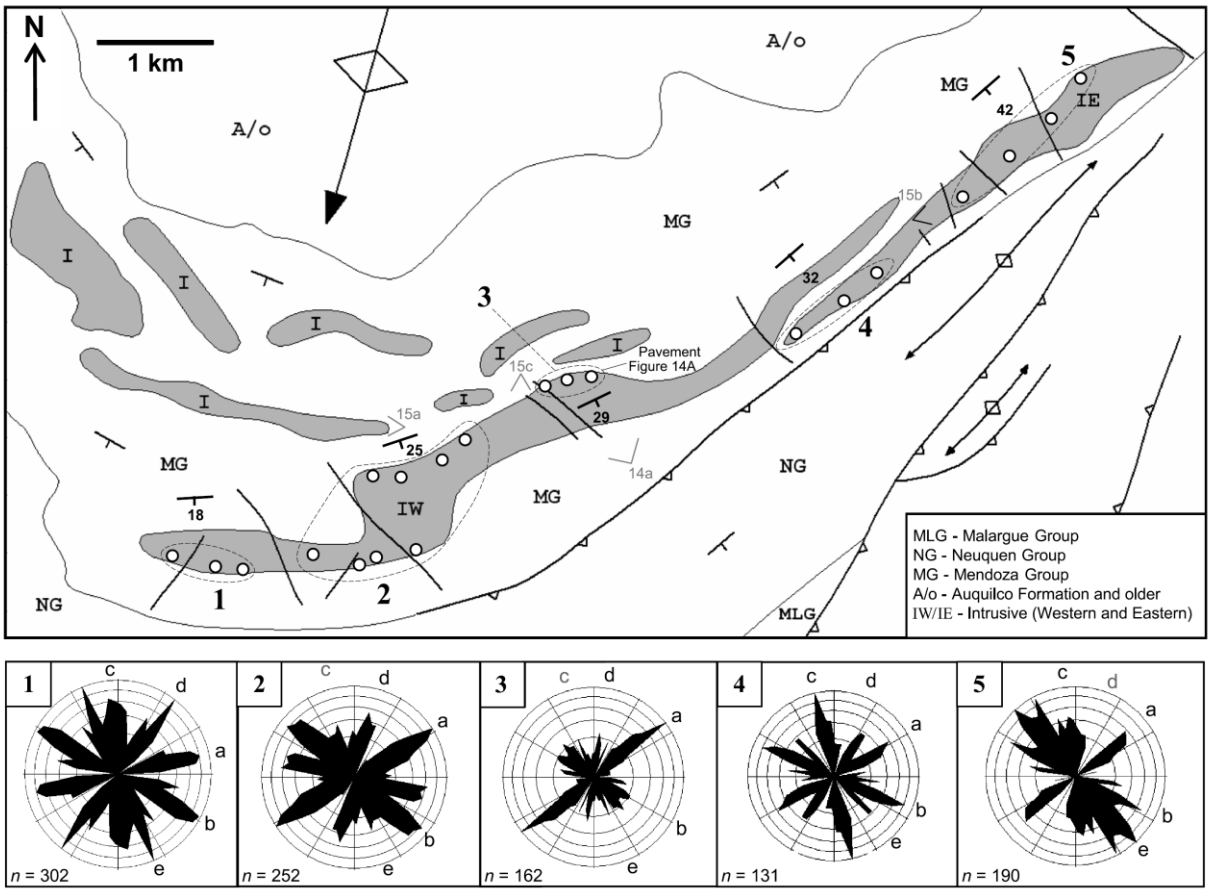

Fig. 6.13: Geologic map of the Sierra Azul outcrops. The stations are marked by circles. Dashed lines indicate dip domains. The orientation data are corrected for local structural dip. The gray numbers indicate the locations of photos (**Fig. 6.15**).

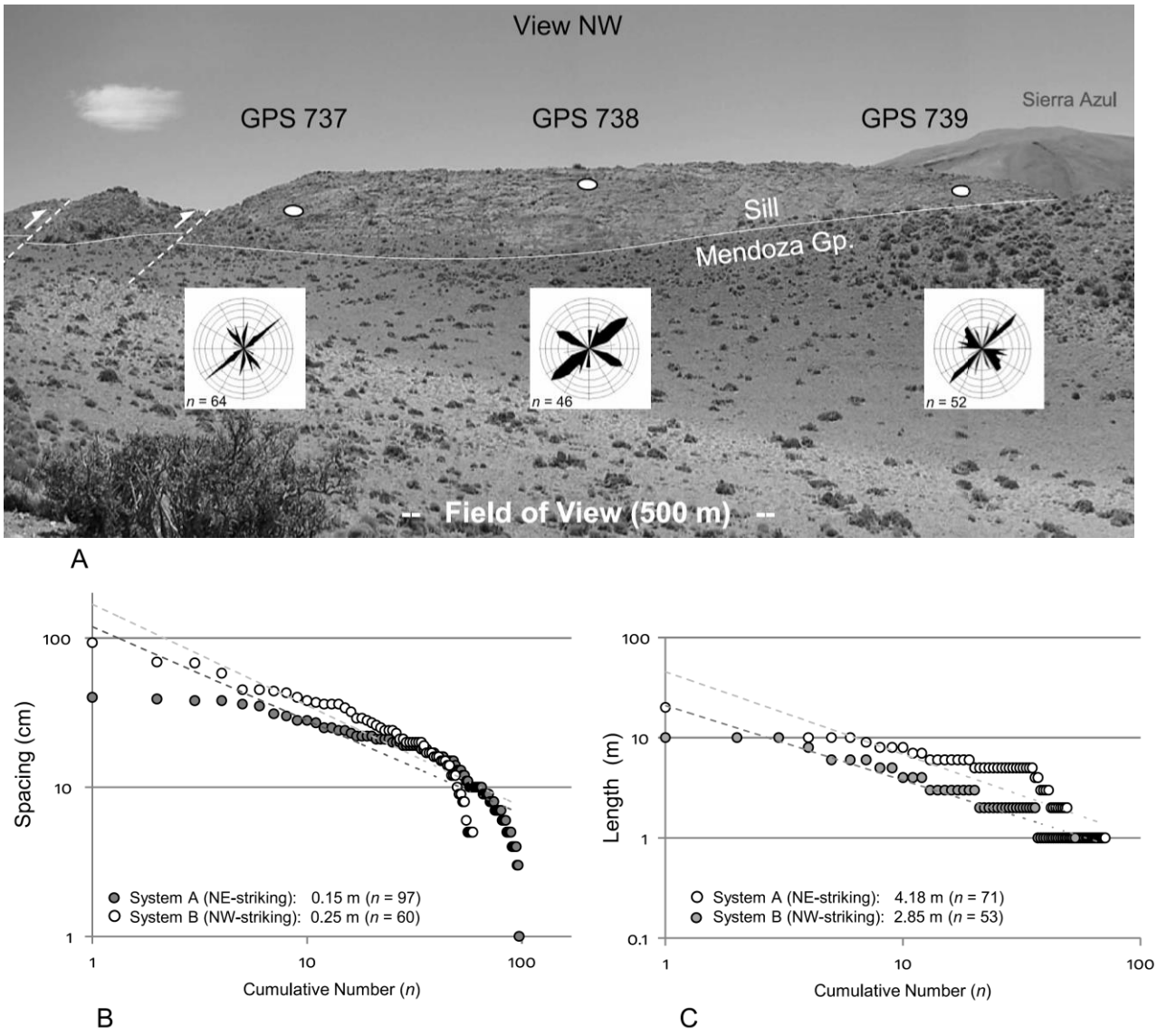

Fig. 6.14: (A) Sill pavement and dip-corrected fracture orientations. Accomodation faults are on the left side. (B) Log-log diagram showing the fracture spacing of the two main sets. (C) Log-log diagram showing the fracture length distribution of the two main sets. GPS = global positioning system.

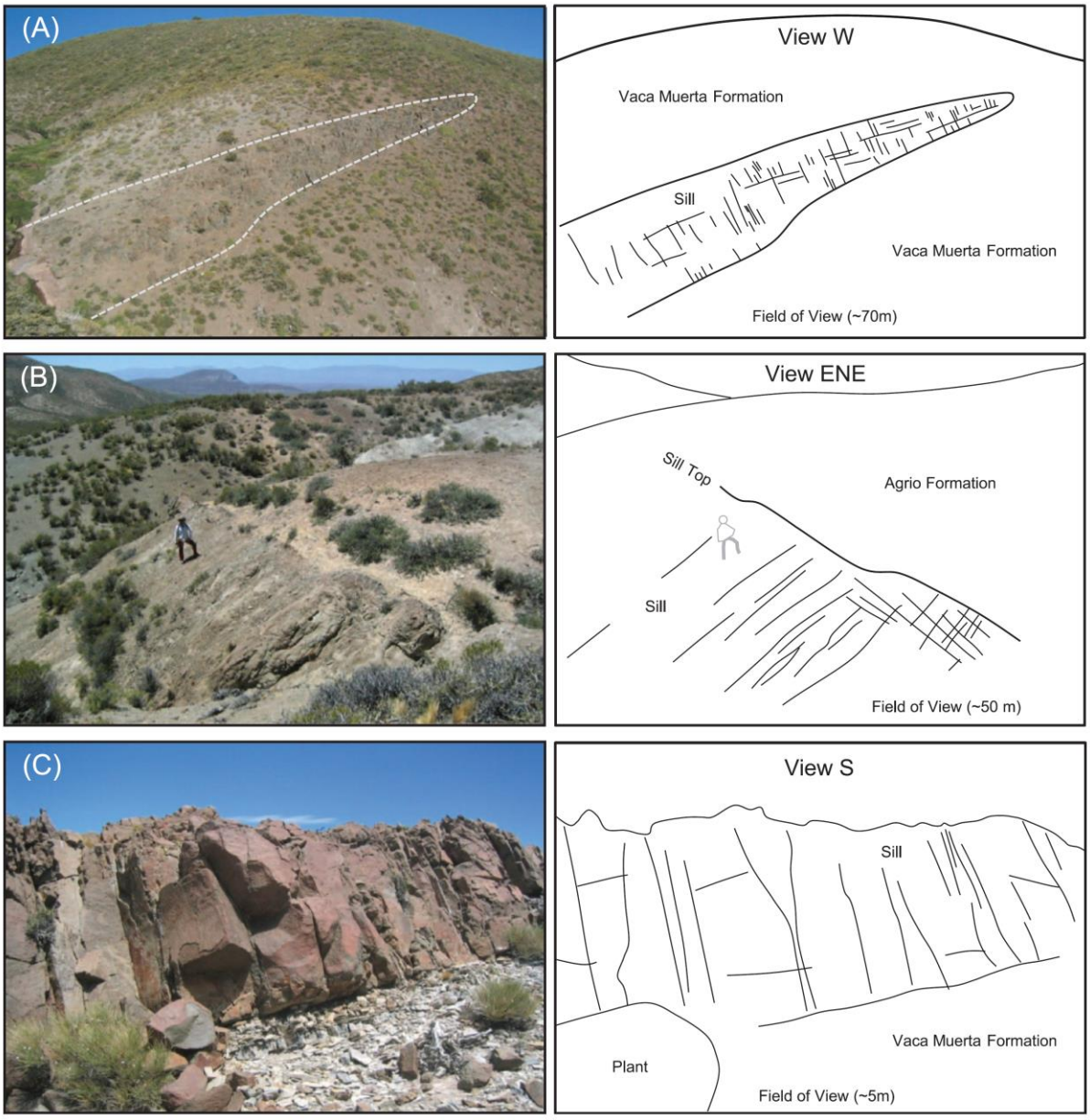

Fig. 6.15: (A) Tip of a sill. Note the thinning and bed-confined fractures. (B) Sharp roof contact of eastern intrusive. Note the bedconfined meter-scale fractures in the intrusive and textureless surrounding shales. (C) Closeup of the western intrusive showing typical fracture spacing. Note the bed-confined fractures, metamorphosed shale at basal contact.

6.6 Discussion

6.6.1 Fracture origin and timing

Different fracturing mechanisms have been identified in igneous rocks, such as cooling, magmatic inflation, tectonism, or unloading (e.g., DeGraff & Aydin, 1987; Schutter, 2003; Kattenhorn & Schaefer, 2008). Major cooling fractures are confined to the igneous body itself (e.g., Kattenhorn & Schaefer, 2008). Locally, metamorphic effects can trigger fractures in the host rock, which typically do not penetrate deeply. We do not observe cooling features typical of surface lava flows, such as bands or hackle marks (e.g., DeGraff & Aydin, 1987), which would indicate abrupt cooling. Cooling fractures in solidifying lava flows grow perpendicularly from the contacts inward (DeGraff & Aydin, 1987; Gil-Imaz et al., 2006) toward the core where densely fractured entablatures may occur (Kattenhorn & Schaefer, 2008). Tectonic fractures may occur in both sills and host rock. From our outcrop and subsurface data, it is not possible to strictly separate cooling and tectonic fractures. Length distributions from outcrop indicate slightly different ages of the main sets. If they are induced by cooling, it would seem plausible that they formed quasi-simultaneously during sill solidification. Striated-cooling joint surfaces may be produced by magmatic inflation, faulting, or folding. We infer that the subvertical fractures were initially created by the thermal contraction of the sill and, during inversion, were tectonically overprinted. Oblique fractures resulting from their orientation are unlikely cooling fractures; we interpret these as a result of the inversion-related arching. We note that fracture formation and shearing on these fractures are not directly related. Andersonian faulting in isotropic bodies should generate fractures, with shear indicators exhibiting downdip (contractional or extensional) kinematics or strike-slip horizontal kinematics. The predominance of an oblique transpressional striae is therefore interpreted as indicating reactivation of existent fractures not only in a modified, but also in a compressional, kinematic regime. Hence, the latter must have undergone changes. In summary, we conclude that at least two phases of fracture generation exist: one caused by cooling and at least one caused by tectonic overprinting.

6.6.2 Kinematics

The present kinematic regime grades from strike slip (σ_{Hmax} ~27°) south of RGV into a thrust regime with prevalent SHmax of approximately 100° at the study area (Guzman et al., 2007; Heidbach et al., 2008). Given the age span embraced by the above map-scale structures, we conclude a fairly constant deformation regime with respect to overall east-west maximum horizontal shortening from middle Miocene to recent times. Most of the kinematic features in the subsurface indicate transpressional

and/or compressional movements. Hence, these fractures were either created by compressional and/or transpressional movements or preexistent fractures were overprinted by such movements.

Sill intrusions represent a stress state where the maximum principal normal stress is oriented horizontally so that magma can overcome the lithostatic pressure and lift the overburden. The sills we investigated show a sharp base and roof in outcrop and subsurface. In addition, sill A reveals a north-south–oriented center bulge, which strongly suggests an underlying north-south feeder dike. The orientation of subvertical basaltic dikes in the wider region is dominantly northeast and north-south, indicating a west-east or northwest-southeast extension. This could indicate that, at the moment of dike intrusion, either the area was under a northwest-southeast–directed extension or that preexisting weakness zones of northeast or north-south orientation acted as conduits. However, geologically, it would be difficult to reconcile north-south–oriented feeder dikes under a west-east–directed compression. We envisage two hypotheses for this apparently conflicting observation: (1) no centered feeder dike under sill A exists and the magma would have intruded from somewhere else and (2) the aforementioned regional stress field is not stable but may have been undergoing short-term changes, a process that temporarily exposed the north-south–oriented preexisting structure to extensional stress, enabling magma to rise. One such mechanism could be a major seismic event at the plate boundary to the west, relaxing the upper plate east-west compression upon rupture. Recent major earthquake events, specifically the Maule earthquake of February 2010, in south Chile, and related global positioning system measurements conducted by Ben Brooks et al. (2011, personal communication) indicate that this event triggered a change in the kinematic regime far into the back-arc. As mentioned above, the deformation of the Palauco anticline, the closest first-order structure from RGV, ceased before 8.14Ma. If the deformation of the RGV structures is related to this first-order structure, then this would constrain the fracture formation and oil charge at RGV to somewhere between the earliest possible time of sill intrusion (10.5 Ma) and the ceased movement of the Palauco anticline (8.14 Ma).

6.6.3 Orientation patterns

Fracture orientations are considered fractal when they are consistent over several orders of scale magnitude (Ortega & Marrett, 2000; Laubach & Gale, 2006). At RGV, we observe broadly consistent fracture orientations over four orders of magnitude (6-mi [10 km] to 3-ft [1-m] scale) (**Figs. 6.16A, 6.16B**). Hence, we infer that fracture orientation is fractal over this scale range. Outcrops show that over 6 mi (9 km), five fracture sets are laterally consistent, so we infer that sills in similar geotectonic

settings may develop consistent fracture sets over many kilometers. Local orientation scatter of individual sets could indicate stress perturbations caused, for example, by inflation fractures (Kattenhorn & Schaefer, 2008).

With respect to the oil-field nose, the four observed fracture sets would be consistent with one longitudinal, one transverse, and two conjugate shear joint sets (Fig. 6.16A). Under the assumption that the fold was contracting while the sills were cooling, the fractures could be explained primarily as cooling related but under an external transpressional confining stress.

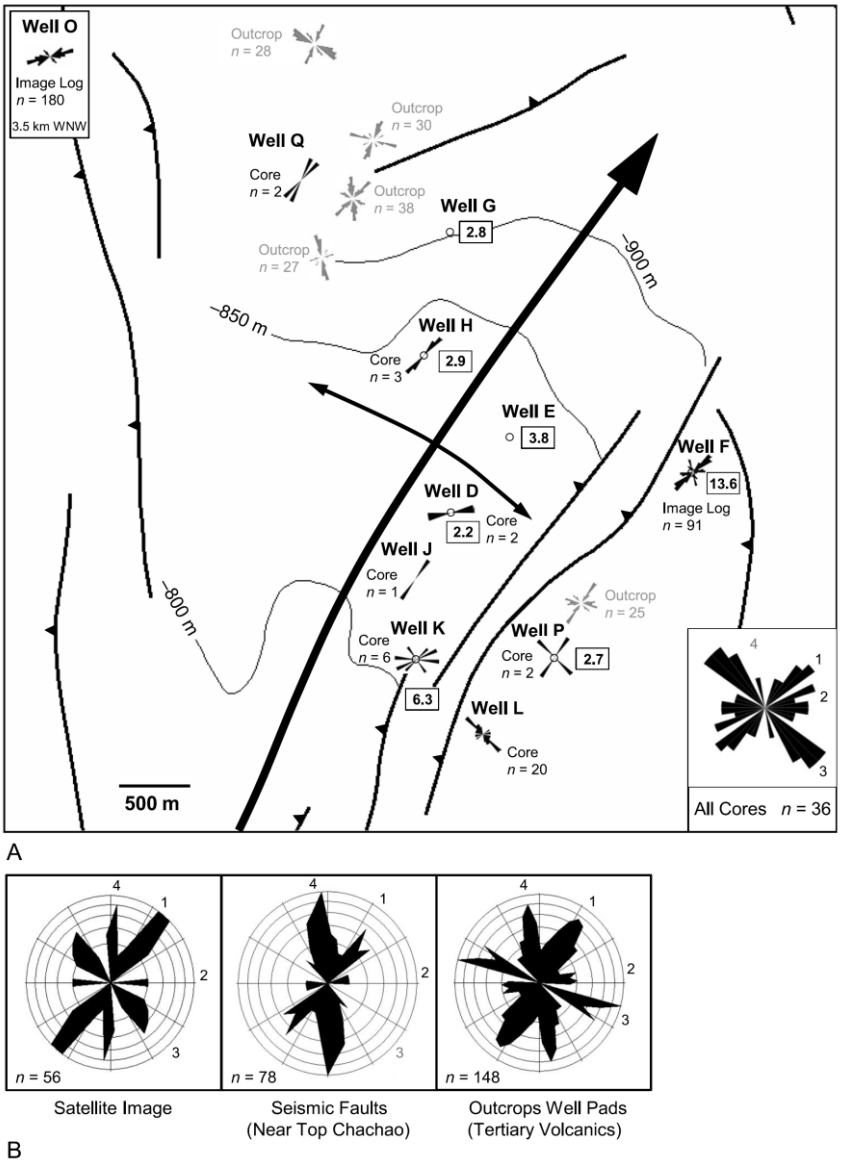

Fig. 6.16: (A) Oil-field scale map of near–top Chachao, with fracture orientations from core, image logs, and well-pad outcrops. Boxes indicate vertical fracture index (fractures per meter). Nonoriented cores were reoriented by aligning the sedimentary dip in the core with the dip from three-dimensional seismic. The error estimate is approximately 5°. (B) Orientation patterns of the main fracture systems at the Los Cavaos oil field at different orders of observation scale.

6.6.4 Spacing

The common approach that joint spacing in sedimentary layers is proportional to layer thickness (e.g., Narr, 1996) is not directly applicable for the sills examined here. These fractures have apparently been created predominantly by cooling effects and superimposed mechanical stresses, so they are unlikely to show the classic mechanical spacing-thickness relationship. Previous studies of fracture spacings in basaltic lava flows report spacing ranges of centimeters to several decimeters (DeGraff & Aydin, 1987; Kattenhorn & Schaefer, 2008), which is in the same range that we observed in core and outcrop. The cumulative spacing frequency of our data suggests a power-law behavior over two orders of magnitude. We do not confirm that fracture spacing is closer at the contact than toward the center, as documented by Kattenhorn & Schaefer (2008). Thicker (and, hence, slower cooling) areas of the outcropping intrusives seem to develop wider fracture spacing, as supported by large block sizes observed at the center of the eastern sill. Vertical fracture indices from core and image logs are in the same range as the outcrops. Abnormally high vertical-fracture indices are found close to major faults, which indicates that faulting may enhance fracture density locally. One key conclusion from the outcrops is that fracture spacing stays relatively constant over many kilometers and seems to be controlled by cooling and tectonic overprinting.

6.6.5 Fracture dimensions

Methods to describe fracture-size properties have been provided by several studies (Marrett, 1996; Ortega & Marrett, 2000). These properties are considered fractal when straight-line distributions over several orders of magnitude are present in log-log diagrams. Our observations indicate that the main fracture sets are perpendicular to the sill base and roof and are sill confined, so their maximum vertical extension would be defined by the sill thickness, an observation that coincides with the findings by Kattenhorn & Schaefer (2008). Ortega & Marrett (2000) use regression correlations to describe fracture-length distributions from pavements and find that scale changes are prone to occur at the length that equals the mechanical layer thickness. The fractures studied herein formed under strong thermal influence. Hence, we doubt that they would correlate with the mechanical bed thickness of the sill. Because of outcrop limitations, we were not able to collect length data beyond the sill thickness, so the question of scale changes in length distribution has to remain open. It is also uncertain if our length measurements reveal power-law or exponential behavior. However, our observation of fracture lengths of greater than 66 ft (>20 m) is independently consistent with predicted maximum lengths from graphical evaluation (Fig. 6.14C). In conclusion, a range of observed fracture lengths can be defined but uncertainty remains regarding their scaling distribution.

6.6.6 Porosity and permeability

To our knowledge, no integrative studies on reservoir-relevant fracture attributes in sills have been published. It has been recognized that fracture aperture data from crystalline rocks predominantly show power-law distributions (McCaffrey et al., 2003; Petford & McCaffrey, 2003), an observation that seems to be confirmed by our data that hint at a power-law distribution over two orders of magnitude. We believe that the similar scaling distributions from apertures in sills and host rocks could indicate similar confining pore fluid pressures and lithostatic conditions because both units have been located at roughly the same depth.Higher aperture values fromoutcrops could be caused by higher accumulated strain or weathering, but scaling still resembles power-law behavior. For aperture analysis, at least 200 data points are recommended to rule out all artifacts (Hooker et al., 2009), so some data uncertainty remains here.

Fracture porosity can be expressed by one-dimensional sampling (Marrett, 1996), which we used in outcrop and core. For our data, simplistic geometric porosity calculations using average aperture (0.5mm), spacing from 3 to 13 fractures per meter of core, lead to fracture porosity ranges of 1 to 8%, which seem in line with the data from oil-producing intrusives ranging from 6 to 10% (McKenny & Masters, 1968; Galloway et al., 1983). Schutter (2003) points out that vesicle porosities in igneous rocks may reach 50%, which is clearly not the case in Los Cavaos. Instead, the sparse and highly localized vesicle layers suggest very low porosity contribution.

Fracture permeability in a reservoir is controlled by the largest fractures in a population (Marrett, 1996), by the number of fracture intersection points (Ortega & Marrett, 2000), and by the degree of cementation (Olson et al., 2007). At RGV, the multiply connected, poorly cemented large fractures and cavities support very high permeabilities and low porosities. For the subsurface, this means that permeabilities are highly localized and, supported by outcrop observation, may be relatively constant over several hundred meters. Early oil coating and protection from mineral overgrowth could explain the weak cementations observed in the fractures at RGV. We support and broadly confirm the findings of Bermudez & Delpino (2008) and Delpino & Bermudez (2009) who recognized the importance of cavity zones in oil-producing sills in the Neuquén Basin. For the first time, we show a map of the sill thickness and its associated cavity zone. On the basis of geometric and lithologic analysis, we suggest that the cavity zones formed from late-stage volatiles in consolidating magmas (e.g., Matthes, 1993). The location of the cavity along the center axis of the sill supports the position of an underlying feeder dikewhere solidification took longest. Cavity zones are also developed in other sills of the RGV and, in several wells, have yielded significant oil flow rates. We suggest that these cavity zones are similar to

the cooling-related entablatures described by Kattenhorn & Schaefer (2008). Our observations confirm that the matrix of the sill is nonpermeable. The reservoir implication of these fracture-cavity networks is that the high degree of connectivity allows high initial production; however, it causes quick pressure drain and makes efficient sweep and secondary recovery very challenging.

6.7 Conceptual model

Based on our observations and the regional geologic context,we propose the following conceptual model for the RGV sills (Fig. 6.17):

1. During the late Miocene, under short-lived periods of west-east directed extension (possibly after major seismic events), andesitic magma rose and intruded along north-south–oriented feeder dikes. Numerous sills were emplaced into the black shales of Mendoza Group strata and triggered an initial oil expulsion, a process known to generate significant overpressure, particularly in a system enclosed by shales. Upon intrusion, liquids were initially driven away from the sills by heat and outward directed pressure gradient.

2. During inward directed solidification, late-stage fluids differentiated from the magma along a tabular zone at the center of the intrusion, creating cavities and vugs and causing alterations. Submillimeter scale fracture networks formed at the shale-sill interface and were impregnated with oil that was expelled locally. Cooling-related contraction caused an inversion of the pressure gradient and oil was now migrating toward the sill because of the inward directed pressure gradient (Aarnes et al., 2008).

3. Ongoing cooling of the sill under resumed west-east compression led to its contraction. Consequently, sill-confined, subvertical cooling fractures formed, connecting cavities and vesicle layers. Sill-confined sub-horizontal fractures formed during this phase. Because of the inward directed pressure gradient and the ongoing oil expulsion from the source rock, oil continued to migrate toward the intrusive being injected into the highly connected fracture-cavity network.

4. Repeated phases of compression and extension controlled by the seismic cycle possibly facilitated the oil charge caused by seismic pumping effects (e.g., Sibson et al., 1975), as indicated by the regional tectonic context.

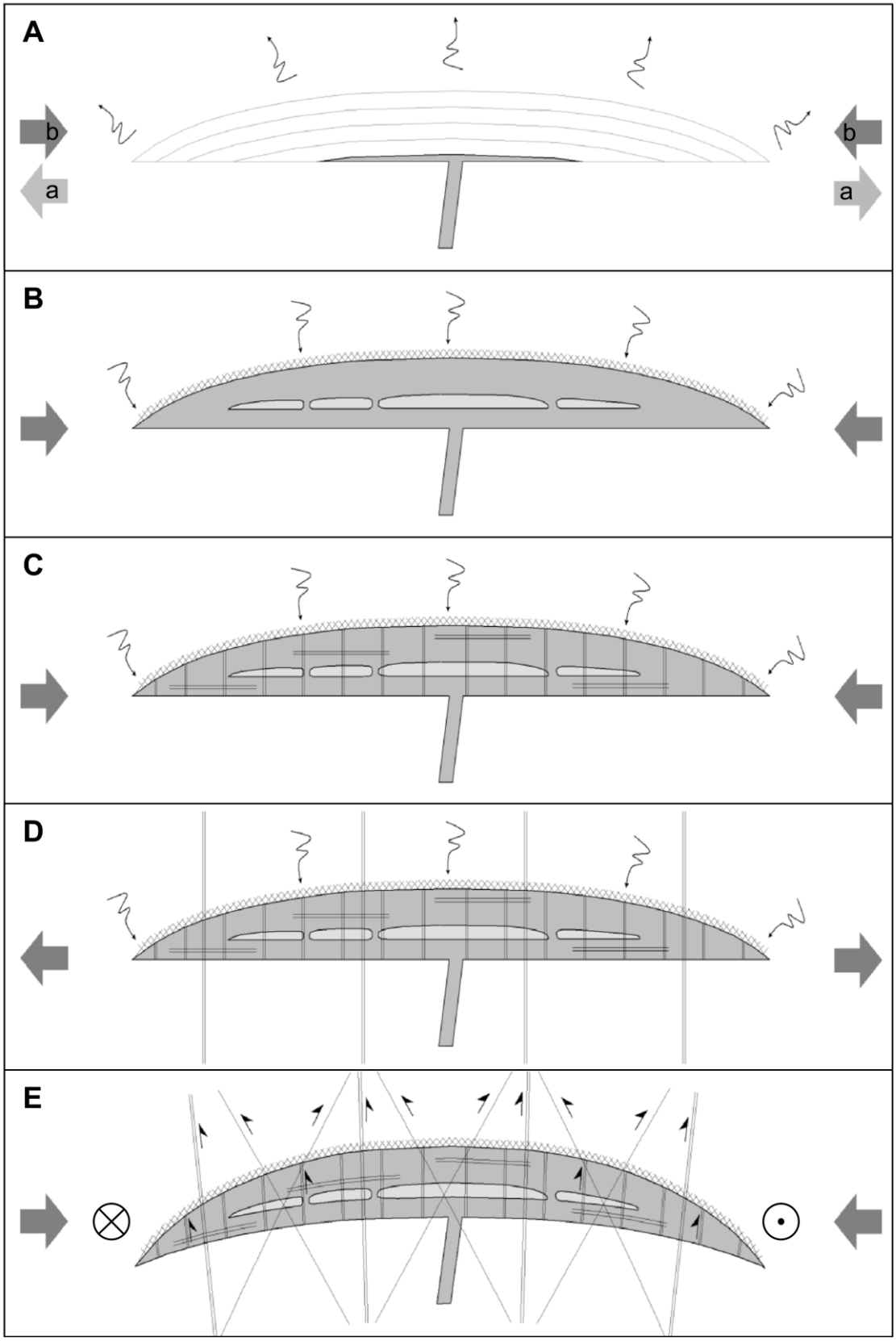

Fig. 6.17: Evolutionary model of sill A. See text for description. a = initial extension; b = subsequent compression.

5. The kinematic regime eventually led to an arching and faulting of the sill. Existing fractures were reactivated transpressionally and new oblique ones formed, leading to additional connectivity. Subtle surface expressions in Neogene strata (e.g., Giambiagi et al., 2008 or Yagupsky et al., 2008) indicate that a west-east contraction and inversion of the structure led to the formation of purely tectonic fractures, affecting sills and host rock.

We encourage that the mechanisms described here, leading to the formation of producible sill reservoirs, be carefully examined in similar oilfield settings, such as the Dineh-bi-Keyah field in Arizona (McKenny & Masters, 1968) or the Wichian Buri field in Thailand (Schutter 2003). We believe that analog applicability depends on several key controlling parameters, such as magma composition (gas content), intrusion depth, cooling history, kinematic history, and richness of source rock.

6.8 Conclusions

Four main fracture sets are identified at Los Cavaos, and their consistent orientation over four magnitudes is an evidence for their fractal organization. The maps of sill A and its associated cavity zone show a north-south thickened center bulge, indicating an underlying feeder dike. High reservoir connectivity through cavity zones and weakly cemented large fractures explain the exceptional initial flow rates of the first oil wells at RGV. Our observations confirm that the bulk oil storage and flow capacity in these atypical oil reservoirs is through fractures and cavity zones. The nonpermeable matrix and poorly connected vesicles do not contribute to the production. Hence, according to the classification provided by Nelson (2001), this is a type-1 reservoir, which has important implications on reservoir development: It is the most challenging of the fractured reservoir types because secondary recovery methods are only poorly applicable. At least two phases of fracture generation are likely, thermal and tectonic; the latter caused shear-failure fractures and transpressional overprint, which enhanced reservoir connectivity.

The parameters spacing, aperture, and length show indications for power-law distribution over two orders of magnitude, an observation that could serve as a prediction tool, as suggested in workflows presented, for example, by Laubach & Gale (2006). Sill reservoirs at RGV are enclosed by shales, and oil-impregnated micro-fracturing networks strongly support local oil expulsion and migration. Because of the subtle relief of the overall structure, we believe that the main entrapment into the fracture-cavity network has a significant stratigraphic component.

Major challenges for future research in sills will be to separate cooling from tectonic fractures and to better grasp fracture-length distributions. Based on our observations of multiscale data and the regional geologic context, we propose a new integrated model explaining fracture evolution, oil migration, and charge in sills of the RGV. Our results may be used as a powerful tool for exploration or field development strategies in similar geologic settings.

6.9 Acknowledgements

We thank Repsol Yacimientos Petrolíferos Fiscales, particularly Pedro Lafourcade and Francisco Dzelalija, for allowing us to publish this paper and for funding the printing. We thank the Faja Plegada Team, particularly Jorge Hechem, Alicia Salinas, Mario Atencio, German Bottesi, and Santiago Periale for the valuable support and fruitful discussions. We thank Daniel Delpino for his assistance and insight. We also thank Nancy Schmidt and Geoff Rait for the geologic discussions during the writing of the paper, as well as Steve Laubach, Jim C. Pickens, Francois M. Roure, and one anonymous reviewer. The AAPG Editor thanks the following reviewers for their work on this paper: Jim C. Pickens, Francois M. Roure, and an anonymous reviewer.

7. CONCLUSIONS

In reference to the key unsolved questions formulated in Chapters 1.2 and 1.3, the main results of this PhD Thesis can be summarized as follows (see below). Note that the results shown here relate to the questions raised in Chapters 1.2. and 1.3:

● What controls the geodynamic situation, structural inheritance, interplay and deformation styles in the back-arc?

Newly integrated multi-scale static and kinematic models that I present here, confirm that in the Peruvian (and Argentinian) back-arcs very different response mechanisms to the Andean contraction exist. Based on regional structural models, covering an area of ~800 km (in N-S direction) and ~150 km (in W-E direction) (**Fig. 4.13**), I present new calculations of the depth to the thick-skinned detachment below the Pachitea and Santiago Basins, which are ~21-24 km and ~19-21 km, respectively. These values coincide closely with published earthquake hypocenters (USGS, 2017) and strongly support published data from across the region (Baby et al., 2005; Sanchez Alvarez, 2007; Devlin et al., 2012). Both areas are located at/near the orogenic front and the lithostratigraphy is very similar across that entire region, although evaporites are more abundant in the Santiago Basin. Based on new seismic data and new structural interpretations, I present a basement-involved transpressional fault system below the San Matias (thin-skinned) thrust that had not been documented previously.

The occurrence of salt structures in Peru has been documented by previous workers (e.g. Benavides, 1968; Hermoza et al., 2006; Moretti et al., 2013; Witte et al., 2015). However, it is the first time that the "Peruvian Salt Belt" domain is proposed in context of the widespread occurrence of salt structures at a preferred longitudinal position along the Peruvian back-arc (**Fig. 4.13**). This interplay of three structural styles (thick-skinned, thin-skinned and salt-tectonics) is common and widespread across the newly defined Peruvian Salt Belt and is more important for the fundamental understanding of structural styles across the region than anticipated. The subduction angle alone does not seem to be the main driver for short-wavelength structures in the Peruvian back-arc. Rather, it appears that the mechanical stratigraphy is the main driver. My observations clearly show that, within the Peruvian Salt Belt, (a) deeply seated and Andean-inverted half-grabens seem to be the exception, (b) across this region, even small salt welds or pillows have the potential to significantly focus the formation of thin-skinned ramps (**Fig. 3.11b**), preferably located near structural basement anomalies and (c) mechanically linked thick- and thin-skinned structures have been (and are) intermittently active over geologic time and, locally, cross-cut each other (**Fig. 3.11c**).

A key observation is that the San Matias thrust represents the easternmost salt-detached thin-skinned structure related to the Andean orogen at this latitude (~10°S).

● **What are the structural timing and the shortening rates, based on the latest interpretations?**

Only very general data on structural timing is available for the greater context of the Santiago Basin (e.g. Naeser et al., 1991; Alemán & Marksteiner, 1993; Prueher et al., 2005; Valdivia et al., 2006; Encarnación, 2008; Chalcatana et al., 2012). Based on newly integrated multi-scale static and kinematic modeling, I present a refined view of the tectonic evolution of the Santiago Basin, whereby the early onset of salt flow occurred already in Albian-Aptian times and contraction can be shown to be active from at least 5.3Ma to post-2.5Ma (**Fig. 4.14**). My kinematic assessments of the Pachitea Basin, located ~600 km south of the Santiago Basin, reveal very similar Cenozoic tectonic activity, as the San Matias thrust there can be demonstrated to be active from 5.3 Ma to post-2.58 Ma. This information broadly supports previously published timing at that latitude (e.g. Mégard, 1984; Gil Rodriguez, 2002; Espurt et al., 2008). For the structures analyzed here, no detailed geological record is available to calibrate the timing after 2.58MA, simply due to the absence of preserved (and deformed) strata. However, geomorphological and modern seismicity data from similar longitudinal and structural positions, near the orogenic front, clearly show that contraction at this longitude is still ongoing at the present-day (Bes de Berc et al., 2005; USGS, 2017). Geomorphological evidence from the thick-skinned Shira Mountains (Pachitea Basin, **Fig. 4.13**), as well as from the central Marañón Basin (~200 km NE of the Balsapuerto Dome), show that deformation is presently ongoing at that longitudinal position (Dumont, 1996; Sanchez Alvarez, 2007). These observations suggest that the structures examined in the Pachitea and Santiago Basins are not likely frozen at 2.58MA.

Based on this PhD Thesis, the amount of thick-skinned shortening at the Pachitea Basin varies between 3.4 km and 5.1 km (~5.5%) (**Figs. 3.7, 3.9**), while the thin-skinned shortening reaches up to 19.6 km (up to 25.5%). At the Santiago Basin overall shortening amounts are between 7.1 km and 7.5 km (~6.1%) (**Fig. 4.6**) (this Thesis), values that are consistent with documented thick-skinned shortening amounts from the Ucayali Basin (Sanchez Alvarez, 2007). The corresponding slip-rates obtained from this PhD Thesis are ~1-1.6mm/yr for the Pachitea Basin and ~1.3-1.4mm/yr for the Santiago Basin. These can be considered slow values when compared with rates from the Eastern Cordillera (Colombia) north of the Santiago Basin where slip rates of up to 5mm/yr have been documented in an approximately similar longitudinal position (Mora et al., 2013). In a greater context, there are indications that the shortening amount (and corresponding slip rates) increase southwards from the Pachitea Basin and northwards from the Santiago Basin, as follows: Across the Southern Ucayali and

Ene Basins Espurt et al. (2008) documented ~56 km of shortening, while from the Huallaga Basin (immediately south of the Santiago Basin) Hermoza et al. (2005) documented ~80 km of overall shortening and Baby et al. (1997) documented even up to 231 km of shortening across the Eastern Cordillera in Bolivia. Possible explanations for these apparent differences in shortening and slip rates at the Santiago Basin and the Pachitea Basin could be (a) the existence of orogenic deflection zones, (b) strain accommodation, (c) shortening may be distributed across numerous structures that are active simultaneously, (d) thick-skinned structures could be are "slower" than salt-detached thin-skinned structures or (e) the existence of unresolved or "blind" structures (Atherton et al., 1983; Marshak, 2004; Oncken et al, 2006; Fildani et al., 2008).

● **What are the implications for the petroleum potential?**

From a petroleum exploration perspective, structural traps should form fast and early on during a basin's tectonic evolution and not suffer from future modifications, so that they can receive oil migration from mature source rocks over time (e.g. Magoon & Dow, 1994). Both, structural style and kinematic evolution are known to have a tremendous impact on the characteristics and associated risks of hydrocarbon traps. Contractional or transpressional thick-skinned structures are often preferred exploration targets as they tend to form higher-relief and simpler (less compartmentalized) domes than thin-skinned structures, as has been documented e.g. from the giant Hassi Messaoud field in Algeria (Bacheller & Peterson, 1991) or the supergiant Ghawar field in Saudi Arabia (e.g. Konert et al., 2001).

Thin-skinned structures, on the other hand, can also host giant fields, as observed in the Camisea region of southern Peru (e.g. Gil Rodríguez, 2002) or at the Cusiana-Cupiagua field complex in central Colombia (Cazier et al., 1995; Last & McLean, 1995). However, these fields tend to develop added complexity, due to fault splays, associated triangle zones, salt welds, salt pillows and increased compartmentalization, as documented from fields in Peru and Colombia (e.g. Cazier et al., 1995; Last & McLean, 1995; Gil Rodríguez, 2002; Wine et al., 2002b), all of which significantly increase operational and commercial risks. Thin- or thick-skinned structures that are active over long periods of (geologic) time, often bear a significant risk of breaching and losing trapped hydrocarbons, an effect that can be mitigated if a given trap – at present – has access to a mature source rock; in that case even a structure that is actively being modified by recent tectonics can host large amounts of hydrocarbons. (e.g. Magoon & Dow, 1994). For the Santiago and Pachitea Basins, where traps are shown to have been repeatedly modified since at least (Upper Cretaceous and) Neogene times, this would mean that the breaching risk is elevated. However, there are strong indications that the known

source rocks in both basins are presently in the oil window (e.g. Mathalone & Montoya, 1995; Martinez et al., 2003, Encarnación, 2008, Disalvo et al., 2008), an observation that has also been confirmed by well results and numerous active oil seeps. This situation makes both Basins attractive exploration targets.

Based on the structural assessments presented here, it can be stated that for the Pachitea Basin significant remaining petroleum potential exists in deeply seated (thick-skinned) transpressional structures, located in the sub-thrust setting of the San Matias thrust sheet (**Fig. 3.10**). This structural play-fairway is about 80 km long (in NNW-SSE direction) and has not been documented in detail before. Additional petroleum potential exists in transverse structures (perpendicular to the Andean trend), such as lateral ramps (**Fig. 3.3**). One such structure can be mapped at the northernmost tip of the San Matias Mountains (**Figs. 3.3, 3.5**). The grain of both structural fairways is likely relatively old (from a petroleum systems perspective), but suffered (possible) Cretaceous and Mio-Pliocene modifications, which increase the risk of trap-breaching. Recognizing prospective undrilled play-fairways is one of the most effective ways to detect significant amounts of reserves. Once proven by the first well, the "string of pearls" can be drilled consecutively, structure by structure, and can potentially add significant volumes to the reserves book. To find undrilled play-fairways, like the one below the San Matias Mountains, becomes exceedingly difficult nowadays. From this perspective, this thick-skinned transpressional play-fairway represents an extremely attractive *thick-skinned* drilling opportunity.

At the Santiago Basin, on the other hand, the attractive exploration potential is hosted in the thin-skinned post-salt stratigraphic section. The thick-skinned structures there are far too deep (e.g. **Fig. 4.5**) and the current seismic data commonly does not have enough resolution to confidently map these deep structures. For these reasons the thick-skinned domain at the Santiago Basin is not considered a realistic exploration target. Regarding the thin-skinned post-salt section it is important to note that the onset of salt flow during Albian-Aptian times was favorable for the early generation of structural relief and for entrapping hydrocarbons early on (**Fig. 4.14**). From this time onwards W-E directed hydrocarbon migration became more complex and would have only worked via a "fill-and-spill" mechanism. However, N-S (strike-parallel) directed migration seems much more likely (Rocha et al., 2008). The latest common critical moment for both source rocks there occurred during Early Miocene times. From this time onwards significant salt-related structural relief already existed across the basin, generating attractive trapping potential.

- **How can the inventory of oil-bearing fractures in igneous reservoirs be better understood?**
- **How can the understanding of scale, dimension and evolution of these fractures be improved?**

Natural fractures are commonly only centimeters to millimeters wide and, hence, the best way to document their scale and dimensions thoroughly is via high-resolution methods, such as drill core, well logs or outcrop observation. Additionally, surface geology, outcrop, core and well log data should be analyzed in combination (integrated) from as many locations as possible (Pollard & Aydin, 1988) and should be assessed in the greater structural-kinematic context. It has been recognized that many fracture studies are biased, which is commonly due to the highly localized nature and orientation of (petroleum) wells, especially when scarce and poorly representative data is used (Narr, 1996). Fractured oil producing volcanic, intrusive or metamorphic rocks have been documented from numerous hydrocarbon basins (Nelson, 2001; Petford & McCaffrey, 2003), however, at present there is no standardized workflow to analyze fractured igneous petroleum reservoirs. Existing studies on fractures in igneous reservoirs are mostly descriptive and rarely try to explain fracture evolution in the kinematic context (e.g. Bermudez & Delpino, 2008). This is likely due to the extremely variable, scarce and often biased data sets. (Static) fracture inventories in igneous rocks have been described previously (e.g. Petford & McCaffrey, 2003; Kattenhorn & Schaefer, 2008) and the tectonic-kinematic evolution of the corresponding basins have been assessed. However, rarely have both elements been analyzed in combination to understand fracture evolution in the greater kinematic context.

In this PhD Thesis, for the first time, an integrative kinematic model concept explaining the formation and evolution of oil-bearing fracture populations in andesitic sills is presented (**Fig. 6.17**). Based on an exceptional data set, including numerous cores, the different kinematic attitudes of the fractures can be linked to magmatic and tectonic events, embedded in the regional context of the Northern Neuquén Basin. I have shown that the challenge of characterizing scale and dimension of fractures (hosted in igneous rocks) can be overcome by a high-density data set that ideally should include abundant core data (and/or image logs). In consequence, this means that cutting abundant cores and registering abundant image log data is absolutely fundamental in (igneous) fracture analysis. Furthermore, I have shown that by analyzing and integrating multi-scale data valuable additional information can be made, allowing for predictions of certain parameters, such as fracture orientation or fracture aperture. A key question is how the fractures fit into the regional context of the Argentinian back-arc. Inter-seismic non-continuous extension reaches far into the back-arc (Ben Brooks, personal communication; Li, 2016) and seems to control the formation and overprinting of these fracture systems and the fluid flow therein (this Thesis). These observations confirm the mechanism of seismic pumping, first established by Sibson et al., 1975.

Some aspects of fractures remain challenging to assess, such as quantifying fracture length, which is practically impossible to quantify from core or log data, as it requires a larger observation window (Pollard & Aydin, 1988). However, even large outcrops are often too small to map fracture lengths in confidently and in statistically meaningful ways. Another challenge in igneous fracture analysis that remains is the precise distinction between cooling and tectonic fractures. This will only be improved by future research if exceptionally exposed fracture surfaces are available, either from core data or outcrop data. My findings and workflows may be (fully or partially) applied in similar settings around the world, wherever a high-resolution data set is available and the greater kinematic context can be reconstructed. This has implications from a petroleum exploration and reservoir management perspective, as oil recovery factors can be optimized and operational and commercial risks will be mitigated.

- **How can uncertainty quantification better constrain multi-scale models?**
- **What are the implications of improved multi-scale models for the petroleum potential?**

In this PhD Thesis, the Malargüe Anticline provides a unique, dense and high-quality data set that was used to build a highly calibrated (pseudo-) 3D model (**Figs. 5.1., 5.6**). Subsequently, a new and systematic workflow, developed here, provides new and detailed insight into uncertainty quantification and helps to better constrain static and kinematic models and drive the genetic model. Previous research has found that the main sources of uncertainty in structural interpretation are related to acquisition, processing and interpretation of data, geometric and kinematic uncertainties (e.g. Victor et al., 2004; Judge & Allmendinger, 2011; Allmendinger et al., 2012, Bond, 2015). In this PhD Thesis I demonstrated, for the first time, that - based on area misfit analysis – the total uncertainty for the Malargüe Anticline cannot be reduced to less than ~7% (**Figs. 5.8., 5.9**). Detailed mapping of the 2-dimensional solution space revealed indications for dependencies of model parameters (**Fig. 5.10**). Major disadvantages of traditional workflows to quantify uncertainties include the lack of not being able to capture small-scale structures (Judge & Allmendinger, 2011), the requirement of very specific strain markers (Poblet & Bulnes, 2007) or not systematically exploring the solution space and interdependencies (Victor et al., 2004).

In contrast, the workflows developed and demonstrated here can be applied in any +/- well constrained 2D or 3D model and, furthermore, can be expanded to different structural settings, such as extensional or salt tectonics. If full 3D data sets are available, differential misfit volumes could be used to map the uncertainties (instead of using 2D differential misfit areas, as shown here). In consequence, and based on the uncertainty quantifications, better constrained static and kinematic

models of the Malargüe Anticline (or other potentially oil-bearing) structures can be constructed. From a petroleum or mineral extraction perspective, this will greatly reduce operational and commercial risks.

8. OUTLOOK – OPEN QUESTIONS

Certain aspects of multi-scale thick-skinned contractional structures and uncertainty analysis remain open at this stage. This chapter summarizes the key remaining questions, as follows:

● **How can the understanding of the structural interplay be improved further?**

Regarding the geodynamic situation and deformation styles, I have shown for different regions of the Subandean back-arc that the interplay of different structural styles is more important than anticipated (at different scales): Thin-skinned deformation is triggered by deep-seated thick-skinned structural growth and can be highly focused by the presence of evaporites (e.g. Moretti et al., 2013) (**Fig. 3.11b**). Further questions, to be approached by future researchers, include the geomechanical impact of ductile shales (e.g. Bolivia) or brittle volcanics (e.g. Argentina, Colombia) on the interplay of structural styles. Regarding structural inheritance, it can be stated that in order to clearly answer the question if a thick-skinned structure has newly formed or has been reactivated by a tectonic increment, it is necessary to understand the state of the structural grain and heterogeneity of the crust ***before*** the structure was formed. And therein lies the challenge: due to the low resolution and indirect nature of the existing methods it is extremely challenging (often impossible) to map the geometry and heterogeneities of the roots of thick-skinned structures. Possible approaches used by future researchers to overcome this challenge could include (a) optimizing the resolution of the existing methods (e.g. gravity, magnetics/magnetotellurics, seismic tomography) or (b) to develop new methods, e.g. based on numeric forward modeling. Some authors have successfully approached these challenges, e.g. by using deep and specially processed seismic data to significantly improve the mapping of the configuration of deep Sub-Andean basement blocks (e.g. Zapata and Allmendinger, 1996) or to better understand the role of basement blocks in terms of stress accommodation and deflection (e.g. Fildani et al., 2008).

Key future challenges will be to analyze the rheological heterogeneities and architecture at the basement level in combination (integrated over several scale-magnitudes) and how they interact with the mechanical stratigraphy of the overburden during the seismic cycle.

● **How can uncertainty quantification in multi-scale kinematic models be improved further?**

Standardized workflows to quantify uncertainty in (multi-scale) structural interpretations are presently lacking. Based on the exemplary data set from the highly constrained Malargüe Anticline I have developed and presented a new workflow that, based on ***two selected*** variables, allows to constrain the uncertainties there to less than ~9% (**Figs. 3.3, 3.5**). Furthermore, my assessment revealed indications for interdependencies between parameters (**Fig. 5.10**). Fundamental questions to be approached by future researchers will be to test additional parameters and, eventually, to examine which interdependencies exist between them and how to map the uncertainty minima in the multi-dimensional solution space.

Which methods and tools could be used? Some methods that come to mind include numerically conducted forward modeling, applying Monte-Carlo-Simulations, which are based on the stochastic analysis of repeated random sampling (of outcomes) (Metropolis et al., 1953) and Bayesian statistics (Bayes & Price, 1763), by simultaneously using all algorithms and their variables in the entire multi-dimensional solution space, with the overall aim to locate the uncertainty minima. Another open – and highly interesting – question will be to test how the workflow I developed can be adapted to other tectonic settings, such as e.g. extensional tectonics, thin-skinned tectonics, shale tectonics or by combining strain modeling with fracture prediction.

● **What are the implications of further improving multi-scale (fracture) models for the petroleum and other industries?**

In fracture analysis it is fundamental to understand fracture origin, orientation, spacing, dimensions (length, height, aperture), permeability, morphology and the current state-of-stress. All of these parameters have significant influence on the amount of fluids that can be stored in a given rock volume and the flowability of that fluid (Pollard & Aydin, 1988; Nelson, 2001). The principal value of conducting petroleum-related multi-scale fracture analyses lies in enabling (lateral and vertical) predictions of the hydraulic reservoir properties in undrilled areas, to minimize operational and commercial risks. In this PhD Thesis I have shown that assessing fractures within their kinematic context can help significantly to develop more robust conceptual models (**Fig. 6.17**) and to better explain (and predict) fracture parameters, such as fracture aperture, spacing and length (**Figs. 6.12, 6.14**).

Remaining challenges, that will be approached by future researchers, include better assessments and more precise predictions of fracture length and to map hydraulic interconnectivity between different fracture sets. Particularly for fractured igneous reservoirs, very few robust and integrative studies are available; while some authors have defined different types of cooling fractures (Kattenhorn & Schaefer, 2008), it remains a major challenge to clearly distinguish cooling from tectonic fractures. Especially in metamorphic rocks, that are usually extremely old, it becomes very difficult to recognize and reconstruct the formation of different fracture populations (Petford & McCaffrey, 2003). The ability to distinguish cooling from tectonic fractures, to better reconstruct fracture sets in metamorphic rocks and to predict fracture length and hydraulic interconnectivity more precisely, have extensive implications for scientific research and numerous fields of technology. Naturally, these applications include optimized extraction of hydrocarbons, but would also yield significant improvements in technologies that are currently gaining significant momentum, such as radioactive waste management, extraction of geothermal energy and the construction of underground cities.

9. REFERENCES CITED

Aarnes, I., Podladchikov, Y.Y. and E. Ragnhild Neumann, 2008, Postemplacement melt flow induced by thermal stresses: Implications for differentiation in sills: Earth and Planetary Science Letters, v. 276, p. 152–166, doi:10.1016/j.epsl.2008.09.016.

Alemán, A. M. and R. Marksteiner, 1993, Structural styles in the Santiago fold and thrust belt, Perú: A salt related orogenic belt: Oxford, UK, Second ISAG, September 21–23, p. 147–153.

Alemán, A. M. and R. Marksteiner, 1997, Petroleum systems and structural styles in the Santiago fold and thrust belt: A salt related orogenic belt: Simposio Bolivariano, http://archives.datapages.com/data/colombia_acggp/simp6/tomo2/033.htm, p. 171–186.

Alemán, A. M., Marksteiner, R. and D. Valasek, 1999, Petroleum systems along the northern Marañon foreland basin and relationship to the Oriente and Putumayo Basins northern South America: Volumen Jubilar No. 5, "75 Aniversario Sociedad Geológica del Perú," Lima, p. 27–43.

Allmendinger, R.W., Cardozo, N. and D.M. Fisher, 2012, Structural Geology Algorithms, Vectors and Tensors; Cambridge University Press; 289 p.; doi.org/10.1017/CBO9780511920202.

Allmendinger, R.W. and P. Judge, 2013, Stratigraphic uncertainty and errors in shortening from balanced sections in the North American Cordillera, GSA Bulletin, 125, p. 1569-1579.

Allmendinger, R., 1998, Inverse and forward numerical modeling of trishear fault-propagation folds; Tectonics 17 (4), p. 640-656.

Allcca Torres, M.A., 2007, La sub Cuenca Pachitea: estructura, nueva estratigrafía y potencial hidrocarburífero. Universidad Nacional de Ingeniería, Facultad de Ingeniería Geologica Minera y Metalúrgica, Lima. September 2007.

Amrouch, K., Lacombe, O., Bellahsen, N., Daniel, J.-M. and J.-P. Callot, 2010, Stress and strain patterns, kinematics and deformation mechanisms in a basement-cored anticline: Sheep Mountain Anticline, Wymoning; Tectonics, 29, p. 1-27.

Angermann, D., Klotz, J., Reigber, C., 1999, Space-geodetic estimation of the NazcaeSouth America Euler vector. Earth Planet. Sci. Lett. 171, p. 329-334.

Artoni, A., Casero, P., 1997. Sequential balancing of growth structures, the late Tertiary example from the central Apennine; Bull. Soc. Géol. France 168, 35-49.

Atherton, M. P., W. S. Pitcher, and V. Warden, 1983, The Mesozoic marginal basin of central Perú: Nature, v. 305, p. 303–306.

Audin, L., Lacan, P., Tavera, H., Bondoux, F., 2008. Upper plate deformation and seismic barrier in front of Nazca subduction zone: the Chololo fault system and active tectonics along the Coastal Cordillera, southern Peru. Tectonophysics, 459, p. 174-185.

Baby, P., Rochat, P., Mascle, G. and G. Herail, 1997, Neogene shortening contribution to crustal thickening in the back arc of the Central Andes. Geology 25 (10), p. 883-886.

Baby, P., W. Hermoza, L. Navarro, R. Bolaños, N. Espurt, M. Roddaza, S. Brusset, and W. Gil, 2005, Geodinámica Mio-Pliocena de las cuencas subandinas peruanas: un mayor entendimiento de los sistemas petroleros: INGEPET, 2005, EXPR-3-PB-20, Lima, 14 p.

Baby, P., M. Rivadeneira, R. Barragán, and F. Christophoul, 2013, Thick-skinned tectonics in the Oriente foreland basin of Ecuador, in M. Nemcok, A. Mora, and J. W. Cosgrove, eds., Thick-skin-dominated orogens: From initial inversion to full accretion: Geological Society, London, Special Publications 377, p. 59–76.

Baby, P. et al., 2014, Thrust propagation and new geochronologic constraints in the Peruvian Subandean fold and thrust belt: VIII INGEPET 2014.

Bacheller, W.D. and R.M. Peterson, 1991, Hassi Messaoud Field – Algeria, Triassic Basin, Eastern Sahara Desert, in Foster, N.H., and Beaumont, E.A., eds., Structural Traps V: AAPG Treatise of Petroleum Geology, Atlas of Oil and Gas Fields, p. 211-225.

Baldauf, P., G. Stephens, F. Nullo, A. Combina, and M. Kunk, 1997, Tertiary uplift, magmatism and sedimentation of the Andes, southern Mendoza Province, Argentina: Geological Society of America Bulletin, v. 29, no. 6, p. A-48.

Bayes, Mr. and Mr. Price, 1763, An Essay towards Solving a Problem in the Doctrine of Chances. By the Late Rev. Mr. Bayes, F. R. S. Communicated by Mr. Price, in a Letter to John Canton, A. M. F. R. S; Philosophical Transactions of the Royal Society of London; 53; p. 370–418. doi:10.1098/rstl.1763.0053

Beacom, L.E., Holdsworth, R.E., McCaffrey, K.J.W. and T.B. Anderson, 2011, A quantitative study of the influence of pre-existing heterogeneities upon fracture-zone development during basement reactivation, in: Holdsworth, R.E, Strachan, R.A., Magloughlin, J.F. an R.J. Knipe, eds., 2001, The Nature and Tectonic Significance of Fault Zone Weakening; Geological Society, London, Special Publications, 186, p. 195-211.

Benavides, V., 1968, Saline deposits of South America: Geological Society of America, Special Papers 88, p. 249–290.

Bergh, S.G., Braathen, A. and A. Andresen, 1997, Interaction of basement-involved and thin-skinned tectonicsm in the Tertiary fold-thrust belt of central Spitsbergen, Svalbard; AAPG Bulletin, 81(4), p. 637-661.

Bermudez, A., and D. H. Delpino, 2008, Concentric and radial joint systems within basic sills and their associated porosity enhancement, Neuquén Basin, Argentina, in K. Thompson and N. Petford, eds., Structure and emplacement of high-level magmatic systems: Geological Society (London) Special Publication, v. 302, p. 185–198, doi:10 .1144/SP302.13.

Berthelon, J., Sassi, W., 2016. A discussion on the validation of structural interpretations based on the mechanics of sedimentary basins in the northwestern Mediterranean fold-and-thrust belts, Bull. Soc. Géol. France 187 (2), p. 83-104.

Bertolotti, R. and Moretti, I., 2009, Deformation history and structural style in the North Ucayali basin. In: X Simposio Bolivariano; Cartagena de las Indias, Colombia.

Bes de Berc, S., Soula, J.C., Baby, P., Souris, M., Christophoul, F. and J. Rosero, 2005, Geomorphic evidence of active deformation and uplift in a modern continental wedge-top – foredeep transition: Example of the eastern Ecuadorian Andes; Tectonophysics, 399, p. 351-380.

Boigk, H., 1981, Erdöl und Erdölgas in der Bundesrepublik Deutschland: Erdölprovinzen, Felder, Förderung, Vorräte, Lagerstättentechnik: Ferdinand Enke Verlag, Bewertungen, 330 p.

Bond, C.E., Gibbs, A.D., Shipton, Z.K., Jones, S., 2007, What do you think it is? “Conceptual uncertainty” in geoscience interpretation; GSA Today 17 (11), p. 4-10.

Bond, C., 2015, Uncertainty in structural interpretation: Lessons to be learnt, Journal of Structural Geology, 74, p. 185-200.

Boyer, S.E., 1995, Sedimentary basin taper as a factor controlling the geometry and advance of thrust belts; American Journal of Science, 295, p. 1220-1254.

British Geological Society, 2019, International geomagnetic reference field; http://www.geomag.bgs.ac.uk/research/modelling/IGRF.html.

Brooks, B.A., Sandvol, E., Ross, A., 2000, Fold style inversion: Placing probabilistic constraints on the predicted shape of blind thrust faults; Journal of Geophysical Research, 105 (B6), p. 13281-13301.

Buiter, S.J.H., 2012, A review of brittle compressional wedge models; Tectonophysics, 530-531, p. 1-17.

Bump, A., L. Kennan, and J. Fallon, 2008, Structural history of the Andean foreland, Perú, and its relation to subduction zone dynamics: AAPG Annual Convention and Exhibition: San Antonio, Texas, AAPG Search and Discovery Article, http://www.searchanddiscovery.com/abstracts/html/2008/ annual/abstracts/412679.htm.

Burchardt, S., 2008, New insights into the mechanics of sill emplacements provided by field observations of the Njardvik sill, northeast Iceland: Journal of Volcanology and Geochemical Research, v. 173, p. 280–288.

Butler, W.H., Tavarnelli, E. and M. Grasso, 2006, Structural inheritance in mountain belts: An Alpine-Apennine perspective; Journal of Structural Geology, 28, p. 1893-1908.

Caër, T., Maillot, B., Souloumiac, P., Leturmy, P., Frizon de Lamotte, D. and C. Nussbaum, 2015, Mechanical validation of balanced cross-sections: The case of the Mont Terri anticline at the Jura front (NW Switzerland); Journal of Structural Geology, 75, p. 32-48.

Calderón, Y., P. Baby, C. Hurtado, and S. Brusset, 2017, Thrust tectonics in the Andean retro-foreland basin of northern Perú: Permian inheritances and petroleum implications: Marine and Petroleum Geology, v. 82, p. 238–250.

Cardozo, N., Bhalla, K., Zehnder, A.T. and R.W. Allmendinger, 2003, Mechanical models of fault propagation folds and comparison to the trishear kinematic model; Journal of Structural Geology, 25, p. 1-18.

Carey, S.W., 1955, The orocline concept in geotectonics Part I; Papers and procedures of the Royal Society of Tasmania, V. 89, p. 255-288.

Cazier, E.C., Hayward, A.B., Espinosa, G., Velandia, J., Mugniot, J-F., and W.G. Leel, Jr., 1995, Petroleum geology of the Cusiana Field, Llanos Basin Foothills, Colombia: AAPG Bulletin, v. 79, p. 1444-1463.

Chacaltana, C., V. Carlotto, W. Valdivia, H. Acosta, D. Peña, and R. Rodríguez, 2011, Estudio geológico de la Cuenca Ene—Sectores Centro y Sur: Boletín No 29 Serie D, Estudios Regionales, Lima, 172 p.

Chacaltana, C., W. Valdivia, and D. Peña Guimas, 2012, Estudio geológico de la Cuenca Santiago sectores centro y sur: Boletín No 30 Serie D, Estudios Regionales, Lima, 183 p.

Chalaron, E., Mugnier, J.L. and G. Mascle, 1995, Control on thrust tectonics in the Himalayan foothills: a view from a numerical model; Tectonophysics, 248, p. 139-163.

Chalco, A., 1961, Compilation geological report Santiago-Nieva region: Informe Técnico Perupetro, IT03154, 45 p.

Cooper,M.A., Addison, F.T., Alvarez, R., Coral, M., Graham, R.H., Hayward, A.B., Howe, S., Martinez, J., Naar, J., Peñas, R., Pulham, A.J. and A. Taborda, 1995, Basin development and tectonic history of the Llanos Basin, Eastern Cordillera, and Middle Magdalena Valley, Colombia: AAPG Bulletin, v. 79, p. 1421–1443.

Chiarelli, A., 1978, Hydrodynamic framework of eastern Algerian Sahara e influence on hydrocarbon occurrence Am. Assoc. Petrol. Geol. Bull., 62, p. 667-685.

Combina, A. M., and F. Nullo, 2005, Tertiary volcanism and sedimentation in the southern Cordillera principal, Mendoza, Argentina: 6th International Symposium on Andean Geodynamics, Barcelona, Spain, September 12–14, 2005, p. 174–177.

Cristallini, E.O., Allmendinger, R.W., 2001. Pseudo-3D modeling of trishear fault-propagation folding: Journal of Structural Geology, 23, p. 1883-1889.

Couzens-Schultz, B. A., B. C. Vendeville, and D. V. Wiltschko, 2003, Duplex style and triangle zone formation: insights from physical modeling: Journal of Structural Geology, v. 25, p. 1623–1644.

Dahlen, F. A., 1984, Non-cohesive critical coulomb wedges: An exact solution: Journal of Geophysical Research, v. 89, p. 10125–10133.

Dalmayrac, B., G. Laubacher, R. Marocco, C. Martinez, and P. Tomasi, 1980, La chaine hercynienne d'amerique du sud structure et evolution d'un orogene intracratonique: Geologische Rundschau, v. 69, p. 1–21.

Davis, D. M., and T. Engelder, 1985, The role of salt in foldand-thrust belts: Tectonophysics, v. 119, p. 67–88.

deAraujo, C. C., J.K.Yamamtot, S. P. Rostirolla,V.Madrucci, and A. Tankard, 2005, Tar sandstone in the Parana Basin of Brazil: Structural and magmatic controls of hydrocarbon charge: Marine and Petroleum Geology, v. 22, p. 671–685, doi:10.1016/j.marpetgeo.2005.01.006.

DeCelles, P. G., and K. A. Giles, 1996, Foreland basin systems: Basin Research, v. 8, p. 105–123.

DeCelles, P., 2012, Foreland basin system revisited: Variations in response to tectonic settings, in C. Busby and A. Azor, eds., Tectonics of sedimentary basins: Recent advances (1st ed.): Blackwell Publishing, Hoboken, p. 405–426.

DeGraff, J. M., and A. Aydin, 1987, Surface morphology of columnar joints and its significance to mechanisms and direction of joint growth: Geological Society of America Bulletin, v. 99, p. 605–617, doi:10.1130/0016-7606(1987)99<605:SMOCJA>2.0.CO;2.

Delpino, H. D., and A. Bermudez, 2009, Petroleum systems including unconventional reservoirs in intrusive igneous rocks (sills and laccoliths): The Leading Edge (July 2009), p. 804–811, doi:10.1190/1.3167782.

Devlin, S., B. L. Isacks, M. E. Pritchard, W. D. Barnhart, and R. B. Lohmann, 2012, Depths and focal mechanisms of crustal earthquakes in the central Andes determined from teleseismic waveform analysis and InSAR: Tectonics, v. 31, p. 1–33.

Dewey, J. F., and S. H. Lamb, 1992, Active tectonics of the Andes, Tectonophysics, v. 205, p. 79–95.

Dickinson, W. R., and W. S. Snyder, 1978, Plate tectonics of the Laramide orogeny, *in* V. Matthews., ed., Laramide folding associated with basement block faulting in the western United States: Denver, CO, Geological Society of America Memoir, 151, p. 355–366.

Diegel, F.A., Karlo, J.F., Schuster, D.C., Shoup, R.C., Tauvers, P.R., 1995, Cenozoic structural evolution and tectono-stratigraphic framework of the northern Gulf coast continental margin. In: Jackson, M.P.A., Rogers, D.G., Snelson, S. (Eds.), Salt Tectonics: a Global Perspective, vol. 65. AAPG Memoir, p. 109-151.

Dimieri, L.V., Turienzo, M.M., 2012, Comment on: "Fault inversion vs. new thrust generation: A case study in the Malargüe fold-and-thrust belt, Andes of Argentina" by J. F. Mescua, and L. B. Giambiagi, Journal of Structural Geology 35 (2012) 51-63, Journal of Structural Geology, 42, 279-282.

Disalvo, A., Chung Ching, J., Seminario, F., Luquez, J., Arteaga, M., Gabulle, J., Davis, S., Valencia, K. and M.B. de Santa Anna, 2008, Sistemas petroleros del "Gran Camisea", Sur de la Cuenca de Ucayali, Perú. In: Cruz, E.C., Rodríguez, J.F., Hechem, J.J., Villar, H.J. (Eds.), Sistemas Petroleros de las Cuencas Andinas; VII Congreso de Exploración y Desarrollo de Hidrocarburos. IAPG, Buenos Aires.

Dumont, J. F., 1996, Neotectonics of the Subandes—Brazilian craton boundary using geomorphological data: The Maranón and Beni Basins: Tectonophysics, v. 257, p. 137–151.

Encarnación, I. B., 2008, Modelado de los sistemas petroleros en las cuencas subandinas del Perú (Cuencas: Madre de Díos, Ucayali, Huallaga, Santiago y Maranón): M.Sc. Thesis, Universidad Nacional de Ingeniería, Lima, 205 p.

Endignoux, L. and J.-L. Mugnier, 1990, The use of a forward kinematic model in the construction of balanced cross sections; Tectonics 9 (5), p. 1249-1262.

Erslev, E.A., 1991, Trishear fault-propagation folding: Geology 19 (6), p. 617-620.

Espurt, N., Baby, P., Brusset, S., Roddaz, M., Hermoza, W., Regard, V., Antoine, P.O., Salas-Gismondi, R. and R. Bolanos, 2007, How does the Nazca Ridge subduction influence the modern Amazonian foreland basin? Geology, 35, p. 515-518.

Espurt, N., S. Brusset, R. Baby, W. Hermoza, R. Bolanos, D. Uyen, and J. Déramond, 2008, Paleozoic structural controls on shortening transfer in the Subandean foreland thrust system, Ene and southern Ucayali basins, Perú, Tectonics, v. 27, p. 1-21. TC3009, DOI: 10.1029/2007TC002238.

Eude, A., M. Roddaz, S. Brichau, S. Brusset, P. Baby, Y. Calderón, and J. C. Soula, 2015, Timing of exhumation and deformation in the Northern Peruvian Eastern Andean wedge (5–8° S) as inferred from low temperature thermochronology and balanced cross section: Tectonics, v. 34, p. 715–730.

Faccenna, C., O. Oncken, A. F. Holt, and T. W. Becker, 2017, Initiation of the Andean orogeny by lower mantle subduction: Earth and Planetary Science Letters, v. 463, p. 189–201.

Fattahi, A., Walker, R., Hollingsworth, J., Bahroudi, A., Nazari, H., Talebian, M., Armitage, S., Stokes, S., 2006. Earth Planet. Sci. Lett. 245, 673-684.

Fildani, A., A. M. Hessler, and S. A. Graham, 2008, Trench forearc interactions reflected in the sedimentary fill of Talara basin, northwest Perú: The Talara Forearc basin: Basin Research, v. 20, no. 3, p. 305–331.

Flöttmann, T. and M. Hand, 1999, Folded basement-cored tectonic wedges along the northern edge of the Amadeus Basin, Journal of Structural Geology, 21, p. 399-412.

Fossen, H., 2010. Structural Geology. Cambridge University Press, p. 463.

Galloway, W. E., T. E. Ewing, C. M. Garrett, N. Tyler, and D. G. Bebout, 1983, Atlas of major Texas oil reservoirs: University of Texas, Bureau of Economic Geology, p. 1–139.

Gautheron, C., Espurt, N., Barbarand, J., Roddaz, M., Baby, P., Brusset, S., Tassan-Got, L. and E. Douville, 2013, Direct dating of thick- and thin-skin thrusts in the Peruvian Subandean zone through apatite (UeTh)/He fission track thermochronometry. Basin Research, 25, p. 419-435.

Gerbault, M., Poliakov, A.N.B., Daignieres, M., 1998, Prediction of faulting from the theories of elasticity and plasticity: what are the limits?; Journal of Structural Geology 20 (2/3), p. 301-320.

Giacosa, R., Allard, J. Foix, N. and N. Heredia, 2014, Stratigraphy, structure and geodynamic evolution of the Paleozoic rocks in the Cordillera del Viento (37° S latitude, Andes of Neuquén, Argentina), Journal of Iberian Geology 40 (2), p. 331-348.

Giambiagi, L.B., Alvarez, P.P., Godoy, E., Ramos, V.A., 2003, The control of pre-existing extensional structures on the evolution of the southern sector of the Aconcagua fold and thrust belt, southern Andes, Tectonophysics, 369, p. 1-19.

Giambiagi, L.B., Bechis, F., García, V. and A.H. Clark, 2008, Temporal and spatial relationships of thick- and thin-skinned deformation: A case study from the Malargüe fold-and-thrust belt, southern Central Andes, Tectonophysics, 459, p. 123-139; doi:10.1016/j.tecto.2007.11.069.

Giambiagi, L.B., Ghiglione, M., Cristallini, E. and G. Bottesi, 2009, Kinematic models of basement/cover interaction: Insights from the Malargüe fold and thrust belt, Mendoza, Argentina, Journal of Structural Geology, 31, p. 1443-1457; doi:10.1016/j.jsg.2009.10.006.

Giambiagi, L.B., Mescua, J., Bechis, F., Tassara, A. and G. Hoke, 2012, Thrust belts of the southern Central Andes: Along-strike variations in shortening, topography, crustal geometry, and denudation, GSA Bulletin, 124, p. 1339-1351; doi:10.1130/B30609.1.

Giambiagi, L. B., P. P. Alvarez, E. Godoy, and V. A. Ramos, 2013, The control of preexisting extensional structures on the evolution of the southern sector of the Aconcagua fold and thrust belt, southern Andes: Tectonophysics, v. 369, p. 1–19.

Gibbs, A.D., 1983, Balanced cross-section construction from seismic sections in areas of extensional tectonics; Journal of Structural Geology, 5 (No. 2), p. 153-160.

Gil Rodriguez, W.F., Baby, P., Marocco, R. and J.F. Ballard, 1999, North-south structural evolution of the Peruvian subandean zone. In: Fourth ISAG, Göttingen (Germany), p. 278-282.

Gil Rodríguez, W. F., P. Baby, and J.F. Ballard, 2001, Structure et contrôle paléogéographique de la zone subandine péruvienne: Earth and Planetary Sciences, v. 333, p. 741–748.

Gil Rodríguez, W. F., 2002, Evolución lateral de la deformación de un frente orogénico; Ejemplo de las Cuencas Subandinas entre 0° y 16°S: Sociedad Geológica del Perú, 146 p, Publicación especial No. 4.

Gil-Imaz, A., A. Pocovi,M. Lago, C. Gale, E. Arranz, C. Rillo, and E. Guerrero, 2006, Magma flow and thermal contraction fabric in tabular intrusions inferred from AMS analysis: A case study in late-Variscan folded sill of the Albarracin massif (southeastern Iberian chain, Spain): Journal of Structural Geology, v. 28, p. 641–653, doi:10.1016 /j.jsg.2005.12.016.

Goulty, N. R., and N. Schofield, 2008, Implications of simple flexure theory for the formation of saucer-shaped sills: Journal of Structural Geology, v. 30, p. 821–817, doi:10 .1016/j.jsg.2008.04.002.

Gries, R., 1983, North-south compression of Rocky Mountain foreland structures, *in* J. D. Lowell, ed., Rocky Mountain foreland basins and uplifts: Denver, CO, Rocky Mountain Association of Geologists, p. 9–32.

Graveleau, F., Malavieille, J. and S. Dominguez, 2012, Experimental modelling of orogenic wedges: A review; Tectonophysics, 538-540, p. 1-66.

Gressier, J.-B., R. Mourgues, L. Bodet, J.-Y. Matthieu, O. Galland, and P. Cobbold, 2010, Control of pore fluid pressure on depth of emplacement of magmatic sills: An experimental approach: Tectonophysics, v. 489, p. 1–13.

Groshong, R. H. and J.-L. Epard, 1994, The role of strain in area-constant detachment folding: Journal of Structural Geology, v. 16, p. 613–618.

Groshong, R.H., Bond, C., Gibbs, A., Ratliff, R. and D.V. Wiltschko, 2012, Preface: Structural balancing at the start of the 21st century: 100 years since Chamberlin; Journal of Structural Geology, 41, p. 1-5.

Guzman, C., E. Cristallini, and G. Bottesi, 2007, Contemporary stress orientations in the Andean retroarc between 34°S and 39°S from borehole breakout analysis:Tectonics, v. 26, p. 1–13, doi:10.1029/2006TC001958.

Hain, M. P., M. R. Strecker, B. Bookhagen, R. N. Alonso, H. Pingel, and A. K. Schmitt, 2011, Neogene to Quaternary broken foreland formation and sedimentation dynamics in the Andes of NW Argentina (25°S): Tectonics, v. 30, p. 1–27, DOI: 10.1029/2010TC002703.

Hampel, A., 2002, The migration history of the Nazca Ridge along the Peruvian active margin: A re-evaluation: Earth and Planetary Science Letters, v. 203, p. 665–679.

Hardy, S. and M. Ford, 1997, Numerical modeling of trishear fault propagation folding; Tectonic, 16(5), p. 841-854.

Heidbach, O., M. Tingay, A. Barth, J. Reinecker, D. Kurfeß, and B. Müller, 2008, The World Stress Map Database Release, 2008. Paris, France, Commission for the Geological Map of the World, Equatorial Scale 1:46,000,000, DOI: 10.1594/GFZ.WSM.Map2009.

Hérail, G., Oller, J., Baby, P., Bonhomme, M. and P. Soler, 1996, Strike-slip faulting, thrusting and related basins in the Cenozoic evolution of the southern branch of the Bolivian orocline. Tectonophysics, 259, p. 201-212.

Hermoza, W., 2004, Dinamica tectono-sedimentaria y restauracion secuencial de la cuenca de antepaís de los Andes Centrales (Doctoral thesis). Université Paul Sabatier, Toulouse.

Hermoza, W., S. Brusset, P. Baby, W. Gil, M. Roddaz, N. Guerrero, and R. Bolanos, 2005, The Huallaga foreland basin evolution: Thrust propagation in a deltaic environment, northern Peruvian Andes: Journal of South American Earth Sciences, v. 19, p. 21–34.

Hermoza, W., P. Baby, N. Espurt, E. Martínez, and R. Bolanos, 2006, The Ucayali Subandean Basin: A complex fold and thrust belt and inverted system, *in* IX Simposio Bolivariano, Petroleum Exploration in the Subandean Basins, Cartagena de las Indias, Colombia, 11 p., http://archives.datapages.com/data/colombia_acggp/simp9/04.htm.

Hermoza,W., Zamora, G., Macellari, C. and R. Tocco, 2011, Paleozoic deformation and its hydrocarbon potential in the northern Andean foreland basin. In: VII INGEPET, EXPR-3-WH-10-E); November 2011, Lima.

Hilley, G.E., Blisniuk, P. and M.R. Strecker, 2005, Mechanics and erosion of basement-cored uplift provinces; Journal of Geophysical Research, 110, p. 1-22.

Hinsch, R., 2001, Frontale Akkretion und Verformungsaufteilung eines gebogenen Falten- und Überschiebungsgürtels, Räumliche Strukturanalyse im Subandin Boliviens, PhD Thesis, FU Berlin, 128 p.

Hooker, J. N., J. F.W. Gale, L. A. Gomez, S. E. Laubach, R. Marrett, and R.M. Reed, 2009, Aperture-size scaling variations in a low-strain opening-mode fracture set, Cozzette Sandstone, Colorado: Journal of Structural Geology, v. 31, p. 707–718, doi:10.1016/j.jsg.2009.04.001.

Hudec, M. R., and M. P. A. Jackson, 2006, Advance of allochtonous salt sheets in passive margins and orogens: AAPG Bulletin, v. 90, p. 1535–1564.

Hughes, A.N., Benesh, N.P. and J.H. Shaw, 2014, Factors that control the development of fault-bend versus fault-propagation folds: Insights from mechanical models based on the discrete element method (DEM), Journal of Structural Geology, 68, p. 121-141.

IHS, 2008, Neuquén Basin Activity Map, Argentina: Global Exploration and Production Service Map, scale 1:1,000,000.

INGEMMET, 1995, Mapa geológico del cuadrángulo de Puesto Llave: Carta geológica del Perú, Hoja 9f, Scale 1:100.000, 1 Sheet, Lima, Perú.

INGEMMET, 1997, Mapa geológico del cuadrángulo de Teniente Pinglo: Carta geológica del Perú, Hoja 9h, Scale 1:100.000, 1 Sheet, Lima, Perú.

INGEMMET, 1997, Boletin No 88, Serie A: Carta Geologica Nacional. In: Geologia de los cuadrangulos de Codo del Pozuzo y Rio Palcazu, Hojas 20-m, 20-n; Lima. IUGS, 2014. International Chronostratigraphic Chart.

INGEMMET, 1998, Mapa geológico del cuadrángulo de Ayambis: Carta geológica del Perú, Hoja 8h, Scale 1:100.000, 1 Sheet, Lima, Perú.

INGEMMET, 1999, Mapa geológico del cuadrángulo de Jiménez Banda: Carta geológica del Perú, Hoja 8g, Scale 1:100.000, 1 Sheet, Lima, Perú.

Isacks, B.L., 1988, Uplift of the central Andean plateau and bending of the Bolivian Orocline; Journal of Geophysical Research, v. 93 (B4), p. 3211-3231.

ISO/JCGM, 2008, Evaluation of measurement data – Guide to the expression of uncertainty in measurement, 134 p.

Jackson, M.P.A., 1995, Retrospective salt tectonics. In: Jackson, M.P.A., Roberts, D.G., Snelson, S. (Eds.), Salt Tectonics: a Global Perspective, vol. 65. AAPG Memoir, p. 1-28.

Jacques, J.M., 2003a, Part I: a tectonostratigraphic synthesis of the Sub-Andean basins: implication for the geotectonic segmentation of the Andean Belt. J. Geol. Soc. London, 160, p. 687-701.

Jacques, J.M., 2003b, Part II: a tectonostratigraphic synthesis of the Sub-Andean basins: inferences on the position of South American intraplate accommodation zones and their control on South Atlantic opening. J. Geol. Soc. London, 160, p. 703-717.

Jaillard, E., G. Herail, T. Monfret, E. Diaz-Martínez, P. Baby, A. Lavenu and J. F. Dumont, 2000, Tectonic Evolution of the Andes of Ecuador, Perú, Bolivia, and Northernmost Chile, *in* U. G. Cordani, E. J. Milani, A. Thomaz Filho, and D. A. Campos, eds., Tectonic evolution of South America, p. 481–559.

Jordan, T. E., and R. W. Allmendinger, 1986, The Sierras Pampeanas of Argentina: A modern analogue of Rocky Mountain foreland deformation: American Journal of Science, v. 286, p. 737–764.

Judge, P.A. and R.W. Allmendinger, 2011, Assessing uncertainties in balanced cross sections: Journal of Structural Geology, 33, p. 458-467, doi: 10.1016/j.jsg.2011.01.006.

Kastelic, V. and M. Carafa, 2012, Fault slip rates for the active External Dinarides thrustand-fold belt. Tectonics, 31, p. 1-18.

Kattenhorn, S. A., and C. J. Schaefer, 2008, Thermal-mechanical modeling of cooling history and fracture development in inflationary basalt lava flows: Journal of Volcanology and Geothermal Research, v. 170, p. 181–197, doi:10.1016/j.jvolgeores.2007.10.002.

Kay, S. M., W. M. Burns, P. Copeland, and O. Mansilla, 2006, Upper Cretaceous to Holocene magmatism and evidence for transient Miocene shallowing of the Andean subduction zone under the northern Neuquén Basin, in S. Kay and V. Ramos, eds., Evolution of an Andean margin: A tectonic and magmatic view from the Andes to the Neuquén Basin (35°–39° S lat): Geological Society of America Special Paper, v. 407, p. 19–60.

Kennan, L., 2008, Fission track ages and sedimentary provenance studies in Perú, and their implications for Andean Paleogeographic evolution, stratigraphy and Hydrocarbon Systems: VI INGEPET, 2008, paper number EXPR-3-LK-36., 13 p.

Kley, J., 1999, Geologic and geometric constraints on a kinematic model of the Bolivian orocline; Journal of South American Earth Sciences, 12 (2), p. 221-235.

Kokkalas, S., E. Kamberis, P. Xypolias, S. Sotiropoulos, and I. Koukouvelas, 2012, Coexistence of thin- and thick-skinned tectonics in Zakynthos area (western Greece): Insights from seismic sections and regional seismicity; Tectonophysics, p. 597–598.

Konert, G., Al-Hajri, S.A., Al Naim, A.A., Afifi, A.M., de Groot, K., and H.J. Droste, H.J., 2001, Paleozoic stratigraphy and hydrocarbon habitat of the Arabian Plate, in Downey, M.W., Threet, J.C., and W.A. Morgan, eds., 2001, Petroleum provinces of the 21st century: AAPG Memoir, 74, p. 483-515.

Kontak, D., A. H. Clark, E. Farrar, and D. F. Strong, 1985, The rift-associated Permo-Triassic magmatism of the Eastern Cordillera: a precursor to the Andean orogeny. Magmatism at a Plate Edge: the Peruvian Andes, in: Pitcher, W.S., M. P. Atherton, J. Cobbing, and R. D. Beckinsale, eds., Magmatism at a plate edge: The Peruvian Andes. Blackie, Glasgow, and Halsted Press. p. 36–44. New York

Last, N.C. and M.R. McLean, 1995, Assessing the impact of trajectory on wells drilled in an overthrust region, Proceedings SPE Annual Technical Conference, Dallas, p. 161-172: SPE Paper 30465.

Laubach, S. E., and J. F. W. Gale, 2006, Obtaining fracture information for low-permeability (tight) gas sandstones from sidewall cores: Journal of Petroleum Geology, v. 29, no. 2, p. 147–158, doi:10.1111/j.1747-5457.2006.00147.x.

Legarreta, L., C. E. Cruz, G. D. Vergani, G. A. Laffitte, and H. J. Villar, 2004, Petroleum mass balance of the Neuquén Basin, Argentina: A comparative assessment of the productive districts and nonproductive trends: AAPG International Conference and Exhibition, Cancun, Mexico, October 24–27, 2004, 6 p.

Li, S., 2016, Geomechanical modeling of earthquake cycles in Chilean subduction zone; PhD Thesis, FU Berlin, 145 p.

Linares, E., and R. R. Gonzales, 1990, Catalogo de edades radimetricas de la republica Argentina, 1957–1987: Publicaciones Especiales de la Asociacion Geologica Argentina, Serie B (Didactica y Complementaria), v. 117, no. 19, 630 p.

Llambías, E.J., Leanza, H.A. and O. Carbone, 2007, Evolución tectono-magmática durante el Pérmico al Jurásico temprano en la Cordillera del Viento (37°05'S - 37°15'S): Nuevas evidencias geológicas y geoquímicas del inicio de la Cuenca Neuquina, Revista de la Asociación Geológica Argentina, 62 (2), p. 217-235.

Lowell, 1979, Structural Styles in Petroleum Exploration. OGCI Publications, Tulsa, p. 504.

Magoon, L.B. and W. G. Dow, 1994, The Petroleum System - From source to trap; AAPG Memoir, 60, AAPG, Tulsa, 644 p.

Manassero, M.J., Cingolani, C.A. and P. Abre, 2009, A Silurian-Devonian marine platform-deltaic system in the San Rafael Block, Argentine Precordillera-Cuyania terrane: lithofacies and provenance; in: Königshof, P. (ed.), Devonian Change: Case Studies in Palaeogeography and Palaeoecology, The Geological Society, London, Special Publications, 314, p. 215-240.

Manceda, R. and D. Figueroa, 1995, Inversion of the Mesozoic Neuquén Rift in the Malargüe fold and thrust belt, Mendoza, Argentina; in: Tankard, A.J., Suárez S., R. and H. J. Welsink, eds.: Petroleum basins of South America; AAPG Memoir, 62, p. 369–382.

Marrett, R., 1996, Aggregate properties of fracture populations: Journal of Structural Geology, v. 18, p. 169–178, doi:10.1016/S0191-8141(96)80042-3.

Marshak, S., 1986, Structure and tectonics of the Hudson Valley fold-thrust belt, eastern New York State: GSA Bulletin, v. 97, p. 354–368.

Marshak, S., 2004, Salients, recesses, arcs, oroclines, and syntaxes—A review of ideas concerning the formation of map-view curves in fold-thrust belts, in K. R. McClay, ed., Thrust tectonics and hydrocarbon systems: AAPG Memoir, 82, p. 131–156.

Martinez, E., E. Fernandez, Y. Calderón, and C. Galdos, 2003, Reevaluation defines attractive areas in Perú's Ucayali-Ene Basin: Oil Gas Journal, v. 101, no. 46, p. 32–38.

Martínez, F., Arriagada, C., Peña, M., Deckart, K. and R. Charrier, 2016, Tectonic styles and crustal shortening of the Central Andes "Pampean" flat-slab segment in northern Chile (27–29°S). Tectonophysics, 667, p. 144-162. https://doi.org/10.1016/j.tecto.2015.11.019

Mathalone, J. M. P., and R. M. Montoya, 1995, Petroleum geology of the Sub-Andean Basins of Perú, in A. J. Tankard, R. Suarez S., and H. J. Welsink, eds., Petroleum basins of South America: AAPG Memoir, 62, p. 423–444.

Matthes, S., 1993, Mineralogie: Heidelberg, Germany, Springer, 461 p.

McCaffrey, K. J. W., J. M. Sleight, S. Pugliese, and R. E. Holdsworth, 2003, Fracture formation and evolution in crystalline rocks: Insights from attribute analysis, in N. Petford and K. J. W. McCaffrey, eds., Hydrocarbons in crystalline rocks: Geological Society (London) Special Publication, v. 214, p. 109–124.

McClay, K.R., Dooley, T., Whitehouse, P., Mills, M., 2002, 4-D evolution of rift systems: insights from scaled physical models, AAPG Bull., 86 (6), p. 935-959. June 2002.

Mcgregor, D.S., 1996. Factors controlling the destruction or preservation of giant light oilfields. Pet. Geosci., 2, p. 197-217.

McKenny, J. W., and J. A. Masters, 1968, Dineh-bi-Keyah field, Apache County, Arizona: AAPG Bulletin, v. 52, no. 10, p. 2045–2057.

McQuarrie, N., 2004, Crustal scale geometry of the Zagros fold-thrust belt, Iran: Journal of Structural Geology, v. 25, p. 519–535.

Megárd, F., 1984, The Andean orogenic period and its major structures in central and northern Perú: Journal of the Geological Society of London, v. 141, p. 893–900.

Mercier, J.L., Sebrier, M., Lavenu, A., Cabrera, J., Bellier, O., Dumont, J.F. and J. Machare, 1992, Changes in the tectonic regime above a subduction zone of Andean type: the Andes of Peru and Bolivia during the Pliocene-Pleistocene. J. Geophys. Res., 97 (11), p. 945-982.

Mescua, J.F., Giambiagi, L.B. and F. Bechis, 2012, Reply to L.V. Dimieri and M.M. Turienzo, 2012 comment on: “Fault inversion vs. new thrust generation: A case study in the Malargüe fold-and thrust belt, Andes of Argentina” by J. F. Mescua and L. B. Giambiagi, Journal of Structural Geology, 35, p. 51-63; doi: 10.1016/j.jsg.2012.05.013.

Mescua, J.F. and L.B. Giambiagi, 2012, Fault inversion vs. new thrust generation: A case study in the Malargüe fold-and-thrust belt, Andes of Argentina, Journal of Structural Geology, 35, p. 51-63; doi:10.1016/j.jsg.2011.11.011.

Messager, G., B. Niviere, J. Martinod, P. Lacan, and J. P. Xavier, 2010, Geomorphic evidence for Plio-Quaternary compression in the Andean foothills of the southern Neuquén Basin, Argentina: Tectonics, v. 29, p. 1-18. TC4003, doi:10.1029/2009TC002609.

Messager, G., Niviere, B., Regard, V., Xavier J., Hervouet, Y., Dhont, D., Bonnel, C., 2012, Geomorphic Evidence for the Deformation Front Propagation of the Malargüe Fold-and-Thrust Belt, Neuquén Andes (Argentina), GSA Annual Conference, Minneapolis (2012).

Metropolis, N., Rosenbluth, A.W., Rosenbluth, M.N., Teller, A.H. and E. Teller, 1953, Equation of State Calculations by Fast Computing Machines. In: The Journal of Chemical Physics; Vol. 21 (6), p. 1087–1092, doi:10.1063/1.1699114.

Miller, D., Nilsen, T. and W. Bilodeau, 1992, Late Cretaceous to early Eocene geologic evolution of the U.S. Cordillera. In: Burchfiel, B., Lipman, P., Zoback, M., eds., The Cordilleran Orogen: Conterminous, vol. G-3. U.S. Geological Society of America, p. 205-260.

Mitra, S., Mount, V.S, 1998, Foreland basement-involved structures, AAPG Bulletin, 82 (1), p. 70-109.

Mon, R., and J. A. Salfity, 1995, Tectonic evolution of the Andes of northern Argentina, in A. J. Tankard, R. Suárez Soruco, and H. J. Welsink, eds., Petroleum basins of South America: AAPG Memoir, 62, p. 269–283.

Mora, A., M. Parra, M. R. Strecker, A. Kammer, C. Dimaté, and F. Rodríguez, 2006, Cenozoic contractional reactivation of Mesozoic extensional structures in the Eastern Cordillera of Colombia: Tectonics, v. 25, p. 1-19. TC2010, DOI: 10.1029/2005TC001854.

Mora, A., T. Gaona, J. Kley, D. Montoya, M. Parra, L. I. Quiroz, G. Reyes, and M. R. Strecker, 2009, The role of inherited extensional fault segmentation and linkage in contractional orogenesis: A reconstruction of Lower Cretaceous inverted rift basins in the Eastern Cordillera of Colombia: Basin Research, v. 21, no. 1, p. 111–137, DOI: 10.1111/j.1365-2117.2008.00367.x.

Mora, A. A. Reyes-Harker, G. Rodriguez, E. Teso, J. C. Ramirez-Arias, M. Parra, V. Caballero, J. P. Mora, I. Quintero, V. Valencia, M. Ibañez, B. K. Horton, and D. F. Stockli, 2013, Inversion tectonics under increasing rates of shortening and sedimentation: Cenozoic example from the Eastern Cordillera of Colombia, in M. Nemcok, A. Mora, J. W. Cosgro, eds., Thick-skin-dominated Orogens: From initial inversion to full accretion: London, Geological Society Special Publication, 377, p. 411–442.

Moretti, I., and J. P. Callot, 2012, Area, length and thickness conservation: Dogma or reality?, Journal of Structural Geology, 41, p. 64-75.

Moretti, I., J. P. Callot, M. Principaud, and D. Pillot, 2013, Salt-pillows and localization of early structures: Case study in the Ucayali Basin, Perú, in M. Nemcok, A. Mora, J. W. Cosgrove, eds., Thick-skin-dominated Orogens: From initial inversion to full accretion: London, Geological Society Special Publication 377, p. 43–58.

Narr, W., 1996, Estimating average fracture spacing in subsurface rock: AAPGBulletin, v. 80, no. 10, p. 1565–1586.

Navarro Zelasco, L.D., 2010, Tectonic Evolution of the Contaya Arch, Ucayali Basin, Peru. t. Texas A&M University (MSc thesis).

Naeser, C. W., J.-Y. Crochet, E. Jaillard, G. Laubacher, T. Mourier, and B. Sige, 1991, Tertiary fission—track ages from the Bagua syncline (northern Perú): Stratigraphic and tectonic implications: Journal of South American Earth Sciences, v. 4, no. 1/2, p. 61–71.

Nelson, R. A., 2001, Geologic analysis of naturally fractured reservoirs: Boston, Gulf Professional Publishing, 332 p.

Noble, D.C., McKee, E.H., Mourier, T., Megard, F., 1990, Cenozoic stratigraphy, magmatic activity, compressive deformation, and uplift in northern Peru. GSA Bull., 102, p. 1105-1113.

Olson, J. E., S. E. Laubach, and R. H. Lander, 2007, Combining diagenesis and mechanics to quantify fracture aperture distributions and fracture pattern permeability, in L. Lonergan, R. J. H. Jolly, K. Rawnsley, and D. J. Sanderson, eds., Fractured reservoirs: Geological Society (London) Special Publication, v. 270, p. 101–116.

Olson, J.E., S.E. Laubach and R.H. Lander, 2009, Natural fracture characterization in tight gas sandstones: Integrating mechanics and diagenesis: AAPG Bulletin, v. 93, no. 11, p. 1535–1549, doi:10.1306/08110909100.

Oncken, O., von Winterfeld, C., Dittmar, U., 1999, Accretion of a rifted passive margin: The Late Paleozoic Rhenohercynian fold and thrust belt (Middle European Variscides), Tectonics 18 (1), p. 75-91.

Oncken, O., G. Chong, G. Franz, P. Giese, H.-J. Götze, V. Ramos, M. Strecker and P. Wigger, 2006, The Andes - Active Subduction Orogeny, Frontiers in Earth Sciences, Springer, 568 p.

Oncken, O., D. Boutelier, G. Dresen, and K. Schemmann, 2012, Strain accumulation controls failure of a plate boundary: Linking deformation of the Central Andes and lithospheric mechanics: Geochemistry, Geophysics, Geosystems, v. 13, no. 12, p. 1–22, AGU.

Ortega, O., and R.Marrett, 2000, Prediction of microfracture properties using microfracture information, Mesaverde Group sandstones, San Juan Basin, New Mexico: Journal of Structural Geology, v. 22, p. 571–588, doi:10.1016 /S0191-8141(99)00186-8.

Ortega, O. J., R. A. Marrett, and S. E. Laubach, 2006, A scale-independent approach to fracture intensity and average spacing measurement: AAPG Bulletin, v. 90, no. 2, p. 193–208, doi:10.1306/08250505059.

Parra, M., A. Mora, C. Jaramillo, V. Torres, G. Zeilinger, and M. R. Strecker, 2010, Tectonic controls on Cenozoic foreland basin development in the north-eastern Andes, Colombia: Basin Research, v. 22, p. 874–903, DOI: 10.1111/j.1365-2117.2009.00459.x.

Pei, Y., Paton, D.A., Knipe, R.J., 2014, Defining a 3-dimensional trishear parameter space to understand the temporal evolution of fault propagation folds, Journal of Structural Geology, 66, p. 284-297.

Perupetro, 1998, Chio 1-X Final Well Report, Lima.

Petford, N., and K. J. W. McCaffrey, eds., 2003, Hydrocarbons in crystalline rocks: Geological Society (London) Special Publication, v. 214, 242 p.

Pilger, R.H., 1981, Plate reconstructions, aseismic ridges, and low-angle subduction beneath the Andes. GSA Bull. Part I 92, p. 448-456.

Plessmann, W., 1972, Horizontal-Stylolithen im französischschweizerischen Tafel- und Faltenjura und ihre Einpassung in den regionalen Rahmen: Geologische Rundschau, v. 61, p. 332–347.

Poblet, J., Bulnes, M., 2007, Predicting strain using forward modelling of restored cross-section: application to rollover anticlines over listric fault, Journal of Structural Geology, 29, p. 1960-170.

Pollard, D.D. and A. Aydin, 1988, Progress in understanding jointing over the past century, GSA Bulletin, v. 100, p. 1181-1204.

Prueher, L. M., R. Erlich, and L. W. Snee, 2005, 40AR/39Ar geochronology of hypabyssal rocks in the Marañón Basin of Perú—A record of thermal history, structure, and alteration: US Geological Survey Scientific Investigations Report 2005—5132, 41 p.

Quispesivana, L., A. Zuloaga, and M. Paz, 1997, Geología de los cuadrángulos de Teniente Pinglo, Santa María de Nieva, Puerto Alegría y Puerto América: INGEMMET Boletín, 99, 185 p.

Rait, G., D. Dolberg, and M. Hearn, 2009, Tectonic evolution of the Situche complex, Marañón Basin, Perú: AAPG Search and Discovery Article #90171 CSPG/CSEG/CWLS GeoConvention 2009, Calgary, Alberta, Canada, May 4-8, 2009, 2 p.

Ramon, M.J., Pueyo, E.L., Briz, J.L., 2015, Detecting and estimating errors in 3D restoration methods using analog models, Geophysical Research Abstracts, 17, EGU General Assembly, 2015.

Ramos, V.A., Cristallini, E.O. and Pérez, D.J., 2002, The Pampean flat-slab of the Central Andes; Journal of South American Earth Sciences, v. 15(1), p. 59-78.

Ramos, V.A., Zapata, T., Cristallini, E.O. and Introcaso, A., 2004, The Andean thrust system – Latitudinal variations in structural styles and orogenic shortening; in: K.R. McClay (ed.): Thrust tectonics and hydrocarbon systems, AAPG Memoir, 82, p. 30-50.

Ramos, V.A. and Mahlburg Kay, S., 2006, Overview of the tectonic evolution of the southern Central Andes of Mendoza and Neuquén (35° – 39°S latitude), in: Mahlburg Kay, S. and Ramos, V.A. (eds.), 2006, Evolution of an Andean margin: A tectonic and magmatic view from the Andes to the Neuquén Basin (35° – 39°S lat), p. 1-17.

Ramsay, J. G., 1967, Folding and fracturing of rocks, The Blackburn Press, Caldwell, 568 p.

Rhea, S., Hayes, G., Villasenor, A., Furlong, K.P., Tarr, A.C. and H. Benz, 2010, Seismicity of the Earth 1900e2007, Nazca Plate and South America; U.S. Geological Survey Open File Report 2010-1083-E; 1 Sheet, Scale 1: 12,000,000.

Rocha, A., R. Gonzales, M. G. De Freitas, and I. Olaya, 2008, Peruvian Santiago Basin revisited: International Congress of Conventional and Unconventional Hydrocarbon Resources, Cartagena, Colombia, February 2008 http://archives.datapages.com/data/colombia_acggp/simp11/181_ROCHA_A.htm

Rodriguez, F., J. H. Villar, and R. Baudino, 2007, Hydrocarbon generation, migration, and accumulation related to igneous intrusions: An atypical petroleum system from the Neuquén Basin of Argentina: SPE Paper 107926-PP, 4 p.

Rodriguez Monreal, F., H. J. Villar, R. Baudino, D. Delpino and S. Zencich, 2009, Modeling an atypical petroleum system: A case study of hydrocarbon generation, migration and accumulation related to igneous intrusions in the Neuquén Basin, Argentina: Marine and Petroleum Geology, v. 26, p. 590–605, doi:10.1016/j.marpetgeo .2009.01.005.

Rosas, S., L. Fontboé, and A. Tankard, 2007, Tectonic evolution and paleogeography of the Mesozoic Pucará Basin, central Perú: Journal of South American Earth Sciences, v. 24, p. 1–24.

Rosenbaum, G., D. Giles, M. Saxon, P. G. Betts, R. F. Weinberg, and C. Dubouz, 2005, Subduction of the Nazca Plate and the Inca Plateau: Insights into the formation of ore deposits in Perú: Earth and Planetary Science Letters, v. 239, p. 18–32.

Rowan, M. G., 1993, A systematic technique for the sequential restoration of salt structures: Tectonophysics, v. 228, no. 3–4, p. 331–348.

Rowan, M.G., 1995, Structural styles and evolution of allochtonous salt, Central Lousiana outer shelf and upper sloper. In: Jackson, M.P.A., Rogers, D.G., Snelson, S. (Eds.), Salt Tectonics: a Global Perspective, vol. 65. AAPG Memoir, p. 199-228.

Rowan, M. G., and R. A. Ractliff, 2012, Cross-section restoration of salt-related deformation: Best practices and potential pitfalls: Journal of Structural Geology, v. 41, p. 24–37.

Sallares, V., and C. R. Ranero, 2005, Structure and tectonics of the erosional convergent margin off Antofagasta, north Chile (23°30'S): Journal of Geophysical Research, v. 110, p. 1–19.

Sanchez Alvarez, J. O., 2007, Structural and stratigraphic evolution of Shira Mountains, Central Ucayali Basin, Perú: M.S. Thesis, Texas A&M University, Universidad Industrial de Santander, 116 p.

Schedl, A., and D. V. Wiltschko, 1987, The role of basement in thrust fault ramping: Journal of Structural Geology, v. 9, p. 1029–1037.

Scherrenberg, A. F., R. J. Holcombe, and G. Rosenbaum, 2014, The persistence and role of basin structures on the 3D architecture of the Marañón Fold-Thrust Belt, Perú: Journal of South American Earth Sciences, v. 51, p. 45–58.

Scherrenberg, A. F., B. P. Kohn, R. J. Holcombe, and G. Rosenbaum, 2016, Thermotectonic history of the Marañón Fold-Thrust Belt, Perú: Insights into mineralization in an evolving orogeny: Tectonophysics, v. 667, p. 16–36.

Scheuber, E. and K.-J. Reutter, 1992, Magmatic arc tectonics in the Central Andes between 21° and 25°S; Tectonophysics, 205, p. 127-140.

Schmidt, C. J., R. B. Chase, and E. A. Erslev, 1993, Laramide basement deformation in the Rocky Mountain Foreland of the Western United States: Geological Society of America Special Paper 280, 446 p.

Schmidt, S., Hetzel, R., Mingorance, F., Ramos, V.A., 2011, Coseismic displacements and Holocene slip rates for two active thrust faults at the mountain front of the Andean Precordillera (~33S). Tectonics, 30, p. 1-15.

Scisciani, V., and R. Montefalcone, 2006, Coexistence of thin and thick-skinned tectonics: An example from the Central Apennines, Italy: Geological Society of America Special Paper, 414, p. 33–54.

Schutter, S. R., 2003, Hydrocarbon occurrence and exploration in and around igneous rocks, in N. Petford and K. J. W. McCaffrey, eds., Hydrocarbons in crystalline rocks: Geological Society (London) Special Publication, v. 214, p. 7–33.

Sdrolias, M., Müller, R.D., 2006, Controls on back-arc basin formation. Geochem. Geophys. Geosyst. 7. April 2006.

Sebrier, M., Mercier, J.L., Machare, J., Bonnot, D., Cabrera, J. and J.L. Blanc, 1988, The state of stress in an overriding plate situated above a flat slab: the Andes of central Peru. Tectonics, 7, p. 895-928.

Sempere, T., Butler, R.F., Richards, D.R., Marshall, L.G., Sharp, W. and C.C. SWISHER III, 1997, Stratigraphy and chronology of Upper Cretaceous-lower Paleogene strata in Bolivia and northwest Argentina. Geological Society of America Bulletin, 109(6), p. 709-727.

Sempere, T., G. Carlier, P. Soler, M. Fornari, V. Carlotto, J. Jacay, O. Arispe, D. Néraudeau, J. Cárdenas, S. Rosas, and N. Jiménez, 2002, Late Permian–Middle Jurassic lithospheric thinning in Perú and Bolivia, and its bearing on Andean-age tectonics: Tectonophysics, v. 345, p. 153–181.

Sibson, R. H., J. M. Moore, and A. H. Rankin, 1975, Seismic pumping: A hydrothermal fluid transport mechanism: Journal of the Geological Society (London), v. 131, p. 653–659.

Silvestro, J., and P. Kraemer, 2005, Evolución tecto-sedimentaria de la Cordillera Principal en el sector surmendocino a los 35° 30’ S, Faja plegada de Malargüe, Republica Argentina: 6° Congreso de Exploración y Desarrollo de Hidrocarburos, Artículo 25, Mar del Plata, CD-ROM.

Silvestro, J. and M. Atencio, 2009, La Cuenca Cenozoica del Río Grande y Palauco: edad, evolución y control estructural, faja plegada de Malargüe (36°S), Revista de la Asociación Geológica Argentina, 65, p. 154-169.

Smart, K.J., Ferrill, D.A., Morris, A.P. and R.N. McGinnis, 2012, Geomechanical modeling of stress and strain evolution during contractional fault-related folding; Tectonophysics, 576-577, p. 171-196.

Spacapan, J.B., Galland, O., Leanza, H.A. and S. Planke, 2017, Igneous sill and finger emplacement mechanism in shale-dominated formations: a field study at Cuesta del Chihuido, Neuquén Basin, Argentina, Journal of the Geological Society of London, v. 174 (3).

Spacapan, J.B., Palma, J.O., Galland, O., Manceda, R., Rocha, E., D’Odorico, A. and H.A. Leanza, 2018, Thermal impact of igneous sill-complexes on organic-rich formations and implications for petroleum systems: A case study in the northern Neuquén Basin, Argentina, Marine and Petroleum Geology, v. 91, p. 519-531.

Spikings, R., M. J. Reitsma, F. Boekhout, A. Mišković, A. Ulianov, M. Chiaradia, A. Gerdes, and U. Schaltegger, 2016, Characterization of Triassic rifting in Perú and implications for the early disassembly of western Pangaea: Gondwana Research, v. 35, p. 124–143.

Strecker, M. R., G. E. Hilley, B. Bookhagen, and E. R. Sobel, 2012, Structural geomorphic, and depositional characteristics of contiguous and broken foreland basins: Examples from the eastern flanks of the central Andes in Bolivia and NW Argentina, in C. Busby and A. Azor, eds., Tectonics of sedimentary basins: Recent advances: Blackwell Publishing, Hoboken, p. 508–521.

Strecker, M. R., P. Cerveny, A. L. Bloom, and D. Malizia, 1989, Late Cenozoic tectonism and landscape development in the foreland of the Andes: Northern Sierras Pampeanas (26°–28°), Argentina: Tectonics, v. 8, p. 517–534.

Suppe, J., 1983, Geometry and kinematics of fault-bend folding: American Journal of Science, 283, p. 684-721.

Surpless, B., Hill, N., Beasley, C., 2015. The unusual 3D interplay of basement fault reactivation and fault-propagation-fold development: A case study of the Laramide-age Stillwell anticline, west Texas (USA), Journal of Structural Geology, 79, p. 42-56.

Tankard, A., 2002, Tectonic framework of basin evolution in Perú: Report for Perupetro, 47 p.

Touzett, P., 1976, Informe de evaluación por hidrocarburos de las estructuras; Dominguiza, Putuime y Piuntza. Compilación de Información diversa sobre exploración por hidrocarburos en el valle del río Santiago: Informe técnico Perupetro, 16 p., USGS, 2017, National Earthquake Information Centre, Earthquake Catalog (https://earthquake.usgs.gov/contactus/golden/neic.php).

Turienzo, M. M., Dimieri, L.V., 2005, Geometría y cinemática de las estructuras que involucran al basamento en la zona del arroyo Tordillo, faja corrida y plegada de Malargüe, Mendoza, Revista de la Asociación Geológica Argentina, 60, p. 651-661.

Turienzo, M.M., 2010, Structural style of the Malargüe fold-and-thrust belt at the Diamante River area (34°30'–34°50'S) and its linkage with the Cordillera Frontal, Andes of central Argentina, Journal of South American Earth Sciences 29, 537-556; doi:10.1016/j.jsames.2009.12.002.

Turienzo, M., Dimieri, L., Frisicale, C., Araujo, V. and N. Sánchez, 2012, Cenozoic structural evolution of the Argentinean Andes at 34°40'S: A close relationship between thick and thin-skinned deformation, Andean Geology, 39, p. 317-357.

USGS, 2017, National Earthquake Information Centre; Golden, USA, http://earthquake.usgs.gov/regional/neic/.

Valdivia, W., C. Chacaltana, E. Grandez, and P. Baby, 2006, Nuevos aportes en el cartografiado geológico y la deformación de la Cordillera de Campanquiz: Cuenca Santiago: XIII Congreso Peruano de Geología, Geological Society of Perú, 4 p., Lima.

Valentine, G. A., and K. E. C. Krogh, 2006, Emplacement of shallow dikes and sills beneath a small basaltic volcanic center: The role of preexisting structure (Paiute Ridge, southernNevada, U.S.A.): Earth and Planetary Science Letters, v. 246, p. 217–230, doi:10.1016/j.epsl.2006.04.031.

Ventura Santos, R., E. L. Dantas, C. Gouveia de Oliveira, C. Souza de Alvarenga, C. W. Dias dos Anjos, E. Mendes Guimaraes, and F. B. Oliveira, 2009, Geochemical and thermal effects of a basic sill on black shales and limestones of the Permian Iratu Formation: Journal of South American Earth Sciences, v. 28, p. 14–24, doi:10.1016 /j.jsames.2008.12.002.

Vergani, G.D., A. J. Tankard, H. J. Belotti and H. J. Welsink, 1995, Tectonic evolution and paleogeography of the Neuquén Basin, Argentina, in A. J. Tankard, S. R. Suarez, and J. Welsink, eds., Petroleum basins of South America: AAPG Memoir, 62, p. 383–402.

Victor, P., Oncken, O. and J. Glodny, 2004, Uplift of the western Altiplano plateau: Evidence from the Precordillera between 20° and 21° (northern Chile), Tectonics, 23, p. 1-24, doi:10.1029/2003TC001519, 2004.

Villar, H. J., G. A. Laffitte, and L. Legarreta, 1998, The source rock of the Mesozoic petroleum system of Argentina: A comparative overview on their geochemistry, paleoenvironments and hydrocarbon generation patterns: AAPG International Conference and Exhibition, Rio de Janeiro, November 8–11, 1998, p. 186–187.

Wiltschko, D. V., and D. Eastman, 1983, Role of basement warps and faults in localizing thrust fault ramps: Geological Society of America Memoir, 158, p. 177–190.

Wine, G., J. Arcuri, E. Martínez, J. Fernández, Y. Calderón, and C. Galdos, 2001a, Santiago Basin—The hydrocarbon potential of NE Perú Huallaga, Santiago and Marañón Basins study: Proyecto de Asistencia para La Reglamentación del Sector Energético del Perú (PARSEP), Lima, 127 p.

Wine, G., D. Vetrici, J. Arcuri, E. Martínez, C. Monges, J. Fernandez, Y. Calderón, and C. Galdos, 2001b, The Huallaga Basin and adjacent area—The hydrocarbon potential of NE Perú Huallaga, Santiago and Marañón Basins study: Proyecto de Asistencia para La Reglamentación del Sector Energético del Perú (PARSEP), Lima, 68 p.

Wine, G., J. Arcuri, E. Martínez, C. Monges, J. Fernandez, Y. Calderón, and C. Galdos, 2002a, Marañón Basin technical report—The hydrocarbon potential of NE Perú Huallaga, Santiago and Marañón Basins study: Proyecto de Asistencia para La Reglamentación del Sector Energético del Perú (PARSEP), Lima, 167 p.

Wine, G., B. Parker, E. Martínez, J. Fernandez, Y. Calderón, and C. Galdos, 2002b, Ucayali and Ene Basins Technical Report—The hydrocarbon potential of the southern sub-andean basins project, Ucayali, Ene and Madre de Díos Basins: Proyecto de Asistencia para La Reglamentación del Sector Energético del Perú (PARSEP), Lima, 160 p.

Witte, C., and J. Bourgois, 2009, Forearc basin formation in the tectonic wake of a collision-driven, coastwise migrating crustal block: The example of the North Andean block and the extensional Gulf of Quayaquil-Tumbes Basin (Ecuador-Perú border area): Geological Society of America Bulletin, v. 122, p. 89–108.

Witte, J., S. Lemieux, and B. Veilleux, 2011, Regional structural styles in the Santiago and Marañón basins of northern Perú: New implications for hydrocarbon trapping from interplay of thick-skin, thin-skin and salt tectonics: VII INGEPET, EXPR-3-JW-E, Lima, 15 p.

Witte, J., J. Rebaza, D. Westlund, M. Stratton, and C. Alegría, 2015, A new structural model of the Pachitea Basin, Perú: Interaction of thick-skinned tectonics and salt detached thrusting: Journal of South American Earth Sciences, v. 63, p. 400–416.

Woodward, N.B., 2012, Evaluation, analysis and prediction of geologic structures; Journal of Structural Geology, 41, p. 76-85.

Yagupsky, D. L., Cristallini, E.O., Fantín, J., Zamora Valcarce, G., Bottesi, G. and R. Varadé, 2008, Oblique half-graben inversion of the Mesozoic Neuquén rift in the Malargüe fold and thrust belt, Mendoza, Argentina: New insights fromanalogmodels: Journal of Structural Geology, v. 30, p. 839–853.

Zapata, T. and Allmendinger, R.W., 1996, Thrust-Front zone of the Precordillera, Argentina: A thick-skinned triangle zone; AAPG Bulleting, v. 80(3), p. 359-381.

Zapata, T. and A. Folguera, 2005, Tectonic evolution of the Andean Fold and Thrust Belt of the southern Neuquén Basin, Argentina; in: Veiga, G.D., Spalletti, L.A., Howell, J.A. and Schwarz, E. (eds), 2005, The Neuquén Basin, Arentina: A Case Study in Sequence Stratigraphy and Basin Dynamics; Geolological Society, London, Special Publications, 252, p. 37-56.

Zelasco, L. D., 2010, Tectonic evolution of the Contaya Arch, Ucayali Basin, Perú: M.Sc. Thesis, Texas A&M University, 57 p.

Der Lebenslauf ist in der Online-Version aus Gründen des Datenschutzes nicht enthalten.

Der Lebenslauf ist in der Online-Version aus Gründen des Datenschutzes nicht enthalten.